COMMUNICATIONS

3
Josef Vican - Jaroslav Odrobinak - Jozef Gocal
ANALYSIS OF OUT-OF-PLANE STABILITY OF BOW-STRING ARCHES

10
Ruzica R. Nikolic - Jelena M. Djokovic - Jan Bujnak
BEHAVIOR OF A SANDWICH BEAM SUBJECTED TO BENDING IN TERMS OF THE CORE'S SHAPE AND DENSITY

15
Jana Izvoltova - Peter Pisca - Pavel Cernota
Marian Mancovic
ADJUSTMENT OF CODE RANGING OF GNSS OBSERVATIONS

19
Libor Izvolt - Janka Sestakova - Michal Smalo
ANALYSIS OF RESULTS OF MONITORING AND PREDICTION OF QUALITY DEVELOPMENT OF BALLASTED AND BALLASTLESS TRACK SUPERSTRUCTURE AND ITS TRANSITION AREAS

30
Antonin Lupisek - Martin Volf - Petr Hejtmanek
Katerina Sojkova - Jan Tywoniak - Peter Op't Veld
INTRODUCTION OF A METHODOLOGY FOR DEEP ENERGY RETROFITTING OF POST-WAR RESIDENTIAL BUILDINGS IN CENTRAL EUROPE TO ZERO ENERGY LEVEL

37
Dasa Fullova - Daniela Durcanska - Dusan Jandacka
Adriana Estokova
MASS DISTRIBUTION OF PARTICULATE MATTER PRODUCED DURING ABRASION OF ASPHALT MIXTURES IN LABORATORY

44
Izabela Major - Maciej Major - Daniela Kucharova
NUMERICAL ANALYSIS OF A MECHANICAL WAVE DAMPING IN THE RUBBER-CONCRETE COMPOSITE USING THE ADINA SOFTWARE

49
Veronika Valaskova, Daniel Papan, Rui C. Barros
ASSESSMENT OF THE ROADWAY DYNAMIC RESPONSE DUE TO THE TATRA 815 LORRY EXCITATION AND EXPERIMENTAL VERIFICATION

56
Jan Celko - Marek Drliciak - Igor Ripka
DATA STRUCTURE OF REGIONAL TRANSPORT FORECAST MODEL

61
Josef Vican - Peter Kotes - Anna Spiewak
Malgorzata Ulewicz
DURABILITY OF BRIDGE STRUCTURAL ELEMENTS

68
Pavol Durica - Peter Juras - Daniela Staffenova
Jan Rybarik
LIGHTWEIGHT WOOD-BASED WALL: THE LONG-TIME EVALUATION OF HEAT-AIR-MOISTURE TRANSPORT

77
Juraj Muzik - Ladislav Kais - Roman Bulko
LOCAL METHOD OF APPROXIMATE PARTICULAR SOLUTIONS FOR TWO-DIMENSIONAL UNSTEADY INCOMPRESSIBLE FLOW

83
Jan Mikolaj - Lubos Remek - Matus Kozel
LIFE CYCLE EXTENSION OF A PAVEMENT STRUCTURE

90
Andrea Kocianova
CAPACITY LIMITS OF BASIC TURBO-ROUNDABOUTS

99
Kamil Borko - Filip Pastorek – Stanislava Fintová
Branislav Hadzima
CORROSION RESISTANCE OF HSLA STEEL AFTER VARIOUS SURFACE TREATMENTS IN CHLORIDE ENVIRONMENT

COMMUNICATIONS

103
Michal Petru – Jaroslav Mlynek – Tomas Martinec
Jozef Broncek
MATHEMATICAL MODELLING OF FIBRE WINDING PROCESS FOR COMPOSITE FRAMES

112
Ladislav Janosik - Ivana Janosikova - Pavel Polednak
ASSESSMENT OF ECONOMIC LIFE OF FIREFIGHTING AND RESCUE APPLIANCES BASED ON CHASSIS RENAULT MIDLUM IN THE ZLIN REGION

117
Silvie Benesova - Isabela Bradacova - Thomas Jager
EVACUATION OF PERSONS FROM SELECTED DEPARTMENTS IN HIGH-RISE BUILDINGS OF HEALTHCARE FACILITIES

123
Cyril Diatka - Jan Ligus
THINKING ABOUT CERTAINTY AND TOLERANCE WITH MICHEL EYQUEM DE MONTAIGNE

129
Milan Kubina - Gabriel Koman
BIG DATA TECHNOLOGY AND ITS IMPORTANCE FOR DECISION-MAKING IN ENTERPRISES

https://doi.org/10.26552/com.C.2016.4.3-9

Josef Vican - Jaroslav Odrobinak - Jozef Gocal*

ANALYSIS OF OUT-OF-PLANE STABILITY OF BOW-STRING ARCHES

Several arch bridge superstructures, designed by the authors of the paper, are presented and analysed. Spatial FEM models were utilised to analyse behaviour of each bridge. Verification of out-of-plane buckling of the arches is discussed in more detail. Comparison of using beam and shell finite elements for the mesh of main beam-arch load-carrying system is given. The variation of top bracing system and its influence on the stability of the arches is presented, as well. A minimum load amplifier to reach the elastic instability of arches is used to estimate the suitability of the bracings. Comparisons of the assessment using results produced by first and second order global analyses are presented. Application of a unique global and local imperfection as the initial geometric imperfection is proposed.

Keyword: *Arch bridges, bow-string girder, buckling, out-of-plane stability of arches, initial imperfection, elastic critical buckling modes.*

1. Introduction

The paper deals with global analysis of bowstring-arch bridges, especially with verification of out-of-plane buckling resistance of the arches. For this purpose, the spatial transformation FEM models of five arch bridge superstructures recently designed by the authors of the paper were utilised. The primary models were modified in the parametric study, focused on effectiveness of different ways of stiffening the arches against the out-of-plane buckling [1]. That parametric study has been extended in this paper by another bridge superstructure and by further FEM models using shell finite elements for the mesh of main girder-arch load-carrying system. The comparison of origin beam models with the shell models is made by the minimum load amplifier to reach the elastic instability of arches. Finally, comparison of the assessment using results produced by first and second order global analyses is presented.

2. Analysed bridge structures

The first bridge passes railway line over the Nosicky Water Canal. The bridge will be situated at km 159.038 of the railway line Bratislava - Zilina and was designed as a four-span two-line steel railway bridge with theoretical lengths of single spans 62.4 m + 124.8 m + 124.8 m + 62.4 m, Fig. 1. All four superstructures of the bridge consist of two bow-string girders with the bottom orthotropic bridge deck and the upper longitudinal bracing. The main beam and the circular curved arches are designed from passable box-sections. The vertical hangers, designed from steel tubes filled with concrete, are hinged to the beams and arches. The more detailed description of the whole bridge can be found in [1 and 2]. In the next study, the superstructure with span of 62.4 m will be designated as bridge "A", while the superstructure with double span (124.8 m) will have designation as "E".

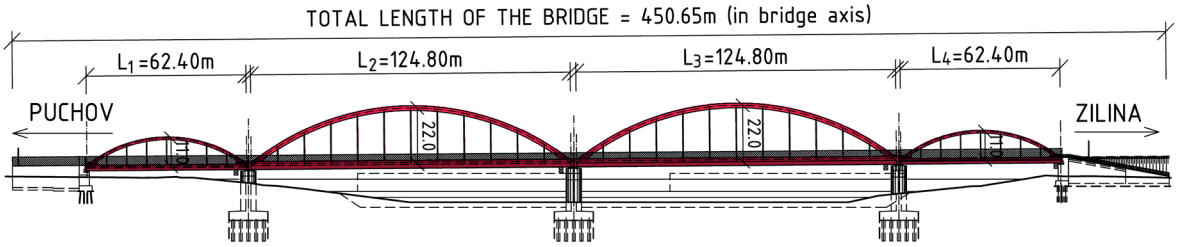

Fig. 1 Longitudinal view of the bridge over the Nosicky Water Canal

* **Josef Vican, Jaroslav Odrobinak, Jozef Gocal**
Department of Structures and Bridges, Faculty of Civil Engineering, University of Zilina, Slovakia
E-mail: josef.vican@fstav.uniza.sk

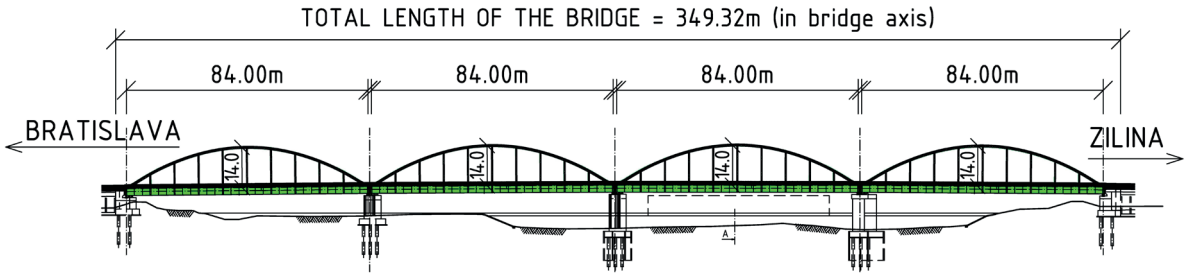

Fig. 2 Longitudinal view of the bridge over the Vah River in Trencin

The second bridge was designed over the Vah River in Trenčín City, just below the confluence of the Vah River and the Kockovsky Water Canal. The bridge is designed as a four-span structure under each railway line with theoretical lengths of single spans of 84.0 m, Fig. 2. The steel superstructures, marked as "B" in the next, consist of two bow-string girders with the bottom orthotropic bridge deck and the upper longitudinal bracing. The plate beams are designed from opened unsymmetrical I-shaped cross sections, while the parabolic curved arches are made of closed box-sections. The vertical hangers are designed from the symmetrical I-shaped cross-sections, fixed to the beams and arches in the plane perpendicularly to the plane of girders. The more detailed description can be found in [3].

The last railway bridge in the study was designed directly behind the railway station Liptovsky Hradok of the railway line Kosice - Zilina and it will cross the Bela River, a right-side inflow of the Vah River. The bridge is designed as two-line steel railway bridge with theoretical span length of 66.0 m, Fig. 3. The steel superstructure "C" consists again of the bow-string girders with the bottom orthotropic bridge deck and the upper longitudinal bracing. The plate beams as well as the circular curved arches are designed from passable box-sections. The vertical hangers positioned in the tenths of span are made of circular hollow sections. The more detailed description of the whole bridge can be found in [3].

Except four abovementioned superstructures of railway bridges, one road bridge superstructure (designated as "D") was included into the presented study. The road bridge on the

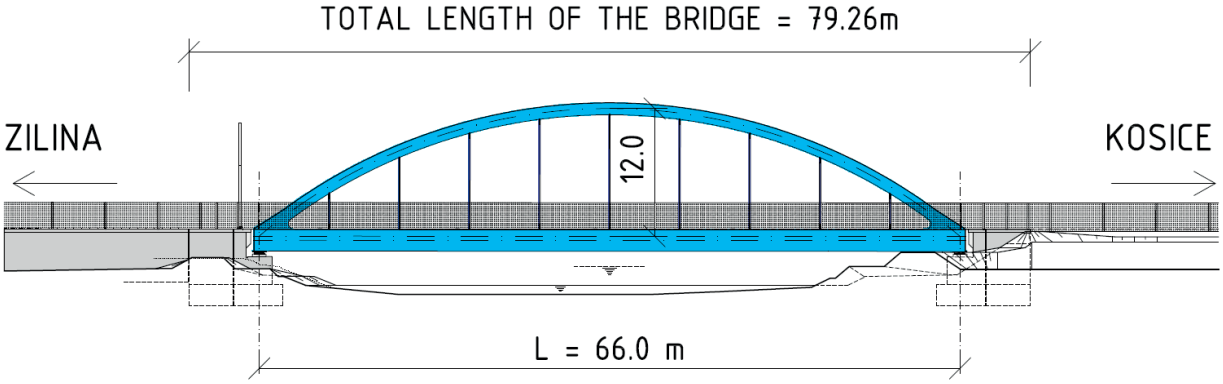

Fig. 3 Longitudinal view of the bridge over the Bela River

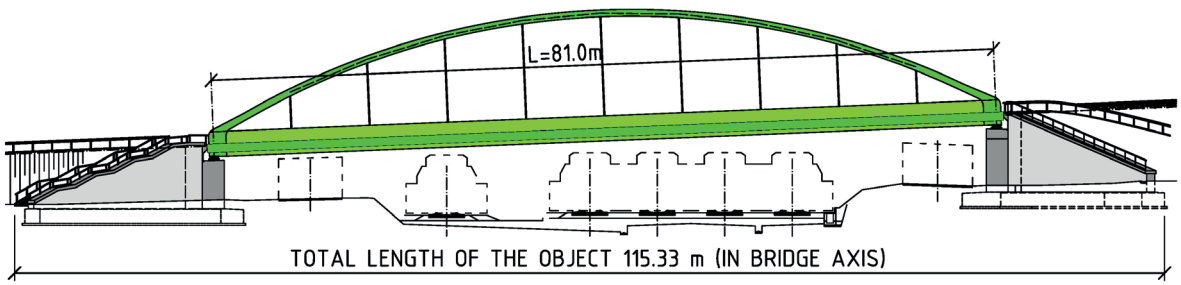

Fig. 4 Longitudinal view of the road bridge in Liptovsky Hradok City

road I/18 in Liptovsky Hradok City spans two local roads and five railway tracks, Fig. 4. The superstructure consists of two steel bow-string girders with theoretical span length of 81.0 m in axial distance of 12 m, connected with the bottom steel and concrete composite bridge deck and the upper longitudinal bracing. The plate beams are designed as opened symmetrical I-shaped cross sections, except for the edge parts, where the single-web cross-section changes to double-web closed cross-section to connect better of the arch box-section. The vertical hangers are designed from steel rods hinged to the girders and arches.

3. Study on stability analysis

3.1 Assumptions of the study

The study, a part of which has been already published in [1], was primarily focused on influence of the upper longitudinal bracing on stability of the arches of two railway bridge superstructures from Fig. 1. Different types of the bracing system were incorporated into original computational models of the railway bridge superstructures. The first comparative model was considered without any top bracing system (I). Then, two basic types of top bracing systems were taken into account: the frame system (II) with varying number of cross-bars and the truss system (III) with various arrangements of diagonals, see Fig. 5. In all cases, the bracing members were designed as circular hollow sections. In case of truss bracing system the slenderness of members did not exceed the value of 150. In this paper, the study has been extended by the additional three superstructures shown in Figs. 2, 3 and 4. Another extension of the study was achieved using further comparative FEM models with shell finite elements for the mesh of main girder-arch load-carrying system. Simplified designation of the bridges from A to E for the purpose of presented study is given in following Table 1.

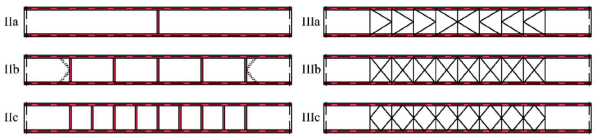

Fig. 5 Considered types of upper longitudinal bracings

3.2 FEM modelling

Utilisation of the commercial software based on Finite Elements Method (FEM) allows for spatial behaviour of bridges. Steel plates of the orthotropic deck of railway bridge superstructures were meshed by shell finite elements, as well as the reinforced concrete deck of the road bridge. Two basic concepts for modelling of the rest bridge geometry were adopted. In so called ”member” models, the beam finite elements were used for modelling main girders, arches, hangers and top bracings. The longitudinal and transversal stiffeners of the steel decks as well as the cross-beams of the steel-and-concrete composite deck were modelled as ribs of the shell members. Considering the actual structural details, all the arch-to-girder joints were considered as rigid. The connections of hangers were approximated by the hinge joints, except for hangers of welded I cross-section of the single track railway bridge D, where the joint was modelled as rigid for out-of-plane bending.

Unlike the previous models, in the “shell” models the main girders and arches, and also their relevant stiffeners and diaphragms, were meshed by the shell elements. The transversal stiffeners or cross beams as well as the frame bracing members and I-shaped hanger members were approximated by 2D elements too. The truss bracing members and also the hangers made of CHS profiles or rods were modelled by beam elements. Modelling of the other parts of bridge superstructures stayed unchanged. Attention was paid to the correct modelling of joints to approximate real

Basic parameters of bridge superstructures — Table 1

Bridge designation	A	B	C	D	E
Arch/bridge span	62.4	66.0	81.0	84.0	124.8
Rise-to-span ratio	1/5.67	1/5.50	1/7.36	1/6.00	1/5.67
Traffic type	two-line railway	one-line railway	two-line road	one-line railway	two-line railway
Span-to-width ratio	5.07	5.28	6.80	13.44	9.90
Bridge deck	steel orthotropic	steel orthotropic	steel-concrete	steel orthotropic	steel orthotropic
Hangers type and joints	hinged tubes	hinged rods	hinged rods	fixed I-section	hinged tubes
Main girder cross-section	box girder	box girder	plate girder	plate girder	box girder
Arch cross-section	box section	box section	box section	box section	box section
Arch-to-girder joint	rigid	rigid	rigid	rigid	rigid

behaviour of structural details. The arch-to-girder connection including corresponding diaphragms in the case of analysed brides E is illustrated in Fig. 6. Type of mesh elements used in FEM models are summarised in Table 2.

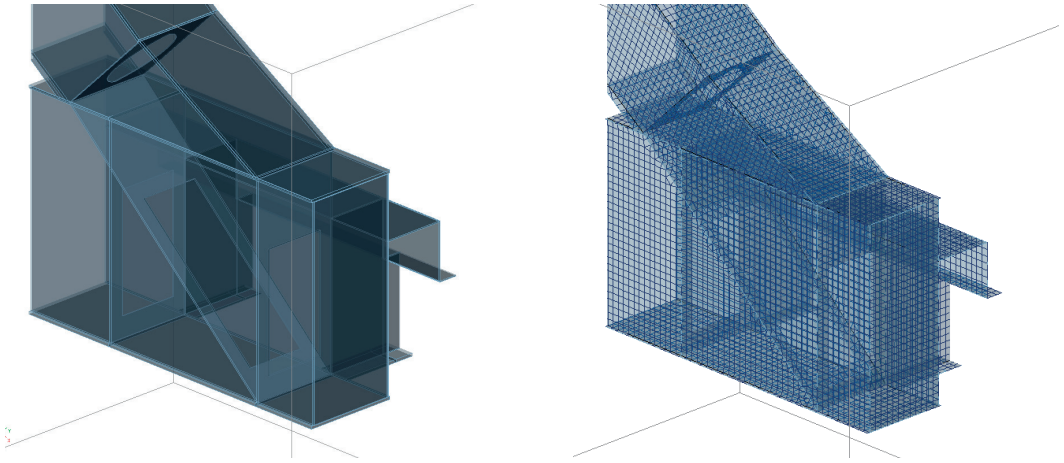

Fig. 6 Detailed view on arch-to-girder connection of the bridge E in shell model alternative

Type of mesh elements used in FEM models — Table 2

Use of element type in FEM models		„MEMBER“ models		„SHELL“ models		
		Railway bridges	Road bridge	Railway bridges		Road bridge
				single-line bridge	two-line bridges	
Applied for bridge		A, B, D, E	C	D	A, B, E	C
Deck parts	steel plates	shells	concrete shells	shells		concrete shells
	longitudinal stiffeners	beams (ribs)	-	beams (ribs)		-
	transversal stiffeners	beams (ribs)	-	shells		-
	cross beams	-	beams (ribs)	-		shells
Main carrying system	main girders	beams		shells (including stiffeners/diaphragms)		
	arches	beams		shells (including diaphragms)		
	hangers	beams		shells	beams	
Bracings	truss alternatives	beams		beams		
	frame alternatives	beams		shells		

Calculated values of the factors α_{cr} for various bracing systems and FEM models — Table 3

Bridge	A		B		C		D		E	
Bracings	$\alpha_{cr,b*}$	$\alpha_{cr,s*}$	$\alpha_{cr,b*}$	$\alpha_{cr,s*}$	$\alpha_{cr,b*}$	$\alpha_{cr,s*}$	$\alpha_{cr,b*}$	$\alpha_{cr,s*}$	$\alpha_{cr,b*}$	$\alpha_{cr,s*}$
I	4.57	4.65	3.83	3.93	0.71	0.76	1.53	1.51	1.76	1.83
IIa	5.06	5.34	4.25	4.21	0.80	0.87	1.90	1.70	1.94	2.02
IIb	5.25	5.36	4.43	4.39	1.29	1.06	2.36	1.88	2.85	2.32
IIc	5.46	5.52	4.48	4.50	1.81	1.21	2.75	2.01	3.43	2.48
IIIa	12.61	13.40	8.82	9.37	5.72	6.20	3.04	3.21	5.69	6.41
IIIb	13.10	12.96	9.18	9.63	5.98	6.49	3.24	3.39	5.64	6.37
IIIc	13.34	12.31	8.80	9.15	7.13	7.32	3.39	3.53	5.71	6.37
* b - beam model, s - shell model										

3.3 Results of stability analyses

All the numerical models (beam models as well as shell models) were used for global stability analysis in order to get the first eigenmodes of the loss of structural stability, especially of the arches. These eigenmodes are quantified by the factor α_{cr}, by which the design load should be increased to cause the elastic instability in a global mode. The values α_{cr} are shown in Table 3, both for the beam models ($\alpha_{cr,b}$) and the shell models ($\alpha_{cr,s}$).

As could be expected, from the comparison of the amplifier values it can be stated that the frame bracing system is generally less effective than the truss one. In the case of narrow bridges with span-to-width ratio greater than 10.0, the frame system appears to be ineffective ($\alpha_{cr} < 3.0$). When using the truss bracing, the rhombic system seems to be the most effective. On the contrary, the K-truss system is the least effective, although only small differences were observed. If no bracing is provided, the out-of-plane stability of arches rapidly decreases with increasing span-to-width ratio, especially in the case of small fixation capability of main girder in arch-to-girder joint. In that case, insufficient stiffness of the opened girder cross-section in horizontal bending and torsion results in arch-ends rotation.

The study outlined a significant role of rigidity of the arch-to-girder connection. More precise modelling using shell elements is generally recommended. However, according to the study, application of shell elements does not necessarily lead to more relevant stability data. Especially, in the case of slender cross-section, when many stiffeners are connected to thin plates, they have to be carefully taken into account in the structure model, including their connection, [4]. If local instability is not considered properly, it can result in an increase of the global deformations, e.g. the horizontal deformation of the arches in stability analysis.

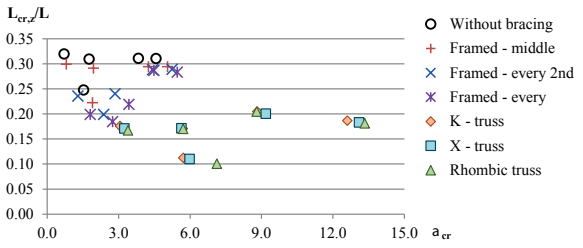

Fig. 7 Relation between $L_{cr,z}/L$ ratio and amplifier α_{cr} in the case of member models

In Fig. 7, the relations between $L_{cr,z}/L$ ratio and amplifier α_{cr} in the case of member models is shown. Actually, the out-of-plane buckling lengths of non-braced arches could be considered under 1/3 of the theoretical arch length for all analysed arches. When truss bracing is applied, the out-of-plane buckling length was under 1/5 of the arch length, regardless of the span and the truss type.

4. Verification of chosen arches

In some cases, it is very difficult to obtain relevant results without application of geometrically nonlinear elastic analysis with initial imperfections included (GNIA), [5]. Next comparative study was done to recognise if linear analysis is sufficient enough for analysis of abovementioned arches.

The obtained shapes of the elastic critical buckling modes (eigenmodes) from stability analyses were used for assessment of critical sections of the arches by means of second order global analysis. The key problem is to estimate the amplitude of so-called unique global and local imperfection. In the case of common structures, especially when uniaxial bending and in-plane buckling are under consideration, the procedure presented in [6 and 7] can be utilised. When biaxial bending and torsion are present combined with more complicated geometry, a complicated iterative procedure allowing for bending moments about both main axes should be executed [8]. These procedures have been also included in EN 1993-1-1 [9]. However, their application is useful provided that the special software able to solve separately internal forces induced by load cases combination and by the initial imperfections, respectively, is available. The work [10] proposes an alternative generalised approach, which is suitable for use in all cases, even when the common computer program is used. According to this approach, the design value of initial bow imperfection $e_{0,d,gen}$ can be obtained from the equation

$$e_{0,d,gen} = e_{0,d} \cdot \frac{N_{crit} \cdot y_{\max}}{M_{e,\max}} = e_{o,d} \cdot v_e \qquad (1)$$

where $e_{o,d}$ is the design value of initial bow imperfection according to [9], N_{crit} is the critical force of the member and $M_{e,max}$ is the maximum bending moment in the member under investigation when it is bent in the shape of the eigenfunction $y(x)$ with the maximum amplitude y_{max}; v_e is an amplification factor.

When using the computer program not giving the values $M_{e,max}$ corresponding to the determined value y_{max}, the amplification factor v_e given by equation (1) can be obtained on the basis of affinity between imperfection shape given by the buckling mode and the deflection $\eta(x)$ and moment $M_z(x)$ diagrams

$$v_e = \frac{N_{crit} \cdot \eta^{II}_{\max}}{M^{II}_{z,\eta,\max}} \qquad (2)$$

where η_{max}^{II} and $M_{z,\eta,max}^{II}$ are the maximum values of deflection and bending moment, respectively, resulting from the second order analysis using the critical buckling mode with arbitrary maximum amplitude y_{max}.

For spaced structures, where the critical buckling mode involves bending moments about both main axes, but when the buckling in y-y direction is decisive, the formula (2) can be modified as follows

$$v_e = \frac{N_{crit} \cdot \eta_{\max}^{II}}{M_{z,\eta,\max}^{II} + M_{y,\eta,\max}^{II} \cdot W_y / W_z} \qquad (3)$$

where $M_{y,\eta,max}^{II}$ is the bending moment about y-y main axis in the same cross section in which $M_{z,\eta,max}^{II}$ occurs and W_y, W_z are elastic section modules of the cross section.

Utilisation grades of chosen arch members Table 4

Bracing	Analysis	A	B	C	D	E
I	LA	0.889	0.817	2,067	1,163	1.242
	GNIA	0.834	0.801	-	-	1,027
IIc	LA	0.870	0.816	1.111	0.750	0.970
	GNIA	0.828	0.793	0.918	0.616	1,002
IIIc	LA	0.762	0.726	0.767	0.678	0.852
	GNIA	0.781	0.726	0.730	0.512	0.896

This approach was used in order to verify the chosen arches from the parametric study. The obtained corresponding global eigenmodes of the loss of structural stability were considered as the unique global and local imperfections η_{init} of the arch members. Applying design amplitudes given by equations (1) and (3) to the member models from the presented parametric study, the internal forces in critical sections were obtained using nonlinear second order global analysis. Consequently, the resistance of these critical cross-sections was evaluated and compared to the standard assessment with the equivalent column method according to 6.3.3 in EN 1993-1-1 [9]. The corresponding utilisation efficiency of the arch members obtained by first order analyses and second order analyses, respectively, are presented in Table 4. Only arches with no bracings, with the frame system in every hanger and with rhombic truss bracing, respectively, were chosen for verification (bracing systems designated as I, IIc and IIIc according to Fig. 5). From the comparison it is evident that the lower stability of arch in the higher differences can be observed. The bridge structure C without bracing (case I) was found to be unstable, therefore its utilisation grades are not given in the table for this case.

5. Conclusions

The paper presents study based on five bow-string arch bridge superstructures. Stability analyses using two types of spatial transformation models by means of FEM software were done. Based on the comparison of applying beam and shell finite elements, respectively, for the mesh of main load-carrying system, it can be stated that application of shell elements does not necessarily lead to more relevant stability data. The rigidity of arch-to-girder connection plays also important role. If excessive local instability occurs in this joint, it can affect the global stability of arches. The study approved an assumption of the higher effectiveness of truss bracing systems comparing to the frame bracings.

Finally, results from geometrically nonlinear analyses using application of initial geometric imperfections into the second order analysis are presented. The amplitudes of elastic critical buckling modes of arches were scaled to be applied as the unique global and local imperfection. The utilisation grades from nonlinear arch verification are compared to the values obtained by the standard assessment by means of the equivalent column method. Results presented above indicate that using of frame bracing systems, in cases of the bridges with rigid connection of box arch to box girder, did not lead into remarkable stability enhancement. Moreover, additional bending moments resulting from framed behaviour of the braced arches caused that the final utilisation of arches stay practically unchanged, in these particular cases.

Acknowledgement

This paper presents results of works supported by the Slovak Research and Development Agency under the contract No. APVV-14-0772 and by the Cultural and Educational Grant Agency KEGA within the project 012ZU-4/2016.

References

[1] VICAN, J., GOCAL, J., ODROBINAK, J., HLINKA, R.: Design and Stability of Long Span Railway Arch Bridge. *Communications - Scientific Letters of the University of Zilina*, 4/15, 2013, p. 33-39.

[2] VICAN, J., ODROBINAK, J., GOCAL, J., HLINKA, R.: *Design of the Two-Line Railway Bridge with the Longest Span in Slovakia.* Proc of 8th intern. conference Bridges in Danube Basin, Timisoara-Belgrade, Romania-Serbia, 2013, Springer Fachmedien: Wiesbaden, 2013, pp. 267-278.

[3] VICAN, J., ODROBINAK, J., GOCAL, J.: *Recently Designed Bow-String Railway Bridges in Slovakia.* Prof. of 7th Intern. Conference on Arch Bridges ARCH 2013, Trogir-Split, 2013, pp. 427-434.

[4] FLODR, J., KREJSA, M., MIKOLASEK, D., BROZOVSKY, J., PARENICA, P.: Numerical Modeling of a Thin-Walled Profile with Respect to the Redistribution of Bending Moments. *Civil-Comp Proceedings*, vol. 108, 2015.

[5] AL ALI, M., TOMKO, M., DEMJAN, I., KVOCAK, V.: Analysis of the Initial Imperfections Effect on the Thin-Walled Cold-Formed Compressed Steel Members. *Communications - Scientific Letters of the University of Zilina*, 4/14, 2012, pp. 83-87.

[6] CHLADNY, E., STUJBEROVA, M.: Frames with Unique Global and Local Imperfection in the Shape of the Elastic Buckling Mode - Part 1, *Stahlbau*, 82, 2013, Ernst & Sohn : Berlin, 2013, pp. 609-617.

[7] BALAZ, I., KOLEKOVA, Y.: S*tructures with UGLI Imperfections*. Proc. of 18th Intern. conference Engineering Mechanics 2012, Svratka, pp. 61-86.

[8] CHLADNY, E., STUJBEROVA, M.: Frames with Unique Global and Local Imperfection in the Shape of the Elastic Buckling Mode - Part 2, *Stahlbau*, 82, 2013, Ernst & Sohn : Berlin, 2013, pp. 684-694.

[9] EN 1993-1-1: Eurocode 3: Design of Steel Structures - Part 1-1: General Rules and Rules for Buildings, CEN : Brussels, 2005.

[10] CHLADNY, E., CHLADNA, M.: *The Application of Initial Bow Imperfection in the Designs of New Danube Bridges in Slovakia*, Proc. of 4th Intern. Conference on Bridges Across the Danube 2001, Bratislava, pp. 179-184.

https://doi.org/10.26552/com.C.2016.4.10-14

Ruzica R. Nikolic - Jelena M. Djokovic - Jan Bujnak*

BEHAVIOR OF A SANDWICH BEAM SUBJECTED TO BENDING IN TERMS OF THE CORE'S SHAPE AND DENSITY

Problem of the multi-layer sandwich beams, subjected to bending, is considered in this paper. The influence of the density and shape of the sandwich beam core on the beam behavior was studied. The two beam configurations were analyzed: the beam whose cross-section is constant along its length and the beam with periodically varying cross-section along the length. Each of the two configurations was considered for the two different core shapes – with the square and the circular holes. The diagrams of the beam deflection in terms of the number of the core unit cells are presented for the two beam configurations and the two core shapes. Based on results presented in this paper, one can conclude that in the given loading conditions, the core density, after reaching certain critical value, ceases to affect the bent sandwich beam behavior. Comparison of the two cores shapes leads to conclusion that, in the same loading conditions, the core with the square holes provides for the better sandwich beam's characteristics, i.e. such a beam has smaller deflection with respect to the beam with the core with the circular holes.

Keywords: *Sandwich beam, bending, core shape, static analysis, optimization.*

1. Introduction

Light multilayer constructions and sandwich structures were studied by numerous investigators: Allen [1] has set the fundamentals for design and analysis of the sandwich structures. In paper by Evans et al. [2] is presented a survey of investigations of the metal cellular systems' mechanical and thermal characteristics. Brittain et al. [3] have created a new method for manufacturing the micro plates with the truss core and they analyzed their mechanical properties. Wicks and Hutchinson [4] have shown that characteristics of the optimized sandwich plates with the truss core are superior to those of plates with the honeycomb core or the stringer-stiffened plates. Wicks and Hutchinson [5] have further extended the previous analysis to sandwich plates with truss core subjected to fracture straining and combination of the bending moment and transversal force, with restraining to buckling and plastic yielding. Valdevit et al. [6] have dealt with the structural optimization of the sandwich plates with the truss core. The multifunctional sandwich plates with prismatic and truss cores were analyzed from the similar point of view in works by Bujnak et al. [7] and Nikolic et al. [8]. The comparison of the two types of plates' performances to plates with honeycomb structure was performed. The estimates of the optimal plates' dimensions and the minimal mass of the sandwich plates with the prismatic and the truss cores were done.

Geometrically considered, these structures represent a result of periodical repetition of the basic cell in one, two, or three dimensions. The sandwich beam is an example of the periodical repetition of a unit cell in one direction (dimension) in order to obtain the multilayer or the sandwich structure.

Sandwich structures are found widely used in the aerospace, automobile and construction industry, as the highly resistant components, since they possess high stiffness and strength, as well as very good heat conductivity and low mass. Functionality of the sandwich beams, columns and other structural elements, can be understood if one analyzes the geometrical and mechanical factors affecting those elements' behavior under loading.

The sandwich beam is viewed as the multi-layer structure with the symmetrical cross-section. The assumption in this paper was that the sandwich structure was formed by the periodical repetition of a unit cell. Here is considered the influence of the unit cell's size, i.e. number of unit cells within structure, on static behavior of a sandwich beam subjected to bending. The static analysis of such a beam is done in this paper, namely the beam's bending stiffness and deflection are determined as a function of the number of the core unit cells, i.e. of the core's density. The

* [1]Ruzica R. Nikolic, [2]Jelena M. Djokovic, [3]Jan Bujnak
[1]Faculty of Engineering, University of Kragujevac, Serbia, Research Center, University of Zilina, Slovakia
[2]Technical Faculty of Bor, University of Belgrade, Serbia
[3]Faculty of Civil Engineering, University of Zilina, Slovakia
E-mail: ruzicarnikolic@yahoo.com

analyzed sandwich beam has length L; it is clamped at one end and free at the other where it is loaded by the transversal force F. The two considered configurations of the sandwich beams are shown in Figs. 1 and 2, each with two different core shapes, for the purpose of comparison of their influence on the beam's behavior in the given loading conditions.

2. The considered problem definition

In Fig. 1 is shown the sandwich beam with a cross section, which is constant along the beam's length L. The cross section consists of two flat plates, the beam's faces, upper and lower, of thickness t_f and width b. The beam's core, of height H_c, is made of a unit cell with two square holes of size a, shown in Fig. 1(a). This is a sandwich structure with $n = 1$, where n represents a number of unit cells, i.e. the core's density. As can be seen in Fig. 1(a), the structure with $n = 2$ has eight square holes. If the structure could be built with sufficient (arbitrary) number of holes, n could be practically limitless ($n = \infty$). In Fig. 1(b) is shown a sandwich structure where the core consists of a unit cell with two circular holes of diameter d and in this case is also $n = 1$. The structure with $n = 2$ has eight circular holes and so on, as far as the number of holes is sufficiently big, when it is taken that $n = \infty$.

In Fig. 2 is shown the sandwich beam with the cross section that is periodically changing along its length. In the A-A section, the beam has the solid cross section, while in the B-B section the cross section has the square or the circular holes. The upper and

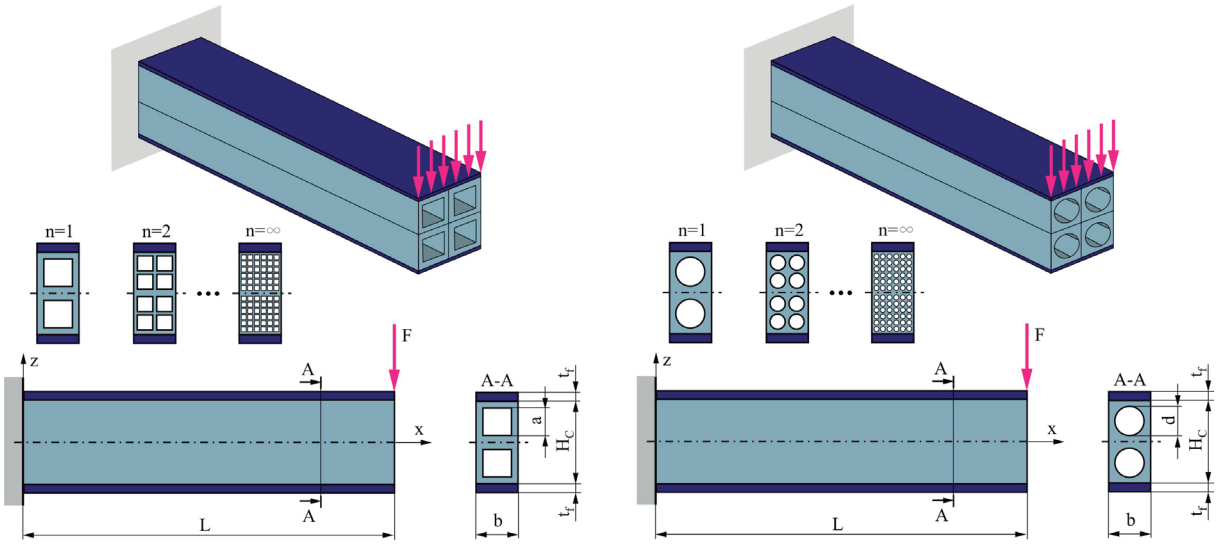

Fig. 1 Schematic presentation of the sandwich beams with the cross section constant along the length: (a) the core with square holes; (b) the core with circular holes

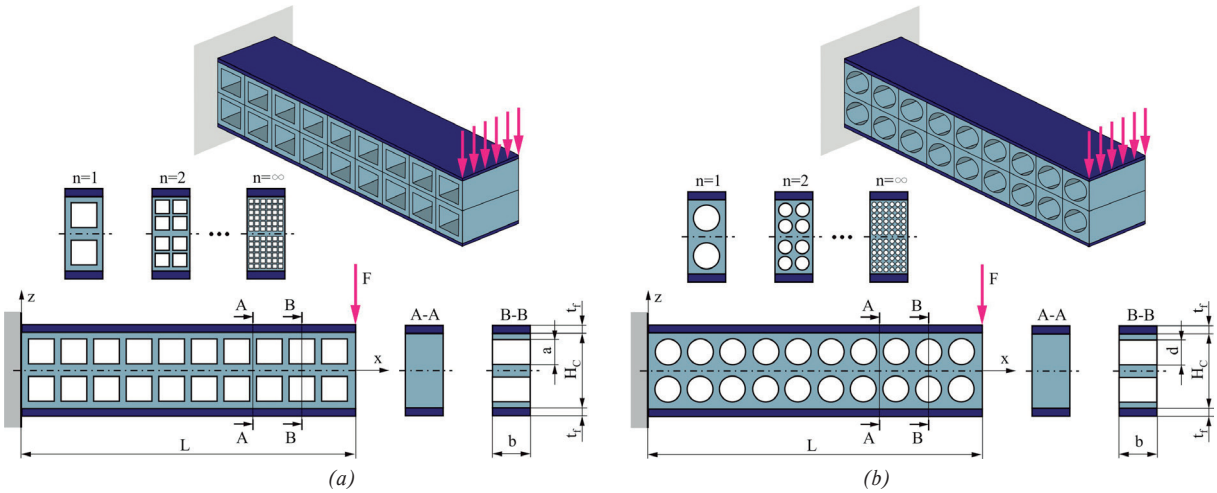

Fig. 2 Schematic presentation of the sandwich beams with the cross section that is variable along the length: (a) the core with square holes; (b) the core with circular holes

the lower beam faces have the same thickness, t_f, while the beam's core height is H_c. The sandwich beams have the square holes of side a and the circular holes of diameter d; the unit cell number is $n = 1$ for both beams.

The faces and cores are made of different materials, thus the Young's elasticity modulus and the Poisson's ratio for the faces' material have subscript 1, i.e. E_1 and v_1, respectively and for the core material subscript 2, E_2 and v_2, respectively.

The differential equation of the beam's elastic (deflection) line reads:

$$B^{(n)}\frac{d^2u(x)}{dx^2} = M(x), \tag{1}$$

where $B^{(n)}$ is the bending stiffness, $u(x)$ is the deflection and $M(x)$ is the bending moment for the cross section defined by coordinate x.

For the beam whose cross section is constant along its length, the bending stiffness is calculated as:

$$B^{(n)} = \sum E_i I_i, \tag{2}$$

while for the beam whose cross section is variable along its length the bending stiffness is calculated as:

$$B^{(n)} = \left(\frac{1}{l}\int_0^l \frac{1}{B(x)}dx\right)^{-1} = l\left(\sum_i \frac{l_i}{B_i}\right)^{-1}, \tag{3}$$

where l is the period's length.

For the loading conditions of beams presented in Figs. 1 and 2, the largest deflection is obtained at the beams' free ends, i.e. for $x = L$, and can be calculated as:

$$u_{\max} = \frac{FL^3}{3B^{(n)}}. \tag{4}$$

For the beam configuration presented in Fig. 1(a) – the beam with the square cross section with the square holes, which does not vary along the beam's length, the bending stiffness in terms of the core's density is obtained as:

$$\begin{aligned} &B^{(n)} = \sum E_i I_i = 2E_1 I_1 + 2E_2 I_2\,,\\ &I_1 = \frac{1}{3}b\left[\left(t_f + \frac{H_c}{2}\right)^3 - \left(\frac{H_c}{2}\right)^3\right],\\ &I_2 = \frac{1}{3}b\left(\frac{H_c}{2}\right)^3 - \frac{1}{3}\frac{a}{n}\sum_{m=1}^{n} n\cdot\\ &\cdot\left[\left(\frac{(2m-1)H_c}{4n} + \frac{a}{2n}\right)^3 - \left(\frac{(2m-1)H_c}{4n} - \frac{a}{2n}\right)^3\right]. \end{aligned} \tag{5}$$

For the beam configuration presented in Fig. 1(b) – the beam with the square cross section with the circular holes, which does not vary along the beam's length, the bending stiffness in terms of the core's density is obtained as:

$$\begin{aligned} &B^{(n)} = \sum E_i I_i = 2E_1 I_1 + 2E_2 I_2\,,\\ &I_1 = \frac{1}{3}b\left[\left(t_f + \frac{H_c}{2}\right)^3 - \left(\frac{H_c}{2}\right)^3\right],\\ &I_2 = \frac{1}{3}b\left(\frac{H_c}{2}\right)^3 - n\sum_{m=1}^{n}\cdot\\ &\cdot\left[\frac{\pi}{2}\left(\frac{d}{2n}\right)^4 - \pi\left(\frac{(2m-1)H_c}{4n}\right)^3\left(\frac{d}{2n}\right)^2\right]. \end{aligned} \tag{6}$$

For the beam configuration presented in Fig. 2(a) – the beam with the square cross section with the square holes, which is varying along the beam's length, the bending stiffness in terms of the core's density is obtained as:

$$\begin{aligned} &B^{(n)} = 2E_1 I_1 + B^{(n)}_{periodic},\\ &B^{(n)}_{periodic} = 2E_2\frac{I_2 I_3 H_c}{(H_c - a)I_3 + 2aI_2},\\ &I_1 = \frac{1}{3}b\left[\left(t_f + \frac{H_c}{2}\right)^3 - \left(\frac{H_c}{2}\right)^3\right],\ I_2 = \frac{1}{3}b\left(\frac{H_c}{2}\right)^3,\\ &I_3 = \frac{1}{3}b\left(\frac{H_c}{2}\right)^3 - \frac{1}{3}\frac{a}{n}\sum_{m=1}^{n} n\cdot\\ &\cdot\left[\left(\frac{(2m-1)H_c}{4n} + \frac{a}{2n}\right)^3 - \left(\frac{(2m-1)H_c}{4n} - \frac{a}{2n}\right)^3\right]. \end{aligned} \tag{7}$$

For the beam configuration presented in Fig. 2(b) – the beam with the square cross section with the circular holes, which is varying along the beam's length, the bending stiffness in terms of the core's density is obtained as:

$$\begin{aligned} &B^{(n)} = 2E_1 I_1 + B^{(n)}_{periodic},\\ &B^{(n)}_{periodic} = \frac{2E_2}{H_c}\left\{\int_0^{\frac{H_c-d}{4n}} dx\Big/\left(\frac{bH_c^2}{24}\right)\int_0^{\frac{H_c-d}{4n}} dx\Big/\left\{\frac{bH_c^2}{24} - \frac{nb}{3}\cdot\right.\right.\\ &\sum_{m=1}^{n}\left[\left(\frac{(2m-1)H_c}{4n} + \sqrt{\left(\frac{d}{2n}\right)^2 - \left(x - \frac{(2m-1)H_c}{4n}\right)}\right)^3\right.\\ &\left.\left.-\left(\frac{(2m-1)H_c}{4n} - \sqrt{\left(\frac{d}{2n}\right)^2 - \left(x - \frac{(2m-1)H_c}{4n}\right)}\right)^3\right]\right\}\\ &\left.+\int_{\frac{H_c+d}{4n}}^{\frac{H_c}{2n}} dx\Big/\left(\frac{bH_c^2}{24}\right)\right\}^{-1},\\ &I_1 = \frac{1}{3}b\left[\left(t_f + \frac{H_c}{2}\right)^3 - \left(\frac{H_c}{2}\right)^2\right]. \end{aligned} \tag{8}$$

3. Results and discussion

In Fig. 3 is presented the variation of the beam's free end's deflection in terms of the core's density for the beam whose cross section does not vary along its length, for the two shapes of the core and the same loading conditions. Results are obtained based on equations (4) to (6) by application of the *Mathematica* ® symbolic programming routine.

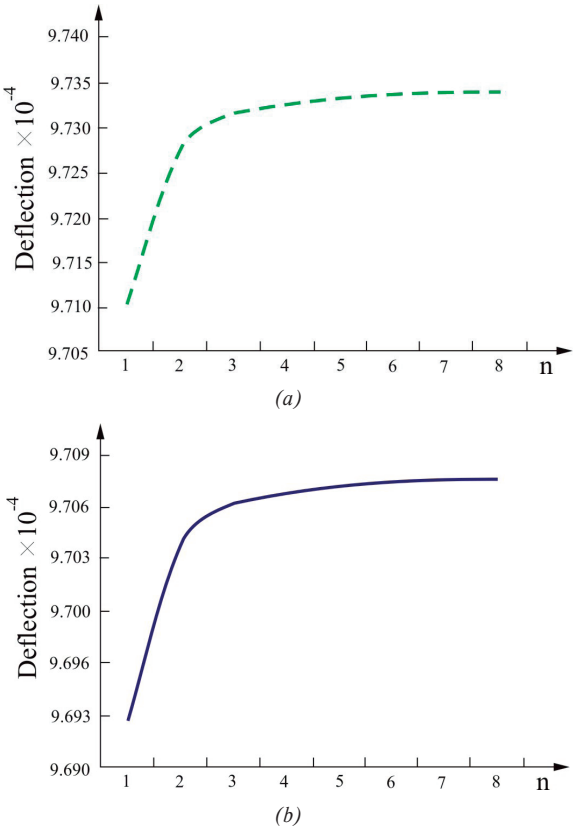

Fig. 3 Deflection of the free end of the bent sandwich beam with the constant cross section along in terms of the core's density n: (a) the core with square holes; (b) the core with circular holes

From Fig. 3, one can notice that the value of the beam's deflection increases with the core density, while after reaching a value of approximately $n = 5$ the deflection almost remains constant.

In Fig. 4 is presented the variation of the beam's free end's deflection in terms of the core's density for the beam whose cross section varies periodically along its length, for the two shapes of the core and the same loading conditions. Results are obtained based on equations (4), (7) and (8) by application of the *Mathematica®* symbolic programming routine.

From Fig. 4 one can see that similarly as for the first beams' configurations, when the cross section is constant, the value of the beam's deflection increases with the core density, while after becoming approximately $n = 5$ the deflection almost remains constant. So, the conclusion is that, regardless of the configuration, after that critical value, the increase of the core density does not significantly influence the sandwich beam's behavior, if at all.

In Fig. 5 is presented variation of the bent sandwich beam free end's deflection in terms of the core density, for the same configuration and for the two shapes of the core.

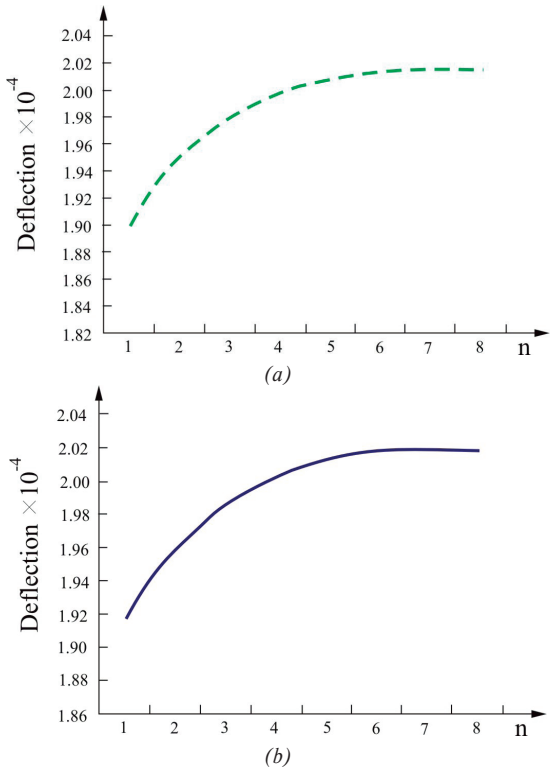

Fig. 4 Deflection of the free end of the bent sandwich beam with the periodically varying cross section in terms of the core density n: (a) the core with square holes; (b) the core with circular holes

From Fig. 5 could be seen that, for the same loading conditions, the beam with the square holes has smaller deflection than the beam with the circular holes.

If the two configurations were compared with respect to the value of the free end's deflection, one could conclude that the beam with the periodically varying cross section is somewhat better than the beam whose cross section is constant along its length, under the same loading conditions.

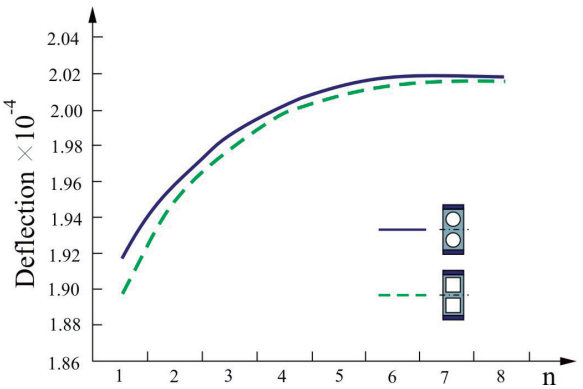

Fig. 5 Deflection of the free end of the bent sandwich beam with the cross section periodically varying along its length in terms of the core density n for the two shapes of the core

4. Conclusion

The influence of the shape and density of the core on behavior of the bent sandwich beam was analyzed in this paper. The sandwich beam was considered as the multi-layered structure with the symmetric cross-section. It was assumed that the sandwich structure is formed by periodical repetition of the core's unit cell. The attention was devoted to influence of the size of the unit cell, i.e. the number of unit cells on behavior of the sandwich beam subjected to bending. The static analysis of that behavior included determination of the sandwich beam free end's deflection in terms of the beam's core density.

The two configurations of the sandwich beams were considered: with the cross-section that is constant and that is varying along the beams length, with the two different shapes of the core: with the square and the circular holes.

The diagrams of the beams' free end's deflection were obtained for all the configurational combinations by application of the *Mathematica* ® symbolic programming routine. Based on obtained results the conclusion was drawn that the core density influences the bent sandwich beam behavior up to a certain critical value (in cases considered in this paper that value was $n = 5$), after which that influence is practically negligible. The other conclusion is that, in the given loading conditions, the beam whose cross section is periodically varying along its length is somewhat better than the beam whose cross section is constant.

Acknowledgement

Parts of this research were financially supported by the Ministry of Education, Science and Technological Development of Republic of Serbia through Grants ON174001, ON174004 and TR32036 and by the European regional development fund and Slovak state budget by the project "Research Center of the University of Zilina" - ITMS 26220220183.

References

[1] ALLEN, H. G.: *Analysis and Design of Structural Sandwich Panels*, Pergamon Press, 1969.
[2] EVANS, A. G., HUTCHINSON, J. W., ASHBY, M. F.: Multifunctionality of Cellular Metal Systems, *Progress in Materials Science*, vol. 43(3), 1998, pp. 171-221.
[3] BRITTAIN S. T., SUGIMURA, Y., SCHUELLER, J. A., EVANS, A. G., WHITESIDES, G. M.: Fabrication and Mechanical Performance of a Mesoscale, Space-Filling Truss Systems, *J. of Microelectromechanical Systems*, 10, 2001, pp. 113-120.
[4] WICKS, N. HUTCHINSON, J. W.: Optimal Truss Plates, *Intern. J. of Solids and Structures*, col. 38, 2001, pp. 5165-5183.
[5] WICKS, N., HUTCHINSON, J. W.: Performance of Sandwich Plates with Truss Cores, *Mechanics of Materials*, vol. 36, 2004, pp. 739-751.
[6] VALDEVIT, L., HUTCHINSON, J. W., EVANS, A. G.: Structurally Optimized Sandwich Panels with Prismatic Cores, *Intern. J. of Solids and Structures*, vol. 41, 2004, pp. 5105-5124.
[7] BUJNAK, J., DJOKOVIC, J. M., NIKOLIC, R. R.: Optimal Plates with Prismatic Cores, *Roczniki Inzynerii Budowlanej - Annals of Civil Engineering*, vol. 13, 2013, pp. 13-20.
[8] NIKOLIC, R. R., DJOKOVIC, J. M., BUJNAK, J.: Optimization of Sandwich Plates with Truss Cores, *Roczniki Inzynierii Budowlanej - Annals of Civil Engineering,* vol. 12*,* 2012, pp. 5-11.

https://doi.org/10.26552/com.C.2016.4.15-18

Jana Izvoltova - Peter Pisca - Pavel Cernota - Marian Mancovic*

ADJUSTMENT OF CODE RANGING OF GNSS OBSERVATIONS

Gauss-Jacobi combinatorial algorithm is a very useful method to adjust code ranging of global navigation satellite observations to find the systematic errors caused by radio waves passing through the atmosphere. The method is used as alternative adjustment technique to the least square method. While, the least square adjustment requires the linearization of nonlinear functions, combinatorial approach seems to be simplier in direct processing the nonlinear models. The diagnostics of observation errors consists in comparison of an evaluated partial positional norm determined in the partial mathematical models with the global one determine by robust estimation.

Keywords: *Code ranging, combinatorial algorithm, observation errors, positional norm.*

1. Introduction

Global navigation satellite system (GNSS) involves two observation techniques to measure the range (pseudorange) between satellite and receiver. Code pseudorange measurement, in short code ranging, is used to measure the time difference between the received code and generated replica code. Phase pseudorange measurement, phase ranging, is based on measurement of phase difference between the received and generated signal. The received carrier is Doppler shifted due to the mutual motion of satellite and receiver [1]. The accuracy of pseudorange obtained by the code or phase ranging depends on random and systematic influences. The whole system error involves the particular errors of determination of satellite time and position, signal transition errors caused by using the incorrect atmospheric model comprising the influence of ionospheric and stratospheric refraction and topography errors known as multipath effect. The great part of system error is generated by a receiver failure, which comprises a variation of phase centre and clock errors. The paper is devoted to a numerical analysis of code ranging especially to diagnose influence of systematic errors by applying the Gauss-Jacobi algorithm [2, 3 and 4].

2. Numerical Approaches of Code Ranging

Gauss-Jacobi algorithm is often used to estimate unknown parameters in nonlinear models [5 and 6]. In geodesy, it is applied as an alternative method to nonlinear Gauss-Markov model, which uses Taylor series for linearization. Application of Gauss-Jacobi combinatorial algorithm in diagnostics of systematic errors in code ranging assumes to arrange the vector of receiver position, which involves the differences between system time t and time delay τ_i of a signal which originates from a satellite position as follows [7, 8 and 9]:

$$\mathbf{r}^T(t-\tau_i) = (r_1(t-\tau_1), r_2(t-\tau_2), ..., r_n(t-\tau_n)). \quad (1)$$

Vector of measurements, which is represented by the pseudorange values $d_i(t)$ and observed in time t can be defined by the formula:

$$\mathbf{y}^T = (d1(t), d_2(t), ..., d_n(t)). \quad (2)$$

Providing $\Delta t_u(t)$ is correction of the system time of a receiver, $\Delta t_i(t-\tau_i)$ is correction of the system time of a satellite and c is signal career, the basic formula for code ranging is as follows:

$$d(t) = c\tau_i + c\cdot\Delta t_u(t) - c\Delta t_i(t-\tau_i), \quad (3)$$

where $c\tau_i = D(t)$ represents the real range, $c\Delta t_u(t) = b(t)$ is the unknown parameter because the system time varies in each satellite and correction of system time of a receiver is an unknown value. The last quantity of an equation (3) $c\cdot\Delta_i(t-\tau_i) = b(t-\tau_i)$ is corrected range, which involves

* [1]Jana Izvoltova, [1]Peter Pisca, [2]Pavel Cernota, [3]Marian Mancovic
[1]Department of Geodesy, Faculty of Civil Engineering, University of Zilina, Slovakia
[2]Institute of Geodesy and Mining, Technical University of Ostrava, Czech Republic
[3]Institute of Continuing Education, University of Zilina, Slovakia
E-mail: jana.izvoltova@fstav.uniza.sk

the time correction of satellites acquired from almanac. Then, the function of code pseudorange can be rewritten into a common formula:

$$\overline{d}(t) = d(t) + b(t - \tau_i) = D(t) + b(t). \tag{4}$$

3. Gauss-Jacobi Combinatorial Algorithm

In conformity with the previously described observation model (4), the mathematical model of code ranging is demonstrated according to formulas [3 and 4] as follows:

$$\mathbf{y} = \sqrt{(\mathbf{r}(t) - \mathbf{r}(t - \tau_i))^T (\mathbf{r}(t) - \mathbf{r}(t - \tau_i))} + \\ + \mathbf{b}(t) + \mathbf{e}, \tag{5}$$

where the vector of receiver position $\mathbf{r}(t)$, vector of clock corrections $\mathbf{b}(t)$ and vector of residuals $\mathbf{e}$ belong to the unknown parameters of model, which are estimated by Gauss-Jacobi combinatorial algorithm. It is a very useful method to ensure both procedures, to estimate the appropriate pseudorange and to identify the possible systematic influence on mathematical model (5). The principle of this method is in creating the minimal number of partial combinations of the model, which satisfies the combinatorial number:

$$C_k = \binom{n}{u} = \frac{n!}{u!(n-u)!}. \tag{6}$$

The rank of the particular matrices of the *p*-models depends on the number of unknown parameters *u*. The solution of the combinatorial algorithm consists in estimating the introductory positional parameters β_i^p from the *i*-th equation of *p*-model as follows

$$\beta_i^p = \begin{pmatrix} \beta_1^p \\ \beta_2^p \\ \vdots \\ \beta_u^p \end{pmatrix} = \mathbf{A}_i^{p^{-1}} \mathbf{y}_i^p \tag{7}$$

and in defining the partial matrices:

$$\mathbf{G}_i^p = \mathbf{A}_i^{p^T} \mathbf{P}_i^p \mathbf{A}_i^p, \tag{8}$$

which have to be positive definite and regular because of their inversion. The unknown parameters of the mathematical model (5) are represented by the weighted averages which are estimated from the equation:

$$\overline{\beta} = \begin{pmatrix} \overline{\beta}_1 \\ \overline{\beta}_2 \\ \vdots \\ \overline{\beta}_u \end{pmatrix} = (\mathbf{G}_i^p + \mathbf{G}_{i+1}^p)^{-1} (\mathbf{G}_i^p \mid \mathbf{G}_{i+1}^p) \begin{pmatrix} \beta_i^p \\ \beta_{i+1}^p \end{pmatrix} \tag{9}$$

The proper identification of the systematic influence in the model consists in comparison of a partial combinatorial positional norm estimated from the *i*-th model:

$$K_i^p = \sqrt{x_i^2 + y_i^2 + z_i^2} \tag{10}$$

with the median positional norm K_{med} in the case of robust estimation or with the "global" positional norm $K_{\overline{\beta}}$ estimated average from the whole model.

4. Verification of Efficiency of Combinatorial Algorithm

The diagnostics of systematic effect on final pseudorange belongs to the fundamental approaches of each GNSS developer and, therefore, there are a lot of hardware and software solutions in engineering practice. Differential GNSS seems to be one of the best methods to avoid this effect by using it in the process of determining the precise receiver position in geodesy applications [1]. However, the actual ionospheric and tropospheric model, precise time delay and satellite ephemerids are always important to know. The efficiency of the Gauss-Jacobi combinatorial algorithm was verified on real raw data arranged in "rinex" format, which were obtained by the static GNSS method. Inter alia, the "rinex" data file contains the number of visible satellites (G4, G31, G29,...) and the appropriate carrier phases (L1, L2), pseudo ranges (P1, P2) and Doppler frequency, as can be seen in Fig. 1.

The precise satellite's position needed for pseudorange calculations is defined by Cartesian coordinates in Global Reference Frame IGS08 and is accessible as a product of NASA and ESA in "sp3" format. For $n = 13$ satellites and $u = 4$ unknown parameters (x, y z, *bias*), we calculated the minimal number of satellite combinations $C_{k,\min} = 715$.The unknown parameters of the partial models were estimated according to the equation (7) to calculate the partial positional norms according to the equation (10):

$$K_i^p = \sqrt{\mathbf{r}_i(t - \tau)^T \mathbf{r}_i(t - \tau)}. \tag{11}$$

The significant difference between the positional norm in model average

$$K_{\overline{\beta}} = \sqrt{\mathbf{r}_{\overline{\beta}}(t - \tau)^T \mathbf{r}_{\overline{\beta}}(t - \tau)} \tag{12}$$

and the positional norm in median:

$$K_{med} = \sqrt{\mathbf{r}_{med}(t - \tau)^T \mathbf{r}_{med}(t - \tau)} \tag{13}$$

```
3953782.5851  1342642.0241  4805763.0479                APPROX POSITION XYZ
      1.4800        0.0000        0.0000                ANTENNA: DELTA H/E/N
   1    1                                               WAVELENGTH FACT L1/2
   6    C1    L1    D1    P2    L2    D2                # / TYPES OF OBSERV
2011    10    27     7    34     0.000000               TIME OF FIRST OBS
2011    10    27     8    36    35.000000               TIME OF LAST OBS
  15                                                    LEAP SECONDS
  16                                                    # OF SATELLITES
       C1    L1    D1    P2    L2    D2                COMMENT
 G 1    0     0     0     0     0     0                 PRN / # OF OBS
 G 2  752   752   752   752   752   752                 PRN / # OF OBS
 G 3    0     0     0     0     0     0                 PRN / # OF OBS
 G 4  413   413   413   413   413   413                 PRN / # OF OBS
 G 5    0     0     0     0     0     0                 PRN / # OF OBS
11 10 27  8  0  0.0000000  0 13 G4G31G29G25G9G2G12R21R11R10R9R20R19
 24176494.240   127048293.21747    -3076.746   24176496.700    98998657.71443    -2397.473
 22845397.200   120053379.65348     2584.396   22845394.980    93548087.05046     2013.815
 21045890.540   110596911.88649     2022.561   21045888.680    86179407.38048     1576.021
 20193365.920   106116851.24949      153.863   20193365.780    82688451.81948      119.893
 24765729.440   130144710.41947    -4214.593   24765734.440   101411442.73744    -3284.112
 21905710.820   115115306.17649     -510.444   21905707.740    89700211.52647     -397.750
 21143870.200   111111779.52349    -1865.957   21143867.720    86580590.79747    -1453.995
 20892791.820   111801573.66808     3003.423   20892794.780    86956794.58608     2335.996
 20260218.720   108264459.41508     2510.455   20260223.840    84205707.26906     1952.575
 19495945.680   103924354.91709    -1781.693   19495952.600    80830062.14807    -1385.763
 22953129.380   122568379.89907    -4255.016   22953141.980    95330990.20607    -3309.467
 19217751.780   102765958.73908     -721.196   19217756.680    79929086.45208     -560.932
 22289583.060   119234200.24408    -3799.061   22289588.120    92737710.35006    -2954.832
```

Fig. 1 Demonstration of raw GNSS data in "rinex" format

gives the view of error influence on observation data. The receiver position calculated from the code ranging obtained from satellites R11 and R19 seems to be influenced by observation error, as we can see from the positional norm differences displayed in Table 1. In practice, the differences from the positional norm demonstrate the pseudorange error, which can be caused by the multipath influence or improper satellite geometry. While, the first reason is easy to eliminate by an appropriate software, the second one is registered as PDOD value in a receiver.

Differences between partial and global positional norms Table 1

Combination number	Partial combinations of satellites	Positional Norm in km	Deviations	
			Average norm	Median norm
1	G4 G31 G29 G25	6366.334	-0.019	-0.013
2	G4 G29 G25 G9	6366.320	-0.032	-0.026
3	G4 G25 G9 G2	6366.302	-0.050	-0.044
4	G4 G9 G2 G12	6366.328	-0.024	-0.019
5	G4 G2 G12 R21	6366.371	0.019	0.025
6	G4 G12 R21 R11	6366.347	-0.005	0.000
7	G4 R21 R11 R10	6366.352	0.000	0.006
8	G4 R11 R10 R19	6366.589	0.237	0.243
9	G4 R10 R19 R20	6366.181	-0.171	-0.166
10	G4 R19 R20 R9	6366.383	0.031	0.036
11	G2 G4 G31 G29	6366.345	-0.007	-0.002
12	G2 G31 G29 G25	6366.336	-0.016	-0.010
13	G2 G29 G25 G9	6366.335	-0.016	-0.011
14	G2 G25 G9 G12	6366.376	0.024	0.029
15	G2 G9 G12 R21	6366.346	-0.006	0.000
16	G2 R12 R21 R11	6366.351	0.000	0.005
17	G2 R21 R11 R10	6366.138	-0.214	-0.209
18	G2 R11 R10 R19	6365.988	-0.363	-0.358
19	G2 R10 R19 R20	6366.358	0.006	0.012
20	G2 R19 R20 R9	6366.397	0.045	0.050
21	G31 G29 G25 G9	6366.352	0.000	0.005
22	G31 G25 G9 G2	6366.342	-0.010	-0.004
23	G31 G9 G2 G12	6366.346	-0.006	-0.001
24	G31 G2 G12 R21	6366.346	-0.005	0.000
25	G31 G12 R21 R11	6366.346	-0.006	0.000

The differences of the partial norms from the global positional norm in median can also be illustrated in Fig. 2.

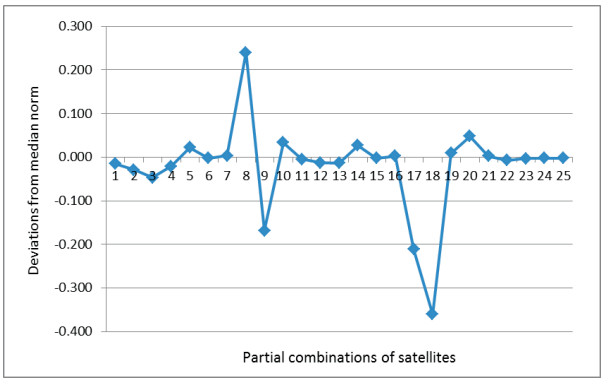

Fig. 2 Comparison of partial positional norm with the global one in median

5. Conclusion

The primary purpose of using Gauss-Jacobi combinatorial algorithm was to amend the endless iterative methods of parameter estimation with the creation of the minimal number of mathematical combinations of observed data. The practical application of this method demonstrates its strength to estimate unknown parameters in nonlinear mathematical models with current diagnostics of observation errors with systematic effect. Comparing the global positional norm with a partial one estimated in *i*-th partial model refers to code ranging error existence probably caused by multipath effect. Gauss-Jacobi combinatorial algorithm enables us to identify improper satellite position in a given system time.

Acknowledgement

This article is a result of the implementation of the project VEGA No. 1/0597/14 "Analysis of methods used to measure the unconventional railway track construction from the point of view of accuracy and reliability" supported by the Scientific Grant Agency of the Ministry of Education, Science, Research and Sport of the Slovak Republic and the Slovak Academy of Sciences.

References

[1] RAO, B., R., K., SARMA, A., D., KUMAR, Y., R.: Technique to Reduce Multipath GPS Signals. *Research Communications, Current Science*, vol. 90, No. 2, 2006, India.
[2] GRAFAREND, E. W.: *Linear and Nonlinear Models*. Walter de Gruyter Berlin : New York, 2006, p. 752.
[3] HEFTY, J., HUSAR, L.: *Satellite Geodesy*, STU : Bratislava, 2003, 186 p.
[4] HOFMANN WELENHOF, B., MORITZ, H.: *Physical Geodesy, 2nd ed*., Springer Wien : New York, 2006, ISBN-13978-3-211-33544-4, 403 p.
[5] AWANGE, J. L., GRAFAREND, E. W.: *Solving Algebraic Computational Problems in Geodesy and Geoinformatics,* Springer Berlin : New York, 2005.
[6] GASINCOVA, S., GASINEC, J.: Adjustment of Positional Geodetic Networks by Unconventional Estimations, *Acta Montanistica Slovaca*, 15/1, 2010, ISSN 1335-1788, pp. 71-85.
[7] HRDINA, Z., PANEK, P., VEJRAZKA, F.: *Position Determination by Radio Ranging*. CVUT : Praha, 1999.
[8] KOCH, K., R.: *Parameter Estimation and Hypothesis Testing in Linear Models.* Springer-Verlag : Berlin, 1988, p. 378.
[9] MUZIK, J., KOVARIK, K., SITANYOVA, D.: Meshless Analysis of an Embankment Using Local Galerkin Radial Point Interpolation Method, *Communications - Scientific Letters of University of Zilina*, 2/2013, ISSN 1335-4205, pp. 34-40.

https://doi.org/10.26552/com.C.2016.4.19-29

Libor Izvolt - Janka Sestakova - Michal Smalo*

ANALYSIS OF RESULTS OF MONITORING AND PREDICTION OF QUALITY DEVELOPMENT OF BALLASTED AND BALLASTLESS TRACK SUPERSTRUCTURE AND ITS TRANSITION AREAS

Securing durability of parameter quality of track alignment design and track geometry is a goal of each railway infrastructure manager. To accomplish this goal, various methods and procedures are applied, but they are all based on regular diagnostics, analysis of its results according to valid legislation and design and implementation of respective maintenance and repair works. The technological and economic optimization of planning and implementation of maintenance and repair works, based on prediction of quality development of railway track, is conditioned by precisely implemented and evaluated monitoring. In relation to these facts, the first part of the paper brings an overview of the problem of monitoring the ballastless structure and its transition areas around portals of the Turecky vrch tunnel by methods of complex diagnostics and quality evaluation of the structure including prediction of the structural quality development. The second part of the paper deals with the analysis of the detected errors of the ballastless track with specific focus on transition areas and on the ballasted track. It also summarizes the possibilities of elimination of these errors in building further sections with ballastless track. Modernization of these sections within modernization of ZSR infrastructure is a topical problem.

Keywords: *Railway track, railway superstructure, diagnostics, track geometry, measuring trolley KRAB™-Light.*

1. Monitoring of the experimental section

The railway track monitoring determines the state of constructions and facilities of railway infrastructure, state of particular structural parts and their functioning, parameters and wear, with regard to tolerances, health, fire and environmental safety, clearances along the track and walking and handling clearance. The operational capability of railway track is verified by inspections and measurements of constructions and facilities of railway infrastructure in prescribed intervals [1].

The diagnostics of the rail route is focused on:

- track skeleton structure
  - parameters of the track geometry of the track and turnout,
  - structural elements of the track and turnout,
- subgrade structure,
  - entire structure,
  - rail bed,
  - substructure,
  - foundation,
- clearances along a line,
- catenary (measurement of the contact wire geometry),
- bridges and tunnels
  - inspections,
  - photogrammetric measurements,
  - clearances along the track and supporting strength,
- moving rail vehicles and detection of their defects (flat wheels, etc.),

  buildings and utilities.

The paper presents the results of diagnostics of track geometry, carried out by the Department of Railway Engineering and Track Management, Faculty of Civil Engineering, University of Zilina since 2012. The diagnostics is performed in the experimental section near the portals of the Turecky vrch tunnel, as shown by Fig. 1. The objective of the diagnostics is to regularly determine and assess the quality of given parameters, monitor continuously the quality development and predict its future development due to optimization of design and implementation of maintenance and repair works.

The experimental section in the area of portals of the Turecky vrch tunnel, its parameters, measuring devices and diagnostics methods, its assessment and partial results were in detail specified in [2] and this monitoring will continue in the future.

The monitored section has a unique superstructure in Slovak Republic: ballasted and ballastless superstructure. Between these two structures there is a transition area, which is the most

* **Libor Izvolt, Janka Sestakova, Michal Smalo**
Department of Railway Engineering and Track Management, Faculty of Civil Engineering, University of Zilina, Slovakia
E-mail: libor.izvolt@fstav.uniza.sk

demanding structure here from the point of view of quality maintenance. The transition area superstructure is formed by railbed in a concrete trough with a variable bottom thickness. From the point of view of diagnostics implementation, the monitored section is divided into subsections:

- section 1.1 (rail no. 1, south portal of Turecky vrch tunnel) and 2.1 (rail no. 2, south portal; both sections are 175 m long; km 102.360 000 – km 102.535 000):
  - km 102.360 000 – km 102.460 500 ballasted superstructure (conventional railway superstructure),
  - km 102.460 500 – km 102.480 500 transition area,
  - km 102.480 500 – km 102.535 000 ballastless track (unconventional superstructure).
- section 1.2 (rail no. 1, north portal of Turecky vrch tunnel) and 2.2 (rail no. 2, north portal); both portals are 640 m long; km 104.200 000 – km 104.840 000):
  - km 104.200 000 – km 104.720 500 ballastless track,
  - km 104.720 500 – km 102.740 500 transition area,
  - km 104.740 500 – km 104.840 000 ballasted superstructure.

The comprehensive diagnostics of the experimental section is carried out by the measuring trolley *KRAB™-Light* using a complex continuous method. As a complementary method, partial point diagnostics by a manual gauge bar was applied here. The implementation and results of the experimental section diagnostics by this method are closely characterized in [4, 5 and 6].

The monitoring method used by the measuring device *KRAB™-Light* is contact while the measured data is recorded in the on-board computer.

After transfer to the computer, on the basis of defined parameter limits of track geometry, for each part of the experimental section there were created: the graph of measured parameters of track geometry, table of local errors with the list of exceeded tolerances and the table of section evaluation which is based on standard deviations of variables (*SDV*), quality marks (*QM*) and quality numbers (*QN*).

The evaluation of a section by the number of quality, calculated according to the equation:

$$QN = \sqrt{0,57 \cdot SDV_{RK}^2 + 1,6 \cdot SDV_{SP,SL}^2 + \\ +1,6 \cdot SDV_{PK}^2 + 1,6 \cdot SDV_{VP.VL}^2} \qquad (1)$$

where:

SDV_{RK} - Standard tolerance of variable of track gauge,
$SDV_{SP, SL}$ - Standard tolerance of variable of direction of the track,
SDV_{PK} - Standard tolerance of variable of track superelevation,
$SDV_{VP, VL}$ - Standard tolerance of variable of rail top level.

where (mm) $$SDV = \sqrt{\frac{1}{n-1}\sum_{i=1}^{n} x_i^2} \qquad (2)$$

expresses irregular course of the track geometry parameter in the section evaluated, where:

n - number of points measured each 0.25 m,
i - marking measuring point,
x - dynamic component of the relevant quantity of track geometry (tolerance from the center line in the wavelength range 1 m to 25 m).

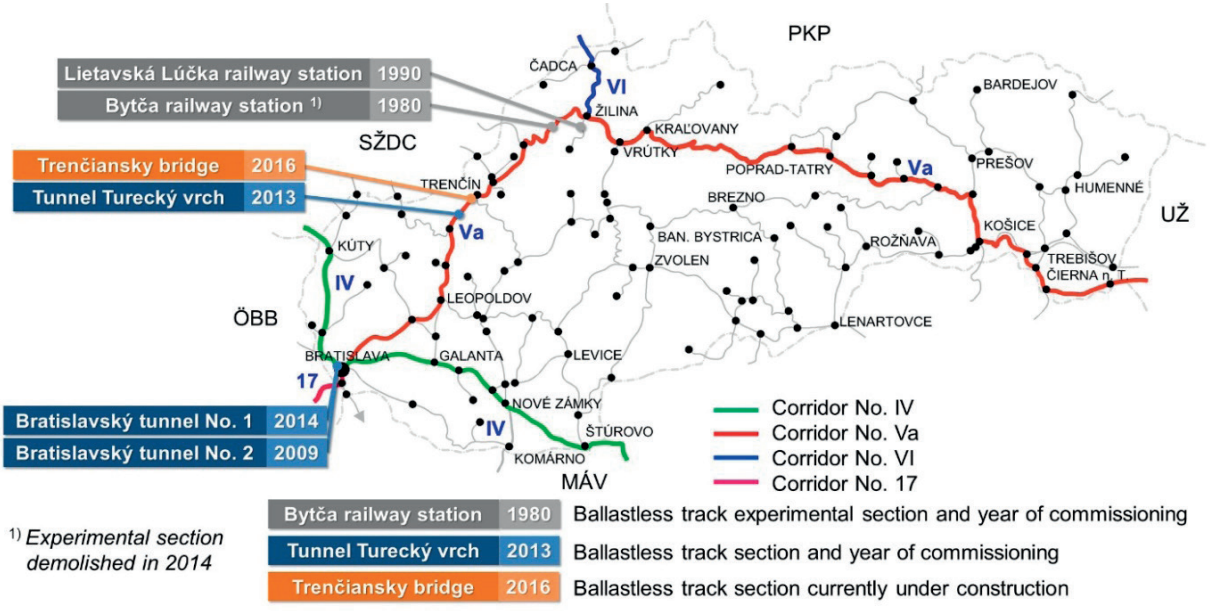

Fig. 1 Ballastless track sections in the railway infrastrucure of the Slovak Republic [3]

The evaluation of section according to quality marks shall be carried out according to the equation:

$$QM = \frac{In\frac{SDV}{b}}{m} \quad (3)$$

where b and m are numerical constants determined on the basis of the SDV statistics of relevant parameter and speed zone.

The evaluation using the list of local errors and the section evaluation respect conditions stated in [7 and 8], for tracks with track speed from 120 km.h^{-1} to 160 km.h^{-1} included (i. e. for speed zone No. 4 /*RP* 4/). The provisions of the currently valid document [9] have so far not been included in the respective legislation by the railway infrastructure manager. The measured parameters were evaluated using software according to maximum input tolerances for acceptance of works with the use of new material (MSO), or according to operational tolerances and maximum operational tolerances for *RP*4 (PO1 to PO7).

The particular measurements in the experimental section were carried out as follows:

- input measurement before putting the structure to operation (MSO), on 10. 7. 2012, 11. 7. 2012, 2. 10. 2012 and 3. 10. 2012,
- first operational measurement (PO1) on 9. 4. 2013, 10. 4. 2013, 21. 4. 2013 and 22. 4. 2013,
- second operational measurement (PO2) on 8. 10. 2013, 9. 10. 2013, 21. 10. 2013 and 22. 10. 2013,
- third operational measurement (PO3) on 25. 5. 2014 and 28. 5. 2014,
- fourth operational measurement (PO4) on 29. 10. 2014,
- fifth operational measurement (PO5) on 25. 3. 2015 and 17. 4. 2015,
- sixth operational measurement (PO6) on 14. 10. 2015 and 15. 10. 2015,
- seventh operational measurement (PO7) on 22. 03. 2016 and 23. 03. 2016.

2. Analysis of results of the experimental section monitoring

The quality of the track geometry of each evaluated section is presented using:

- graphs of measured parameters of track geometry,
- tables of local errors with an overview of exceeded maximum values (standard tolerances) of measured parameters and
- tables of section evaluation which show:
  - standard tolerances (SDV) and quality marks (QM) of particular geometric quantities – alignment of the track (SK), track gauge (RK), superelevation (PK) and rail top level (VK),
  - overall quality mark (OQM) which serves for assessment of track geometry in the evaluated section as a whole,
  - tamping mark (TM), which helps decide whether to deploy a tamping machine. Unlike OQM, it does not consider gauge tolerances (RK). (They are not maintained by tamping machines).
  - quality number (*QN*).

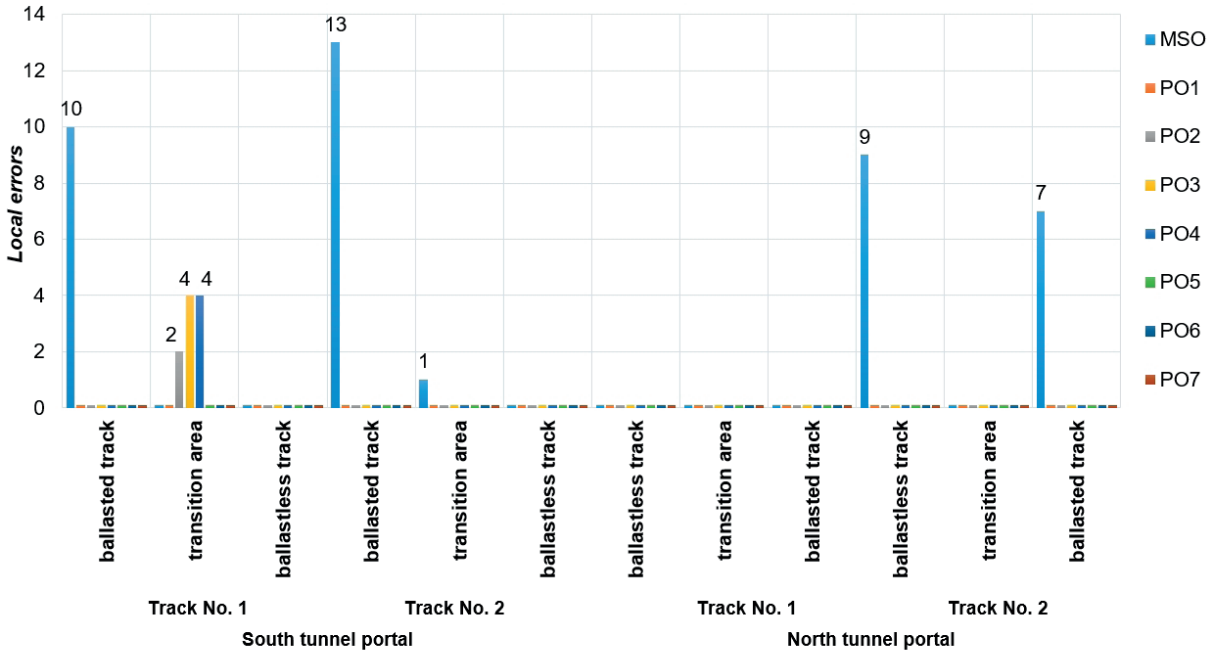

Fig. 2 Incidence of local errors in the monitored section- measurements carried out using measuring trolley KRAB™-Light

The overview of quality development of the track geometry of the monitored section is shown in Figs. 2 - 7. The incidence of local errors of measured parameters is stated separately for ballasted track sections, transition areas and for ballastless track sections (Fig. 2).

2.1 Local errors

The experimental section monitoring has been carried out since July 2012, with six-month periodicity. The input measurement (MSO) was carried out 2 days before putting the track in operation. Within the input measurement, 40 local errors were recorded, out of them 30 in sections with ballasted track, 9 in sections with ballastless track and 1 local error was diagnosed in the transition area of the section 2.1. After this measurement, the supplier carried out the repair of track geometry and microgeometry of rail heads by grinding in the transition areas and in the sections with gravel superstructure (unfortunatelly, the supplier did not provide the details of repair works). The operational diagnostics has been applied seven times (PO1 to PO7).

In the second operational measurement (PO2), the local errors of the rail top level of the right rail (*VP*) and the top level of left rail (*VL*) were for the first time recorded in the transition area of the section 1.1, confirmed by the track geometry car of ZSR (Zeleznice Slovenskej republiky – the Railways of the Slovak Republic). In the following measurements – PO3 and PO4 – further quality degradation of the section 1.1 was diagnosed, confirmed by the increased number of local errors (Fig. 2) as well as worsening value (increase) of the overall number of quality (Fig. 7). In November 2014, the railway infrastructure manager carried out repair interventions in the transition areas of the sections 1.1 and 2.1. In this way the diagnosed local errors were removed. The complex continuous diagnostics, carried out by the measuring trolley *KRAB*^{TM}*- Light*, and monitoring by the railway infrastructure manager applying the levelling method from December 2014 to August 2015 in the sections 1.1 and 1.2 confirm further lowering of the track. Their values cannot at present be considered local errors as the operational tolerances were not exceeded. However, due to further degradation of particular parameters of the sections in question, incidence of local errors is expected in the near future. The sections 1.2 and 2.2 in the transition areas do not show any errors in values. The quality development in the measurements carried out so far do not indicate any probability of their incidence in further measurements [5, 6 and 10].

2.2 Section evaluation

The quality marks of the alignment of the right rail (after calculation also of the left one) QM_{SK} (Fig. 3) were within MSO, PO1, PO2 and PO3 measurements placed in the interval $2 < QM \leq$

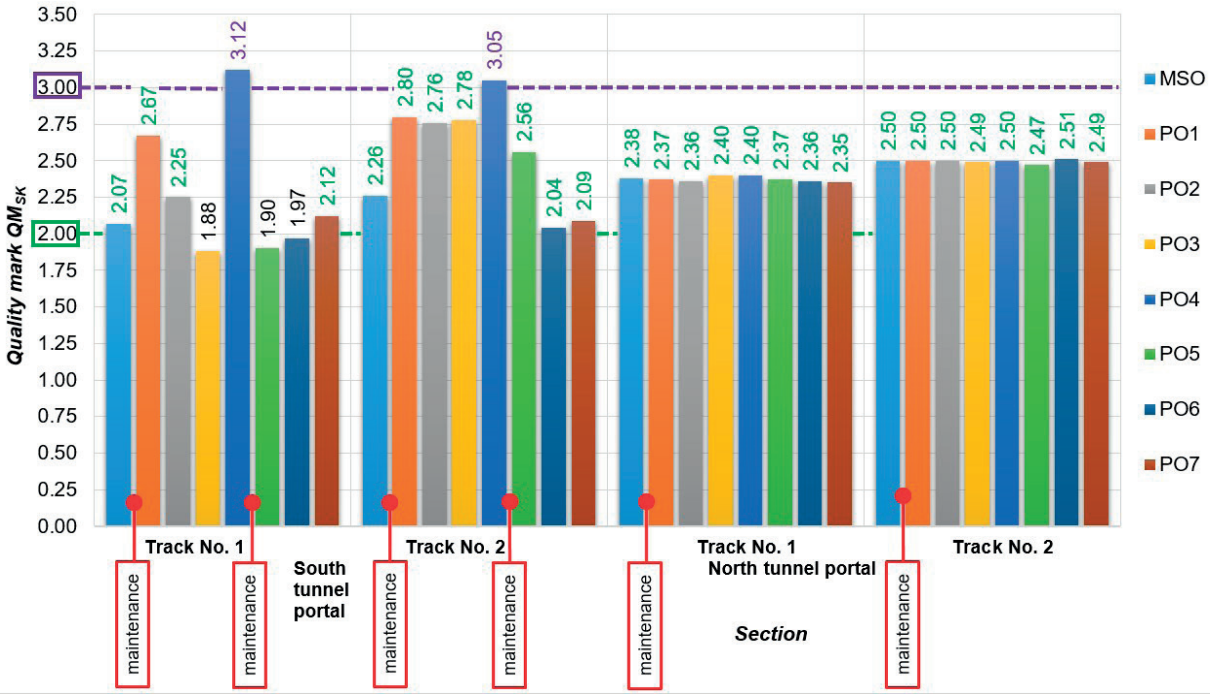

Fig. 3 Quality marks of the geometric quantity alignment of the right rail in respective monitored sections – measurement carried out by measuring trolley KRAB^{TM}*-Light*

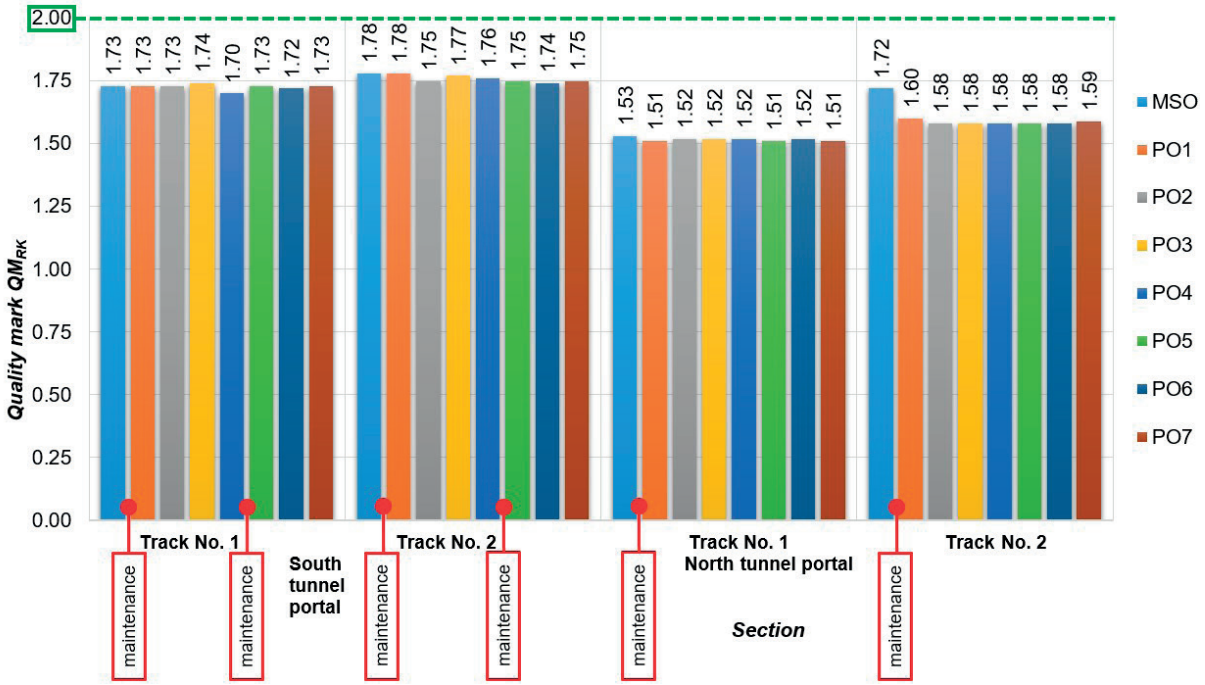

Fig. 4 Quality marks of the geometric quantity rail gauge tolerance in respective monitored sections – measurements carried out by measuring trolley KRAB™-Light

3 (recommendation: to design the repair of track geometry in the maintenance work plan) in all the monitored sections. The quality marks in the interval $3 < QM \leq 4$ (recommendation: to carry out the repair of the track geometry until the nearest inspection) were reached in the sections 1.1 and 2.1 within PO4 measurement. After repair interventions before PO5 measurement, the values of quality marks improved (decreased) to the interval $0 < QM \leq 2$ (the state of the track geometry in the evaluated section is

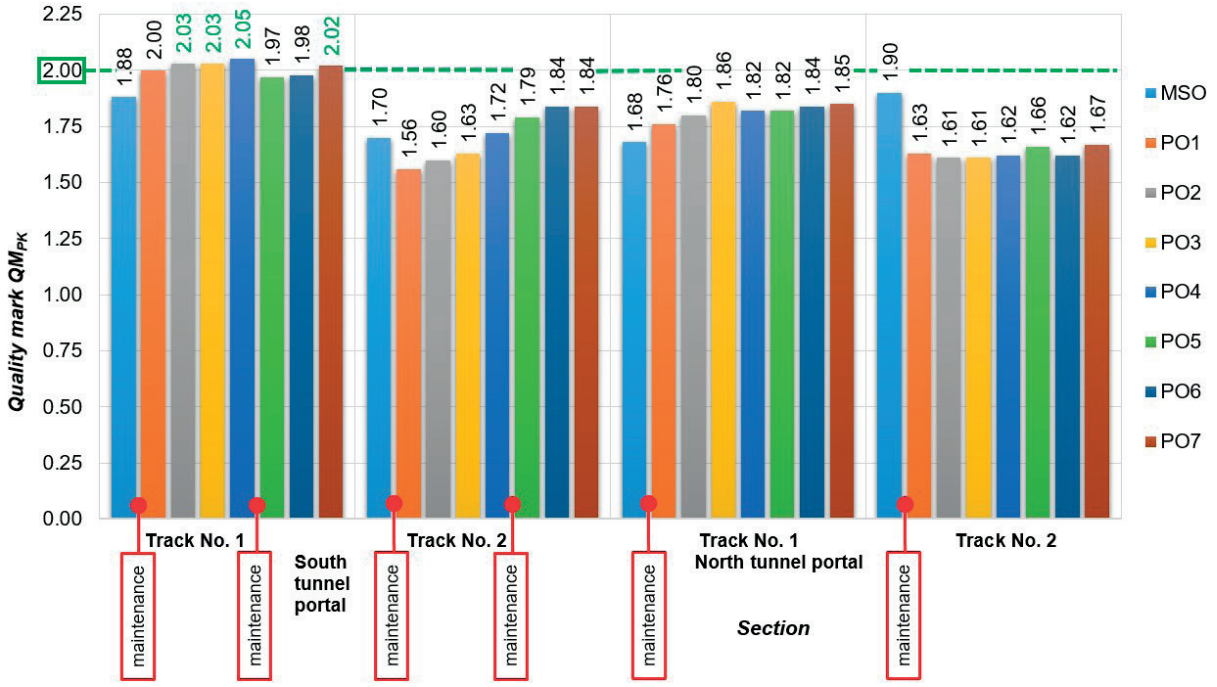

Fig. 5 Quality marks of the geometric quantity rail superelevation in respective monitored sections – measurements carried out by measuring trolley KRAB™-Light

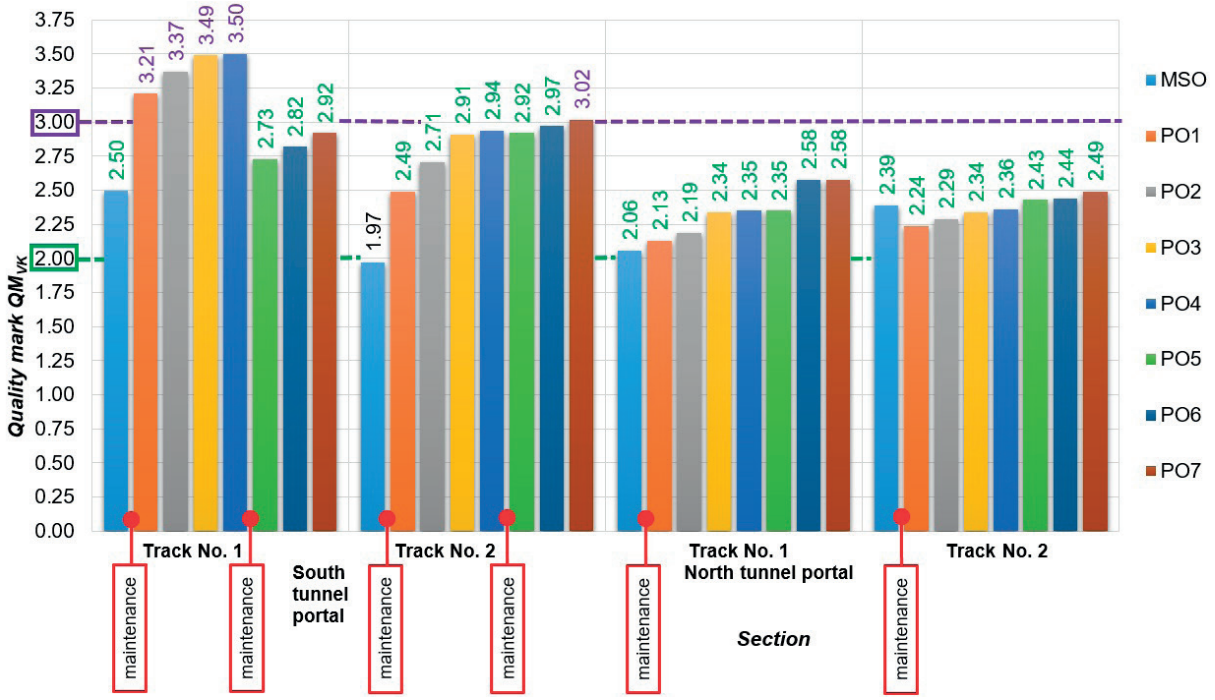

Fig. 6 Quality marks of geometric quantity rail top level of the right rail in respective monitored sections - measurement carried out by the measuring trolley KRAB™-Light

satisfactory) in the section 1.1 or to $2 < QM \leq 3$ in the section 2.1. In PO7 measurement, slight deterioration of QM_{SK} in the section 1.1 was found out placing it to the interval $2 < QM \leq 3$.

The quality marks of rail gauge tolerance QM_{RK} in all the sections and measurements are in the interval of values $0 < QM \leq 2$, which indicates that the state of track geometry is satisfactory (Fig. 4). Higher values of quality marks QM_{RK} in the sections 1.1 and 2.1 result from higher share of ballasted track sections compared to the sections 1.2 and 2.2 with prevailing better quality ballastless track (also securing higher durability of rail position). The values of QM_{RK} obtained by monitoring carried out during operation (measurements PO1 to PO7) present the rail gauge as a parameter with permanently satisfying quality development.

The quality marks of superelevation QM_{PK} are in the interval of values $0 < QM \leq 2$ in all the sections and $2 < QM \leq 3$ in measurements PO2, PO3, PO4 and PO7 in the section 1.1. After repair interventions (after PO4 measurement) the values moved into the interval $0 < QM \leq 2$. The trend of quality increase in this section proven by measurements PO5 and PO6, is indicated as stopped by measurement PO7: the quality mark QM_{PK} is in the interval $2 < QM \leq 3$ (Fig. 5).

The quality mark with the worst development according to the measurements carried out so far seems to be the quality mark of the top level of the right (after calculation also of the left) rail QM_{VK} (Fig. 6).

The errors of the parameter of the top level of rails are the most frequently occurring defects, which is also confirmed by evaluation of measurements by the track recording car of ZSR. With the exception of measurement MSO in the section 2.1, in all the measurements of monitored sections the determined values were $2 < QM \leq 3$ and in the measurements PO1, PO2, PO3 and PO4 in the section 1.1 the values were $3 < QM < 4$ which indicates the necessity to carry out the repair of track geometry until the nearest inspection. By the repair intervention carried out in sections 1.1 and 2.1, before measurement PO5, the values of QM_{VK} decreased. The measurements PO5 and PO6 placed these values into the interval $2 < QM \leq 3$. In the measurement PO7 QM_{VK} reached values in the interval $3 < QM < 4$, in the section 2.1. The tendency of quality mark deterioration in the section 1.1 predicts the determination of QM_{VK} value within the interval $2 < QM \leq 3$ in the near future.

Within PO1, PO2, PO3 and PO4 measurements, further continuous quality deterioration of sections 1.1. and 2.1 was determined, as indicated by the overall quality number. The repair interventions, carried out in November 2014 by the railway infrastructure manager with the aim to remove the local errors of the parameter *VK* (top level of rail) as a priority, decreased significantly the values of quality numbers of respective sections, from the value 2.36 (PO4 measurement) to the value 1.31 (PO5) in the section 1.1 and from the value 1.86 (PO4) to the value 1.59 (PO5) in the section 2.1. The tendency of results of measurements PO5, PO6 and PO7 indicates certain increase and thus quality deterioration of sections 1.1 and 2.1. In the sections 1.2 and 2.2, the quality deterioration (*QN* increase) is slight only.

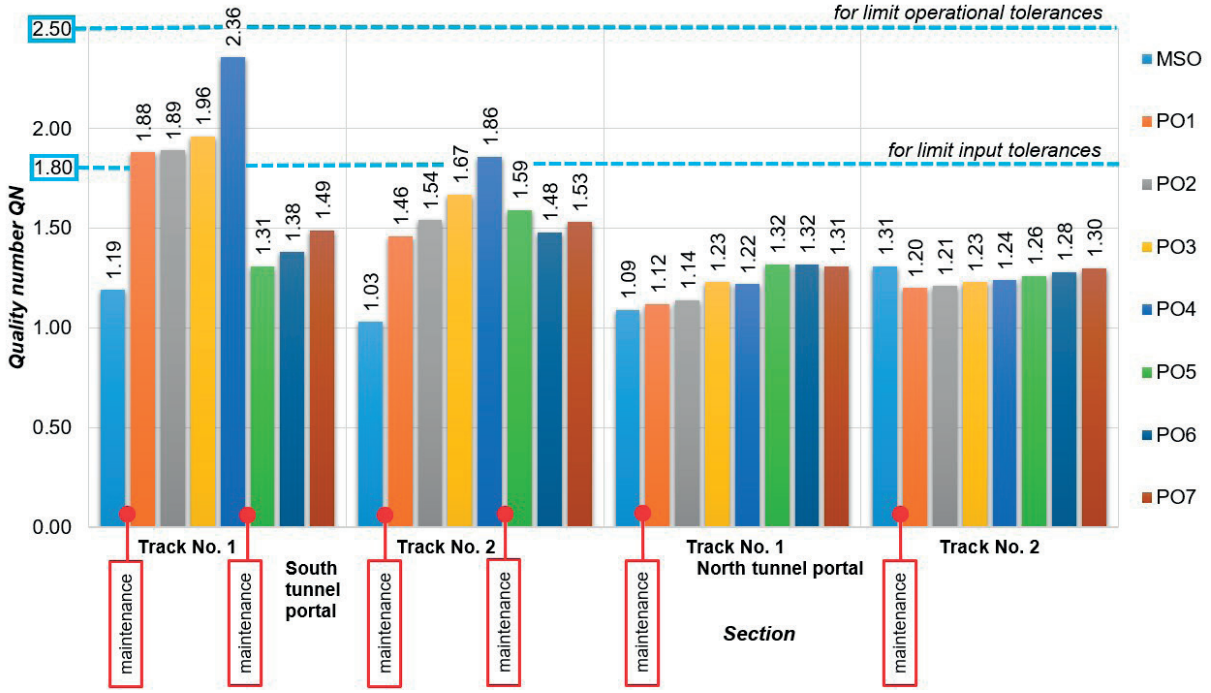

Fig. 7 Overall quality number in respective monitored sections – measurement carried out by measuring trolley KRAB™-Light

3. Development predictions of structural behavior

The development prediction of structural behavior of the structure as a whole is related to transition areas from the ballastless structure to the ballasted structure as these sections are on the basis of long-term observations considered the most problematic ones. The development monitoring was carried out on the basis of data obtained by the complex continuous method by the measuring trolley *KRAB™-Light*. The quality marks reaching the highest values since the first measurement are the quality marks of the selected geometric quantity – top level of the right rail. On the basis of measured data, there were prepared graphs of tolerances of top level of the right (Fig. 8) and left (Fig. 9) rail in the transition area 1.1. The respective transition area (rail 1 of the south portal) is the most problematic one from the point of view of maintenance, error incidence and reached quality marks. However, it is necessary to mention here that after implementation of repair intervention before the fifth operational measurement, there were recorded slightly higher values of quality marks for top level of right rail in the adjacent rail (section 2.1). It is probably related to the lower quality of repair intervention implementation in the rail no. 2.

The tolerances of the top level of the right (after calculation also of the left) rail in the transition area of the section 1.1 (Figs. 8 and 9) detect the parameter errors on the level of exceeded operational tolerance defined by values ± 6 mm in the fourth operational measurement for the right rail, or in the third and fourth operational measurement (upper limit + 6 mm) and in the second and fourth operational measurement (lower limit – 6 mm) for the left rail. The parameter error on the level of exceeded operational tolerance can be confirmed by errors detected by the measuring car of ZSR in individual measurements carried out within regular measurements in compliance with regulations for rail diagnostics. The completed repair of the track geometry in the transition area decreased the tolerance values but the places with limit tolerance values remained the same (contact of transition area with ballastless track and the start of the ballasteless track structure).

In the adjacent rail (section 2.1), errors of the parameters *VP*, *VL* on the level of exceeded operational tolerance were not recorded, but the manager carried out a repair intervention in the same time in both rails. The repair intervention carried out in the transition area of the rail no. 2 did not improve the values of parameter tolerances in any way, only a displacement of irregularities and places with reached limit values occurred here. This can also be confirmed by the development of quality marks of considered geometric quantity – top level of the right (after calculation also the left) rail (Fig. 6), where, unlike in the rail no.1, the values of quality marks did not significantly improve after repair interventions.

From the point of view of further quality development and subsequent maintenance planning, there was observed a tendency of development of maximum tolerances of both rails (Figs. 10 and 11) with the prediction of reaching the tolerance of the top level of

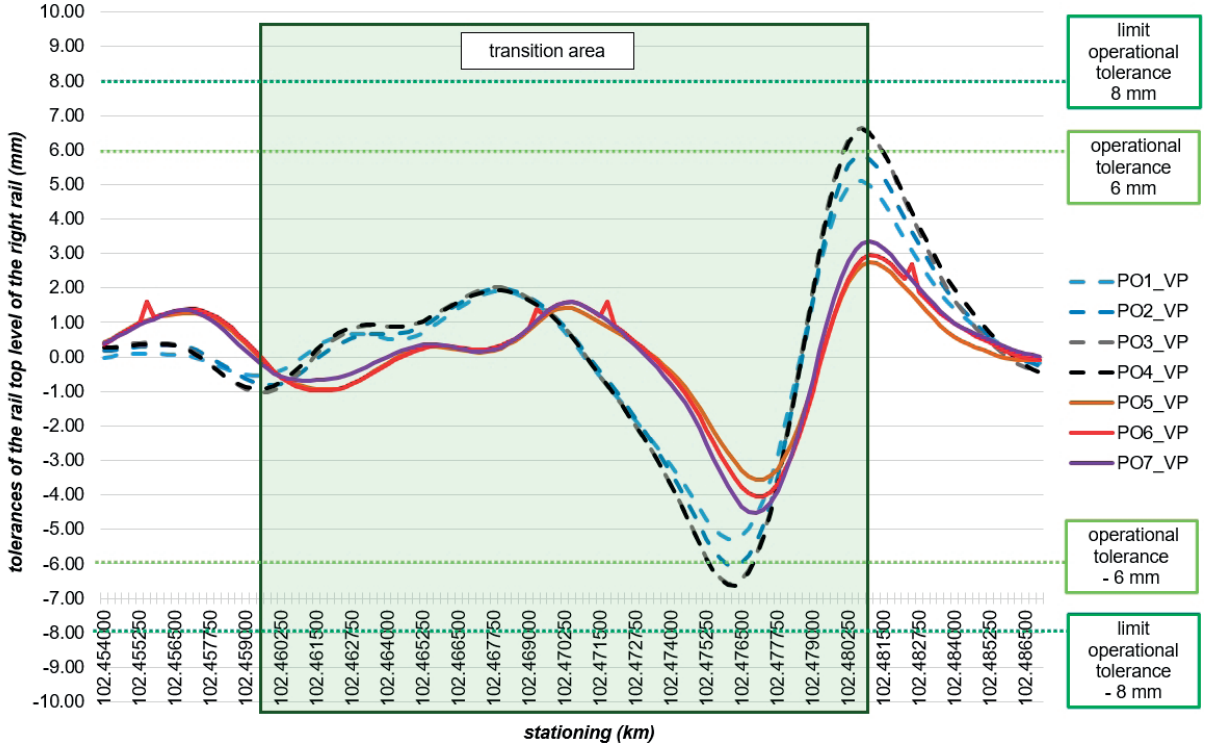

Fig. 8 Tolerance of the top level of the right rail in the transition area of the section 1.1 (km 102.460 500 - km 102.480 500)

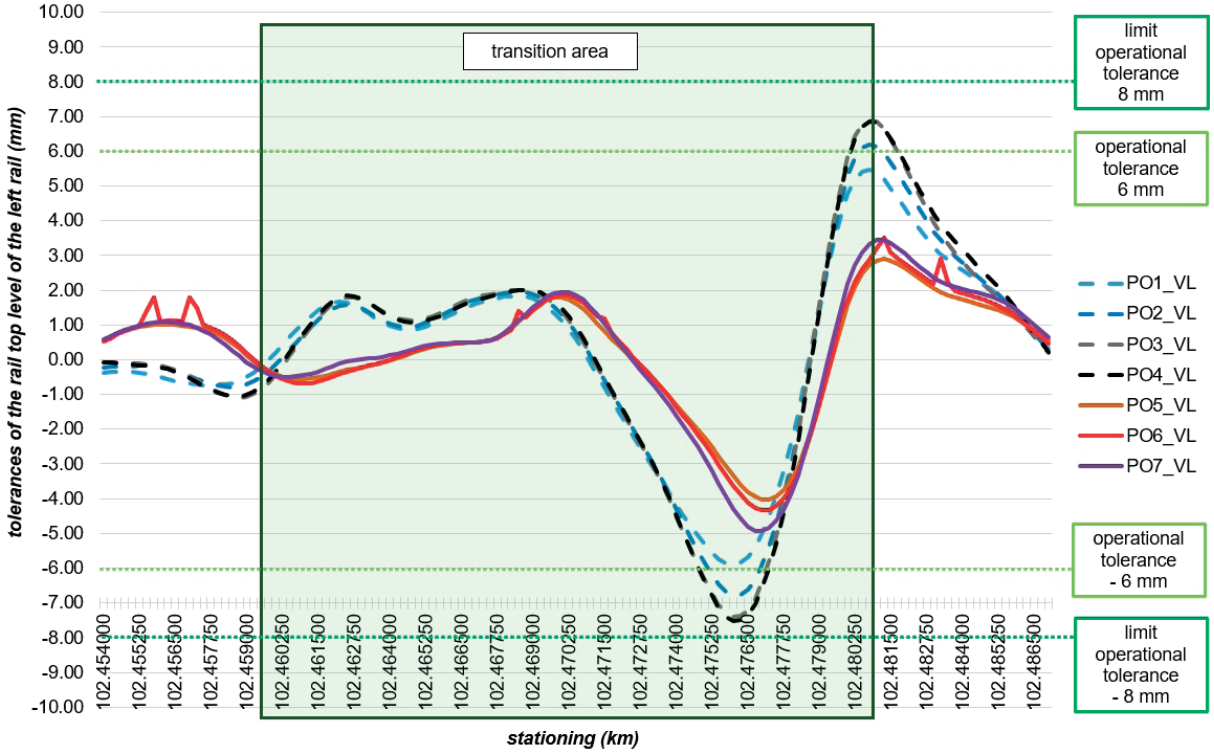

Fig. 9 Tolerance of the top level of the left rail in the transition area of the section 1.1 (km 102.460 500 - km 102.480 500)

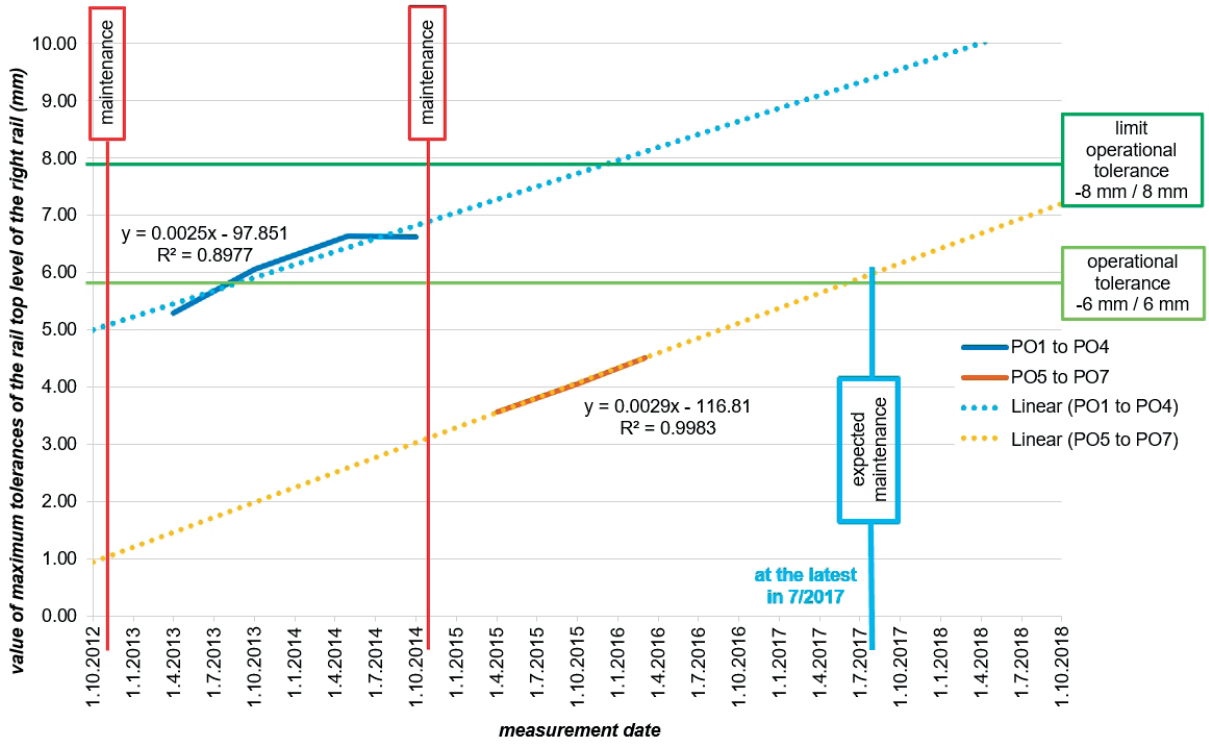

Fig. 10 Measurements PO1 to PO7 and the developmental tendency of maximum tolerances of the right rail in the transition area of the section 1.1 and its vicinity (km 102.454 000 - km 102.487 000)

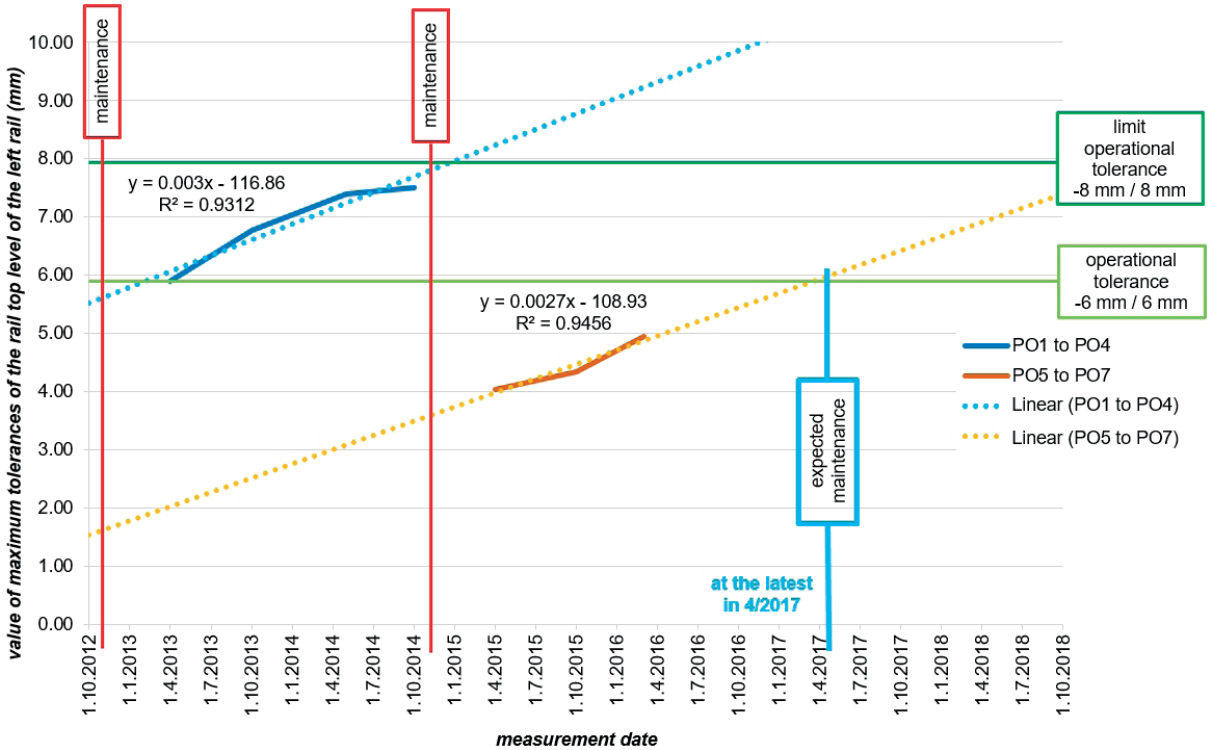

Fig. 11 Measurements PO1 to PO7 and the developmental tendency of maximum tolerances of the left rail in the transition area of the section 1.1 and its vicinity (km 102.454 000 - km 102.487 000)

the right (left) rail on the level of exceeded operational tolerance. The developmental tendency shows that the absolute value of maximum tolerance of the top level of right rail will reach the level of operational tolerance at the latest in July 2017, the absolute value of the maximum tolerance of top level of left rail will reach the level of operational tolerance probably earlier – at the latest in April 2017, and these levels of exceeded operational tolerances should be detected within the second measuring campaign of the measuring car ZSR (in summer 2017). After detection of these tolerances, the infrastructure manager is supposed to plan and, as soon as possible, also to carry out the repair of track geometry in the respective section.

4. Conclusion

The structural parts and parameters of track geometry in the time of operation show signs of quality deterioration. Its monitoring and recording in the experimental section has been carried out for five years. At present the measurements confirm the significant quality deterioration in the transition areas of sections 1.1 and 2.1. The implementation of repair intervention after measurement PO4 caused certain improvement, but later there was again recorded further quality number (*QN)* deterioration – especially by decreasing quality of parameter *VK* (the top level of the rail). With the exception of the parameter *RK* (rail gauge), all the other monitored parameters of track geometry of the experimental section contribute to the quality number deterioration by their continuous degradation. The described tendency of quality decrease is expected in the further periods of operation of respective sections. The repair will be feasible only by repair interventions of track geometry carried out as soon as possible after the error detection but no later than the nearest inspection of the track state.

With regard to quality number, the sections 1.2 and 2.2 seem to be sections with slightly deteriorated quality which can be explained by the quality change of operated railway track with mixed train operation. Considering the quality development in the previous monitoring period, there is supposed a permanent decrease of construction quality, provided the operation is without any extraordinary operational events. The improvement of structural quality will be carried out by repair of track geometry as a part of the repair work plan.

Acknowledgement

The paper contains partial results of the grant project VEGA 1/0597/14 "Analysis of methods used to measure the unconventional railway track construction from the point of view of accuracy and reliability".

References

[1] IZVOLT, L., SESTAKOVA, J., SMALO, M.: *Railway Engineering 2: Diagnostics, Mechanisation and Track Works Technology on Railway Track* (in Slovak), EDIS : University of Zilina, 2015, ISBN 978-80-5541-169-9.

[2] IZVOLT, L., SESTAKOVA, J., SMALO, M., GOCALOVA, Z.: Monitoring of the Track Geometry Quality around the Portals of new Tunnel Construction Turecky vrch – Preliminary Result, *Communications - Scientific Letters of the University of Zilina,* vol. 16, No. 4, 2014, 9-20, ISSN 1335-4205.

[3] IZVOLT, L., SESTAKOVA, J., SMALO, M.: Monitoring of the Track Alignment and Track Geometry Parameters of Ballastless Track Sections and Transition Areas in Vicinity of Portals of Turecky Vrch Tunnel (in Slovak), *NTT: New Railway Trends - Transport - Telematics,* vol. 24, No. 3, 2016, 12-16, ISSN 1210-3942.

[4] SESTAKOVA, J., GOCALOVA, Z.: *Comparison of Results of Geometrical Position of the Track Diagnostics – Spot and Continuous Measurement,* Procedia Engineering [electronic source] : XXIII R-S-P seminar: Theoretical Foundation of Civil Engineering: ISSN 1877-7058 : vol. 91, 2014, online, p. 447-452 : http://ac.els-cdn.com. /S1877705814030410/1-s2.0-S1877705814030410-main.pdf?_tid=7ac2c2f8-c709-11e4 -aaf7-00000aab0f6b&acdnat=1425980605_3c52ef455ea61af04fe1b951e4d82550.

[5] SESTAKOVA, J.: Quality of Slab Track Construction - Track Alignment Design and Track Geometry, *Civil and Environmental Engineering* [electronic source]: De Gruyter Open: vol. 11, No. 1, 2015, ISSN: 1336-5835, online, pp. 2-9: http://www.degruyter.com/dg/viewarticle.fullcontentlink:pdfeventlink/$002fj$002fcee.2015.11.issue-1$002fcee-2015-0001$002fcee-2015-0001.pdf?format=INT&t:ac=j$002fc ee.2015.11.issue-1$002fcee-2015-0001$002fcee-2015-0001.xml.

[6] IZVOLT, L. et al.: *Monitoring of Sections of a Non-conventional Construction of the Railway Superstructure and the Transition Areas - 7st and 8st Stage*. ZSR Modernization of Railway Track Nove Mesto nad Vahom - Puchov, km 100.500 to 159.100, part 24-32-01 Nove Mesto - Trencianske Bohuslavice (in Slovak), Zilina: KZSaTH: SvF: University of Zilina, 12/2015.

[7] STN 73 6360 (1999) *Track Alignment Design and Track Geometry of Normal-Gauge Tracks* (in Slovak), SUTN Bratislava and Amendment 1 (2002), SUTN Bratislava.

[8] ZSR SR 103-7 (S) *Measurement and Evaluation of Track Geometry by Measuring Trolley KRAB* (in Slovak), GR ZSR, 2008.

[9] STN 73 6360-1 (2015) *Railway Applications. Track. Part 1: Geometrical Position Arrangement of 1 435 mm Gauge Railways* (in Slovak), SUTN Bratislava.

[10] SMALO, M., IZVOLT, L.: Assessment of Track Quality in Trial Test Sections by Spot and Continuous Method, *Communications - Scientific Letters of the University of Zilina,* vol. 17, No. 4, 2015, ISSN 1335-4205.

https://doi.org/10.26552/com.C.2016.4.30-36

Antonin Lupisek - Martin Volf - Petr Hejtmanek - Katerina Sojkova - Jan Tywoniak - Peter Op't Veld*

INTRODUCTION OF A METHODOLOGY FOR DEEP ENERGY RETROFITTING OF POST-WAR RESIDENTIAL BUILDINGS IN CENTRAL EUROPE TO ZERO ENERGY LEVEL

Buildings are responsible for 35% of greenhouse gas emissions released in Europe. The highest potential for reduction of the environmental impacts is in the existing buildings' energy efficiency improvement. The paper introduces a development of new methodology for a rapid deep energy retrofitting of existing buildings applicable to residential housing stock in Central Europe. It briefly describes the steps from production of building information model of existing building to complete renovation. It presents experience from pre-production phases on a case study from the Czech Republic. Technical and non-technical barriers to be solved in the near future are summarised in the discussion.

Keyword: *Deep energy retrofitting, zero energy buildings, energy efficiency, residential buildings, renovation strategy.*

1. Introduction

The European Union aims at the goal of erecting only near-to-zero operation energy level buildings after 2020; according to further-going Roadmap for moving to a competitive low carbon economy in 2050 [1], the European Council also sets the goal of 80 to 95% cuts in emissions by 2050.

The building sector is one of the main energy consumers and emission polluters; about 40% of overall EU energy consumption together with about 35% of overall CO_2 emissions release is attributed to buildings [2]. The construction industry is pushed tough for the highest possible energy and emission cuts. At least 3% of renovations yearly must comply with the low energy level to reach the EU's energy targets.

In the Czech Republic – as in any European country with long history – the building stock consists nowadays of rather old buildings. Most of dwellings have been built after World War II, when the demand for new building soared. Today, these buildings still present the largest group among all dwellings (see Fig. 1). To reach the environmental goals in the foreseen future, it is needed not only to build up the low energy buildings, but also to focus on the energy and emission cuts in the existing building stock.

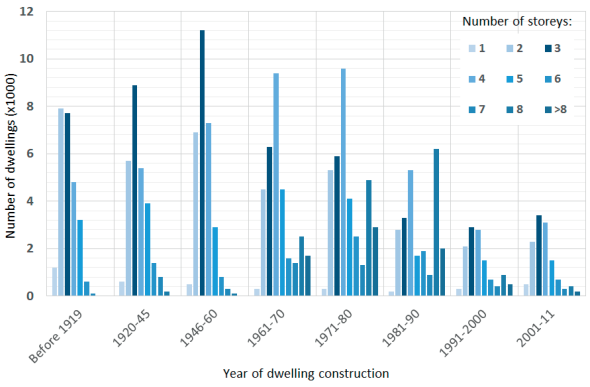

Fig. 1 Building stock in the Czech Republic (with former Czechoslovakia) [3]

For example, the recent requirements for the thermal resistance (or thermal transmittance) of the buildings' envelopes are driving the new construction automatically to a more sustainable operation of the buildings. The older building designs had to fulfil much less strict requirements, sometimes no limits for the energy performance were set in their year of construction. Figure 2 illustrates the development of the requirement for the mean U-value of building's exterior wall with openings in relation to various fenestration ratios. Just the operational energy cuts are definitely not the only goals that can be achieved to reach by

* [1]Antonin Lupisek, [1]Martin Volf, [1]Petr Hejtmanek, [1]Katerina Sojkova, [2]Jan Tywoniak, [3]Peter Op't Veld
[1]University Centre for Energy Efficient Buildings, Czech Technical University in Prague,Czech Republic
[2]Faculty of Civil Engineering, Czech Technical University in Prague, Czech Republic
[3]Huygen Installatie Adviseurs, Maastricht, Netherlands
E-mail: antonin.lupisek@cvut.cz

a refurbishment, but enhanced comfort level and higher quality of the indoor environment is usually expected these days. Many related parameters are required also by legislation. Summary of legal requirements was published in [4]. It can be though assumed that a simple refurbishment to the recently required quality level can bring significant savings and major quality improvement.

Although the straightforward idea, it means a very complex refurbishment process. To investigate the possibilities of energy saving renovations in the Czech Republic, the most frequent dwelling was chosen as a pilot building. Moreover, the refurbishment process was led to make more significant progress: the renovated building should reach nearly zero operation energy level in the same way like the newly-built houses after 2020.

The described situation is a starting point for a European project MORE-CONNECT under H2020 [5] which tries to solve the problem of complex renovations of existing residential buildings by developing prefabricated multifunctional renovation elements for the total building envelope (façade and roof) and installations and building services.

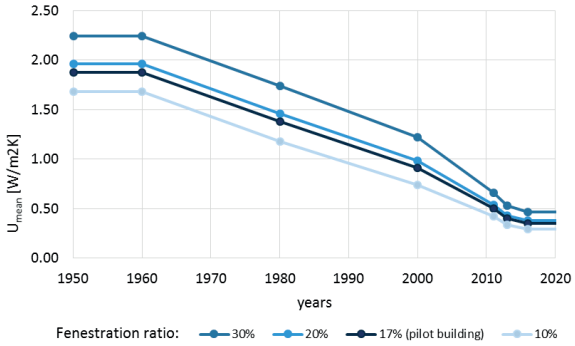

Fig. 2 The decrease of mean thermal transmittance (mean U-value) since 1950 for residential buildings for various fenestration ratios.

Objectives

The objectives of the design renovation process are based on a MORE-CONNECT project prerequisite that the energy consumption of a subject building has to be reduced from its actual level to net-zero level and the time needed for complex renovation of a block of flats shall not take more than 2 weeks (assembly on site). At the same moment there is a requirement for reduced negative environmental impacts, especially amount of embodied carbon dioxide equivalents.

The objectives of present paper are to introduce a novel renovation methodology designed in the project for post-war Central-European residential housing and to present an experience with application of the process from its beginning to pre-production phase.

2. Methods

The methodology comprises the following steps:

- Assessment of the actual condition of the existing building and its operation;
- Production of detailed building information model (BIM);
- Analysis of today's energy performance;
- Definition of clients' needs;
- Design of technical improvements;
- Energy simulation of building after implementation of designed energy-saving and energy production measures;
- Draft plan and time schedule of construction process;
- Design of planned measures in BIM;
- (Semi-) automated production of modular elements;
- Transportation on site;
- Dismantling of old structures and preparation for installation of new elements;
- Assembly of new elements;
- Quality control;
- Commissioning and handover of finished renovation;
- Monitoring.

The steps of the proposed methodology are closely described in the following sections.

Assessment of the actual condition of the existing building and its operation

Each building is a unique exemplary and has to be carefully probed. After the inception of the renovation process and general agreement with the investor, the first onsite inspection takes place. The main objective of this step is to collect the basic information about the building in question, but also to compare it with other similar buildings.

Production of detailed building information model from a point cloud obtained by scanning

The next step is to create an information model of the building. The model has to be detailed and accurate enough to enable export of information needed for energy simulations of the present state, for design and planning of the technical improvements and for pre-production modelling of each element.

For this task are usable several methods; the most suitable are laser scanning or photogrammetry. These techniques are provided by professional surveyors and the raw output is usually a digital map of the building in form of point cloud. To enable use of the obtained data for simulations and modelling the point-cloud, it has to be converted into a vector format, which can be to a high degree done automatically, but still usually some additional manual corrections of data are required. Additionally, information on building structures, used materials and basic properties of elements (such as windows, doors etc.) are added into the information model.

Energy analysis of present building

In this step the information model is used for compilation of a simplified parametric representation of building's envelope. It is then combined with the information on building volume, the use patterns of whole building and individual apartments, data on number of buildings' occupants, data on historic energy consumption, local boundary conditions and localised climate data to generate a simplified energy calculation of building's primary energy demand.

Definition of clients' needs

In the next step the investor of the renovation is briefed about the results of the energy analysis and is guided through a list of choices of energy improvement of the building with the aim of defining potential variant sets of modules that can be added to the building to improve its usability, comfort, indoor environment and to reduce the energy demand of the building.

Design of technical improvements and energy simulation of building after implementation of designed energy-saving and energy production measures

Based on the interaction with the client, the technical variants are designed into detail using sets of modules that combined together form comprehensive renovation packages, which are modelled in BIM. Energy performance of each of the variant renovation packages is simulated and the results are together with visualisations, detailed descriptions and cost estimations conveyed to the investor in order to get a decision on choice.

Draft plan and time schedule of production and construction process

After selection of the renovation package, the whole production and construction process is planned into detail. The planning comprises design of all modules, their prefabrication and transportation to the construction site (just in time for assembly), preparation of the construction site, dismantling of old structures, installation of new components and assemblies, finalisation, quality control and final handover of finalised renovation to the investor.

Pre-production design of modules in BIM

Based on the selection of design variants by the investor, each module will be designed in BIM, which will automatically produce a bill of quantities and list of environmental impacts and embodied primary energy. The data will be transferred to the production facilities.

(Semi-) automated production of modular elements and transportation

Based on the BIM data, each element will be produced on semi- or full-automated production line, packed, labelled and then just in time sent to the construction site for assembly.

Dismantling of old structures, site preparation and assembly of new elements

The construction site preparation of a typical residential building includes preparation of the construction site by installation of dust and dirt protection and packaging of furniture, and handover of each flat, removing obsolete building components (windows, doors, roof elements or whole roof, building services, old pipes and wiring) and installation of anchors for new modules. The preparatory works are followed by a continuous assembly of the new external modules accompanied by connection of the internal installation and finished by cladding of roof elements and building integrated renewable energy sources.

Quality control, commissioning and handover of finished renovation

Depending on the variant, the finished installation of the renovation packages undergoes a standardised set of quality checks and commissioning of new building elements and technical systems. Each step is protocolled within the BIM, which is at the end of the process handed over to the building owner and can be used for facility management.

Monitoring

Higher levels of renovation packages include detailed set of sensors for complete monitoring of the regular operation of the building and preventive warning system which automatically sends alert messages in case of non- standard operational state occurrence.

3. Results

The proposed methodology was tested by project partners on several buildings representing the target buildings' typologies over Europe. The following sections present the experience from the practical application of the methodology on pilot building in the Czech Republic.

Fig. 3 The view of the pilot building in Milevsko in its present state

Assessment of the actual condition of the existing building and its operation

The pilot building for the Central-European geo-cluster is a masonry residential house with a lateral load bearing system from 1950's in Milevsko (Fig. 3); the house is used as social housing. The building has a simple, rectangular floor plan, and a hip roof. It has three floors with 24, similarly designed flats used with area of approx. 30 m^2. The house has a usable floor area 995.3 m^2 and energy related area 1107.3 m^2. The fenestration ratio is 17.2%. Typical floor height is 2.5 m, each apartment has floor area of 35 m^2. The building has a pitched wooden roof structure with ceramic tiles (33°) and is partly provided with cellars.

A reconnaissance to describe the weaknesses of the building was done. A number of problems was observed, such as an old-fashioned appearance of the house and devastated common areas, or the ruptures in the plaster. From the perspective of energy consumption, the original wooden windows' insulation level was considered insufficient, the users experienced winter overheating by dysfunctional control of heating system. An insufficient ventilation rates probably cause a mould growth in the basement floor, the leaking water-proofing amplifies the problem.

The deep renovation process has to take into account the causes of these problems. The overall energy performance of the building is planned to be improved, the poorly functional elements will be replaced and the failures fixed. The final design process is led up to solve the problems in the same time of one fast refurbishment.

Production of detailed building information model from a point cloud obtained by scanning

The age and original construction technology does not allow the simplification of the buildings' geometry, the facade cannot be assumed plain. To ensure the sufficient speed of renovation process, the 3D scanning or a digital photogrammetry is used as a basis for the building information model (BIM) development.

The comparative study was performed to show the possibilities of both technologies – see Fig. 4 [6]. Generally, both methods are convenient. Digital photogrammetry appears to be less demanding to perform in praxis, but not all cameras are precise enough.

The studies also showed the need for further development - the link between point cloud to a BIM model appears to be cumbersome; the current tools need large amount of human's support to deliver sufficient outputs for further production.

Energy analysis of present building

A preliminary analysis was performed to show the possibilities of the deep energy retrofit. The present state was modelled as a reference level. Building's mean *U*-value is 1.18 W/(m^2K)

a)

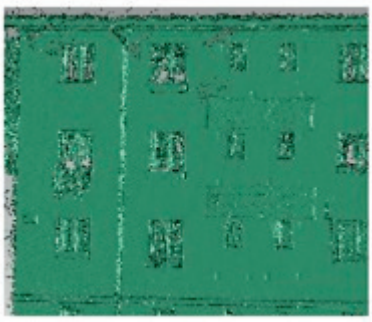

b)

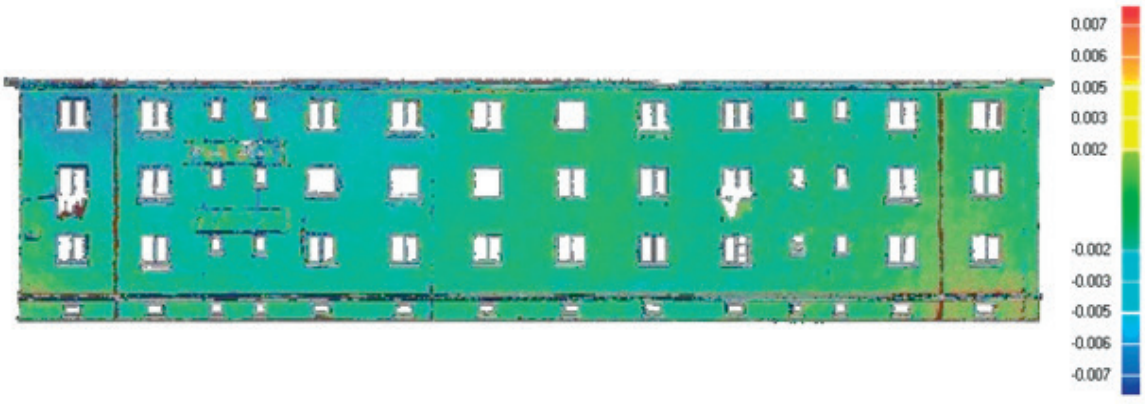

c)

Fig. 4 The best in-comparison performing digital camera's (Pentax 645D) outcomes: a) original picture, b) a point cloud, c) accuracy of the final model (in metres) [6]

which significantly exceeds the required value of 0.51 W/(m^{2}K). The total heat transfer coefficient reaches 2037 W/K. The total energy need for heating is 186 MWh, which corresponds to 168 kWh/(m^{2}a). The building is connected to district heating system and equipped with traditional heating bodies. Total calculated delivered energy is 291 MWh (263 kWh/(m^{2}a)), annual consumption of non-renewable primary energy reaches 309 MWh (279 kWh/(m^{2}a) respectively).

Definition of clients' needs

Other step was to describe and fulfil the possible users' requirements as broadly as possible. The already finished refurbishment projects were considered together with the possible business plans. The investors can choose from many optional features to improve their building in number of combinations. To enable variability in the renovation offering, the three scenarios were set, all aiming at the zero primary energy building (ZEB) level:

a) *Low-cost but complex ZEB renovation* – economically the least demanding scenario; the building will reach ZEB level by refurbishment at minimum cost. This scenario contains no additional lofts or extra balconies, the technologies are designed at minimal needed level. A ventilation system with heat recovery, equitherm control system and an integrated photovoltaic system are installed.

b) *Economic extension and renovation* – ZEB refurbishment creates extra flats, the income from their sale partly covers the renovation cost. This scenario contains a new roof structure, roofing, individual room control system (user can control indoor climate separately for each room).

c) *High-tech renovation (see Fig. 5)* – this scenario tends to accommodate the best available technologies; the additional apartments in the duplex apartments are created (again to cover the refurbishment expenses), a new roof structure is created, and a model predictive control system (to adjust the operational control of the building by data obtained in real-time simulation in the mathematical model) will be installed. The flats may be provided with additional balconies or additional rooms. The new structures contain a vacuum insulation panels to provide a high insulation level (U = 0.11 W/(m^2.K)). To the basic scenario is added a new wiring for cable TV or Internet routers to provide the user with all technologies at once and improve the standard of the building.

Fig. 5 The visualisation of the refurbished building – the high-tech scenario.

The elements designed for various scenarios can be used in arbitrary combinations.

Design of technical improvements and energy simulation of building after implementation of designed energy-saving and energy production measures

Three variants of energy improvement levels were developed:

1. Variant complying Czech nearly zero energy definition [7];
2. Variant leading to 80% reduction of primary energy use for space heating, ventilation, domestic hot water, pumps and other auxiliary energy;
3. ZEB level, i.e. the net primary energy use on annual basis is zero kWh/(m^2 a), covering the same extent of needs as in the previous variant.

For each of the variants, combination of range of U-values with various kinds of energy sources supplemented with PV and/or solar thermal panels were considered within energy calculations to reach given (primary) energy consumption targets. Driven by the results of variant calculations, prerequisite basic level of *U*-values was set as follows: U_{walls} = 0.14 W/(m2K), $U_{ceiling/roof}$ = 0.10 W/(m2K), U_{floor} = 0.32 , $U_{windows}$ = 0.7 W/(m2K), solar thermal transmittance of windows g = 0.5. These values were used for the *Low-cost but complex ZEB renovation* and *Economic extension and renovation* scenarios. For *High-Tech renovation* scenario U_{walls} = 0.11 W/(m2K) was assumed. Based on calculation of the heat loss of individual flats, considering given parameters of building envelope, warm air heating system with heating recovery has proved to be sufficient apart from the most unfavourable flat at *Economic extension and renovation* and *High-Tech renovation* scenarios where supplementary heating would be needed during the coldest days. After retrofit, mean U-value = 0.23 W/(m2K) and calculated energy demand for heating at Low-Cost variant (geometry without changes) decreased to 24 kWh/(m2a). Delivered total energy dropped to 67 kWh/(m2a) or 80 kWh/(m2a) for district heating and pellet boiler respectively. To achieve that level 254 m^2 or 120 m^2 of PV would be needed to reach ZEB level considering district heating or pellet boiler respectively.

Pre-production design of modules

The main design objectives were set before: the ZEB level of refurbishment, complex renovation process and high speed of retrofit process. Namely, the last objective pushes the design to prefabrication and additive technology; the original structure mostly remains and the new elements are added during the retrofit. A modular system was chosen as the most feasible solution. Apart

from the most frequent standard wall and roof modules, the pre-production showed the need of auxiliary modules: roof extension, corner, entrance or gable modules etc. – see example of a division of building envelope into modules in Fig. 6.

The CAD and 3D BIM model was used to illustrate all the technologies in the modules. The virtual design process pointed out the problematic details in the structure and missing or non-complying elements. These need to be designed or adjusted to its final form to fit in the system. On the other hand, every newly designed element creates new expenses and must be though further optimised.

Fig. 6 An example of building envelope's division into retrofit modules

The production phases will be subject of further research in the MORE-CONNECT project.

4. Discussion

During the work on the Czech projects were identified various non-technical and technical barriers that limit the applicability of the proposed approach.

Non-technical barriers

Some of buildings' owners are mentally locked in the typical scenario of step-by-step renovations, which includes at some point replacement of old obsolete windows (usually for new low-cost double-glazed with plastic frames) and then later on installation of an external thermal insulation composite system (ETICS). Independently on the previous steps roof covering gets replaced when needed. The problem is that the owners of buildings are usually not well informed about all available options for advanced retrofitting enabling rapid installation (and thus reducing the negative effects of construction); improvement of the indoor environment by installation of mechanical ventilation system with heat recovery, controlled by CO_2 concentrations; new installations of cabling for data networks and TV; possible addition of new balconies; integration of shading devices; and building integrated solar systems.

Another type of barrier is represented by the economic feasibility of complex renovation. The feasibility parameters are strongly dependent on the socio-economic situation of the tenants and their willingness or even possibilities to pay extra for improved standard of living. The barrier can be mitigated by seeking for additional sources of finance, which can come for instance from adding new flats for rent or sale in roof extension of the building.

Technical barriers

One group of technical barriers depends on the potential for rapid development of production technologies in the near future. For example, at the moment a manual polishing of data is still needed in the process of scanning of building envelopes and conversion of point-cloud data to BIM, but it is expected that this step soon becomes automated. Another leap forward is needed to enable to connect the building information modelling phase more tightly with the production phase. At the same moment the obsolete manual production of prefabricated elements is due for replacement by highly flexible automated production lines, which will represent a significant shift in construction practice (as drafted for instance in [8]).

Another group of technical barriers is represented by limitations resulting from the parameters of the existing building. For instance, there is limit for the thickness of the additional external thermal insulation layer imposed by the dimensions of windows and related requirements on indoor daylight factors. It can be solved with help of superinsulation (as shown for instance in solutions developed in [9 and 10]), but with a significant improvement of project cost. Another restriction by dimensions is for new ventilation ducts, wiring, piping or even new boilers and heat storage tanks. Some of the installations can be led directly in the facade modules (leading in some cases to need of superinsulation due to limited space in the facade thickness) or in new building extensions dedicated to these installations. Building extensions can be in some cases used also for installation of new energy sources.

5. Conclusions and future work

The up to date usual step-by-step partial renovations of buildings do not represent a systemic solution to achieve nearly-zero and zero primary energy levels. With the advancing climate change a rapid renovation action is needed. Modular retrofitting with use of prefabricated elements might not be suitable for all existing buildings, but there is a significant portion of building stock, for which this approach is advantageous. As shown on the pilot building, the described methodology offers several scenarios of renovation, each of them utilising set of prefabricated modules that can be variably combined to offer a broad variety of options to the potential investors. Such approach to deep energy

retrofitting generally seems to be viable, however, there are still some challenges in process waiting to be solved. While the 3D scanning and use of its outcomes for modelling seems to be manageable, the main challenge will be in close interconnection of the pre-production and the production phases. Also some non-technical challenges still wait to be tackled.

The complete design and production process will be further validated and improved during the remaining time of the MORE-CONNECT project duration and it is expected to be proven on real retrofitting projects in partnership with a selected municipality owning suitable buildings.

Acknowledgements

The project MORE-CONNECT has received funding from the European Union's H2020 framework programme for research and innovation under grant agreement no 633477. This work has been supported by the Ministry of Education, Youth and Sports of the Czech Republic within National Sustainability Programme I, project No. LO1605.

References

[1] European Commission: A Roadmap for Moving to a Competitive Low Carbon Economy in 2050, 2011.
[2] Directive 2010/31/EU of the European parliament and of the council of 19 May 2010 on the energy performance of buildings
[3] ANTONIN, J.: *Housing Stock and Energy Savings Possibilities Survey.* Prague : Czech Green Building Council; 2014.
[4] KALAMES, T. et al.: *What Kind of Requirements nZEB and Deep Renovation Sets for Building Envelope?* Proc. of Central Europe towards Sustainable Building 2016, Prague : Czech Technical University, 2016; in print
[5] MORE-CONNECT: Concept and Approach [online]. 2016 [cit. 2016-05-30]. Available from: http://www.more-connect.eu/the-project/concept-and-approach/
[6] MATOUSKOVA, E., FALTYNOVA, M.: *Advanced Geomatics for Modular Building Reconstruction* (MORE-CONNECT Deliverable 4.1), Prague, 2016.
[7] Regulation No. 78/2013 Sb. *About Energy Performance of Buildings* (in Czech), Ministry of Industry and Trade of the Czech Republic, 2013.
[8] MICIETA B., BINASOVA, V., HALUSKA, M.: The Approaches of Advanced Industrial Engineering in Next Generation Manufacturing Systems. *Communications. Scientific Letters of the University of Zilina*, vol. 16, No. 3a, 2014, 101-105, ISSN 1335-4205, 2013.
[9] KOBLER, R., L., et al: *Retrofit Module, Design Guide*. EMPA, March 2011. ISBN 978-3-905594-60-7.
[10] TYWONIAK, J., LUPISEK A., BURES, M., VOLF, M.: *Wood Based Curtain Wall for Building Retrofit - Development and Performance.* Proc. of Advanced building skins 2015 Conference, Graz : Graz University of Technology, 2015, 213-218. ISBN 978-3-85125-397-9.

https://doi.org/10.26552/com.C.2016.4.37-43

Dasa Fullova - Daniela Durcanska - Dusan Jandacka - Adriana Estokova*

MASS DISTRIBUTION OF PARTICULATE MATTER PRODUCED DURING ABRASION OF ASPHALT MIXTURES IN LABORATORY

Non-exhaust emissions of particulate matter from road traffic can come from abrasion of vehicle parts (tyres, brake linings, clutch and bodywork) or from pavement surface abrasion and also from resuspension of dust. A differentiation between PM emissions from road pavement abrasion and resuspension is very difficult due to their similar elemental composition. The research is focused on abrasion of pavement surface from asphalt mixtures. Experimental tests are conducted for measuring of particulate matter production in the atmosphere during the rutting of various asphalt mixtures used for wearing courses. The tests are performed in wheel tracking machine in the laboratory. Particle sampling in the laboratory makes it possible to sample PM with very low contamination from surrounding sources and no influence from exhaust emissions. The paper presents an example of the results of measurements on six trial samples of asphalt mixtures with different composition.

Keywords: *Particulate matter (PM), abrasion, wearing courses, laboratory tests, chemical elements.*

1. Introduction

The air is polluted mainly by traffic, industry, agriculture and households. Although the production of emissions has been decreased in recent decades and some of the contaminants have been reduced, the problem is far from solving. These are particularly the two substances - particulate matter (PM) and ground-level ozone, which cause respiratory problems, cardiovascular diseases and reduce life expectancy [1].

Road traffic is one of the main sources of pollution in the vicinity of roads. Particulate matter air pollution can come from combustion or non-combustion processes. Non-combustion emissions of particulate matter can come from abrasion of vehicle tyres, abrasion of brake linings, clutch, and vehicle bodywork, abrasion of pavement surface and also from resuspension of dust (Fig. 1) [2, 3 and 4].

We have decided to deal with non-combustion emissions, especially with the production of particulate matter from abrasion of the pavement surface. This decision is based on information obtained from several foreign and Slovak scientific papers [5 and 6], studies and researches about production of particulate matter from road traffic [7, 8, 9 and 10]. The issue of abraded particulate matter (PM) from pavement surfaces and the contribution of those emissions to air pollution is mostly solved in the Nordic countries [11and 12]. This problem has attracted attention especially in Norway, Finland and Sweden because of the use of studded tyres and winter gritting.

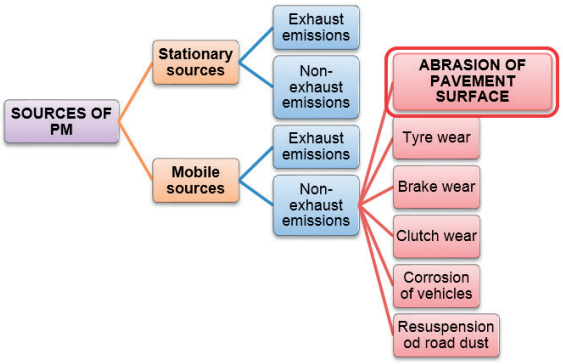

Fig. 1 The separation of particulate matter sources and non-exhaust emissions of mobile sources

It is a very difficult process to identify pavement surface abrasion as a source of particulate matter and separate it from other abrasions and quantify its share of the amount of produced particulate matter directly in the field. One possible way leads through chemical analysis of particulate matter and multivariate statistical analysis. But it is necessary to know which chemical elements this source (pavement surface) can contain and release.

* [1]Dasa Fullova, [1]Daniela Durcanska, [1]Dusan Jandacka, [2]Adriana Estokova
[1]Department of Highway Engineering, Faculty of Civil Engineering, University of Zilina, Slovakia
[2]Technical Institute of Environmental Engineering, Faculty of Civil Engineering, University of Kosice, Slovakia
E-mail: dasa.fullova@fstav.uniza.sk

There are few data about the chemical composition of road surface materials and particulate matter from abrasion of wearing courses available in the literature. Emissions from abrasion of pavement surface are more difficult to quantify separately than emissions from tyre and brake wear.

The task of our research is to monitor the separation of abraded particulate matter from the selected group of samples used for the asphalt wearing courses. An important phase of the research is to determine chemical elements in the collected particulate matter and to confront it with the representation of these elements in the chemical composition of the asphalt mixture. The next step is to attempt to determine the share of the mechanical separation of PM from the pavement by evaluating the chemical composition of the materials used in the studied asphalt mixtures of wearing courses and subsequently collected particulate matter. The research is aimed at finding dependence between the composition of asphalt mixture and collected PM.

An aggregate, asphalt binder, additives, or recycled material are basic materials for the production of different types of asphalt mixtures. The choice of materials and technological procedures for their construction or renovation affects the structural design of pavements. Vehicle motions cause mechanical wearing of the asphalt pavement surface - wearing course by vehicle tyres. That leads to gradual fragmentation and abrasion of aggregate.

2. Methodology of experimental measurements

The resulting abrasion and production of inhalable PM emissions are dependent on a number of factors that are difficult to quantify in real world environments. Therefore, the measurements are performed in the laboratory at the Department of Highway Engineering. Particle sampling in the laboratory makes it possible to sample pure abraded particles with very low contamination from ambient particles. The samples of asphalt mixtures for creation of wearing courses are used for laboratory measurements. The samples are rutted in wheel tracking machine DYNA-TRACK which is used to assess the rutting resistance of asphalt materials under conditions, which simulate the effect of traffic (Fig. 2). The objective of the experimental measurements is to verify the effect of the composition of the asphalt mixture for the production of PM emissions.

Each of the tested samples is specific in its composition - the type of asphalt, the amount of asphalt, the type of aggregate, the different lines of granularity of aggregate. In connection with the material are created samples with different structure of surface, which can ultimately affect abrasion of the samples. Detailed specification of asphalt mixtures is described in the catalog [13].

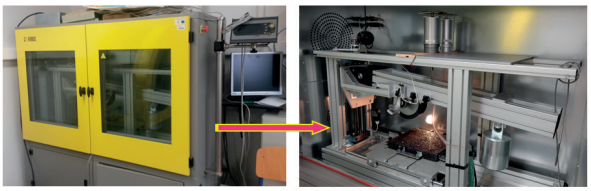

Fig. 2 Wheel tracking machine DYNA-TRACK

The wheel tracking equipment consists of a loaded wheel, which bears on a sample held on a moving table. The wheel tracker is fitted with a temperature controlled cabinet with a temperature range from laboratory environment to 65°C ± 1.0°C. The wheel is fitted with a solid rubber tyre of outside diameter 200 mm. The wheel load under standard conditions is 700 ± 10 N. The sample may be either a 200 mm diameter core or a 300 x 400 mm slab of asphalt mixture from 25 mm to 100 mm thick [14].

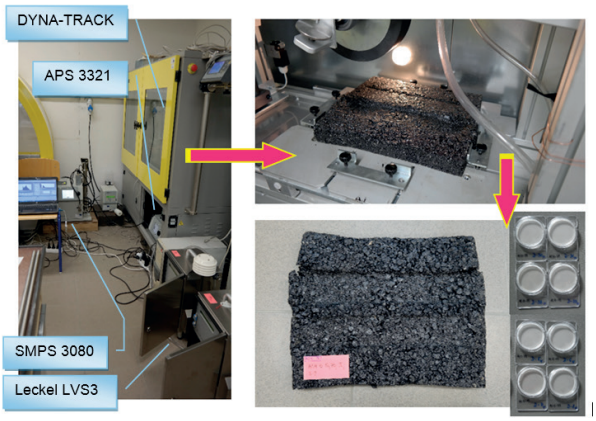

Fig. 3 The used machine technology and rutted sample of the tested asphalt mixture (AC 11 O 50/70, II, S-9) with the contaminated nitrocellulose filters of diameter 47 mm

The used asphalt mixture samples are plates of size 320 x 260 mm and thicknesses of 40 mm. The sampling of the air from inside of the machine DYNA-TRACK during the rutting of samples is performed by equipment APS 3321 (Aerodynamic Particle Sizer) and SMPS 3080 (Scanning Mobility Particle Sizer) which intercept and distribute particle range from 0.012 to 20 µm and 2 pieces of Leckel LVS3 which intercept particulate matter $PM_{2.5}$ and PM_{1} on the filters for the subsequent chemical analysis (Fig. 3).

The air in the vicinity of the sample is circulated (it is swirled by two fans which are part of the device), so that the temperature is stable in the whole space around the sample. This is obtained by the swirling of particles produced during abrasion of the sample and their subsequent sampling by spectrometers APS, SMPS and low volume sampler Leckel. The asphalt mixture samples are rutted by typified wheel for 12 hours through the steady working

conditions. It performs 20 000 cycles during the 12 hours (i.e. 40 000 running gear).

There are specified chemical elements (markers) which are contained in the basic materials of asphalt mixture for identification of particulate matter originating from the asphalt mixture abrasion. These elements will be determined by analyses of the components of the road wearing courses (asphalt mixtures), and they are the aggregate as a filler and the asphalt as a binder. Identified elements will subsequently be confronted with the elements of the particulate matter collected on the filters.

3. The results of current chemical analyses and experimental measurements

The tests of chemical composition of materials (aggregates, asphalt) of samples were carried out before the rutting of these asphalt mixture samples by XRF analyzer (X-ray fluorescence spectroscopy). From the analysis of each material the percentage of each selected element has been found. For the experiments the machine SPEKTRO iQ II (AMATEK, Germany) was used. It is used for analysis of the majority, minor and trace elements in all types of material with sensitivity at the level of ppm.

The tests of chemical composition were performed in the laboratory of the Faculty of Civil Engineering of the Technical University in Košice. The first step was to start with a selected group of elements (Na, Mg, Al, V, Fe, Mn, Ni, Cu, Zn, As, Mo, Sb, Cd, Ba, Pb, Ca, and Cr).

The chemical analyses were performed for all kinds of aggregates used in tested samples. In the samples aggregates from six quarries were used:

- ⇨ Maluzina - **melaphyre1**
- ⇨ Biely Potok - **dolomite**
- ⇨ Badin - **andesite**
- ⇨ Tunezice - **silicious limestone**
- ⇨ Solosnica - **melaphyre2**
- ⇨ Zirany - **quartzite**

XRF analyzer used and evaluated the powder samples (crushed aggregates). The results are shown in the following

Percentage share of the chemical elements of aggregate used in the tested samples — Table 1

Chemical element/ Aggregate	Mg	Al	Si	P	S	Cl	K	Ca	Ti	V	Cr
Melaphyre1	3.62	7.60	23.81	0.086	0.015	0.027	1.034	7.23	0.848	0.030	0.005
Andesite	1.88	10.3	28.12	0.077	0.009	0.028	1.020	6.35	0.476	0.023	<
Melaphyre2	6.25	7.87	23.65	0.151	0.013	0.035	0.923	7.13	0.890	0.032	0.012
Dolomite	17.56	0.95	2.041	0.023	0.010	0.052	<	30.42	0.047	0.011	0.039
Silicious limestone	4.69	0.55	2.622	0.025	0.018	0.038	0.112	48.29	0.029	0.012	0.036
Quartzite	1.51	0.24	0.510	0.004	0.007	0.022	<	51.31	0.011	0.008	0.021

Percentage share of the elements of aggregate used in the tested samples – continuation — Table 2

Chemical element/ Aggregate	Mn	Fe	Cu	Zn	Rb	Sr	Y	Ba	Ta	Share of identified elements
Melaphyre1	0.197	5.747	0.005	0.011	0.005	0.014	0.002	0.019	0.037	50.35%
Andesite	0.098	4.068	0.003	0.004	0.004	0.030	0.001	0.013	0.029	52.56%
Melaphyre2	0.205	7.466	0.004	0.023	0.004	0.019	0.004	0.015	0.044	54.76%
Dolomite	0.040	0.352	<	<	0.001	0.010	<	<	<	51.58%
Silicious limestone	0.035	0.348	<	<	0.001	0.070	<	<	<	56.89%
Quartzite	<	0.14	<	<	<	0.015	<	<	<	53.82%

Note: < - Elements under the detection limit

Tables 1 and 2. The maximum obtained values are highlighted in blue.

The chemical composition analysis (XRF-analyzer) showed that the tested asphalt (binder of asphalt mixture) does not contain any elements from the selected group of elements. Therefore, it will be necessary to extend or replace some elements by organic elements, or by organic compounds. Asphalt contains about 4.8% of inorganic elements and the rest are organic elements. The sulfur S has the largest representation, it represents 4.19%. Silicon Si (0.21%) and chlorine Cl (0.17%) represent a higher share of identified inorganic elements.

Till now, the measurements of particulate matter were performed on six trial samples of asphalt mixtures with different composition. Two plates of each mixture were rutted in the laboratory and each plate was rutted two times:

- ⇨ AC 11 O 50/70, II, **D – 5**
- ⇨ AC 11 O 50/70, II, **K – 4**
- ⇨ AC 11 O 50/70, II, **R – 9**
- ⇨ AC 11 O 50/70, II, **S – 9**
- ⇨ AC 11 O PMB 45/80-75, I, **R – 8**
- ⇨ SMA 11 PMB 45/80-75, **S – 4**

All six samples had the same conditions in the space of rutting during abrasion of asphalt mixtures. The measurements were performed in the period from 24th August 2015 till 23rd

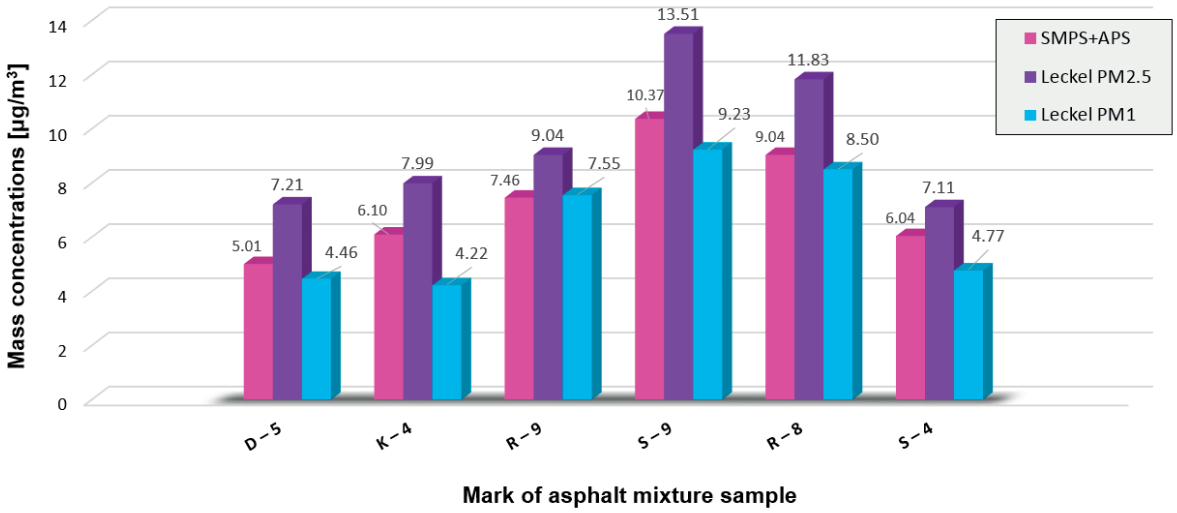

Fig. 4 The average measured concentrations of PM during rutting of the samples

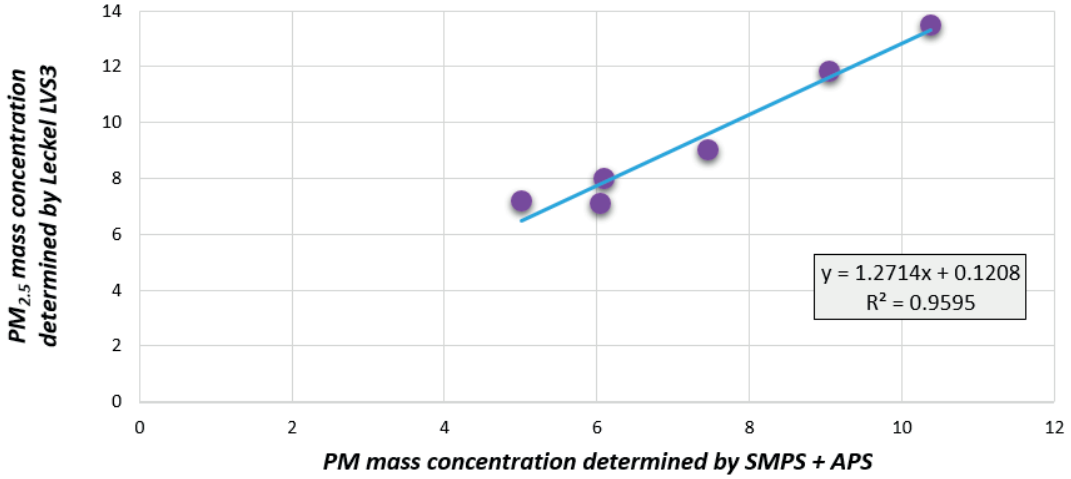

Fig. 5 The correlation between particulate matter mass concentrations determined by spectrometers (SMPS+APS) and low volume sampler (Leckel LVS3)

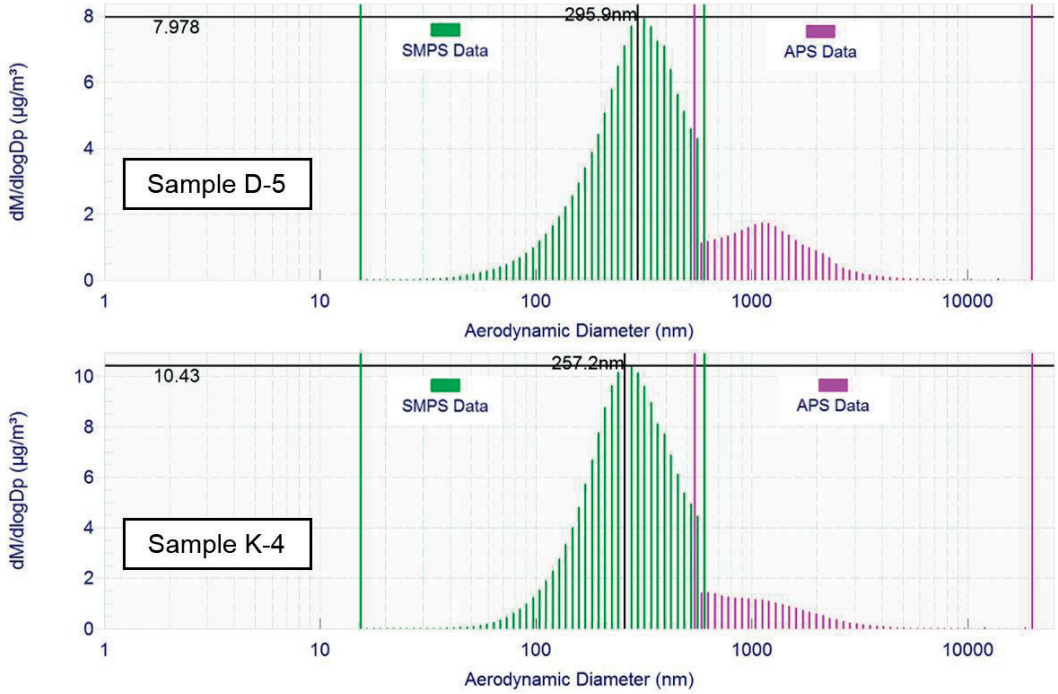

*Fig. 6 The average mass distribution of particulate matter according to the aerodynamic diameter for the rutted samples **D – 5** and **K – 4***

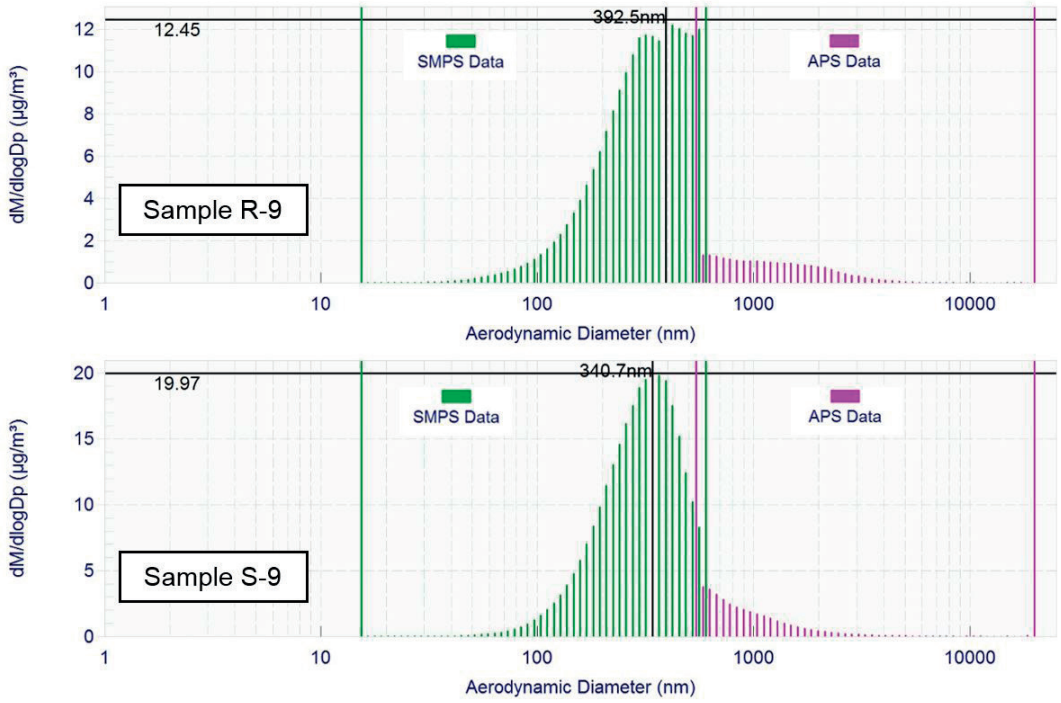

Fig. 7 The average mass distribution of particulate matter according to the aerodynamic diameter for the rutted samples R – 9 and S – 9

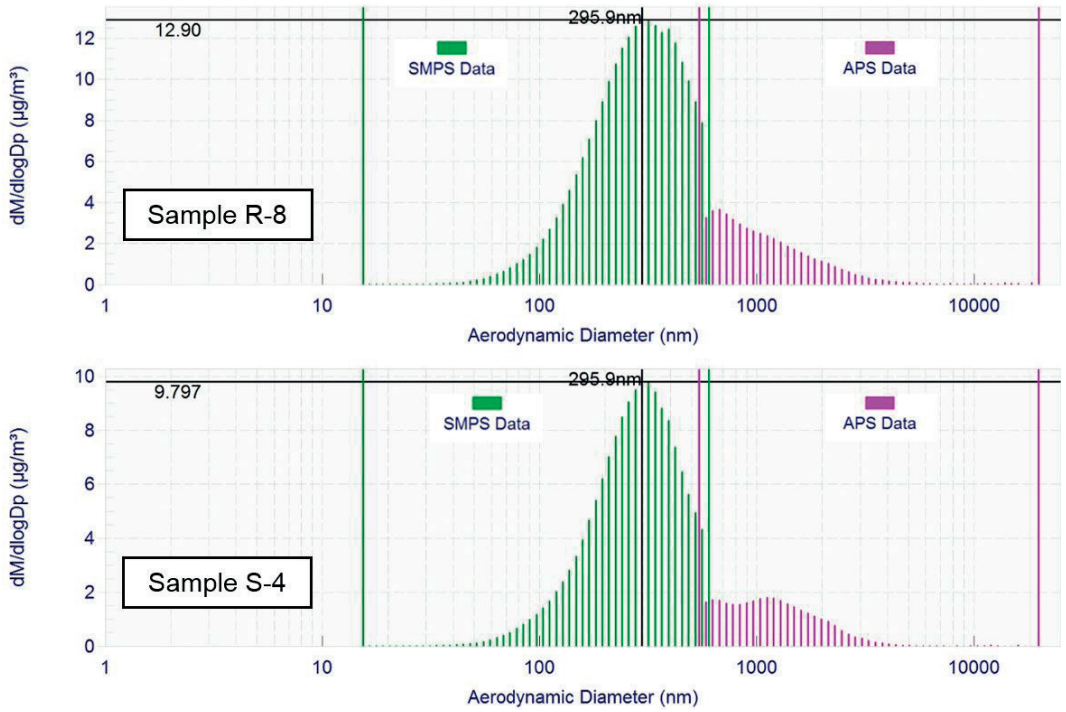

Fig. 8 The average mass distribution of particulate matter according to the aerodynamic diameter for the rutted samples ***R – 8*** *and* ***S – 4***

September 2015. The total length of measurement was 12 hours. The four measurements were performed for each of the asphalt mixtures, it means two ruttings on each sample. The air sampling from inside of the machine DYNA-TRACK during the rutting was performed by means of spectrometers SMPS, APS and two Leckels. In order to determine mass concentrations by SMPS and APS, 180 air samplings were performed. The air sampling was carried out every 4 minutes during 12 hour measurements. Mass concentrations of PM_1 and $PM_{2.5}$ were determined by the gravimetric method (Leckels) and 12 hour air samplings were performed. The results of the measured PM are shown in the following figure as mass concentrations (Fig. 4).

Spectrometers APS 3321 and SMPS 3080 intercepted and distributed particle range from 0.012 to 20 µm and 2 pieces of Leckel LVS3 intercepted particulate matter $PM_{2.5}$ and PM_1. Particulate matter of concern includes "fine particles" $PM_{2.5}$ with a diameter smaller than 2.5 µm and "ultrafine particles" PM_1 smaller than 1 µm in diameter.

The highest concentrations of particulate matter were measured for the mixture AC11 with classic binder, especially for the sample wih the mark S - 9 (used aggregates - melaphyre and quartzite) and the lowest concentrations of particulate matter for the sample with the mark D - 5 (used aggregate - siliceous limestone).

Particulate matter concentrations were determined by two methods. The first is determination by the two spectrometers SMPS and APS and the second is determination by low volume sampler Leckel. The results correlate with each other - Leckel $PM_{2.5}$ vs. SMPS+APS (r = 0.98) (Fig. 5).

The following Figs. 6 - 8 present the average mass distribution of PM according to the aerodynamic diameter for six rutted mixtures. The values are given in the units dM/dlogDp (µg/m^3) for the mass concentration at 32 aerodynamic diameter for a decade.

The values measured by spectrometers APS 3321 are highlighted in violet and the values measured by SMPS 3080 are highlighted in green. The mode (the aerodynamic diameter that appears most often in a set of data) at the mass concentration is 296 nm for the rutted sample with the mark D – 5, 257 nm for the sample K – 4, 393 nm for the sample with the mark R – 9 and 341 nm for the sample S – 9 (Figs. 6 - 7). The mode is 296 nm for the rutted sample with the mark R – 8 and also 296 nm for the sample with the mark S – 4 (Fig. 8).

As regards the comparison of six different asphalt mixtures, the sample with the mark S - 9 shows the highest mass concentration of particulate matter and the sample with the mark D - 5 shows the lowest concentration. The average mass concentration of the sample D – 5 is by 5.36 µg/m^3 less than the average mass concentration of the sample S – 9. These concentrations were determined by means of spectrometers APS and SMPS. The difference between these two samples was determined on 6.30 µg/m^3 for the particulate matter of fraction

$PM_{2.5}$ and 4.77 μg/m^3 for the particulate matter of fraction PM_1 by using the gravimetric method (by the machine Leckel).

4. Discussion to the issue

For our research the initial measurements of abrasion of asphalt mixture samples for wearing courses and chemical analysis of aggregates and asphalt were carried out. Chemical analyses revealed a number of facts about content of individual elements in the investigated materials. While the elements such as Si and Ca have a dominant representation in the aggregates, the presence of Mg, Al and Fe is lower. Asphalt contains primarily elements of organic chemistry but sulfur S prevails over other inorganic elements.

The findings from chemical analyses can be further applied for the research of particulate matter released from asphalt roads abrasion. The subsequent phase of the research will be to determine chemical elements in the collected particulate matter and to confront it with the representation of these elements in the chemical composition of the asphalt mixture. Till now 24 tests have been performed and 6 asphalt mixtures have been rutted in wheel tracking machine. Four measurements of PM concentrations are available for each type of asphalt mixture.

The samples were different not only by the used aggregate type but also by the used binder. The highest concentration of particles PM was measured for the sample S – 9 (AC 11) with the asphalt 50/70. The lower values of mass concentration were measured for the sample S – 4 (SMA 11) with modified asphalt PMB 45/80-75 and the lowest mass concentration was determined for the sample with the mark D – 5 (AC 11) with the asphalt 50/70. Aerodynamic diameter is the substantial value of measured particulate matter during the rutting of asphalt mixture samples by means of APS and SMPS. The aerodynamic diameter is less than 1 μm.

The continuation of our research should include a comparison of individual types of asphalt mixtures by monitoring the chemical composition of produced particulate matter and subsequent comparison of mixtures from the perspective of particulate matter production from the pavement surface. As this paper presents partial results, the task for the continuation of the research is to test and compare the largest possible number of asphalt mixtures. The final evaluation should be based on the results of a sufficient number of measurements for statistical evaluation of the experiment.

References

[1] EEA Report No 5/2014. Air quality in Europe - 2014 report

[2] AMATO, F., et al.: Urban Air Quality: The Challenge of Traffic Non-Exhaust Emissions. *J. of Hazardous Materials*, 275, 31-36, 2014. Retrieved from www.scopus.com

[3] JANDACKA, D.: *Road Transport Impact on the Occurrence of Particulates*, Dissertation thesis. University of Zilina, 134 p., 2012.

[4] JANDACKA, D.: Contributory Assessment of Creation of PM_{10} as Impacted by Vehicular Traffic Based on the Presence of Heavy Metals. *Communications - Scientific Letters of the University of Zilina*. vol. 15, No. 3, 2013, pp. 96-101, ISSN 1335-4205.

[5] DURCANSKA, D.: Analysis of Particulate Matter Composition. *Communications - Scientific Letters of the University of Zilina,* vol. 12, No. 3A, 2010, 17-22, ISSN 1335-4205.

[6] POSPISIL, J., LICBINSKY, R., HUZLIK, J.: Dispersion of Pollutants from Line Sources in Small Municipalities. *Transactions on Transport Sciences,* vol. 7, No. 4, 2014, 161-168. ISSN 1802-971X.

[7] DURCANSKA, D., et al.: *Analysis of Methods of Evaluation of the Air Pollution from Road Traffic: Analysis Task.* Zilina: Faculty of Civil Engineering, Department of Highway Engineering, September 2014.

[8] GEHRIG, R., ZEYER, K., BUKOWIECKI, N., LIENEMANN, P., POULIKAKOS, L. D., FURGER, M., BUCHMANN, B.: Mobile Load Simulators - A Tool to Distinguish between the Emissions Due to Abrasion and Resuspension of PM_{10} from Road Surfaces. *Atmospheric Environment*, 44(38), 4937-4943, 2010.

[9] PIRJOLA, L., KUPIAINEN, K. J., PERHONIEMI, P., TERVAHATTU, H., VESALA, H.: Non-Exhaust Emission Measurement System of the Mobile Laboratory SNIFFER. *Atmospheric Environment*, 43(31), 4703-4713, 2009.

[10] TERVAHATTU, H., KUPIAINEN, K. J., RAISANEN, M., MAKELA, T., HILLAMO, R.: Generation of Urban Road Dust from Anti-Skid and Asphalt Concrete Aggregates. *J. of Hazardous Materials*, 132(1 spec. iss.), 39-46, 2006.

[11] FOLKESON, et al., SPENS: *Sustainable Pavements for European New Member States, Guidelines for the environmental assessment of various pavement types including recommendations to road authorities in NMS*, European commission DG research, Sixth framework programme, 29 May 2009.

[12] GUSTAFSSON, M., BLOMQVIST, G., GUDMUNDSSON, A., DAHL, A., JONSSON, P., SWIETLICKI, E.: Factors Influencing PM_{10} Emissions from Road Pavement Wear. *Atmospheric Environment*, 43(31), 4699-4702, 2009.

[13] KLAZ 1/2010 *Catalog Sheets - Asphalt Mixture Guide*. MDPaT SR, 2010.

[14] Wheel Tracking Machine DYNA-TRACK. Cernusco, Italy: Controls S.R.L., 2000.

https://doi.org/10.26552/com.C.2016.4.44-48

Izabela Major - Maciej Major - Daniela Kucharova*

NUMERICAL ANALYSIS OF A MECHANICAL WAVE DAMPING IN THE RUBBER-CONCRETE COMPOSITE USING THE ADINA SOFTWARE

This paper presents numerical analysis concerning a rubber-concrete composite which can be considered as a structural element designed to form walls. Structural elements that carry the compressive load have a rubber with a specific shape embedded during the technological process. Therefore, the prefabricated block offers an additional damping property of a mechanical wave resulting from the dynamic load. The numerical analysis using the ADINA software revealed significant mechanical wave damping in the composite analysed in the study for different types of dynamic load.

Keywords: *Composites, Mooney-Rivlin, non-linear hyperelastic material, damping, ADINA.*

1. Introduction

Nowadays, due to specific mechanical properties, composite materials are frequently used in civil engineering to build various types of structures. There are a number of composites manufactured today, whereas the most popular solution is to combine concrete with steel. It should be noted that, depending on the type of structure, at least few different composites can be used. For example, glued laminated timber can be considered to be used in wooden structures. Materials such as concrete-steel composites combine advantages of these two different materials, which results in a more efficient transfer of tensile and compressive stresses in the structure. Moreover, combination of rubber and other materials such as steel are also desirable from the engineering point of view. These compounds are used mainly in bridge construction as bearings and the use of rubber allows for reduction in vibration from dynamic load i.e. moving vehicles, pedestrians etc. However, there are various types of composites and the research on concrete-rubber materials remains to be at the initial stage.

Nowadays, expensive experimental tests are more frequently replaced with the numerical analysis based on the finite element method due to its reduced time consumption and lower costs. FEM software does not only help compute structural displacements and internal stresses. It is also possible to analyse mechanical wave propagation.

It is assumed that the first researchers to start experimental tests on rubber in order to describe its behaviour were Mooney and Rivlin [1 and 2]. In the forties and the fifties of the 20th century, they developed a mathematical model describing the rubber behaviour caused by external load. In the following years, their research was continued by Zahorski [3 and 4], who modified the Mooney-Rivlin mathematical model to describe rubber behaviour for higher external loads. It is assumed that Mooney-Rivlin model can be safely applied to rubber materials where the value of strain equals 1.4, whereas for Zahorski this value equals 3. The study of shock wave phenomena in selected rubber materials was presented in [5], where the evolution and reflection of particular waves is considered. Experimental tests of mechanical wave propagation in layered composite materials were also the focus of the study by Kosiński [6]. Due to rapid technological advances many research centres at the end of the 20th century were already equipped with computers and finite element method based software, which resulted in many publications concerning the FEM method used in different fields of science (see [7]). A great number of papers have used FEM to examine mechanical wave propagation in different materials. One example is modelling of wave propagation with a hyperelastic Mooney-Rivlin and Zahorski material model presented in [8 and 9], based on the ADINA software using the finite element method.

This paper presents a numerical analysis of damping of mechanical wave propagation caused by different types of dynamic

* [1]Izabela Major, [1]Maciej Major, [2]Daniela Kucharova
[1]Faculty of Civil Engineering, Czestochowa University of Technology, Poland
[2]Faculty of Civil Engineering, University of Zilina, Slovakia
E-mail: imajor@bud.pcz.czest.pl

load in a composite made of concrete with rubber pads compared to the solid concrete block. Four different types of dynamical load were studied: concentrated force, vertical line load, horizontal line load and pressure on the frontal surface of the block, respectively. The ADINA software which is fully based on the finite element method was chosen to perform numerical analysis.

2. Hyperelastic Mooney-Rivlin material

The constitutive equations describe the behaviour of the specified material medium under the influence of various types of external factors.

The constitutive relation for the hyperelastic Mooney-Rivlin material can be written as:

$$W(I_1, I_2) = C_1(I_1 - 3) + C_2(I_2 - 3) \quad (1)$$

where: C_1, C_2 are the material constants, whereas I_1, I_2 are invariants of deformation tensor. According to the above equation, one can be stated that the elastic energy for the discussed incompressible isotropic hyperelastic Mooney-Rivlin material is linearly dependent on invariants of deformation tensor.

Table 1 presents elastic constants for rubber analysed in this study. The values are based on the study [3] and were obtained by computing into the SI system.

Constants C_1, C_2 Table 1

Constants	C_1 [Pa]	C_2 [Pa]
Value	$6.278 \cdot 10^4$	$8.829 \cdot 10^3$

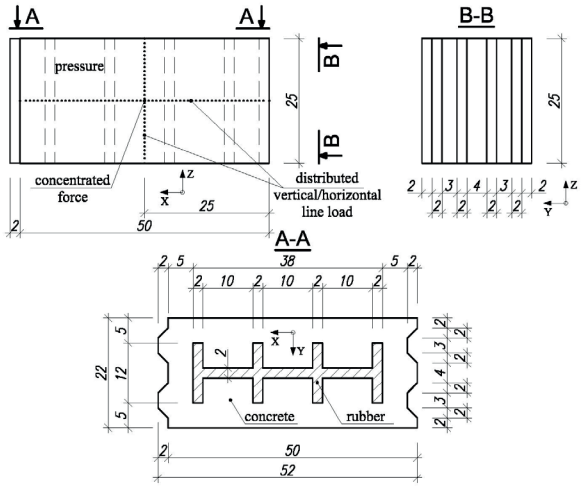

Fig. 1 Scheme of the analysed concrete-rubber block

as mechanical wave propagation. In the following stages of the analysis, the effective stress values resulting from the pulse load were read in the measurement points 1 to 4 (see Fig. 2) and 1R–4R which were the reflection of points 1 to 4 located on the rear side of the block. The effective stress was read as a mean value from the adjacent elements to the black dots denoting the measurement points presented in Fig. 2.

The following boundary conditions were used in the model with respect to the Cartesian coordinate system presented in Fig. 1: bottom surface of the block located on the XY plane was fixed in the direction of Z axis, whereas side surfaces of the block located on the YZ plane were fixed both in the X and Y axis direction.

Discretization of the block model was obtained using 3D-Solid finite elements (tetrahedrons), with the size of each

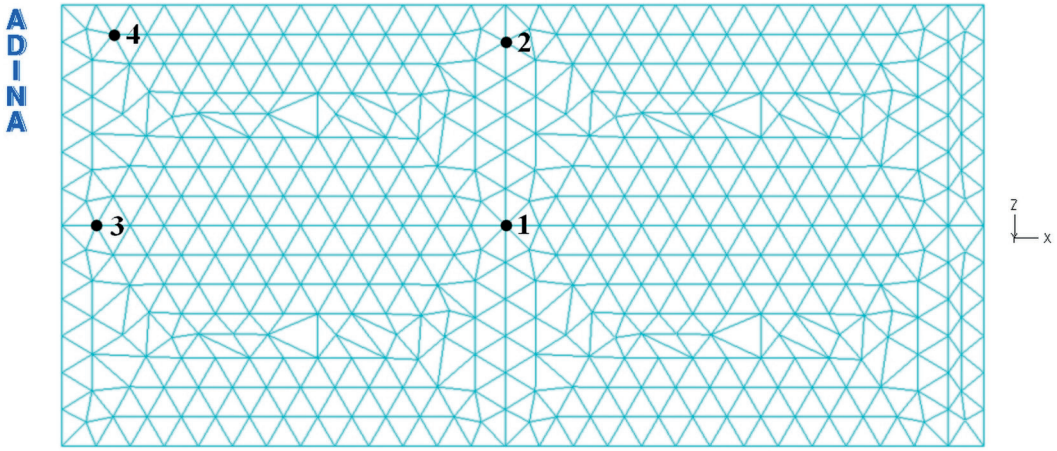

Fig. 2 Discrete model of the analysed concrete-rubber block and effective stress measurement points 1-4; Points 1R-4R are the reflection of points 1-4 located on the rear surface of the block

were adopted for reading of the effective stress: $t_1=1\times10^{-5}$ s and $t_2=6\times10^{-5}$ s. Furthermore, the disturbance propagation resulting from the different types of dynamic load in the composite and solid concrete block was presented in Figs. 3-6.

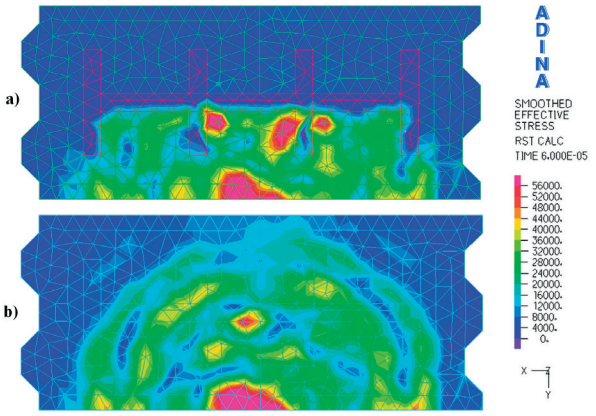

Fig. 3 Effective stress at t = 0.00006 s,
(a) composite blocks made of concrete and rubber,
(b) solid concrete block (a dynamic concentrated force load)

Comparison of the effective stress redistribution on the top surface of the block shown in Fig. 3-6 reveals that perpendicular mechanical wave propagation in the composite (see Figs. 3a-6a) at time $t=6\times10^{-5}$ s is significantly reduced behind the rubber pads, whereas in the solid concrete block (see Fig. 3b-6b), the wave is only slightly damped with material properties. It is noticeable that the effective stress on the rear block side in the composite ranges from 4 to 8 kPa, while in the concrete block, stresses fit the range of 4 – 36 kPa.

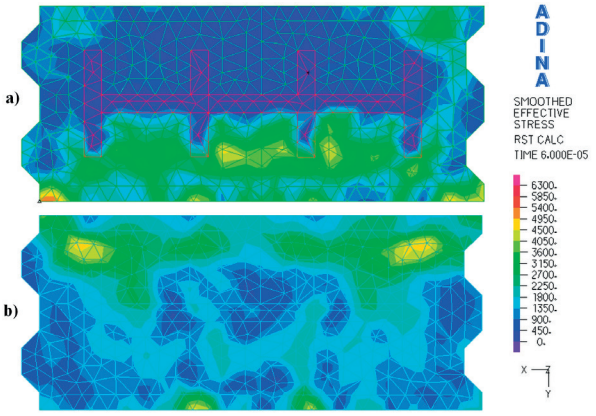

Fig. 4 Effective stress at t = 0.00006 s,
(a) composite blocks made of concrete and rubber,
(b) solid concrete block (a dynamic pressure load)

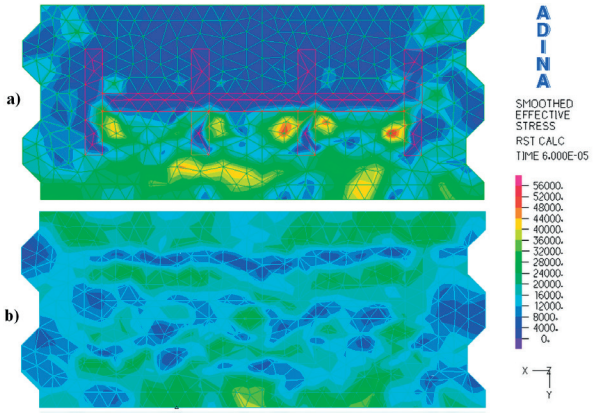

Fig. 5 Effective stress at t = 0.00006 s,
(a) composite blocks made of concrete and rubber,
(b) solid concrete block (a dynamic horizontal line load)

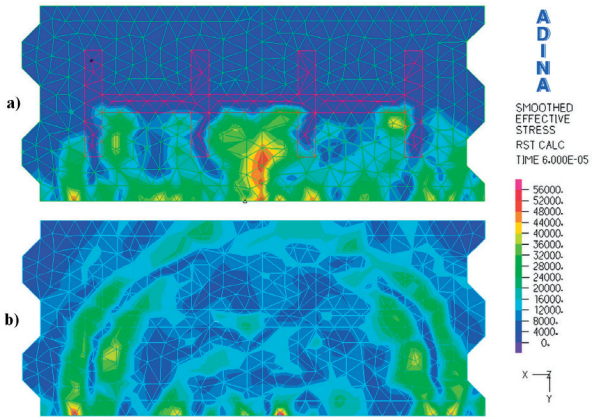

Fig. 6 Effective stress at t = 0.00006 s,
(a) composite blocks made of concrete and rubber,
(b) solid concrete block (a dynamic vertical line load)

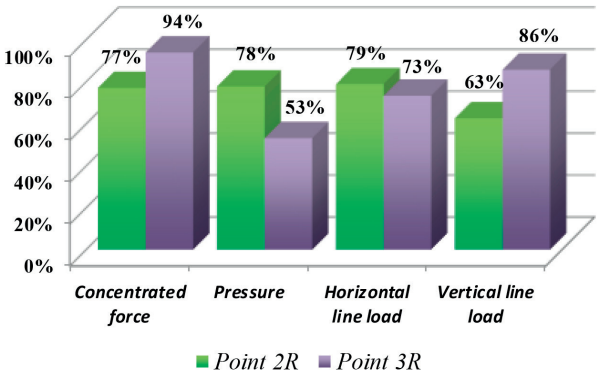

Fig. 7 Mechanical wave percentage damping on the outer surface ("XZ" plane) of the composite block in relation to the solid concrete block at the 2R and 3R measurement points for a different dynamic loads applied; Time $t=6\times10^{-5}$ s

Comparison of the effective stress in selected measurement points in the composite and solid concrete block for different types of dynamical load and two different time values $t_1=1\times10^{-5}$ s and $t_2=6\times10^{-5}$ s Table 2

Concentrated force					Pressure load				
Effective stress [Pa]					Effective stress [Pa]				
Point	Composite		Solid concrete block		Point	Composite		Solid concrete block	
	t_1	t_2	t_1	t_2		t_1	t_2	t_1	t_2
1	1.50E+06	1.75E+05	1.50E+06	1.78E+05	1	5.73E+03	4.11E+03	5.72E+03	2.37E+03
1R	8.59E-02	4.79E+03	2.43E+00	1.09E+04	1R	1.24E-01	2.82E+03	2.41E-01	2.45E+03
2	5.54E+02	5.88E+04	5.51E+02	5.75E+04	2	5.88E+03	3.15E+03	5.87E+03	2.03E+03
2R	7.32E-02	2.34E+03	3.93E-01	1.02E+04	2R	3.54E-02	4.67E+02	3.24E-01	2.10E+03
3	5.90E-01	2.40E+04	5.56E-01	2.47E+04	3	6.45E+03	4.86E+03	6.44E+03	2.51E+03
3R	7.90E-04	5.89E+01	4.95E-02	9.80E+02	3R	2.45E-01	1.34E+03	4.40E-01	2.86E+03
4	2.18E-01	9.19E+03	2.22E-01	8.75E+03	4	5.50E+03	559E+03	5.49E+03	2.30E+03
4R	7.71E-04	9.13E+01	2.29E-02	5.25E+02	4R	2.74E-01	1.95E+03	4.35E-01	2.85E+03

Horizontal line load					Vertical line load				
Effective stress [Pa]					Effective stress [Pa]				
Point	Composite		Solid concrete block		Point	Composite		Solid concrete block	
	t_1	t_2	t_1	t_2		t_1	t_2	t_1	t_2
1	3.86E+05	1.06E+05	3.86E+05	9.29E+04	1	3.86E+05	6.73E+04	3.86E+05	6.66E+04
1R	2.17E-01	5.14E+03	3.58E+00	1.27E+04	1R	8.49E-01	1.89E+04	1.90E+00	1.11E+04
2	5.04E+02	3.34E+04	4.96E+02	3.28E+04	2	4.40E+05	7.69E+04	4.40E+05	7.25E+04
2R	1.19E-01	3.53E+03	8.25E-01	1.67E+04	2R	2.60E-01	3.85E+03	2.20E+00	1.03E+04
3	4.62E+05	4.98E+04	4.62E+05	4.99E+04	3	8.67E-01	2.79E+04	8.50E-01	2.97E+04
3R	1.85E+00	3.78E+03	3.29E+00	1.42E+04	3R	1.07E-02	2.26E+02	8.74E-02	1.59E+03
4	2.82E+02	2.32E+04	2.78E+02	1.73E+04	4	1.23E+00	3.55E+04	1.15E+00	3.92E+04
4R	5.22E-01	1.39E+04	9.03E-01	1.91E+04	4R	1.54E-03	1.16E+02	8.71E-02	1.54E+03

The values presented in Table 2 show that the effective stress on the frontal XZ plane of the block is slightly higher for the composite compared to the solid concrete. This is due to lower amount of concrete material in the block and its higher stiffness compared to rubber, which results in higher force distribution in this material. It should also be noted that at the time $t=6\times10^{-5}$ s there were both higher and lower values of effective stress on the frontal block surface, caused by the mechanical wave interference and refraction of the reflected wave in the rubber material. Figure 7 shows damping of mechanical wave propagation in the composite block made of concrete and rubber pads for different types of dynamical load in the measurement points 2R and 3R at $t=6\times10^{-5}$ s compared to the solid concrete block.

Based on the results presented in Fig. 7, it can be found that damping in the composite material fits the range of 53 – 94% for different types of dynamical load applied to the frontal surface of the block. The highest damping was observed for the concentrated force, because the mechanical wave had to propagate through the rubber material for both 2R and 3R points.

Damping for the above force is higher at the 3R point because the rubber pads were not only inserted in the XZ plane of the block, but they were also located in the YZ plane, providing additional damping in the longitudinal direction of the block. With the pressure and horizontal-line dynamical load shown in Fig. 7, it is noticeable that damping at point 3R is relatively smaller for the point 2R. This phenomenon was connected with the location of the point 3R: mechanical wave propagation from both pressure and horizontal line load propagated through the solid concrete material near side surface located on the YZ plane. It is remarkable that with longer distances from the applied

dynamic load to the measurement point and more rubber inserts present in the way of disturbance propagation, the disturbance could be efficiently diminished on the outer side of the block.

5. Conclusion

This paper presents the reduction in disturbance wave propagation in the composite block made of concrete and rubber. It was found that despite the type of the dynamic load to the frontal surface of the composite block, the disturbance wave propagation on the outer block side was significantly reduced from 53% up to 94% compared to the solid concrete block. Therefore, composite blocks could be used in wall structures to transfer compressive forces as well as to provide a barrier from the external sources of vibrations.

The main advantages of the innovative composite solution include: low cost of implementation in the technological process, where special mould would have to be embedded in the beginning of the process and, after the mould removal, rubber pads could be either inserted or injected. The blocks are symmetrical in the horizontal plane to prevent from incorrect assembly of the block. Another advantage is also that the materials are recyclable. The main drawback is a small reduction in load bearing capacity of each block. The bigger the rubber pads, the more significant reduction in load bearing capacity, whereas optimal dimensions of inserts and concrete blocks could be easily determined via numerical analysis. It should be noted that the configuration of rubber pads and its dimensions presented in the paper are only the examples of possible patterns. Therefore, they can be considered as the basis for further modifications and experimental tests of these construction materials.

References

[1] MOONEY, M.: A Theory of Large Deformations. *J. Appl. Phys.*, 11, 1940.
[2] RIVLIN, R. S., SAUNDERS, D. W.: *Large Elastic Deformations of Isotropic Materials*, VII Experiments of the deformation of rubber, Phil. Trans. Roy. Soc. Lond. 243, 1951, 251-288
[3] ZAHORSKI, S.: Experimental Study of some Mechanical Properties of Rubber (in Polish), *Rozprawy inzynierskie*, vol. 10 (1), 1962.
[4] ZAHORSKI, S.: *A Form of Elastic Potential for Rubber-Like Materials*. Arch. of Mechanics, 5, 1959.
[5] KOSINSKI, S.: *Reflection and Evolution of the Shock Wave in the Selected Hyperelastic Materials* (in Polish), Wydawnictwo IPPT PAN: Warszawa, 1995, ISSN 0208-5658.
[6] KOSINSKI, S.: *Elastic Waves in the Rubber-Like Layered Composites* (in Polish), Wydawnictwo Politechniki Lodzkiej : Lodz, 2007. ISBN 978-83-7283-220-7. 116p.
[7] MELCER, J.: A Vehicle Bridge Interaction, *Communications - Scientific Letters of the University of Zilina*, 2007, 3/2007, 5-10.
[8] MAJOR, I., MAJOR, M.: Comparative Analysis of the Distribution of Effective Stress in Mooney and Zahorski Materials using Adina Software, *Advanced Material Research*, 2014, 1020, 165-170.
[9] MAJOR, I., MAJOR, M.: Travelling Waves in a thin Layer Composed of Nonlinear Hyperelastic Zahorski Material, *J. of Theoretical and Applied Mechanics*, 2009, 47, 1, 109-126.

https://doi.org/10.26552/com.C.2016.4.49-55

Veronika Valaskova - Daniel Papan - Rui C. Barros*

ASSESSMENT OF THE ROADWAY DYNAMIC RESPONSE DUE TO THE TATRA 815 LORRY EXCITATION AND EXPERIMENTAL VERIFICATION

The effect of moving load represents the current problem which is analyzed in engineering practice. The response of the vehicle and its dynamic effect on the pavement can be analyzed in an experimental or computational way. The road-vehicle interaction effect is one of the most important problems for the vibration propagation due to traffic. This paper shows the practical analysis of the Tatra 815 Lorry passing effect using two software systems based on the Finite Element Method (FEM). First system is better for a vehicle model and its passing on a simple road model based on Winkler-Pasternak theory of elastic half-space. In the second system, the vehicle model is not supported but it is better and more accurate for the road and geological environment model - where the subsoil layers were modeled separately. The computing is carried out in time domain. The results obtained by the FEM simulation are compared with the result obtained by the experiment in frequency domain.

Keywords: *Finite element method, dynamic analysis, vibration propagation, time domain, frequency domain*

1. Introduction

The heavy road vehicles are at present one of the induced seismicity sources. The moving load generates vibrations which are propagated in geological environment. The assessment of the vibration effect can be performed numerically (FEM dynamic numerical analysis) or it can be experimentally extrapolated. For the FEM dynamic solution many commercial computing systems are currently available. Every system is comfortable for different analysis. That is the reason for a more difficult analysis of decomposition to subsystems. Each system is conformably modeled. In this case (road dynamic response due to vehicle passing) the MODEL 1 (M1) is created in ADINA system. Subsystem of MODEL 2 (M2) is used in Visual FEA for the road-soil dynamic response.

2. Dynamic Simulation of the Tatra 815 Lorry Moving Load – M1

For M1 model it is necessary to describe the basic vehicle and road technical parameters. This model is planar and interactive. It is also necessary to define the basic mathematical principles of the ADINA system.

2.1. Description of the Tatra 815 Half-Part Model

One of the most important parts of the process of numerical simulation is to create a proper computing model. For this case the half-part model of the TATRA 815 was chosen as the most representative vehicle (Fig. 1). The theoretical solution is based on the FEM. The FEM has been mostly used since computer calculations started as one of the possible ways to find solution to systems of differential equations. In this particular case the vehicle was moving steadily on the pavement. These actions are described by the following differential equation:

$$[M]\cdot\{\ddot{u}(t)\}+[C]\cdot\{\dot{u}(t)\}+[K]\cdot\{u(t)\}=\{F(t)\}, \quad (1)$$

where [M], [C] and [K] are mass, damping and stiffness matrices.

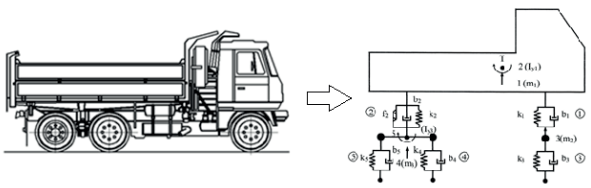

Fig. 1 Half-part model of the lorry T-815

* [1]Veronika Valaskova, [1]Daniel Papan, [2]Rui C. Barros
[1]Department of Structural Mechanics and Applied Mathematics, Faculty of Civil Engineering, University of Zilina, Slovakia
[2]Department of Civil Engineering, Structural Division, FEUP - Faculty of Engineering of the University of Porto, Portugal
E-mail: veronika.valaskova@fstav.uniza.sk

Important part of simulation is to choose the appropriate model of vehicle. The model has to be represented with appropriate mathematical formulation. Half-part models are usually preferred and used for 2D analysis as a combination of mass, spring and beam elements. This discrete model of the vehicle with finite degrees of freedom makes solution easier from the mathematical point of view. This assumption changes partial differential equations to the ordinary differential equations [1 and 2].

The main characteristic of the half part model is defined by three diagonal matrices. They are the mass *[m]*, stiffness *[k_i]* and damping *[b_i]* matrices which contain experimentally measured values [2].

$\{\mathbf{m_i}\}_D = \{m_1, I_{y1}, m_2, m_3, I_{y3}\}_D = \{11475; 31149; 455; 1070; 466\}_D$ [kg, kg.m^2]

$\{\mathbf{k_i}\}_D = \{k_1, k_2, k_3, k_4, k_5\}_D = \{143716.5; 761256; 1275300; 2511360; 2511360\}_D$ [N/m]

$\{\mathbf{b_i}\}_D = \{b_1, b_2, b_3, b_4, b_5\}_D = \{19228, 260197, 2746, 5494, 5494\}_D$ [kg/s]

2.2. Description of the Interaction Model between the Tatra 815 and Soil

In this article a numerical 2D model of the vehicle as well as of pavement are created using computer software ADINA. Computer software ADINA offers all options that are in demand. It offers to define contact pairs between the elements of vehicle that ensured the interaction between the pavement and the vehicle [1].

The computational model of the road is based on Kirchhoff theory of thin plates on a flexible substrate. For the purposes of numerical calculations the following composition of road layers was chosen:

CC I - cement concrete plate h_1 = 240 mm, E_1 = 37500 MPa, v_1 = 0.20

CA II - coated aggregate as Class II. h_2 = 40 mm, E_2 = 4500 MPa, v_1 = 0.21

CS I - cement stabilization as Class I. h_3 = 200 mm, E_3 = 2000 MPa, v_1 = 0.23

PL - protective layer of gravel h_4 = 250 mm, E_4 = 120 MPa, v_1 = 0.35

SS - subsoil h_5 = ∞ mm, E_5 = 30 MPa, v_1 = 0.35

The pavement is modeled as a rigid surface. It is composed of the surface for acceleration (15m) and the surface for braking (15m) (see Fig. 2).

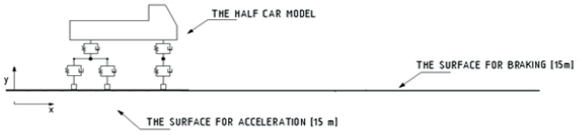

Fig. 2 The numerical model of interaction system

2.3. Description of the Computing Software ADINA

ADINA is a commercial engineering simulation software program which is used in industry and academia to solve structural, fluid, heat transfer, and electromagnetic problems. ADINA can also be used to solve multiphysics problems, including fluid-structure interactions and thermo-mechanical problems. ADINA is the acronym for Automatic Dynamic Incremental Nonlinear Analysis. The program consists of four core modules:

- *ADINA Structures* for linear and nonlinear analysis of solids and structures
- *ADINA Thermal* for analysis of heat transfer in solids and field problems
- *ADINA CFD* for analysis of compressible and incompressible flows, including heat transfer
- *ADINA EM* for analysis of electromagnetic phenomena.

These modules can be used fully coupled together to solve multiphysics **problems, where the response of the system is affected by the interaction of several distinct physical fields (e.g.** fluid-structure interaction, thermo-mechanical analysis, piezoelectric coupling, Joule heating, fluid flow-mass transfer coupling, electromagnetic forces on fluids and structures, etc.) [3].

2.3.1. Principles of Numerical Solver

An effective implicit time integration scheme was proposed for the finite element solution of nonlinear dynamics problems. Direct time integration is widely used in the finite element solutions of transient wave propagation problems. However, accurate solutions are difficult to obtain because of numerical dispersion and dissipation, resulting from period elongations and amplitude decays. In the solution of transient wave propagations, the errors from the spatial and temporal discretizations appear together and affect each other. Analyses of these errors have led to the use of linear combinations of consistent and lumped mass matrices. Another approach is to reduce the solution errors by evaluating the mass and stiffness matrices using modified spatial integration rules. Such schemes can improve the accuracy of solutions of multi-dimensional wave propagation problems when using certain elements and meshes.

We analyze the dispersion errors resulting from the spatial discretization coupled with the temporal discretization. We consider the Bathe method and the Newmark trapezoidal rule. For this purpose, we handle the solution obtained for the scalar wave governed by:

$$\frac{\partial^2 u}{\partial t^2} - c_0^2 \nabla^2 u = 0 \qquad (2)$$

where u is the field variable and c_0 is the wave velocity. Here, body forces are not considered since we focus on the dispersion associated with the propagations of disturbances due to initial conditions. The associated finite element discretization gives

$$\mathbf{M}\ddot{\mathbf{U}} + \mathbf{c}_0^2\mathbf{K}\mathbf{U} = \mathbf{0} \tag{3}$$

where K and M are the stiffness and mass matrices, and for element (m) with volume $V^{(m)}$

$$\mathbf{M}^{(\mathbf{m})} = \int_{V^{(\mathbf{m})}} \mathbf{H}^{(\mathbf{m})^{\mathrm{T}}}\mathbf{dV}^{(\mathbf{m})} \tag{4}$$

$$\mathbf{K}^{(\mathbf{m})} = \int_{V^{(\mathbf{m})}} \left(\nabla\mathbf{H}^{(\mathbf{m})}\right)^{\mathrm{T}}\left(\nabla\mathbf{H}^{(\mathbf{m})}\right)\mathbf{dV}^{(\mathbf{m})} \tag{5}$$

Here, $H^{(m)}$ and U are the element interpolation matrix and the nodal values of the solution, respectively. The matrices M and K in Eq. (3) are obtained by the usual summation process.

In the Bathe method, the following relations are employed

$${}^{t+\Delta t/2}\dot{U} = {}^{t}\dot{U} + \left[\frac{\Delta t}{4}\right]\left({}^{t}\ddot{U} + {}^{t+\Delta t/2}\ddot{U}\right) \tag{6}$$

$${}^{t+\Delta t/2}U = {}^{t}U + \left[\frac{\Delta t}{4}\right]\left({}^{t}\dot{U} + {}^{t+\Delta t/2}\dot{U}\right) \tag{7}$$

$${}^{t+\Delta t}\dot{U} = \frac{1}{\Delta t}\left(U - \left[\frac{4}{\Delta t}\right]^{t+\Delta t/2}U + \frac{3}{\Delta t}\right)^{t+\Delta t}U \tag{8}$$

$${}^{t+\Delta t}\ddot{U} = \frac{1}{\Delta t}\left(\dot{U} - \left[\frac{4}{\Delta t}\right]^{t+\Delta t/2}\dot{U} + \frac{3}{\Delta t}\right)^{t+\Delta t}\dot{U} \tag{9}$$

Using Eq. (3) at times t, $t + \Delta t/2$ and $t + \Delta t$, where t denotes the current time and Δt the time step, with Eqs. (6)-(9), we obtain a linear multistep form of the Bathe method

$$\left(72M + 8c_0^2\Delta t^2 K\right)^{t+\Delta t}U + \left(-144M + 5c_0^2\Delta t^2 K\right)^{t+\frac{\Delta t}{2}} U + \left(72M + 5c_0^2\Delta t^k K\right)^{t}U = 0 \tag{10}$$

Using the definition of the *CFL* number, = , where h is the 'characteristic length' of a finite element (or fundamental length used) , Eq. (10) becomes

$$\left(72M + 8\gamma K\right)^{t+\Delta t}U + \left(-144M + 5\gamma K\right)^{t+\frac{\Delta t}{2}} U + \left(72M + 5\gamma K\right)^{t}U = 0 \tag{11}$$

where $\gamma = CFL^2h^2$ [4].

2.4. The Dynamic Analysis Results

The vehicle passes on a pavement at a constant speed during the whole simulation. The used speed is 40, 60 and 80 km/h.

The time step for simulation has a value 1/50 of second. The following Fig. 3 shows the displacement in the pavement for variable speed.

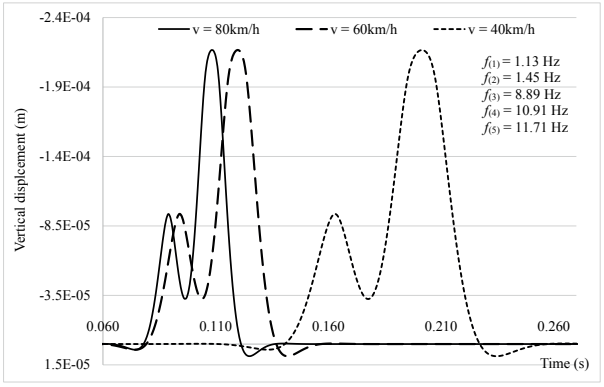

Fig. 3 The displacement on the pavement for variable vehicle speed with natural frequencies

3. The Road and Soil Dynamic Response – M2

The time response function obtained from model M1 for 60km/h is used as basic dynamic load for M2 model. This function was time shifted with step **Δt** = 0.14s corresponding to simulated vehicle model speed and road FE dimension l = 2m. The number of the dynamic load functions was 50. Each function was step by step applied to nodes in the central line of the road upper surface layer. The example of the first 22m dynamic load is shown in the Fig. 4.

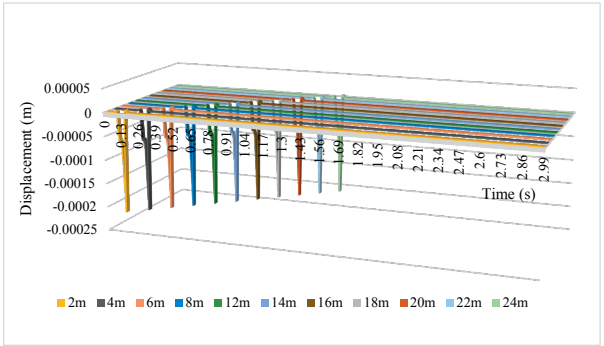

Fig. 4 The dynamic load example for the first 11 time functions

3.1. Description of the Road-Soil Model

The road-soil computing model is created in VisualFEA system. The reference part of the half space [5] used for road-soil is created as a cuboid with length 100m. All finite elements are 3D solid type. Width of the model is 25m and road layer width is 6m. The mechanical properties and thicknesses of created layers are summarized in Table 1. The mechanical properties of the road sublayers are averaged. Geological environment properties are the same as geological properties of the locality for in-situ measurement in [6]. Support of the M2

model is only on the bottom surface of a rock soil layer. The colors in Table 1 correspond with colors on model M2, Fig. 5.

Geometric and material parameters of the M2 layers Table 1

Layer	E	Poisson ratio	Unit weight	Thickness
	(MPa)		(kg/m^3)	(m)
Road layers	12457	0.21	2186	0.48
Subsoil	1500	0.15	1800	10
Rock soil	15000	0.25	2600	10

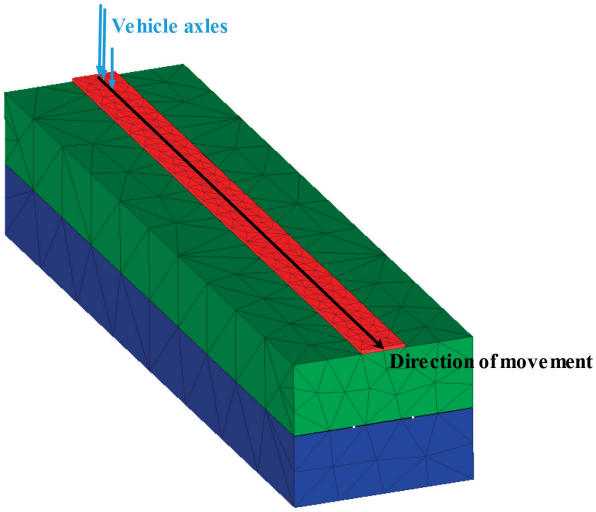

Fig. 5 The road-soil FEM model M2

3.2. Description of the Visual FEA Software

Visual FEA is innovative software for finite element (FE) analysis, which is an advanced technique to solve and analyze physical problems arising in many fields of science and engineering. This program is a full-fledged software integrated with ease-of-use but powerful functions for pre- and post-processing as well as for FE processing. Visual FEA has functions for studying FE analysis and it uses deformation variant of the FEM. The various computational aspects and concepts involved in FE modeling can be easily understood through computational simulation. Its preprocessing capability includes the most advanced 2 and 3-dimensional mesh generation techniques. The analysis can be divided into three phases [7]:

- Preprocessing - these functions are to create, edit and check the modeling data necessary for FE analysis. The data are constructed in a few steps: creation of boundary curves and surface primitives, mesh generation and data assignment (Boundary condition, Element property, Load condition etc.),
- Processing – this phase is the kernel of FE analysis. Processing does not require user interaction and proceeds with various stages of computing element equations, assembling system equations, solving them, and executing other related computations,
- Postprocessing - Functions of this group are used for graphic visualization or further processing of the computed results of the analysis to facilitate their interpretation and understanding.

4. The Results of the Dynamic Analysis and their Comparison with the Experiment

The numerical simulation results of the Tatra 815 are presented for the point on the road edge (right and left are the same if it is symmetric) in 25m distance from the start point 0m. The central point of M2 results are presented because there is minimal effect of mirrors [8]. Figure 6 shows the results in time domain.

The experimental measurement of the road dynamic response due to traffic seismicity was performed in 2008 as a part of the dissertation thesis research [6]. The measurement conditions were considered in the M2 numerical simulation. Only recordings in the point on the road surface were taken into account. In Figs. 7 and 8 are spectral characteristics of the vibration acceleration due to the Tatra 815 road response in vertical and horizontal directions. The average speed of vehicles was 60km/h. The dash-dot curve in Figs. 7 and 8 represents enveloping curve of results.

Figure 9 presents comparison between the experimental and numerical results. Owing to the fact that the experimental results in time domain are non-filterable, experimental verification is relevantly possible in a frequency domain only. The enveloping curve from the experiment overlaps with numerical PSD for vertical and horizontal directions.

5. Conclusions

Problems with the vibrations of civil and traffic structures due to technical seismicity resources are current. Soil-borne vibrations and their effects on civil structures can be solved theoretically (using FEM simulations) and can also be detected experimentally. This paper shows one of the simplified theoretical approaches to traffic seismicity vibration assessment. Both computing systems are useful tools for numerical simulations but each of them is more comfortable for another specialized analysis. Combination of these FEM systems has achieved interesting results but there is more than one precision deficient. Here are some of them:

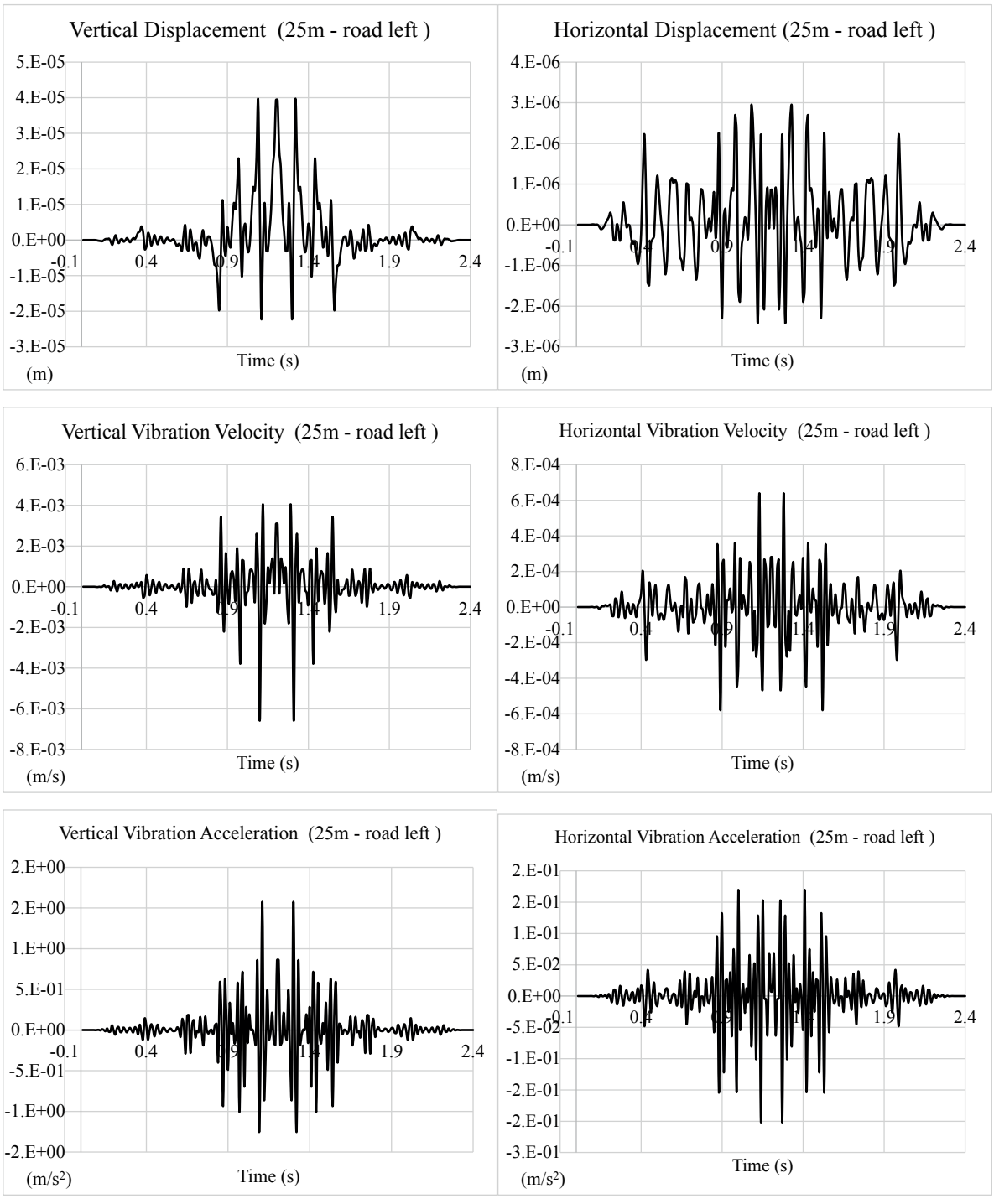

Fig. 6 The results of simulation in the time domain

- Live interaction between M1 and M2 is not possible in this approach.
- No unevenness was modeled in M1, therefore, vehicle excitation is not involved in the model.
- Only symmetric line of the vehicle movement is present.

Though, using this approach, significant results for the future discussion can be obtained:

- Average heavy-duty vehicle (similar to the Tatra 815) moving on the road with a low unevenness level generates only two impacts between the axles. This effect is verified by Fig. 9

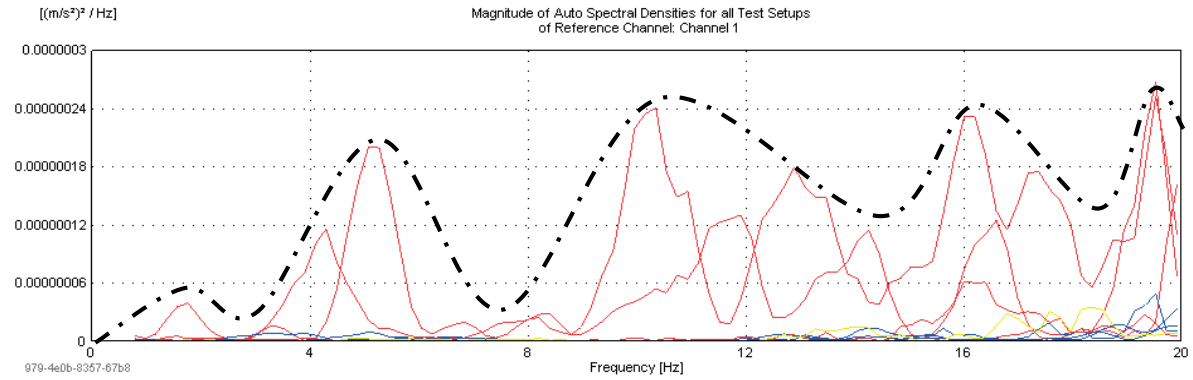

Fig. 7 Measured vertical Dynamic response at the edge of the road surface in frequency domain - vertical acceleration Power spectral density (PSD)

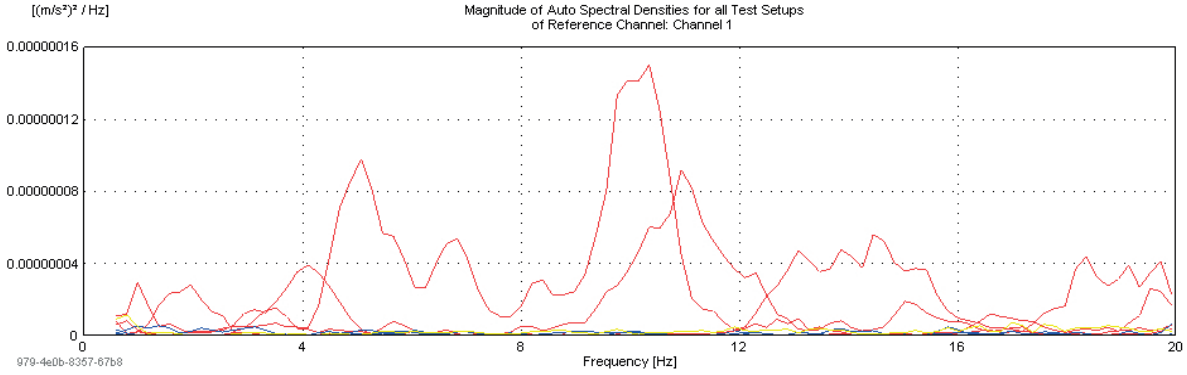

Fig. 8 Measured vertical Dynamic response at the edge of the road surface in frequency domain - horizontal acceleration Power spectral density (PSD)

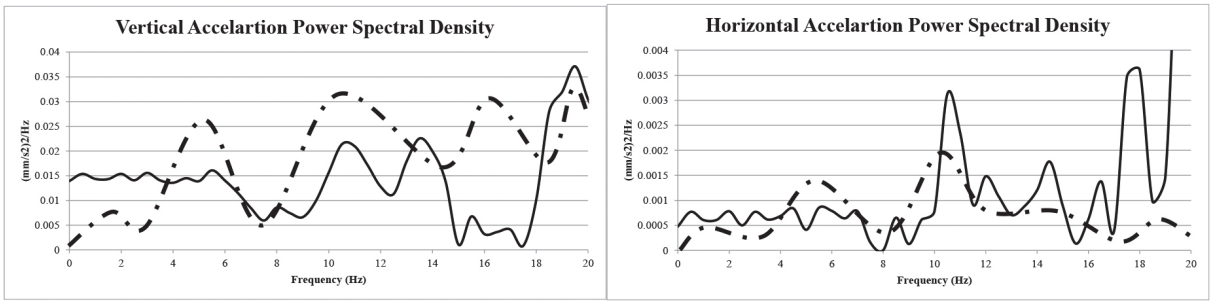

Fig. 9 The acceleration Power Spectral Density comparison - numerical and experimental

where a frequency band from 8 to12 Hz shows similar peaks. The vehicle speed of about 60km/h with the axle distance similar to that of the Tatra 815 generates just the frequency of 10 Hz.

- It is possible to add some simple civil structures into the model M2 and in many cases vibration effects on these structures can be assessed.

The results obtained by FEM simulation are in relatively good accordance with the experiment. It is necessary to know the basic parameters of the soil for a complex computing model. If we want to estimate the effects of technical seismicity, the most efficient is to use theoretical and experimental approaches [9].

References

[1] DANIEL, L., VALASKOVA, V., KORTIS, J.: Numerical Simulation of Moving Vehicle across the Obstacle. *Civil and Environmental Engineering,* vol. 10, No. 2, 108-112, ISSN 1336-5835, 2014.

[2] MARTINICKA, I.: Calculation of Natural Frequencies and Vibration Shapes its own Computational Models of Vehicles, *Land Communications and Tracks*, vol. 6, No. 1-2, 41-50, 2010, ISSN 1336-7501.

[3] ADINA R & D, Official Website.

[2] PERSSON, P., A., HOLMBERG, R., LEE, J.: *Rock Blasting and Explosives Engineering.* Boca Raton, Fla.: CRC Press, 1993, 560, ISBN 0-8493-8978-X.

[4] GUNWOO, N., SEOUNGHYUN, H., BATHE, K., J.: Performance of an Implicit Time Integration Scheme in the Analysis of Wave Propagations, *Computers and Structures*, 123, 2013, 93-105.

[5] BENCAT, J., STYPULA K.: Buildings Structure Response Due to Railway Traffic. *Communications - Scientific Letters of the University of Zilina,* vol. 15, No. 2, 2013, 41-48 (Civil-Comp Proceedings, 102. ISSN 1759-3433), ISSN 1335-4205.

[6] PAPAN, D.: *Spectral Characteristics of the Load and Response of Bridges Due to Technical Seismicity*, Thesis, University of Zilina, 2008.

[7] http://www.visualfea.com/manual-normal/index_online.html, Manual of the computing system VisualFEA.

[8] PAPANOVA, Z., PAPAN, D., KORTIS, J.: Microtremor Vibrations in the Soil Experimental Investigation and FEM Simulation, *Communications - Scientific Letters of the University of Zilina,* vol. 16, No. 4, 2014, 41-47, ISSN 1335-4205.

[9] MORAVCIK, M.: Analysis of Vehicle Bogie Effects on Track Structure - Non-Stationary Analysis of Dynamic Response. *Communications - Scientific Letters of the University of Zilina,* vol. 13, No. 3, 2011, 33-40, ISSN 1335-4205.

https://doi.org/10.26552/com.C.2016.4.56-60

Jan Celko - Marek Drliciak - Igor Ripka*

DATA STRUCTURE OF REGIONAL TRANSPORT FORECAST MODEL

There are several ways to define basic transport relations in an studied area. Generally, the values have to represent relevant and real situation. The quality of data sources is the determining factor of transport forecast quality. The basic purpose of transportation planning and management is to match transportation supply with travel demand, which represents 'need'. A thorough understanding of existing travel pattern is necessary for identifying and analysing existing traffic related problems. Detailed data on current travel pattern and traffic volumes are needed also for developing travel forecasting/prediction models. The prediction of future travel demands is an essential task of the long-range transportation planning process for determining strategies for accommodating future needs.

The transport forecast process estimates the number of vehicles or people that will use a specific transportation facility in the future. The article describes gathering and analysing process of available data for Slovak regions. The mathematical model of forecast transport relations needs a unique form of input data and special computing parameters. The aim of paper is to describe the implementation of the existing data to the transport forecast calculation.

The output data, which are evaluated from the forecast transport model, have to describe a real vision of the region development. The sets of function parameters (measurable or unmeasurable) are edited by using different results of surveys that are often complicated and very time-consuming.

Keywords: *Transport forecast, 4-step model, modelling.*

1. Introduction

Solutions of traffic problems in the town, which are formatted by the influence of strong inter-zone relations and other development intentions, are necessary to be carried out complexly in a general context in order to ensure sustainable regional development. This can be ensured also by creation of a traffic model. The correctly defined traffic model allows evaluating new development activities impact on the road infrastructure loading and allows evaluating alternative solutions of increased traffic problems, too. We can monitor, in addition, the impact of individual phases of highways and highway feeder construction on the urban network loading. The transport analysis and transport prediction models are generally solved by using the Four-step model that was for the first time implemented in Detroit at the Metropolitan Area Traffic Study in 1950. In spite of the time span, the model has still been unchallenged [1].

2. Four-step model

Trip Generation is the first step in the conventional four-step transportation forecasting process, followed by Trip distribution, Modal Split (Mode Choice), and Route Assignment (Fig. 1). Trip generation predicts the number of trips originating in a particular traffic analysis zone. For the residential side of things, trip generation is thought of as a function of the social and economic attributes of households. Households and housing units are very similar measures but sometimes housing units have no households, and sometimes they contain multiple households. Clearly, housing units are easier to measure, and thus are often used in model. Clear definition of the used parameter is very important for an exact model creation. The second step of four-step model - Trip distribution (or destination choice or zonal interchange analysis) - matches trip makers' origins and destinations to develop a "trip table". The trip table is described by the O-D Matrix (Origin – Destination matrix) that express the number of trips between start and final zones. Historically,

* [1]Jan Celko, [1]Marek Drliciak, [2]Igor Ripka
[1]Department of Highway Engineering, Faculty of Civil Engineering, University of Zilina, Slovakia
[2]Institute of Transportation, Technical University of Vienna, Austria
E-mail: jan.celko@fstav.uniza.sk

trip distribution has been the least developed component of the transportation planning model [2].

The trip distribution's zonal interchange analysis yields a set of origin - destination matrices that inform where the trips will be made. The mode choice (Modal split) is a third step of the model, which determines the transport mode using [3].

To determine facility needs, costs, and benefits, the number of trips on each route and link of the network is necessary to determine. The route like a simple chain of links between origin and destination zones is assigned to the network of highways and transit systems. The first required information is the present pattern of travel times and flows, followed by determination of the activity [2].

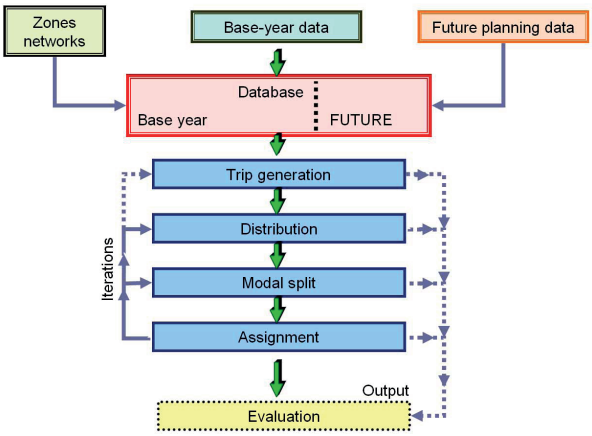

Fig. 1 Four-step model [4]

The solved region is divided into zones dependent on selected parameters which are defined by a detailed analysis of urban, transport, economic and sociological conditions. The basic requisite parameter for traffic forecast is generation of the trips by origin zones [4]. The number of trips depends above all on the zone character. The greatest source of the trips is a living zone. The majority of the trips are connected with a household. The home based trips mean that one end of the trip is connected with home (home – work, sport - home, etc.). On the other hand, the industrial zones are the most attractive for trips induced by a destination zone.

3. Data gathering

The gathering of social and traffic data is the essential step in the process of traffic relation calculations in the studied area. The choice and quantity of questioned samples of population indicates the quality and reliability of results of the transport demand model. The quantity of data collected will be a function of the number of respondents in the final dataset and the amount of information obtained from each respondent. This, in itself, presents a trade-off situation because any attempt to collect more information from each respondent (beyond a threshold level of information) may result in fewer respondents responding. The total number of respondents will obviously depend on the size of the sample drawn from the population and the response rate obtained from that sample.

3.1. Input data

There are several ways to define basic transport relations in the studied area. Generally, the values must represent relevant and real situation. The quality of data sources of transport behaviours of inhabitants is the determining factor of transport forecast quality. It is possible to use several sources to fill the database in Slovakia [3]. The first useful source is the Statistical Office of the Slovak Republic (SO SR).

The system of demographic statistics in Slovakia based on monthly processing of data on demographic events drawn from the exhaustive population survey, regularly performed censuses of population and housing and supplementary population surveys (microcensuses); provides the decisive bulk of information on population as a whole, its spatial distribution, number, structures, and characteristics in the specific period of time.

Labour Market Statistics provide information on present situation and trends in employment, unemployment, job vacancies, wages, labour costs and strikes. Primary source of this information consists of regular statistical surveys carried out in enterprises and households. Labour Force Survey (LFS) quarterly monitors labour force supply focusing on economic activity of population, employment and unemployment.

Social statistics aims at obtaining relevant and comparable statistical information on social protection, income and living conditions of households, labour and wages, education and learning, health, culture and criminality. This information is needed for making and monitoring policy on each level of public administration management including international organisations and for meeting users´ requirements on national and international level.

The system of quarterly and annual enterprise surveys represents the key instrument of data collection in the labour and wages statistics. It provides information on the number of employees, hours worked, job vacancies, average nominal and real wage (classified by branches, size of enterprises, regions) for operative measures of central bodies as well as for experts and for general public. Information on a level of average monthly nominal wage of employees published by the SO SR is a basis for calculation of other significant social indicators (e.g. basis of pension assessment, earnings of institutional representatives, limit of deposit protection etc.). For the purpose of a regional overview, the employment and wages have been surveyed in annual periodicity referring to work place. Furthermore, a total

employment balance has been compiled for the national economy along with regional breakdowns.

3.2. Data gathering process

The first step in data gathering process is a sharing the sophistic data system DATAcube. Database DATAcube contains multidimensional tables for indicators of economic and socio-economic development. The classification system of individual tables is based on maintaining the structure of domains and fields similarly as in the web Portal. Data from various statistical fields are presented in the form of multidimensional tables in monthly, quarterly or yearly time series and allow to create specific own selections. The outputs can be exported to the select format.

Despite of data foundation the demand characteristics for a demand model are not possible to obtain from available sources. The mobility information is to be determined by a classic questionnaire system, where inhabitants are requested for daily transport activities with determination of number of trips, modal choice, traffic chains, and range of the trips.

The next required data contain information about infrastructure for the network model. The source of data is available in the sources of the Road databank (RDB) that is a branch of the Slovak Road Administration. Through its own facilities, in close cooperation with road owners and administrators, it executes:

- collection and processing of technical data of roads,
- pavement diagnostics,
- development and building of the GIS (Geographical Information System),
- information service of databank.

In addition, RDB operates the application system for assessment and determination of routes for the transport of excessive and oversized cargo. The RDB also offers the summary data of the road network SR, selected data of objects in the road network, length of the roads since 1995 and the basic and thematic maps of the road network (road sections with toll, international road E, TEM, TEN-T), maps of regions, districts, map sheets and maps of intersections. Other urban streets are not included in RDB

4. Parameter setting

The transport demand model is based on a large base of evaluated data which are processed into the mathematical function. The most popular functions are: BoxCox, Logit, Kirchhoff function. Mentioned functions are used in trip distribution, mode choice and assignment process (Fig. 2).

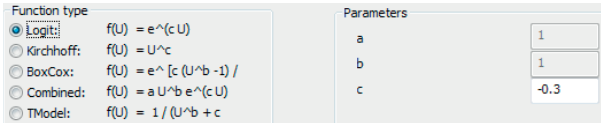

Fig. 2 Definition of Function type [5]

Table 1 presents the example of data evaluation from mobility survey and application to the demand model parameters. Restraint functions were used for trips distribution. The parameters adjust the shape of the logit function.

The example of restraint function for utility travel time [6] Table 1

Group	town	work	school	shop	private
Student	<5000		0.056	-0.0756	-0.0619
	5000-50000			-0.086	-0.075
	>50000			-0.106	-0.075
Employed with car	<5000	-0.059		-0.070	-0.044
	5000-50000	-0.062		-0.087	-0.049
	>50000	-0.072		-0.082	-0.046

4.1. Volume delay function

The key element of the road assignment process using equilibrium method is the volume-delay function (VDF). There are several different formulas for description of VDF (from a simple linear with the breakpoint to much more complicated). In most traffic assignment methods, the effect of road capacity on travel times is specified by means of volume-delay functions t(v) which expressed the travel time (or cost) on a road link as a function of the traffic volume (V). Usually these functions are expressed as the product of the free flow time multiplied by a normalised congestion function.

$$t_v = t_o * f\left(\frac{v}{q}\right), \quad (1)$$

where

t_o - free flow time,
V - traffic volume,
q - capacity (it may be full capacity, capacity on the level or saturation flow).

The function should have several conditions. For the formulation of VDF the conditions can be divided into two groups – mathematical and behavioural [7].

Mathematical

From the mathematical point of view, having in mind the system optimal principle, the function should be [8]:

- continuous,

- strictly increasing,
- non – negative.

Behavioural

Following facts should be kept in mind [7]:

- in urban traffic most of the trips are made every day – users have a lot of experience with traffic conditions in different times of the day on different routes,
- the user can make also "on-time" decisions – if he sees there is a congestion on the street in front of him or when he hears about congestion on the radio, he can turn and choose another route,
- time spent in the congestion weighs much more for the user than travel time at an acceptable speed – the user is strongly forced to choose another route,
- free flow speed - defined as a speed of the traffic flow without any disturbances on the road; free flow speed decreases after implementing the traffic lights, but many users choose a route without acceptance this decrease.

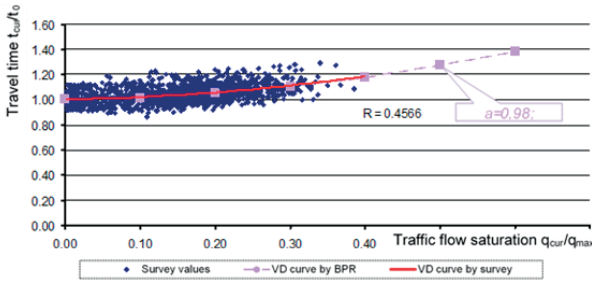

Fig. 3 Definition Volume delay function [9]

Figure 3 presents the example of the parameters of VDF function for for urban main street. Parameters were derived from large measurements in Zilina. The parameter „a" of exponential function was derived from mentioned measurements.

4.2. The impedance

One of the most difficult steps - mode choice - calculates a discrete distribution model. The trip of each route is calculated for a person group first, and one from transport modes is chosen. The modes are divided into two groups: exchangeable modes (generally walk, passenger and public transport), and non-exchangeable modes (car, bike). Changing the mode during the same trip creates a trip chain. If the first mode is a non-exchangeable mode, the entire trip chain is maintained independent of its attributes. If an exchangeable mode was selected for the first trip, mode choice is carried out for the remaining chain trips, however, only within the exchangeable modes.

$$P_{gij}(m) = \frac{e^{U_{gij}(m)}}{\sum_{k=1}^{M} e^{U_{gij}(k)}} \qquad (2)$$

where

i,j indices of origin and destination zones,
$P_{gij}(m)$ choice probability for mode m by person group g,
$U_{gij}(m)$ objective utility value of mode m for person group g,
m number of alternative modes.

The structure of the utility function is of special importance in this respect. The following utility function from [8] illustrates possible components of the function for the mode choice:

$$U_{gij}(m) = p_{1gm} * T_{ijm} + p_{2gm} * Z_{ijm} + p_{3gm} * \ln\frac{D_{ij}}{p_{4gm}} + \\ + p_{5gm} * C_{ijm} + p_{6gm} \qquad (3)$$

with the parameters per group g and mode m:

p_{1gm} marginal utility of one-minute ride time,
p_{2gm} marginal utility of one-minute access/egress time,
p_{3gm} marginal utility of logarithmic relative distance increases (impact of distance advantage),
p_{4gm} advantage distance of mode m,
p_{5gm} marginal utility of one monetary unit of a ticket price,
p_{6gm} constant utility of mode m,

and the mode dependent attributes:

T_{ijm} ride time from i to j with mode m,
Z_{ijm} sum of access time at i and egress time at j for mode m,
C_{ijm} costs of trip from i to j with mode m,
D_{ij} distance from i to j.

The parameters p1, p2 and p5 have a negative utility, so they have a negative sign. The parameter p4 (advantage distance) indicates from what distance a particular mode of transport is considered to be useful by travellers of a specific group. Only when the distance d_{ij} exceeds the advantage distance p4 (d_{ij} > p4) the quotient d_{ij} / p4 is greater than 1 and the logarithmical term ln (d_{ij} / p4) turns positive. As a consequence, distances below the advantage distance result in a negative utility. The distance relevant parameters p3 and p4 are important to give preference to the modes walking and cycling on short distances, as their p4 is defined smaller than for the modes of transport car und PrT and their p3 is negative compared to the others.

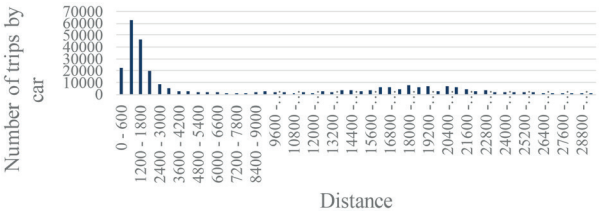

Fig. 4 The final graphical expression of trips by car according to the distance. (Source: Authors)

The parameters of utility function were calibrated by results from mobility survey. The final modal split was evaluated according to many parameters. Figure 4 presents the evaluation according to the length of trips, Fig. 5 presents the observed modal split by the groups of inhabitants defined for Zilina.

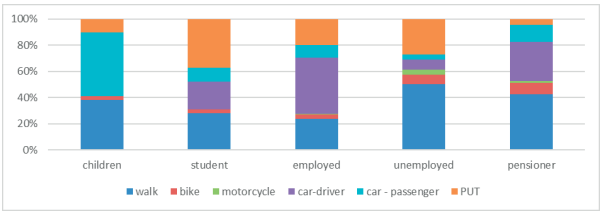

Fig. 5 Modal split in Zilina (Source: Authors)

5. Conclusion

The structure of database of the transport forecast model, especially multimodal, is set by the experience of a model maker. Every step of transport forecast model offers several ways for calculation with different structure of parameters. Therefore, the very large database of the mobility data is necessary for the model solution. The article does not provide detailed information from realised mobility surveys. Authors present only several results of data evaluation from the mobility survey in Zilina.

Acknowledgement

This contribution/publication is the result of the project implementation:

Centre of excellence for systems and services of intelligent transport, ITMS 26220120028 supported by the Research & Development Operational Programme funded by the ERDF.

Európska únia
Európsky fond regionálneho rozvoja

Operačný program VÝSKUM a VÝVOJ

Agentúra Ministerstva školstva, vedy, výskumu a športu SR pre štrukturálne fondy EÚ

"Podporujeme vyskumne aktivity na Slovensku/Projekt je spolufinancovany zo zdrojov EU."

References

[1] WEINER, E.: *Urban Transportation Planning in the United States: An Historical Overview*, p. 26, ISBN 0-275-96329-2
[2] LEVINSON, D., LIU, H., GARRISON, W., DANCZYK, A., CORBETT, M.: *Fundamentals of Transportation/Mode Choice/Solution,* https://upload.wikimedia.org/ wikipedia/commons/7/79/Fundamentals_of_Transportation.pdf.
[3] CELKO, J., DRLICIAK, M., GAVULOVA, A.: Transportation Planning Model. *Communications - Scientific Letters of the University of Zilina*, vol. 9, No. 3, 2007, pp. 28-32. ISSN 1335-4205.
[4] ORTUZAR, J., D., WILLUMSEN, L. G.: *Modelling Transport*, Wiley, p. 23, 2001, ISBN 978-0-471-86110-2 (H/B).
[5] PTV Visum 15, User manual.
[6] RIPKA, I.: *Determination of the Resistance Functions at Prediction of the Inter-Zonal Relations* (in Slovak). Doctoral thesis, University of Zilina, 2011.
[7] JASTRZEBSKU, W. P.: *Volume Delay Functions*, Proc. of 15th Intern. EMME/2 User's Group Conference, Vancouver, B. C., October 2000.
[8] DRLICIAK, M., CELKO, J.: *Social-traffic Data for Mezoscopic Traffic Model*, Proc. of 12th Intern. Conference Reliability and Statistics in Transportation and Communication (RelStat'12), October 2012, Riga, pp. 204-210. ISBN 978-9984-818-49-8.
[9] BARTOVIC, M.: *Models for Division of Transport Work* (in Slovak), Doctoral thesis, University of Zilina, 2009.

https://doi.org/10.26552/com.C.2016.4.61-67

Josef Vican - Peter Kotes - Anna Spiewak - Malgorzata Ulewicz*

DURABILITY OF BRIDGE STRUCTURAL ELEMENTS

Due to environmental actions evocated by the atmospheric behaviour, the material degradation processes are started. The effects of material deterioration due to corrosion cause the loss of cross-sectional or member resistance, but the limit state method does not directly reflect design and verification allowing for failures caused by this influence. The time-variant loss of steel and reinforced concrete moment cross-sectional resistances were computed respecting specific corrosion models to express the time-dependent approximation function taking into account effects of corrosion degradation. The paper presents the general principles of structural elements design for durability based on the limit state concept and their application in the case of moment cross-sectional resistance respecting the effects of corrosion degradation.

Keywords: *Corrosion, corrosion models, cross-sectional resistance, numerical analyses, design for durability.*

1. Introduction

The general approach to durability design is given by the standard [1] but the form of the procedure is not appropriate for design practice. The shortage of information related to the transformation processes of the environmental changes on the environmental actions, which is e.g. corrosion of steel, is the basic reason of this. On the other hand, the corrosion process has random character depending on many random variable parameters, therefore, its mathematical interpretation is somewhat complicated.

Generally, two approaches could be applied to verify durability of structures. The first approach is based on the concept of the design structural service life t_s [2]. The second one is based on the limit state concept design considering effects of environmental actions in the following form

$$P_f(t) = P\{R(t) - E(t) \leq 0\} \leq P_{fd}, \tag{1}$$

where $E(t)$ represents the random variable time-dependent action effects and $R(t)$ is the random variable time-dependent structural member resistance. $E(t)$ and $R(t)$ are functions of random variables X_i, which are also time-dependent functions in relation to the models of material degradations.

2. Corrosion of structural steel and reinforcement

The mathematical description of the theoretical background of corrosion processes by means of differential equations is very complicated. Therefore, the development of semi-empirical models was preferred to apply for practical utilisation respecting the appropriate sophisticated level of approximation. This concept introduces need for systematic research and obtaining data related to the corrosion effects. Therefore, the most corrosion models are based on certain assumptions or results of experimental measurements. If the degradation influences of the corrosion process are known, the possibility of modelling corrosion effects using extrapolation of experimentally gained data exists and a mathematical model can be calibrated by means of them. Even though several long-term experimental investigations were performed in the past and many factors influencing corrosion process are known, the models of time-dependent prediction of corrosion loss are more or less simplified. Regarding random character of many parameters entering the corrosion process, the mathematical statistics and probability theory are the most appropriate approaches to describe the corrosion effects. At present, several corrosion models are known, which should be used to analyse corrosion effects from the viewpoint of structural reliability. The application in bridge engineering is not sufficiently verified, because the developed corrosion models based on laboratory tests are dependent on the modelling of actual environment by means of laboratory equipment. The review

* [1]Josef Vican, [1]Peter Kotes, [2]Anna Spiewak, [2]Malgorzata Ulewicz
[1]Department of Structures and Bridges, Faculty of Civil Engineering, University of Zilina, Slovakia
[2]Faculty of Civil Engineering, Czestochowa University of Technology, Czestochowa, Poland
E-mail: josef.vican@fstav.uniza.sk

Probabilistic structural steel corrosion models — Table 1

Author	Mean value [mm]	Standard deviation [mm]	Distribution
Southwell-Melchers [3]	$0.084t^{0.823}$	$0.056t^{0.823}$	Normal
Frangopol [4]	$0.03207t^{0.5}$	$0.00289t^{0.045}$	Normal
Qin-Cui [5]	$1.67\left[1-\exp(-t/9.15)^{1.97}\right]$	$0.0674\left[1-\exp(-t/0.181)^{0.0294}\right]$	Normal
Guedes- Soares [6]	$d_{corr}(t)=1.5\left(1-e^{(-t/10)}\right)$ and t is time in years		–

of the most applied structural steel corrosion models describing the time-dependent material loss is presented in Table 1.

Examples of application of those corrosion models were introduced e.g. in [2, 7, 8 and 9].

In the case of the reinforcement corrosion, two models are usually used to describe the change of the reinforcement diameter in time due to corrosion taking into account uniform type of corrosion [10 and 11]. The process of degradation due to corrosion consists of two stages - passive stage and active stage. The passive stage means time t_0 from the beginning of the bridge operation, when degradation agents penetrate through the concrete cover up to the level of reinforcement, but reinforcement does not corrode. After that time, the concrete loses its passivation protection and the reinforcement corrosion starts – so called active stage (t-t_0). The process of time-dependent change of reinforcement diameter can be described using following equations

$$\phi(t)=\phi, \text{ for time } t\le t_0, \tag{2a}$$

$$\phi(t)=\phi-0.0232\cdot(t-t_0)\cdot i_{corr}, \text{ for time } t>t_0, \text{ or} \tag{2b}$$

$$\phi(t)=\phi-(t-t_0)\cdot r_{corr}, \text{ for time } t>t_0, \tag{2c}$$

where r_{corr} = corrosion rate [μm/year]; i_{corr} = corrosion current density [μA/cm^2] (1 μA/cm^2 is equal to 11.6 μm/year of corrosion); t = time [years]; t_0 = length of time of passive stage for longitudinal main reinforcement in years.

Formula (2b) was assumed according to [10] and formula (2c) was taken over from [11]. The length of the passive stage t_0 could be calculated according to the simplified model described in many references, e.g. [12 and 13]

$$t_0=\frac{c^2}{2\cdot D} \tag{3}$$

where D = material constant [mm^2.s^{-1}].

3. Moment resistance of steel cross-section considering corrosion

To determine the effect of corrosion on the moment cross-sectional resistance, the parametric study of six welded beams of the I-shape was performed. As random variables, the cross-sectional dimensions b_f, t_f, h_w, t_w were considered together with random variable steel yield strength f_y. The basic statistical parameters of those random variables (mean μ and standard deviation σ) are presented in Table 2 and designations are defined in Fig. 1.

Standard deviations of those cross-sections were determined using standard tolerances a according to standard [14] valid for tolerances of the web height and flange width and in accordance with standard [15] for tolerances of web and flange thickness under assumption that 95 % of values of all realisations of the random variables normally distributed occurs in the interval

$$\langle \mu_x-a;\mu_x+a\rangle \tag{4}$$

Then the standard deviation σ is approximately possible to determine as $2a$. According to above mentioned procedure, the standard deviations of the heights and widths of the investigated cross-sections were estimated.

$$h\le 900\ mm ... \Delta h=\pm 3\ mm ... \sigma_{hw}=1.5\ mm$$
$$h\le 300\ mm ... \Delta b=\pm 3\ mm ... \sigma_{bf}=1.5\ mm$$

Statistical characteristics of the parameters of analysed cross-sections — Table 2

	Cross-section 1		Cross-section 2		Cross-section 3		Cross-section 4		Cross-section 5		Cross-section 6	
	μ	σ	μ	σ	μ	σ	μ	σ	μ	σ	μ	σ
f_y [MPa]	284.44	18.18	284.44	18.18	284.44	18.18	284.44	18.18	284.44	18.18	284.44	18.18
b_f [mm]	150	0.987	150	0.987	175	0.987	175	0.987	200	0.987	200	0.987
t_f [mm]	8	0.165	16	0.197	10	0.165	20	0.197	12	0.165	25	0.263
h_w [mm]	284	0.987	268	0.987	380	0.987	360	0.987	476	0.987	450	0.987
t_w [mm]	6	0.132	6	0.132	8	0.165	8	0.165	8	0.165	8	0.165

Standard deviations of web and flange thickness are presented in Table 3.

The numerical calculation of the time-dependent moment cross-sectional resistance was processed using software Matlab, where the effect of the random variable cross-sectional dimensions and steel yield strength were taken into account. The normally distributed random variables were generated by means of Latin Hypercube Sampling (LHS) for 10 000 samples.

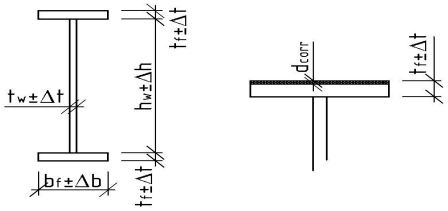

Fig. 1 Cross-sectional dimensions and considered tolerances

Standard deviations of cross-section thickness Table 3

Nominal thickness [mm]	Limit values [mm]		Standard deviation σ_t [mm]
	lower	upper	
$3 \le t < 5$	-0.4	0.8	0.300
$5 \le t < 8$	-0.4	1.1	0.375
$8 \le t < 15$	-0.5	1.2	0.425
$15 \le t < 25$	-0.6	1.3	0.475
$25 \le t < 40$	-0.8	1.4	0.550

The courses of the moment resistances were calculated using all above mentioned corrosion models (see Table 1) for lifetime of 100 years in dependence on the time *t*. Corrosion loss d_{corr} according to individual models from Table 1 was implemented into the calculation by means of flange thickness reduction using formulae $t_{f,red} = t_f - d_{corr}$, where t_f is the flange thickness without corrosion loss. To determine the moment cross-sectional resistance considering the corrosion degradation due to flange corrosion, two approaches were applied.

For plastic time-dependent moment resistance $M_{pl}(t)$, the following equation was used

$$M_{pl} = \left[t_w h_w^2/4 + b_f\left(h_w + t_f - d_{corr}\right)\left(t_f - d_{corr}\right)\right] f_y, \quad (5)$$

while the elastic time-dependent moment resistance was expressed by the equation $M_{el}(t)$

$$M_{el} = \left[\frac{\left(t_w h_w^3/12 + b_f\left(t_f - d_{corr}\right)^3/6 + b_f\left(t_f - d_{corr}\right)\left(h_w + t_f - d_{corr}\right)^2/2\right)}{\left(h_w/2 + t_f - d_{corr}\right)}\right] f_y \quad (6)$$

Time-dependent course of the means of the plastic and elastic moment resistances of the cross-section 1 respecting the corrosion models according Table 1 are presented in Figs. 2 and 3.

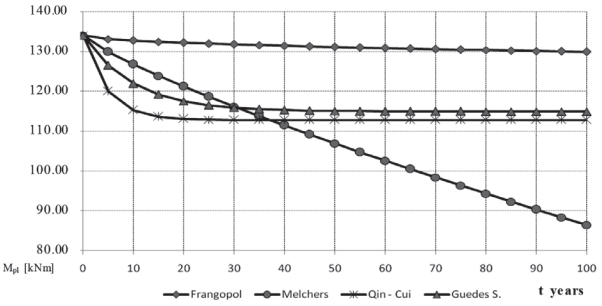

Fig. 2 Plastic cross-sectional moment resistances of cross-section

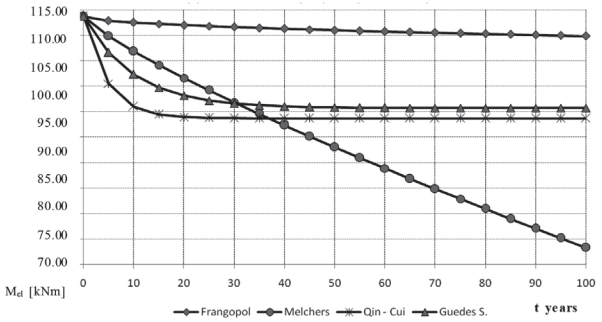

Fig. 3 Elastic cross-sectional moment resistances of cross-section

Time-dependent degradation function *F(t)* was derived as the ratio of the moment resistance *R(t)* of the cross-section degrading in time to the moment resistance R_0 at the beginning of the structure exploitation when it was not affected by the degradation effects

$$F(t) = R(t)/R_0. \quad (7)$$

For further general utilisation, the degradation function *F(t)* was approximated using software MATLAB by means of the following relation

$$F(t) = a \cdot e^{-b \cdot t} + c. \quad (8)$$

The values of the coefficients *a, b, c* determined using approximation proved very good compliance with courses of the approximated and actual degradation functions defined by the coefficient of regression R^2.

Concurrently, it was found that the value of the coefficient *b* was constant for every corrosion model and the values of coefficients *a, c* were changing while those coefficients were nearly independent on the cross-sectional classes defining the application of the plastic or elastic moment resistance.

Therefore, the given model of the prediction of corrosion loss should be applied from the viewpoint of environment type using the "degradation coefficient" *b* and "shape coefficients" *a, c,* by means of which the time-dependent course of the degradation function of the cross-sectional resistance could be calculated for the designed cross-section and its lifetime.

Considering that degradation coefficient *b* represents time-dependent corrosion process depending on relevant corrosion model and when for coefficients *a* and *c* the relation $a + c = 1$ is valid, then the shape coefficient *a* is only necessary to determine according to following equation valid for Frangopol or Melchers corrosion models

$$a = \frac{b_f\left(h_w + t_f - b_0 t^{b_1}\right)\left(t_f - b_0 t^{b_1}\right) - b_f\left(h_w + t_f\right)t_f}{W_{pl,0}\left(e^{-bt} - 1\right)}, \quad (9)$$

where coefficients b_0, b_1 are considered in accordance with the appropriate Frangopol or Melchers corrosion models (0.03207, 0.5 or 0.084, 0.823). The resulting value of the coefficient *a* is the minimum value in time interval within the element lifetime. The approach presented above is relatively complicated for practical utilisation. Therefore, it would be appropriate to process the value of the coefficient *a* in tabular form.

The Qin-Cui and Guedes-Soares corrosion models enable a more simple calculation of the coefficient *a.* Its value could be directly obtained when the corrosion loss determined according to the appropriate model in time $t = \infty$ is taken away from the relation (9). Then, the relation (9) should be adjusted in the following form

$$a = \frac{b_f\left(h_w + t_f - d_{corr,t=\infty}\right)\left(t_f - d_{corr,t=\infty}\right) - b_f\left(h_w + t_f\right)t_f}{W_{pl,0}\left(e^{-bt} - 1\right)}. \quad (10)$$

The value of $d_{corr,\ t=\infty}$ =1.67 mm for Qin-Cui model and $d_{corr,\ t=\infty}$ =1.50 mm for Guedes-Soares corrosion model should be substituted into the equation (10). To prove the correctness of the assumptions related to the coefficients *a, b* and derivation of the general solution, the new parametric study was worked up for 2500 beams having welded I-shaped cross-section, whose cross-sectional characteristics and yield strength were considered as random variables.

It follows from the new parametric study that the degradation coefficient *b* has the constant value for given corrosion model and values of coefficients *a, c* were only changing. Degradation coefficient *b* is dependent on the relevant corrosion model and also on the environmental condition. It is also clear that calculation of the shape coefficient *a* could be simplified using the following relation

$$a = \frac{b_f\left(2t_f + h_w\right)}{W_{pl,0}}\alpha_{\text{corr.model}}, \quad (11)$$

where $\alpha_{\text{corr.model}}$ introduces the corrosion coefficient given in Table 4 according to the appropriate corrosion model.

Final values of the degradation and corrosion coefficients b and $\alpha_{\text{corr.model}}$ Table 4

Corrosion model	Coefficient	
	b	$\alpha_{\text{corr.model}}$
Frangopol	0.0194	3.278E-04
Melchers	0.0055	8.460E-03
Qin-Cui	0.2158	1.655E-03
Guedes-Soares	0.1003	1.490E-03

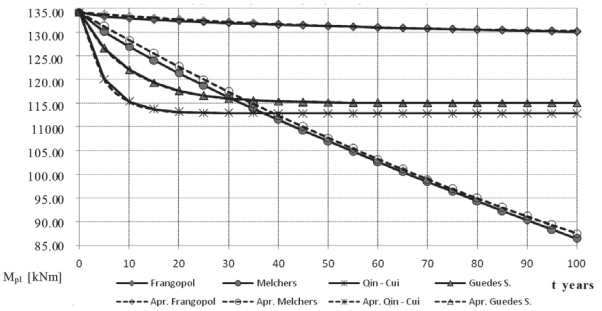

Fig. 4 Comparison of numerically obtained time-dependent course of plastic moment resistance to the resistance calculated according to proposed analytical relation (12)

Finally, the time-dependent moment resistance of I-shaped cross-section with degradation of the both flanges could be determined according to following equation

$$M_{Rd}(t) = M_{Rd,t=0}\left[1 + a\left(e^{-bt} - 1\right)\right], \quad (12)$$

where value of the coefficient *a* should be calculated using equation (11) and degradation coefficients *b*, $\alpha_{\text{corr.model}}$ should be considered in accordance with Table 4.The comparison of the numerically determined courses of the plastic moment resistance of the cross-section 1 to calculations according to relation (12) for individual corrosion models is introduced in Fig. 4. The very good compliance of the analytical model with numerical analyses can be identified.

4. Moment resistance of reinforced concrete cross-section considering reinforcement corrosion

Concrete structures shall be adequately safe against failure and must also exhibit satisfactory performance in service. The internal forces as bending moments *M* and shear forces *V* are considered as the relevant structural response to actions. Vertical bending seems to be the main action effect determining the cross-sectional dimensions and arrangement of the longitudinal reinforcement, which are firstly contemplated to provide the necessary moment resistance.

Bending limit state comes into being when the limit strain is achieved at least in one of the materials (concrete in compression or reinforcement in tension) [16 and 17]. In the case of girder bridges, the bridge deck is always connected with beams, therefore, the cross-section is considered as flanged beam (cross-section of the T shape). The time-dependent moment resistance $M_{Rd}(t)$ of the reinforced concrete flanged beam is given in accordance with standard [18] by formula

$$M_{Rd}(t) = F_s(t) \cdot z(t) = A_{s1}(t) \cdot f_{yd} \cdot z(t) = A_{s1}(t) \cdot f_{yd} \cdot \left(\left[h - c - \frac{\phi(t)}{2} \right] - \frac{A_{s1}(t) \cdot f_{yd}}{2 \cdot b_{eff} \cdot f_{cd}} \right) \quad (13)$$

where $F_s(t)$ is the time-dependent force in tensioned reinforcement changed due to corrosion, $z(t)$ is the time-dependent lever of internal forces, f_{yd} is the design steel yield strength, f_{cd} is the design compressive strength of concrete, h is the cross-sectional height, h_s is the height of slab (beam flange), b is the beam cross-sectional width, b_{eff} is the effective cross-sectional width, c is the concrete cover thickness, n is the number of longitudinal reinforcements in cross-section, $A_{s1}(t)$ is the time-dependent reinforcement cross-sectional area changed due to reinforcement corrosion and $\varphi(t)$ is the longitudinal reinforcement diameter (see Fig. 5).

As it was presented in [19 and 20], equation (13) could be modified into its final form for moment resistance depending only on time

$$M_{Rd}(t) = M_{Rd}(0) + k_1 \cdot (t - t_0) + k_2 \cdot (t - t_0)^2 + + k_3 \cdot (t - t_0)^3 + k_4 \cdot (t - t_0)^4 \quad (14)$$

where k_1, k_2, k_3, k_4 are the parameters depending on material and geometrical characteristics with their physical significance

$$k_4 = A \cdot 0.0232^4 \cdot i_{corr}^4, \text{ or } k_4 = A \cdot r_{corr}^4, \quad (15a,b)$$

$$k_3 = (4 \cdot A \cdot \phi + B) \cdot 0.0232^3 \cdot i_{corr}^3, \text{ or } k_3 = (4 \cdot A \cdot \phi + B) \cdot r_{corr}^3, \quad (16a,b)$$

$$k_2 = (6 \cdot A \cdot \phi^2 + 3 \cdot B \cdot \phi + C) \cdot 0.0232^2 \cdot i_{corr}^2, \text{ or } k_2 = (6 \cdot A \cdot \phi^2 + 3 \cdot B \cdot \phi + C) \cdot r_{corr}^2, \quad (17a,b)$$

$$k_1 = (4 \cdot A \cdot \phi^3 + 3 \cdot B \cdot \phi^2 + 2 \cdot C \cdot \phi) \cdot 0.0232 \cdot i_{corr}, \text{ or} \quad (18a)$$

$$k_1 = (4 \cdot A \cdot \phi^3 + 3 \cdot B \cdot \phi^2 + 2 \cdot C \cdot \phi) \cdot r_{corr} \quad (18b)$$

where *A, B, C* are the time-independent parameters

$$A = -\frac{\pi^2 \cdot n^2 \cdot f_{yd}^2}{32 \cdot b_{eff} \cdot f_{cd}} \quad (19)$$

$$B = -\frac{\pi \cdot n \cdot f_{yd}}{8} \quad (20)$$

$$C = \frac{\pi \cdot n \cdot f_{yd} \cdot (h - c)}{4} \quad (21)$$

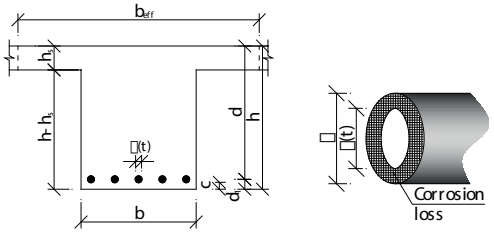

Fig. 5 Flanged beam - denotation

The parametric study was performed in accordance with the approach described above.

5. Experimental application

The influence of longitudinal reinforcement corrosion on moment resistance of the bridge structural element was investigated. The reinforced concrete flanged beam subjected to bending with material and geometrical characteristics given in Table 5 obtained from measurement on the real bridge structure was used.

Material characteristics used in parametric study Table 5

Material characteristics	Notation	Unit	Value
Strength of concrete in compression	f_{cd}	N.mm^2	20.0
Yield strength of reinforcement	f_{yd}	N.mm^2	179.23
Height of cross-section	h	m	0.837
Width of cross-section	b	m	0.322
Effective width of cross-section	b_{eff}	m	1.545
Concrete cover thickness - main	c	mm	29.6
Concrete cover thickness - stirrups	c_s	mm	15.6
Number of bars (reinforcement)	n	pcs	7
Slab height	h_s	m	0.186
Bar diameter – main longitudinal	φ	m	0.030
Bar diameter - stirrups	$φ_s$	m	0.014
Corrosion current density	i_{corr}	μA/cm^2	0.5
			1.0
			3.0
			5.0
Material constant	D	mm^2.s^{-1}	$4.82 \cdot 10^{-7}$

From the results of the bridge diagnostics follows that the concrete of C30/37 was used and the beams are reinforced with the rebar of A (10210) in two layers (5ϕ in the lower layer and 2ϕ in the upper layer). The design lifetime for bridge structural element is equal to T_d = 100 years. Firstly, the length of time of passive stage t_0 for longitudinal reinforcement was calculated using formula (3). Then, the active stage (t-t_0) was calculated according to formula (2b) in the parametric study. Due to the parametric study, various corrosion current densities (i_{corr}) were considered. The influence of the corrosion on the time-dependent moment resistance of the reinforced concrete flanged beam is shown in Fig. 6.

The length of the passive stage for main longitudinal reinforcement was calculated as t_0 = 28.8 years (for D = $4.82 \cdot 10^{-7}$ mm^2s^{-1}). The basic value of the moment resistance at time t = 0 year is equal to $M_{Rd}(t=0)$ = 689.621 kNm. Hypothetically, the decrease of moment resistance during the whole lifetime was 5.3 % in the case of i_{corr} = 0.50 μA/cm² (small aggressive environment), 10.4 % for i_{corr} = 1.00 μA/cm² (average aggressive environment), but as much as 29.7 % for i_{corr} = 3.00 μA/cm² (very aggressive environment in Slovakia) or 46.7 % for i_{corr} = 5.00 μA/cm² (very aggressive environment recommended for coastal areas).

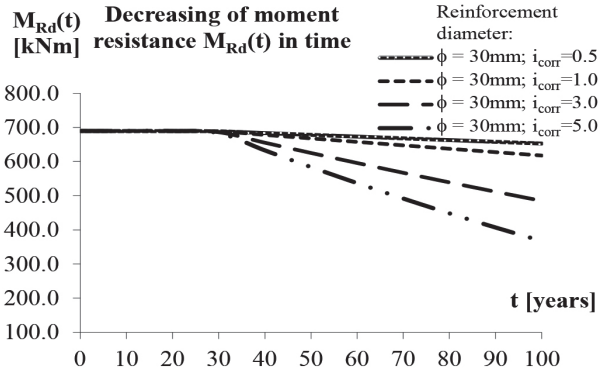

Fig. 6 Change of moment resistance $M_{Rd}(t)$ in time of reinforced concrete beam due to reinforcement corrosion

Diagnostics of the investigated bridge structural element was performed in 2006. At that time, the bridge was approximately 65 years old. The corrosion caused the rebar diameter loss from the initial value 30 mm to average value 29.37 mm (the minimal measured value was 28.7 mm). Now, it is possible to calculate backwards from the formulas (2b, 2c) the length of time, i.e. in how many years reinforcement would corrod from the basic diameter of ϕ = 30 mm to average value ϕ = 29.37 mm depending on environmental aggressiveness (i_{corr}). That length of time is called an active stage. The formulas (2b) or (2c) are changed after modification to

$$t = \frac{\phi - \phi(t)}{0.0232 \cdot i_{corr}} + t_0, \text{ or } t = \frac{\phi - \phi(t)}{r_{corr}} + t_0. \quad (22a, 22b)$$

Using formula (22a) and if t_0 = 0, the reinforcement diameter changes due to corrosion from the basic diameter ϕ = 30 mm to the average value ϕ = 29.37 mm would be 54.31 years (for i_{corr} = 0.50 μA/cm²), 27.16 years (for i_{corr} = 1.0 μA/cm²), 9.05 years (for i_{corr} = 3.0 μA/cm²), or 5.43 years (for i_{corr} = 5.0 μA/cm²).

The corresponding length of the passive stage t_0 can be obtained by modification of formulas (22a, 22b), if t is equal to age of the bridge (t = 65 years). The shortest length of the passive stage was obtained for i_{corr} = 0.50 μA/cm² and was equal to t_0 = 10.69 years. The lengths of time of passive stages are equal to t_0 = 37.84 years for i_{corr} = 1.00 μA/cm², t_0 = 55.95 years for i_{corr} = 3.00 μA/cm² and t_0 = 59.57 years for i_{corr} = 5.00 μA/cm². Now, it is possible to predict the moment resistance change of reinforced concrete flanged beam up to the end of design lifetime T_d = 100 years. The results are shown in Fig. 7.

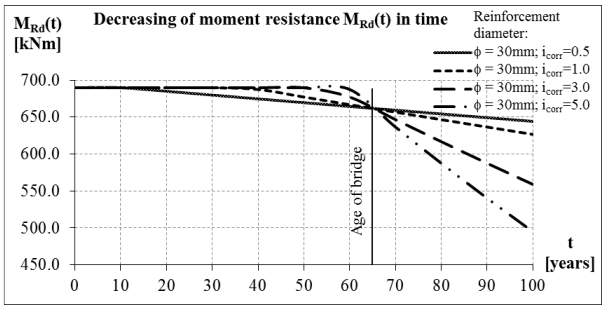

Fig. 7 Prediction of moment resistance change $M_{Rd}(t)$ in time of the reinforced concrete bridge beam due to reinforcement corrosion

6. Conclusions

The paper presents the results of the research concerning the influence of the corrosion of the structural steel or reinforcement on the time-dependent moment cross-sectional resistances of I-shaped cross-section and also on the cross-section of the flanged bridge beam. Two approaches are introduced related to the expressing the effect of corrosion on the moment cross-sectional resistance. The first approach is based on the assumption taking into account the effect of corrosion of structural steel using approximated degradation function $F(t)$ and multiple it by the moment cross-sectional resistance in time t =0 to obtain the actual moment resistance in time t respecting the known corrosion models. The second approach was derived to allow for effect of reinforcement corrosion on the moment cross-sectional resistance of reinforced concrete flange beam respecting the known corrosion models valid for reinforcement corrosion. It follows from result analysis that the reinforcement corrosion has significant influence on change of resistances in time.

Acknowledgement

The research was supported by the European Regional Development Fund and the Slovak state budget for the project "Research Centre of University of Zilina", ITMS 26220220183 and by the Slovak Research and Development Agency under contract No. APVV-14-0772 and also by the project SK-PL-2015-0004 in frame of bilateral cooperation.

References

[1] ISO DIS 13823: *General Principles on the Design of Structures for Durability*. ISO/TC 98/SC 2.

[2] VICAN, J., SYKORA, M.: Design of Compression Members for Durability. *Communications - Scientific Letters of University of Zilina*, vol. 11, No. 4, pp. 9-15.

[3] MELCHERS, R. E.: Corrosion Uncertainty Modelling for Steel Structures. *J. of Constructional Steel Research*, Elsevier, 1999.

[4] AKGUL, F., FRANGOPOL, D., M.: Lifetime Performance Analysis of Existing Steel Girder Bridge Superstructures. *J. of Structural Engineering*, v. 130, No. 12, pp. 1875-1888.

[5] QIN, S., CUI, W.: Effect of Corrosion Models on the Time-Dependent Reliability of Steel Plated Elements, *Marine Structures*, Elsevier, 2003.

[6] GUEDES SOARES, C., GARBATOV, Y.: Reliability of Maintained, Corrosion Protected Plates Subjected to Non-Linear Corrosion and Compressive Loads, *Marine Structures*, Elsevier, 1999.

[7] VICAN, J., KURCIK, F.: *Corrosion Effect on Truss Bridge Compression Chord Reliability*. Intern. Conference "Bridges in Danube Basin 2007", Budapest 2007, pp. 449-460.

[8] VICAN, J., SYKORA, M.: Numerical Analysis of the Bridge Orthotropic Deck Time-Dependent Resistance, *Communications - Scientific letters of the University of Zilina*, vol. 15, No. 3, pp.112-118, ISSN 1335-4205.

[9] KVOCAK, V., VARGOVA, R., BEKE, P., TERPAKOVA, E.: Effects of Atmospheric Corrosion on the Car Park Roof Structure, *Communications - Scientific letters of the University of Zilina*, vol. 14, No. 1, pp. 80-87, ISSN 1335-4205.

[10] ANDRADE, C., SARRIA, J., ALONSO, C.: *Corrosion Rate Field Monitoring of Post-Tensioned Tendons in Contact with Chlorides.* Durability of building materials and components, Stockholm, 1996, pp. 959-967.

[11] THOFT-CHRISTENSEN, P.: *A Reliability Based Expert System for Bridge Maintenance*, Tekno Vision Conference, 1992, Denmark.

[12] BILCIK, J.: Prediction of Service Life with regard to Reinforcement Corrosion, *Slovak J. of Civil Engineering,* vol. 2-3, 1998, pp.34-38.

[13] Ceb-Fip Model Code 2010, 2011. Special Activity Group 5, 653 p.

[14] STN EN 1090-2 + A1: *Execution of Steel Structures and Aluminium Structures - Part 2: Technical Requirements for Steel Structures.* Slovak Office for Standards, Metrology and Testing, Bratislava, 2012.

[15] STN EN 10029: Hot-rolled steel plates 3 mm thick or above - Tolerances on dimensions and shape. Slovak Office for Standards, Metrology and Testing, Bratislava, 2011.

[16] HALVONIK, J., BENKO, V., HUBOVA, O., SOKOL, M., STUJBEROVÁ, M., BORZOVIC, V.: *Design of Bearing Structures of Constructions. Basis of Design and Actions,* 1st ed. (in Slovak), STU : SvF : Bratislava, 2009. 144 p.

[17] BENKO, V., FILLO, L., KENDICKY, P., KNAPCOVA, V.: *Experimental and Numerical Analysis of Concrete Slender Columns by Stability Failure,* Applied Mechanics and Materials : selected, peer reviewed papers from the Engineering Mechanics 2015, Svratka, 11. - 14. 5. 2015, vol. 821, 2016, pp. 747-752.

[18] STN EN 1992-2: Eurocode 2: *Design of Concrete Structures - Part 2: Concrete Bridges, Design and Detailing Rules + National Annex*. Slovak Office for Standards, Metrology and Testing, Bratislava, 2007.

[19] KOTES, P., VICAN, J., IVASKOVA, M.: Influence of Reinforcement Corrosion on Reliability and Remaining Lifetime of RC Bridges. *Materials Science Forum*, 2015, ISSN: 1662-9752, vol. 844, pp. 89-96.

[20] KOTES, P., DUBALA, K., SELEJDAK, J.: *Influence of Reinforcement Corrosion on Moment Load-Carrying Capacity of RC Bridge Girder Subjected To Bending*. Proc. of the 11th European conference of young researchers and scientists "Transcom 2015", University of Zilina, June 22-24, pp. 52-57.

https://doi.org/10.26552/com.C.2016.4.68-76

Pavol Durica - Peter Juras - Daniela Staffenova - Jan Rybarik*

LIGHTWEIGHT WOOD-BASED WALL: THE LONG-TIME EVALUATION OF HEAT-AIR-MOISTURE TRANSPORT

Five lightweight timber-frame wall sections with various thermal insulations and outdoor coating colors have been exposed to real outdoor boundary climate conditions since 2010. The indoor boundary conditions were set as constant. This article compares measured temperatures inside individual sections of the wall fragment to non-steady Heat-Air-Moisture (HAM) simulations in WUFI and ESP-r. The wall sections differ from each other in used thermal insulation: mineral wool, glass wool and hemp. Another difference is in color of outdoor surface: yellow, white and dark grey. Some wall compositions are equipped with vapor retarder. Each section has attached some thermal sensors.

Keywords: *Platform frame, wood, experiment, HAM, moisture, thermal conductivity.*

1. Introduction

Slovakia has a great potential for the construction of wooden buildings due to high forest coverage and wood availability. The number of wooden houses increases every year and has growth from 1 % to 10 % in around 5 years [1], but it is still low in comparison to Austria, Germany or Scandinavia (40 - 80 %). The natural conditions and increasing energy, ecology and economy requirements [2] created the need for long-term evaluation of different wooden structures, which are represented in this five sections of the experimental wall. The sandwich exterior wall fragment was designed and realized in all alternatives in the thermal-technical standard for passive buildings [2 and 3]. Comparing to standard structures, it differs from them in the inverse range of layers. The thermal-accumulating layer is situated from the exterior and the thermal-insulating layer is situated from the interior side of the wall fragment, so as we know it from some layer compositions used in Nordic countries [1].

2. Construction of the laboratory and experimental wall

Construction of the Laboratory Centre of the Department of Civil Engineering and Urban Planning started in 2010. Process of construction is shown in Figs. 1-5. The laboratory is constructed as a pavilion type and consists of two climatic chambers and office with recording equipment (Fig. 6). The chambers have controlled indoor environment (AC unit), which is set to maintain 20 °C and 50 % relative humidity at all the time. From the exterior, test wall sections were exposed to real boundary conditions of the external climate.

Later, since 2013, the laboratory center has been equipped also with detached experimental weather station, which records all necessary climatic parameters [4]. One climatic chamber has built-in lightweight wood-based experimental wall fragment, which consists of five different sections, the other one has three windows [5].

Fig. 1 Beginning of construction work on the laboratory - prepared opening for wooden frame (April 2010)

Dimensions of monitored experimental wall fragment are 3670 x 2670 mm and it consists of 5 sections (Fig. 7). They differ

* **Pavol Durica, Peter Juras, Daniela Staffenova, Jan Rybarik**
Department of Building Engineering and Urban Planning, Faculty of Civil Engineering,University of Zilina, Slovakia
E-mail: pavol.durica@fstav.uniza.sk

from each other in material composition and surface coloring. Sections 1, 2, 4 and 5 are diffusional closed constructions and the third section is made as a diffusional open construction (Fig. 8). Detailed composition of the sections is shown in the Table 1. Used material properties are summarized in the Table 2. All compositions had to meet the requirements of Slovak standard STN 730540:2012, which is U = 0.15 W/m^2.K after year 2020 (zero energy building). The main device for temperature measuring in tested sections is Ahlborn Almemo 5690-2M used as a datalogger with connected Ahlborn thermocouples (totally 22 pieces), which have deviation up to 0.4 K [6]. Some of the wall sections were later additionally equipped with combined temperature/relative humidity HUMI sensors and Raspberry Pi as a datalogger [7]. The thermocouples are generally located on the exterior surface, under the coating, on the internal surface of MDF board and on internal surface of the filling thermal insulation. Several sensors are located also on the wooden columns (Fig. 8). More detailed description is mentioned in [1 and 7]. The temperatures were recorded in 30 minutes time periods.

Fig. 2 View at wooden frame (May 2010)

Fig. 3 Montage of MDF board (September 2010)

Fig. 4 Montage of thermocouples on the wooden columns from inside (November 2010)

Fig. 5 Thermal insulation prior fitting vapor barrier (January 2011)

Fig. 6 View at data recording device ALMEMO 5690-2M in the office next to the laboratory rooms (May 2011)

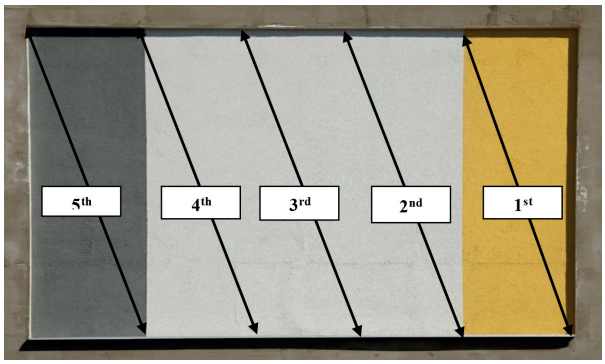

Fig. 7 Exterior view at the experimental wall fragment (3670 x 2760 mm) with marked five different sections (works were finished in November 2010)

The parameters of external environment were recorded by the detached experimental weather station at the same time step period (30 minutes) and captured were: temperature and relative humidity of external air, wind velocity and direction, the intensity of global solar radiation on a horizontal plane and the vertical plane identical to the orientation of the test wall fragment.

Evaluation of the wall structure

After the construction of the wall fragment and laboratory climatic chamber there were made several measurements made [1]. The outer surface temperatures were also measured with thermal camera several times. In the Fig. 10 is image from March

Composition of five sections within the experimental wall fragment — Table 1

Thickness [mm]	4	100	220	-	12
1st section	Yellow coating	MDF board	Glass wool	Vapor barrier	OSB board
2nd section	White coating				
3rd section			Hemp	-	
4th section			Mineral wool	Vapor retarder with changeable permeability	
5th section	Grey coating				

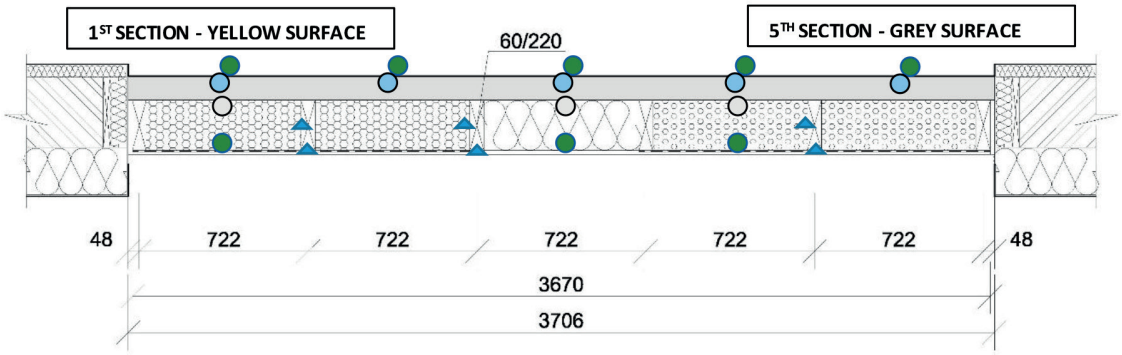

Fig. 8 Sketch showing measuring points in the construction of wall sections. Thermocouples: 1 - the exterior surface, 2 - under the coating, 3 - under the thermal insulation, 4 - under the infill thermal insulation, 5 - in the middle of the column, 6 - the inner surface of the column

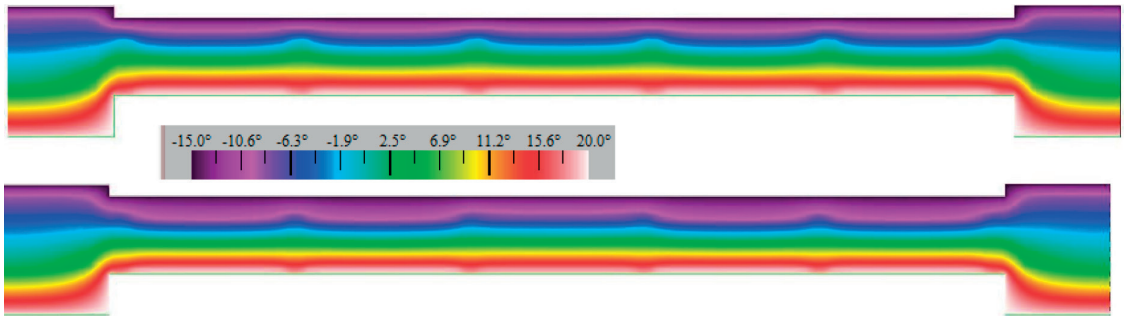

Fig. 9 Isotherm in the experimental wall fragment for boundary conditions $\theta_{a,i}$ = 20 °C, $\theta_{a,e}$ = - 15 °C in finite element simulator Therm v 5.2; Top: with usage of design thermal conductivities for materials (Table 2), bottom for measured conductivities in May 2015[8]; Noticeable is the decrease by MDF board across the wall and in 3rd section with Hemp

Material properties of used materials in the experimental wall Table 2

MATERIAL	DESCRIPTION	d	λ	$\lambda_{current}$ [8]	ρ	c	μ
		m	W/(m.K)	W/(m.K)	kg/m³	J/(kg.K)	-
External plaster	StoSilco	0.004	0.7	0.7	1900	720	40
Woodfiber MDF board	HofaTex SysTherm	0.1	0.045	0.10	210	2100	5
Stone wool insulation (MW)	Rockwool MW W	0.22	0.037	0.039	40	840	1
Hemp insulation	Cannabest Plus	0.22	0.040	0.039	36	1200	1.9
Glass wool insulation (GW)	Isover ENV	0.22	0.035	0.063	24	840	1
Vapour barrier with changeable diffusion resistance	Isover Vario KM Duplex	0.0004	1	-	2000	1470	90000
Vapour barrier	PE foil	0.0002	0.4	0.14	400	1470	10200
OSB board 3	OSB 3 MUPF/PMDI	0.012	0.14		700	2100	240

2011 after completing the thermal insulation layers. Exterior air temperature was -10 °C at around 4:00AM during measurement. In the figure are also shown the measured temperatures from thermocouples on the surface with the values obtained with the thermal camera, which showed very good match.

Long-term temperature measurement

To show long-term temperature measurement results in different layers of the wall fragment, a one week measurement during the winter season [9] from 27-01-2012 to 02-02-2012 was chosen ($\theta_{ae,\ min}$ = -18.9 °C, $\theta_{ae,\ max}$ = 4.6 °C). Outer surface temperatures of each section are shown in Fig. 11. Different temperatures in the structure were affected not only by its material composition, but also by natural influences of the environment as well as by the different light absorption and reflectance caused by various coating colors. The highest surface temperatures were measured on the dark coating. Such a coating has the lowest reflectivity of solar radiation and absorbs most short wave solar radiation. Maximum during clear days was above 48 °C, and higher by about 30 °C when we compared it to other surfaces. From sections with white coating, section no. 3 had the lowest surface temperature which is caused by the higher heat flow. During nights of the whole reference week, the surface temperature in all sections was lower than the ambient air temperature due to the cold sky radiation. At this time, the minimum temperatures were recorded mainly in the 4th section with white finish, and 1st section with yellow finish [9]. Significant influence of deviation of external conditions at the temperature course in the structure was noticed in monitored positions closest to the interior under the additional thermal insulation MDF board Hofatex. On the contact of the infill insulation with OSB board it was observed more significant impact of the technology of internal environment (AC unit used to maintain the indoor climate).

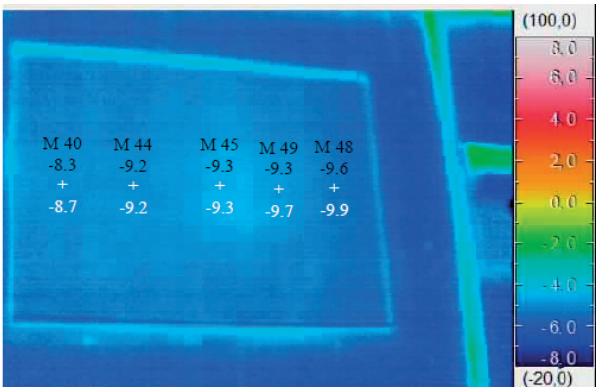

Fig. 10 Results from thermal camera NEC TH7700 measured on 09-03-2011, $\theta_{a,e}$ = -10 °C; black values are from thermocouples on the surface, white are measured with thermal camera

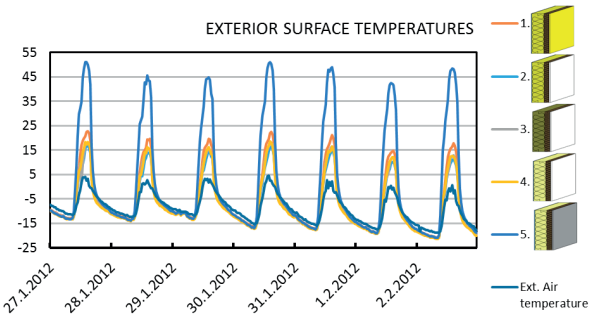

Fig. 11 Temperature courses at the exterior surface of the structure are from 27-01-2012 to 02-02-2012, surface finish coloring yellow (1st), white (2nd, 3rd and 4th) and dark grey (5th) [9]

During the winter period, the mechanism of heating and cooling process had positive effect on heat loss of the building, because minimum temperatures under the additional insulating layer and therefore the largest cooling of storage layer was thank to the thermal inertia and with it connected phase shift of the temperature oscillation recorded in time, when the experimental wall fragment was exposed to the solar radiation from the exterior side and therefore its energy was accumulated [1, 2 and 9].

Thermal conductivity measurements during exploitation

There were conducted measurements of thermal conductivity in the materials with use of Isomet 2104. By finding out properties of individual thermal insulations after 4 years from assembling it was observed that by 24-hour testing of thermal conductivity coefficient [10 and 11] of fibrous insulations this changed during the day only minimal or insignificantly (Table 3). By 24-hour testing in the additional insulation MDF board Hofatex, there were monitored significant changes in all sections, mostly in the 5th section with dark grey finish.

More significant changes were compared to the design or by manufacturer measured values. Based on measurements of water content in insulating materials, the following conclusions can be stated: The measured values of moisture in sections no. 1, 4 and 5 have no significant impact on the thermal conductivity of glass wool and mineral wool (infill insulations). The moisture of glass wool was measured 1.09 % and the thermal conductivity was measured max. 0.039 W/(m.K). The moisture of mineral wool was measured 3.47 % and the thermal conductivity 0.0402 W/(m.K), which are values close to the design values stated in [8]. These sections were constructed as diffusional closed constructions. On the other hand, moisture in section no. 3 has a big impact on the thermal conductivity of hemp insulation (11.63 %), because the design thermal conductivity of hemp insulation is 0.04 and the measured one is 0.0637 W/(m.K). That section was constructed as a diffusional open construction. The moisture has a big impact also on the thermal conductivity of MDF boards (moisture max. 13.42 %), the design value is 0.049 W/(m.K) (Table 2), but the maximal measured value is 0.129 W/(m.K) (Table 3).

Color of the façade surface has an impact on moisture content in MDF board but not on the individual layers of insulation between wooden columns. The moisture in MDF boards under the dark grey plaster was on average 27 % lower than under the white plaster. Also moisture under the yellow plaster was lower but only an average of 9 % [9].

Measured values of moisture in 3rd and 4th section are nearly the same, which can be influenced by the moisture transport from the wetter 3rd section, because the MDF board is not separated between the individual sections.

The measured thermal conductivities have crucial impact on the thermal resistance of MDF board and hemp insulation in 3rd section. The difference in temperatures in the wall composition is shown in Fig. 9, calculated with measured and designed values in Therm software. Also comparisons in *U*-values and thermal resistance are summarized in Table 4. The *U*-value is lower in average about 20 % with exception in the 3rd section, where the *U*-value is lower by 42 %, which is a crucial finding.

Moisture measurements during exploitation

After three years of exploitation, in autumn 2014 (before the cold period of the year) and in spring 2015 (after the cold season of the year), the water content in thermal insulations, was measured. Mass moisture of MDF fibreboard and infill insulations was determined by the gravimetric method (STN EN ISO 12570/A1); mass moisture of wooden support poles by the resistance meter Greisinger GMH 3850. Gravimetric method is based on weighing wet and dry samples. Figure 13 shows the collection of samples for the gravimetric test, in this case from 5th section. Three samples were taken from each layer – the bottom, middle and top. From each section 9 samples were taken (1st, 2nd layer of infill insulation and MDF board). The difference between the positions in the layer was not significant. After being collected,

Measured thermal conductivities in the wall fragment materials. No measurement made in 2nd section — Table 3

	1st section			3rd section			4th section			5th section		
	thermal conductivity coefficient λ [W/(m.K)]											
Area of Insulation	min	max	Δ	min	max	Δ	min	max	Δ	min	max	Δ
infill insulation	0.039	0.039	0.001	0.062	0.064	0.002	0.038	0.040	0.003	0.038	0.039	0.001
MDF insulation	0.104	0.112	0.007	0.102	0.108	0.006	0.106	0.121	0.015	0.099	0.129	0.029

Comparison of designed and current thermal resistance *R* and *U*-value based on the thermal conductivity measurement (in the STN 73 0540:2012 is required 0.15 W/(m^2.K) after year 2020) — Table 4

	$R_{HOF,D}$	$R_{INS,D}$	$R_{HOF,C}$	$R_{INS,C}$	U_d	U_c	ΔU [%]
1st section	2.22	5.95	1.00	5.64	0.122	0.151	**18.70**
2nd section	2.22	6.29	1.00	5.64	0.118	0.151	**21.94**
3rd section	2.22	5.50	1.00	3.49	0.129	0.223	**41.83**
4th section	2.22	6.29	1.00	5.64	0.118	0.151	**21.94**
5th section	2.22	6.29	1.00	5.64	0.118	0.151	**21.94**

the samples were put into a hermetic and vapor proof package and brought to the lab. The samples were weighed precisely before being placed into the drying oven. The drying oven Kendro-Heraeus was used for drying and the electronic scale Radwag PS 6000/C/2 was used for weighing (with an accuracy of 0.01 g). The drying temperature for insulating materials is 105 °C. After 24 hours of drying, samples were weighed, and drying and weighting cycles were repeated in 6 hour intervals. After reaching the constant weight of the samples, the cycle was completed and the values recorded. The difference in weight was equal to the amount of evaporated water.

Measurements of water content in sections 1, 4, 5 (in 2nd there were no measurements performed, because optical cables are used for the measurement and it is not possible to collect samples from it) in fibrous insulations confirmed constant low content [8] in both measured time periods. On the contrary, the increased water content was noticed in hemp layer with diffusional open compositions. The mass water content at the wool board oscillated in a range of 8.50 % to 13.42 %, while lower values were reached under darker surfaces (Fig. 14 - 1st and 5th). The highest moisture was recorded again in the part of the diffusional open construction (3rd).

By the wooden columns, the mass water content oscillated in a range of 10.00 to 15.20 %, which are appreciative values for wood (columns are numbered as in Fig. 12, from the left to the right). Lower values were obtained at fronts of the columns from the interior side as at their sides – measured in the middle of columns (Fig. 13). With the same methodology the measurement was repeated in May 2015 after the cold period of the year. The comparisons of the measured values are shown in Fig. 13.

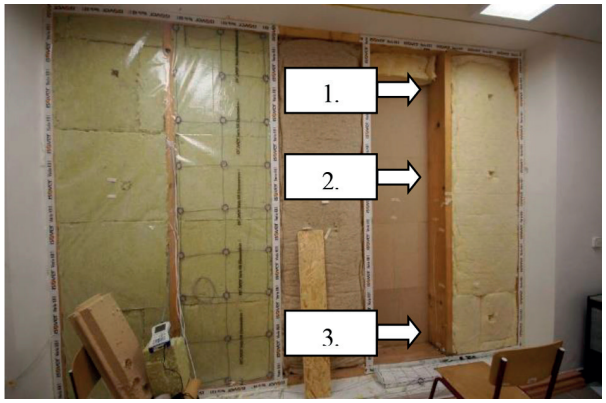

Fig. 12 Tested wall fragment from the interior during collecting of samples for the 5th section (in 2nd section optic cables are visible, we were not allowed to collect samples and do other measurements)

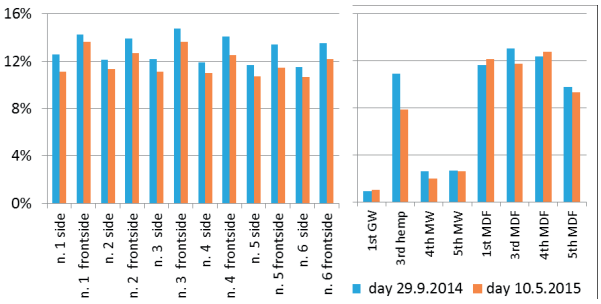

Fig. 13 Water content in wooden columns (left) and thermal insulations (right) in the wall composition

HAM simulation in WUFI and ESP-r

Two simulations were made. First were compared the measured temperatures through the wall fragments with calculation of temperatures with ESP-r, which is available via GPL-license. It has been the subject of sustained developments since 1974 with the objective of simulating the building performance and in this case uses finite volume method [12] and WUFI Pro [13], which also allows to calculate moisture transport and measured mass moisture from previous chapter was used. WUFI Pro allows calculation in multi-layer building components exposed to the natural weather of the transient coupled one dimensional heat and moisture transport described by Kunzel [14] (Eq. 1 and 2):

$$\frac{\partial H}{\partial \theta}\frac{\partial \theta}{\partial t} = \frac{\partial}{\partial x}\left(\lambda \frac{\partial \theta}{\partial x}\right) + h_v \frac{\partial}{\partial x}\left(\frac{\delta}{\mu}\frac{\partial p}{\partial x}\right) \quad (1)$$

$$\rho w \frac{\partial u}{\partial \varphi}\frac{\partial \varphi}{\partial t} = \frac{\partial}{\partial x}\left(p_w D_w \frac{\partial w}{\partial \varphi}\frac{\partial \varphi}{\partial x}\right) + \frac{\partial}{\partial x}\left(\frac{\delta}{\mu}\frac{\partial p}{\partial x}\right) \quad (2)$$

- D_w is liquid transport coefficient[m²/s],
- H is enthalpy of the material [J/m³],
- h_v is enthalpy of the water [J/kg],
- p is partial pressure of water vapor [Pa],
- w is water volume in component [m³/m³],
- δ_A is water vapor diffusion coefficient in air [kg/(m.s.Pa)],
- θ is temperature [°C],
- λ is thermal conductivity coefficient [W/(m.K)],
- μ is water vapor diffusion resistance factor [-],
- ρ_w is bulk density of water [kg/m³],
- φ is relative air humidity [-].

It is based on the newest findings regarding vapor diffusion and liquid transport in building materials and it has been validated by detailed comparison with measurements obtained in the laboratory and on outdoor testing field [15].

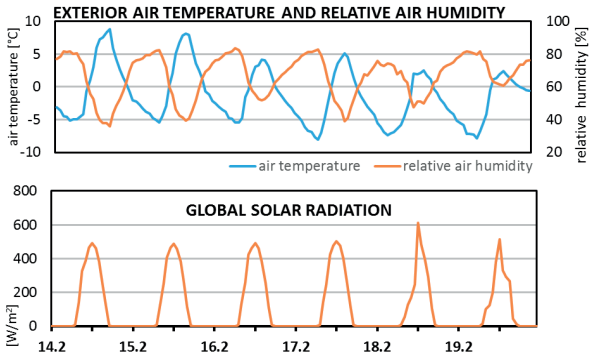

Fig. 14 Daily courses of air temperature, relative humidity (up) and global solar radiation (down) between the 14-02-2015 and the 19-02-2015 obtained by the detached experimental weather station [16]

As a basis for climate data, the measured data from the weather station were served. Different combinations of material properties from manufacturer`s data sheets were used and compared to measured ones at the time of five years after completing the wall fragment. The thermal conductivity, especially, caused an increase of heat transfer and influenced the temperatures within the wall, which is significant for this comparison. The short-wave radiation absorptivity was used as 0.4 for yellow section and 0.6 for dark grey section. For calculating temperatures, the winter time period from the 14th of February to the 19th of February 2015, was used. The outdoor climate for the selected time period (Fig. 14) combines freezing temperatures (up to -10 °C) during the night with longwave radiation [17] and clear, sunny days which warmed the façade. The difference between the surface temperatures can be clearly seen.

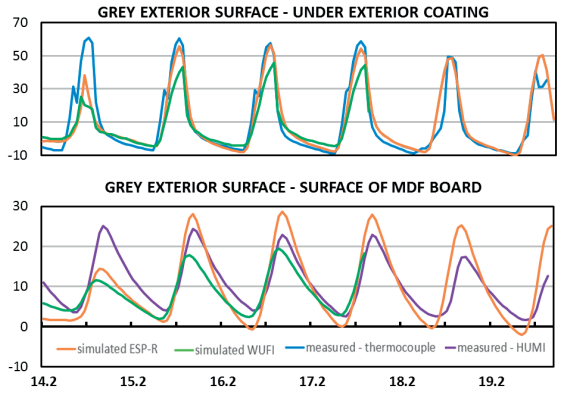

Fig. 15 Daily courses of temperature between the 14-02-2015 and the 19-02-2015 in the wall section with grey surface for positions under the exterior coating and inner surface of the MDF fiberboard [16]

Regarding the comparison of measurement and simulation, there is very good match between measurement and ESP-r for the temperatures under the exterior coating as shown in Fig. 15. This shows that the handling of solar radiation by the numerical model is on high level. On the other hand, the WUFI calculates the day peaks temperatures around 10 K lower.

On the inner surface of MDF board, temperatures are slightly overestimated by ESP-r and underestimated by WUFI for dark grey surface.

It should be noted that after 4 years of assembly of the experimental wall fragment, the reflectance and short-wave solar radiation absorptivity is changed due to the dust and age. This comparison shows very good results for calculation of outdoor surface and undersurface temperatures, where the ESP-r obtained very good results. Disadvantage is the use of direct normal global solar radiation, which is not available in most cases and has to be approximated. In this comparison, WUFI mostly underestimates calculated temperatures, but this is on the safe side [16].

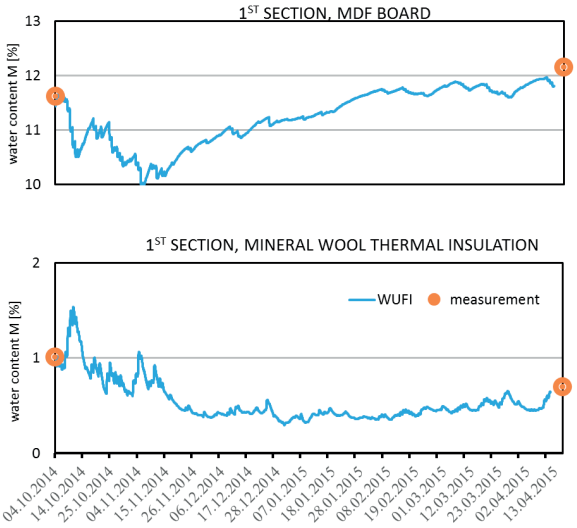

Fig. 16 Daily course of simulated water content (from 01-10-2014 to 10-05-2015) and results from the gravimetric measurement, 1st section [18]

The other simulation [18] incorporated WUFI software with measured outdoor climate from October 2014 to May 2015, measured initial water content in materials and thermal conductivities from previous chapters [8, 9]. The course of mass moisture is showed in Fig. 16.

Destruction, discussion and future

This long-term measurement of experimental wall fragment shows some rarely seen outputs. First of all, the high decrease of thermal resistance of the third section should be noticed. This is caused by the high moisture content in the hemp thermal insulation. On the other hand, in the rest of sections, there is not such a high impact of the exploitation to the outer climate. The

MDF board was not separated between sections, so the vapor diffusion and capillary water transport were possible inside the construction and it seems so, that it was there from the wetter third section. Another problem was the inner climate, because with current AC unit it was not possible to maintain the relative humidity in the room over the year constant. Another negative aspect was that there was no possibility to set direct value, if there was need to simulate another boundary condition such as kitchen or bathroom. Also the lack of funds causes no thermocouples inside the 5th section. The thermocouples provide good accuracy but there was also a lack of sensors for measuring relative humidity inside the fragments. This was later tried to improve with low-cost solution [7] with good results.

Nowadays is the wall dismantled and is being replaced by new one, which should reflect some consequences of these measurements, such as strictly divided sections, sensors for temperatures and relative humidity. The sections are more different, there will be also wood paneling with ventilated layer and massive wooden wall with inner thermal insulation. Also another climate room will be built with better AC unit with the possibility to set temperature and relative humidity strictly.

3. Conclusion

During long-term measurements it was shown as expedient to use the unconventional composition with inverse range of layers according to the model of Nordic countries in climate zone of central Europe too. The thermal-accumulative layer was warmed during winter days, which caused the improvement of boundary conditions for heat transport and decreasing heat loss. Moreover, the negative influence of external environment was decreased (temperature extremes, UV radiation, dust, moisture, etc.) on filling fibrous thermal insulations, which thermal-insulating properties have not changed significantly during the day due to this fact. What is more, it was thus possible to avoid reinforcing OSB board from the exterior side, which has a positive impact not only on moisture transport through the structure, but in economic terms, the absence of one layer has positively influenced both - the amount of acquisition costs or labor content. The comparison of measurement results and simulations showed favorable accord in radiation model with ESP-r and moisture transport in WUFI.

Measured moistures in diffusional closed sections are low, without significant increase in thermal flow. In contrary is the section without vapor barrier (3rd), which thermal resistance decreases about 40 % and its composition cannot be recommended for zero energy buildings and also does not complain the Slovak standard after five years of exploitation.

Based on the research course the conclusions for actions in lightweight wall in built-in state were formulated. However, it is needed to remark that these are valid for specific conditions of interior environment of air-conditioned room without presence of thermal gains from internal sources and without thermal gains from solar radiation through transparent constructions.

Acknowledgement

The research is supported by VEGA No. 1/0729/13 and VEGA 1/0945/16. Thanks to Caroline Kyzek, M.A. for language proofreading.

References

[1] BADUROVA, S.: *Theoretical, Technical and Technological Aspects of the Design and Manufacturing of Wood-Based Buildings* (in Slovak). Dissertation thesis. Zilina, 2012.

[2] PONECHAL, R., BADUROVA, S.: The Comparative Analysis of External Walls, a Passive House with Respect to Environment and Energy. Advanced Materials Research: *Buildings and Environment*, vol. 649, 2012, 129-132, ISSN 1022-6680.

[3] DURICA, P. et al.: Energy and Environmental Evaluation of Selected Wooden Family Houses, *Communications - Scientific Letters of the University of Zilina*, No. 1, 2013, 88-95, ISSN 1335-4205.

[4] STAFFENOVA, D. et al.: Climate Data Processing for Needs of Energy Analysis. *Advanced Materials Research: enviBUILD,* vol. 1041, 2014, 129-134, ISSN 1022-6680.

[5] DURICA, P. et al.: Thermal Properties of Selected Lightweight Wooden Walls and Windows in the Regime of Long Time Testing, *Advanced Materials Research*, vol. 899 2014, 450-456, ISSN 1022-6680.

[6] NiCr-Ni thermocouple T190-0, website < http://ahlborn.com/getfile.php?2052.pdf>

[7] JURAS, P., SLAVIK, R.: Usage of Raspberry Pi for Temperature and Relative Humidity Measurements and Comparison with HAM Simulation, *Applied Mechanics and Materials*, vol. 824, 2016, 552-559, ISBN 978-3-03835-689-9.

[8] DURICA, P. et al.: *Long-Term Monitoring of Thermo-Technical Properties of Lightweight Constructions of External Walls Being Exposed to the Real Conditions*, XXIV R-S-P seminar, Theoretical Foundation of Civil Engineering (24RSP), Procedia Engineering, 111, 2015, 176-182, ISSN 1877-7058.

[9] SUSTIAKOVA, M., DURICA, P.: Monitoring Thermal Parameters of Lightweight Wood-Based Perimeter, *Advanced Materials Research*, vol. 1041, 2014, 315-318, ISSN 1022-6680.

[10] ANDERSON, B. R.: *Conventions for U-Value Calculations*, 2nd ed., IHS - BRE Press. 2006, ISBN 1860819249.
[11] ANDERSON, B. R.: *The Measurement of U-values on Site*, (online), homepage: http://web.ornl.gov/sci/buildings/2012/1985%20B3%20papers/001.pdf, (date of access: 2013-11-4).
[12] ESP-r website < *http://www.esru.strath.ac.uk/Programs/ESP-r_overview.htm*>
[13] WUFI website < https://wufi.de/en/>
[14] KUNZEL, H. M.: *Simultaneous Heat and Moisture Transport in Building Components. One- and Two-dimensional Calculation using Simple Parameters*, Stuttgart : IBP Verlag, 1995.
[15] DURICA, P., VERTAL, M.: Verification of the Water Transport Parameter - moisture Storage Function of Autoclaved Aerated Concrete - Approximately Calculated from a Small Set of Measured Characteristic Values, *Communications - Scientific Letters of the University of Zilina*, No. 4, 2011, 35-42, ISSN 1335-4205.
[16] JURAS, P., PONECHAL, R.: Measurement of Lightweight Experimental Wall and Comparison with Different Simulation Programs, *Applied Mechanics and Materials*, vol. 820, 2016, 262-269. ISBN 978-3-03835-689-9.
[17] CEKON, M.: Accuracy Analysis of Longwave Sky Radiation Models in the MZELWE Module of the ESP-r Program, *Energy and Building*, 103, 2015, 147 - 158, ISSN 0378-7788.
[18] DURICA, P. et al.: *Lightweight Wood-Based Walls with Different Thermal Insulations: Long-Time Measurement and Subsequent Comparison with Ham Simulation*, Building Simulation, 14th Conference of IBPSA, 2015, 2371-2376, ISBN 978-93-5230-118-8.

https://doi.org/10.26552/com.C.2016.4.77-82

Juraj Muzik - Ladislav Kais - Roman Bulko*

LOCAL METHOD OF APPROXIMATE PARTICULAR SOLUTIONS FOR TWO-DIMENSIONAL UNSTEADY INCOMPRESSIBLE FLOW

A meshless local method of approximated particular solutions (LMAPS) is used to analyze incompressible fluid flow in a two dimensionalcavity. The method solves the incompressible Navier-Stokes equations in terms of theprimitive variables using the fractional step scheme. The basic equations are derived via interpolation using integrated multiquadrics radial basis functions. Lid-driven cavity benchmark case for various Reynolds numbers is presented in the article. The procedure produces stable solutions with results comparable to those in literature.

Keywords: *Meshless, localized method of approximated particular solutions, incompressible flows, Navier-Stokes equations.*

1. Introduction

The isothermal incompressible viscous flow is used to describe flows taking advantage of simplified flow equations that describe fluid motion, which is known as the incompressible Navier-Stokes equations. There are numerous approaches developed to solve the incompressible Navier-Stokes equations; the algorithm used in this article represents the Chorin's projection method (fractional step) that belongs to the class of the decoupled methods which are more commonly used in computational fluid dynamics (CFD). Other way to classify the algorithms is to determine the version of the underlying governing equations, whether they are expressed using the primitive variables, velocity component and pressure, or not [1]. The mentioned fractional step method uses primitive variable formulation of the Navier-Stokes equations.

The fractional step algorithm is chosen to approximate the solutions of the incompressible Navier-Stokes equations in conjunction with the localized method of approximated particular solutions (LMAPS) that represents meshless collocation method [2].

The fractional step method solves the incompressible Navier-Stokes equations in three steps. In the first step the simple form of the momentum equations is obtained by dropping the pressure source term; this results in the intermediate velocities. In the next step the intermediate velocities are projected on the divergence-free plane using the solution of the Poisson's pressure equation and, subsequently obtaining velocity corrections using the pressure gradients [1].

The main drawback of mesh-based numerical methods is the requirement of the mesh generation, which may be difficult to process during the numerical implementations, especially for multi-dimensional problems. In order to avoid mesh generation process many meshless numerical methods, such as the local boundary integral element method (LBIEM) [3 - 7], smoothed particle hydrodynamics (SPH) method [8], meshless strong (collocation) method [9 - 11] and meshless local Petrov-Galerkin method (MLPG) [12 and13] have been developed. The LMAPS used in this study represents a stable, accurate tool for simulating the two-dimensional incompressible viscous flow field with the projection method. Numerical experiment of the two-dimensional lid-driven cavity flow problem is presented in the article with the comparison against literature data [14], which verifies the performance of the LMAPS.

2. Governing equations

An unsteady incompressible flow is governed by Navier-Stokes equations, which can be in a two dimensional case written in dimensionless form using the primitive variables as

$$\frac{\partial u}{\partial t}+u\frac{\partial u}{\partial x}+v\frac{\partial u}{\partial y}=\frac{1}{\mathrm{Re}}\left(\frac{\partial^2 u}{\partial x^2}+\frac{\partial^2 u}{\partial y^2}\right)-\frac{\partial p}{\partial x} \tag{1}$$

$$\frac{\partial v}{\partial t}+u\frac{\partial v}{\partial x}+v\frac{\partial v}{\partial y}=\frac{1}{\mathrm{Re}}\left(\frac{\partial^2 v}{\partial x^2}+\frac{\partial^2 v}{\partial y^2}\right)-\frac{\partial p}{\partial y} \tag{2}$$

$$\frac{\partial u}{\partial x}+\frac{\partial v}{\partial y}=0 \tag{3}$$

* **Juraj Muzik, Ladislav Kais, Roman Bulko**
Department of Geotechnics, Faculty of Civil Engineering, University of Zilina, Slovakia
E-mail: juraj.muzik@fstav.uniza.sk

where u, v is the velocity vector component in the direction x and y respectively, p is the pressure, and Re represents Reynolds number, assuming that density and characteristic velocity equals to unity. A fractional step algorithm is used to solve this problem (see [1, 15 and 16]). The time derivative of the velocity in momentum equations Eq.(1, 2) can be replaced with a difference and the following relation is obtained:

$$u^{n+1} = u^n + \Delta t\left[\frac{1}{\mathrm{Re}}\left(\frac{\partial^2 u^n}{\partial x^2} + \frac{\partial^2 u^n}{\partial y^2}\right) - u^n\frac{\partial u^n}{\partial x} - v^n\frac{\partial u^n}{\partial y} - \frac{\partial p^{n+1}}{\partial x}\right] \quad (4)$$

$$v^{n+1} = v^n + \Delta t\left[\frac{1}{\mathrm{Re}}\left(\frac{\partial^2 v^n}{\partial x^2} + \frac{\partial^2 v^n}{\partial y^2}\right) - u^n\frac{\partial v^n}{\partial x} - v^n\frac{\partial v^n}{\partial y} - \frac{\partial p^{n+1}}{\partial x}\right] \quad (5)$$

where upper indexes n and $n+1$ indicate time level and Δt is the length of the timestep. The first order finite difference, used here to discretize unsteady term, is preffered beacuse the explicit nature of the momentum equations. Eq. (4, 5) arean explicit formula for the convection andviscous terms, and an implicit one for the pressure term. Eq. (4, 5) are simplified using the fractional time step approximation (e.g., [15 and 16]), which computes the intermediate velocity $\tilde{u}, \tilde{v}$ using the simplified momentum equation

$$\tilde{u} = u^n + \Delta t\left[\frac{1}{\mathrm{Re}}\left(\frac{\partial^2 u^n}{\partial x^2} + \frac{\partial^2 u^n}{\partial y^2}\right) - u^n\frac{\partial u^n}{\partial x} - v^n\frac{\partial u^n}{\partial y}\right] \quad (6)$$

$$\tilde{v} = v^n + \Delta t\left[\frac{1}{\mathrm{Re}}\left(\frac{\partial^2 v^n}{\partial x^2} + \frac{\partial^2 v^n}{\partial y^2}\right) - u^n\frac{\partial v^n}{\partial x} - v^n\frac{\partial v^n}{\partial y}\right] \quad (7)$$

Comparing (4, 5) and (6, 7) respectively gives

$$u^{n+1} = \tilde{u} - \Delta t\frac{\partial p^{n+1}}{\partial x} \quad (8)$$

$$v^{n+1} = \tilde{v} - \Delta t\frac{\partial p^{n+1}}{\partial x} \quad (9)$$

The intermediate velocity components $\tilde{u}, \tilde{v}$ do not satisfy the continuity equation in (3). The velocity components u^{n+1}, v^{n+1} must satisfy the continuity equation, which implies

$$\frac{\partial}{\partial x}\left(\tilde{u} - \Delta t\frac{\partial p^{n+1}}{\partial x}\right) + \frac{\partial}{\partial y}\left(\tilde{v} - \Delta t\frac{\partial p^{n+1}}{\partial y}\right) = 0 \quad (10)$$

A pressure Poisson equation then results directly from equation (10)

$$\frac{\partial^2 p^{n+1}}{\partial x^2} + \frac{\partial^2 p^{n+1}}{\partial y^2} = \frac{1}{\Delta t}\left(\frac{\partial \tilde{u}}{\partial x} + \frac{\partial \tilde{v}}{\partial y}\right) \quad (11)$$

3. Localized method of approximated particular solutions

In order to apply the LMAPS, the following procedure may beadopted to solve physical variable u with any given differential operator.Even though the implementation details of the LMAPS are quite similar to the meshless collocation methods, its origin follows the globally defined method of approximated particular solution (MAPS) (see [2]). In this study the LMAPS is treated as special case of the meshless collocation methodwith the support domain concept already included in the formulation.

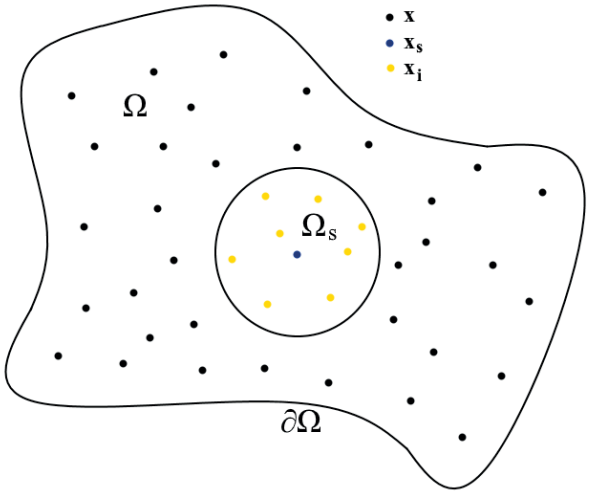

Fig. 1 The diagram of global domain Ω, local support domain Ω_s of point x_s, global points xand local point x_i

The area of interest Ω with the boundary ∂Ω is covered by points within the area and also on the global boundary (see Fig. 1). Consider a local circular sub-domain Ω_s centered at every point s. This sub-domain is regular around all the points, and it is called support domain. Then using the points in a particular support domain any function can be expressed using just nodal values as

$$u(\mathbf{x}) = \sum_{i=1}^{NS} \alpha_i F(\| \mathbf{x} - \mathbf{x}_i \|), x \in \Omega \quad (12)$$

where NS is the total number of computational nodes in the support domain, F is the radial basis function, $\mathbf{x}$ is coordinate vector and α_i are the local weighting coefficients to be determined. Because the values of u expressed using Eq. (12) at the computational nodes should be the same as$u$ specified in these nodes, we can write following matrix expression

$$\mathbf{u} = \mathbf{F}\alpha \quad (13)$$

where

$$\mathbf{u}_i = \left[u(\mathbf{x}_1) \ \ldots \ u(\mathbf{x}_{N_S})\right]^T \quad (14)$$

$$\mathbf{F}=\begin{bmatrix} F(\|\mathbf{x}_1-\mathbf{x}_1\|) & \cdots & F(\|\mathbf{x}_1-\mathbf{x}_{NS}\|) \\ \vdots & \ddots & \vdots \\ F(\|\mathbf{x}_{NS}-\mathbf{x}_1\|) & \cdots & F(\|\mathbf{x}_{NS}-\mathbf{x}_{NS}\|) \end{bmatrix} \tag{15}$$

$$\alpha=\begin{bmatrix}\alpha_1 & \cdots & \alpha_{NS}\end{bmatrix}^T \tag{16}$$

Since **F** is invertible, we will obtain the unknown weighting coefficients as

$$\alpha=\mathbf{F}^{-1}\mathbf{u} \tag{17}$$

Now, for operators concerned in solving Navier-Stokes equations, we firstly consider the operator with highest order, the Laplace operator ∇^2, and let

$$\nabla^2 u(\mathbf{x}_i)=\sum_{i=1}^{NS}\alpha_i f(\|\mathbf{x}-\mathbf{x}_i\|)=\mathbf{f}\alpha \tag{18}$$

where f is the radial basis function with the essential condition as $f=\nabla^2 F$. Replacing α_i with Eq. (17) we get

$$\nabla^2 u(\mathbf{x})=\mathbf{f}\mathbf{F}^{-1}\mathbf{u}=\varphi\mathbf{u} \tag{19}$$

where φ is the vector of shape functions Laplacian. We apply similar procedures to the gradient operator ∇ and we get

$$\nabla_j u(\mathbf{x}_i)=\sum_{i=1}^{NS}\alpha\frac{\partial F(\|\mathbf{x}-\mathbf{x}_i\|)}{\partial x_j}=\mathbf{G}_j\alpha= \\ =\mathbf{G}_j\mathbf{F}^{-1}\mathbf{u}=\gamma\mathbf{u} \tag{20}$$

where γ is the vector of shape function gradients and subscript j represents the coordinate of the gradient.

The processed operators may now be applied directly into numerical implementations, which discretizes the governing equations and the essential conditions into formulation of linear systems. All boundary conditions in this paper have also been processed using the LMAPS. Numerical procedures for solving Navier-Stokes equations will be elaborated in subchapter 3.3, and more details of the LMAPS can be found in Ref. [2].

3.1 Integrated multiquadrics radial basis functions

The trial function basis used in the LMAPS incorporates multiquadrics RBF, but different approach than the standard meshless collocation methods is adopted. In the case of LMAPS the MQ-RBF [2 and 17] represents the form of basis function after differentiation using highest order operator. To obtain the basis function, MQ-RBF needs to be integrated.

In this article the two-dimensional integrated multiquadrics radial basis function (integrated MQ-RBF) is used as the basis function F. The MQ-RBF

$$f(r)=\sqrt{r^2+c^2} \tag{21}$$

and the integrated MQ-RBFs [2]

$$F(r)=\frac{1}{9}(r^2+4c^2)\sqrt{r^2+c^2}-\frac{1}{3}c^3 \\ \ln(\sqrt{r^2+c^2}+c) \tag{22}$$

where r depicts the distance between the collocation points and c is a shape parameter.

3.2 Handling derivative boundary conditions

Strong-form methods can produce accurate results for partial differential equations, when the boundary conditions are all of Dirichlet type. If there is any derivative boundary condition, the accuracy of the solution deteriorates drastically, and the solution can be unstable; small changes in the setup of the problem can lead to a large change in the solution. The discretized

system equation behaves like an ill-posed problem in which errors introduced into the system are magnified in the output. A number of strategies can be used to impose the derivative boundary conditions in the strong form methods. The method using fictitious points is used in this article to enforce the pressure gradient on the boundary.

Along the derivative boundaries, a set of fictitious points is added outside the problem domain. In this case, two sets of equations are established at each derivative boundary node, one for the derivative boundary condition, and the other for the governing equation.

3.3 Discretization of Navier-Stokes equations

In this section, the numerical procedures for the approximation of the Navier-Stokes equations via the fractional step method and the LMAPS will be explained. The fractional step begins with Eq. (6, 7), where the intermediate velocity can be obtained for ith node explicitly as follows:

$$\tilde{u}_i=u_i^n+\Delta t\left[\frac{1}{\mathrm{Re}}\varphi_i\mathbf{u}_i^n-u_i^n\gamma_{i,x}\mathbf{u}_i^n-v_i^n\gamma_{i,y}\mathbf{u}_i^n\right] \tag{23}$$

$$\tilde{v}_i=v_i^n+\Delta t\left[\frac{1}{\mathrm{Re}}\varphi_i\mathbf{v}_i^n-u_i^n\gamma_{i,x}\mathbf{v}_i^n-v_i^n\gamma_{i,y}\mathbf{v}_i^n\right] \tag{24}$$

The boundary conditions of intermediate velocity are given as the same as the boundary conditions of the original velocity in

the present study. Next, we obtain pressure term from Poisson's equation of the second stage, which can be written as

$$\varphi \mathbf{p}^{n+1} = \frac{1}{\Delta t}\left(\gamma_x \tilde{\mathbf{u}} + \gamma_y \tilde{\mathbf{v}}\right) \tag{25}$$

Then, in the third stage we execute the velocity correction explicitly as

$$u_i^{n+1} = \tilde{u}_i - \Delta t \gamma_{i,x} \mathbf{p}^{n+1} \tag{26}$$

$$u_i^{n+1} = \tilde{v}_i - \Delta t \gamma_{i,y} \mathbf{p}^{n+1} \tag{27}$$

The convergence criterion for steady state is given as $\varepsilon = 10^{-7}$ for all numerical experiments in this paper. The fractional time step algorithm described above is now used to solve the Navier-Stokes equations at every time step [15]:

- Step 1: Computation of the intermediate velocities $\tilde{u}$, $\tilde{v}$ from the velocities at the previous time step using (23, 24).
- Step 2: Solution of pressure Poisson equation (25).
- Step 3: Computation of velocities at the current time step from (26, 27).

4. Numerical example

The solution of the Navier-Stokes equations using the LMAPS developed in the previous sections is validated here by solving lid-driven cavity flow examples. Lid-driven cavity flow is used as a standard test problem for the validation of numerical solutions of incompressible Navier-Stokes flow. The top wall of the cavity moves with a velocity $u_0=1$, and no-slip impermeable boundary conditions are assumed along the other three walls. The geometry and boundary conditions arepresented in Fig. 2. The difficulty of this problem lies in the presence of singularities of pressure and velocity at the two upper corners of the cavity [15]. Therefore, the density of points used increases toward the corners of the cavity (see Fig. 2).

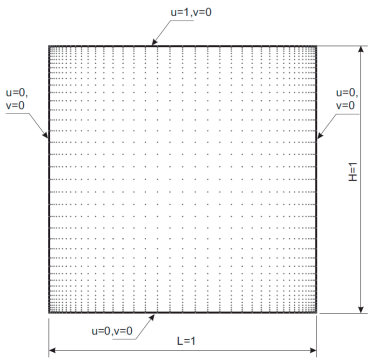

Fig. 2 Lid-driven cavity, boundary conditions, 41x41 points distribution

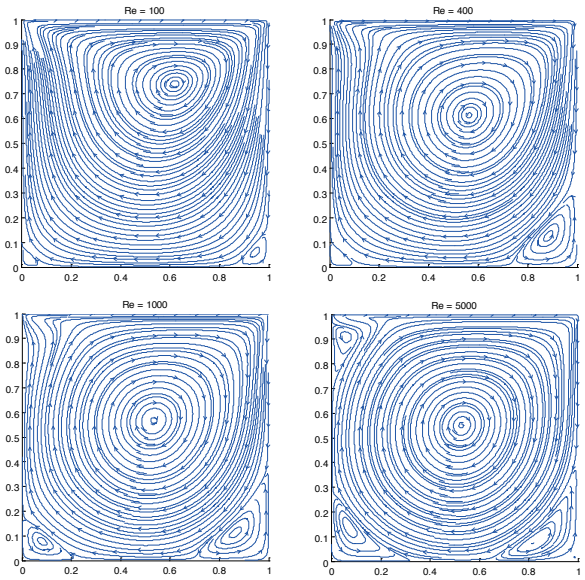

Fig. 3 Lid-driven cavity, streamlines pattern for different Reynolds numbers

Three different meshes are tested here (61×61, 81×81, and101×101 points), with each having a non-uniform distribution similar to that used in [15]. For all calculations the uniform timestep $\Delta t=10^{-3}$. The strategy of finding neighboring points for RBF interpolation is the main problem facing the use of anon-uniform distribution of points.

The segmentation strategy (see [7]) gives the best results for this type of network. For higher Reynolds numbers the solution found using a coarse network does not converge and denser networks must be used. This problem probably arises because the point distribution in the coarse network is unable to capture the velocity gradient within a thin boundary layer for higher Reynolds numbers. The results of the LMAPS are compared with the solutions presented in [14] for the Reynolds number Re=100, 400, 1000 and 5000. The vertical velocity components along a horizontal line through the center ofthe cavity and the horizontal velocity components along a vertical line through the center of the cavity are plotted in Fig. 4.

These comparisons for the three types of mesh show that, as expected, the most dense mesh (101×101 points) leads to the results closest to those of [14]. Figures 3, 5 and 6 present streamlines, velocity magnitude and pressure contours for Reynolds numbers Re=100, 400, 1000 and 5000.

5. Conclusions

A possible use of the localized method of approximate particular solutions with integrated MQ-RBF interpolation

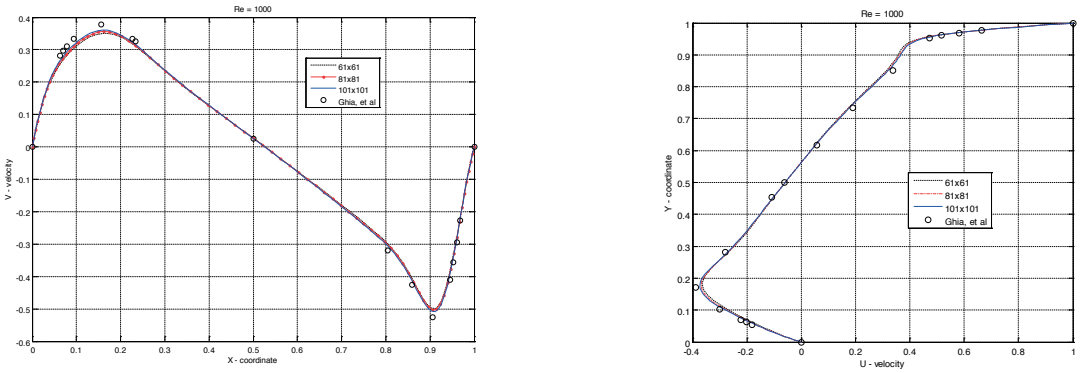

Fig. 4 Lid-driven cavity, Re=1000,vertical velocity components along horizontal line y=0.5 and horizontal velocity components along vertical line x=0.5

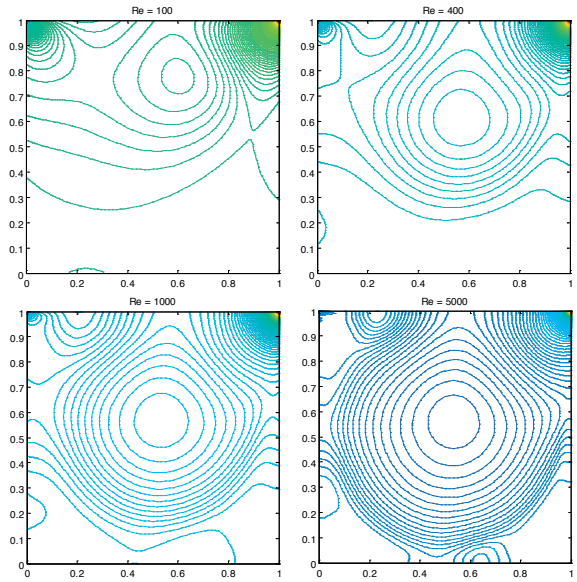

Fig. 5 Lid-driven cavity, pressure contours for different Reynolds numbers

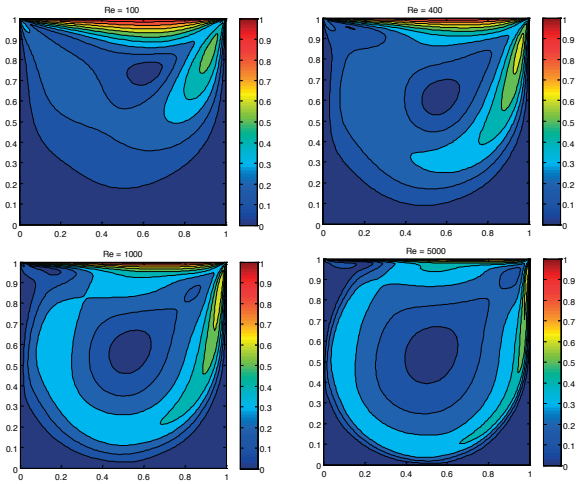

Fig. 6 Velocity magnitude for different Reynolds numbers

ispresented here for the computation of incompressible flows. The primitive variable formulation of the Navier-Stokes equations and the fractional step scheme is used to achieve stable and accurate results. The suitability of this procedure is tested in the solution of the lid-driven cavity flow problem for various meshes and Reynolds numbers. The results demonstrate that the method is effective and useful forsolving this type of flow.

References

[1] NITHIARASU, P, ZIENKIEWICZ, O.: Analysis of an Explicit and Matrix Free Fractional Step Method for Incompressible Flows, *Comput Methods Appl Mech Eng,* 2006, 195:5537-51.

[2] LIN, C. Y., GU, M. H., YOUNG, D. L., SLADEK, J., SLADEK, V.: The Localized Method of Approximated Particular Solutions for Solving Two-Dimensional Incompressible Viscous Flow Field, *Eng Anal Bound Elem*, 2015, 57:23-36.

[3] KOVARIK, K.: Numerical Simulation of Groundwater Flow and Pollution Transport Using the Dual Reciprocity and RBF Method, *Communications - Scientific Letters of the University of Zilina*, No. 3a, 2010, pp.5-10, ISSN 1335-4205.

[4] KOVARIK, K.: The New Numerical Methods for Mathematical Modelling of Pollutant Transport, *Communications - Scientific Letters of the University of Zilina*, No. 4, 1999, pp. 59-68, ISSN 1335-4205.
[5] ZHU, T., ZHANG, J., ATLURI, S.: A Meshless Numerical Method Based on the LocalBoundary Integral Equation (LBIE) to Solve Linear and Non-Linear BoundaryValue Problems. *Eng Anal Bound Elem* 1999, 23:375-89.
[6] SLADEK, V, SLADEK, J, ATLURI, S. N., VAN KEER, R.: Numerical Integration of Singularities in Meshless Implementation of Local Boundary Integral Equations. *Comput Mech*, 2000, 25:394-403.
[7] KOVARIK, K, MUZIK, J.: A Meshless Solution for Two Dimensional Density-Driven Groundwater Flow, *Eng Anal Bound Elem*, 2013, 37:187-96.
[8] GINGOLD, R. A., MONAGHAN, J. J.: Smoothed Particle Hydrodynamics: Theory and Applications to Non-Spherical Stars, *Mon Not R Astron Soc*, 1977, 181:375-89.
[9] KANSA, E. J.: Multiquadrics- a Scattered Data Approximation Scheme with Application to Computational Fluid Dynamics, *Comput Math Appl*, 1990, 19:127-45.
[10] SANYASIRAJU, Y, CHANDHINI, G.: Local Radial Basis Function Based Gridfree Scheme for Unsteady Incompressible Viscous Flows, *J. Comput Phys*, 2008, 227:8922-48.
[11] SHU, C, DING, H, YEO, K. S.: Local Radial Basis Function-Based Differential Quadrature Method and its Application to Solve Two-Dimensional Incompressible Navier-Stokes Equations, *Comput Methods Appl Mech Eng*, 2003, 192:941-54.
[12] ATLURI, S. N., KIM, H-G., CHO, J. Y.: A Critical Assessment of the Truly Meshless Local Petrov-Galerkin (MLPG), and Local Boundary Integral Equation (LBIE) Methods, *Comput Mech*, 1999, 24:348-72.
[13] Lin, H., ATLURI, S. N.: The Meshless Local Petrov-Galerkin (MLPG) Method for Solving Incompressible Navier-Stokes Equations, *Comput Model Eng Sci*, 2001, 2:117-42.
[14] GHIA, U., GHIA, K. N., SHIN, C. T.: High-resolutionsfor Incompressible Flow Using the Navier-Stokes Equations and a Multigrid Method, *J. Comput Phys*. 1982, 48:387-411.
[15] KOVARIK, K, MUZIK, J, MAHMOOD, M. S.: A Meshless Solution of Two Dimensional Unsteady Flow, *Eng Anal Bound Elem*, 2012, 36:738-43.
[16] NAJAFI, M., AREFMANESH, A., EJILELA, V.: Meshless Local Petrov-Galerkin Method Higher Reynolds Numbers Fluid Flow Applications, *Eng Anal Bound Elem*, 2012, 36:1671-85.
[17] HARDY, R. L.: Theory and Applications of the Multiquadrics-Biharmonic Method (20 years of discovery 1968-1988), *Comput Math Appl*, 1990, 19:163-208.

https://doi.org/10.26552/com.C.2016.4.83-89

Jan Mikolaj - Lubos Remek - Matus Kozel*

LIFE CYCLE EXTENSION OF A PAVEMENT STRUCTURE

The pavement structure, namely pavement surfacing must meet the criteria required to provide operational service during the whole life cycle of the pavement. Surfacing design composed of layer strengths and proposed materials is defined by design method which calculates the stress state during long-term transport and environmental conditions. The designed surfacing life cycle is defined in respect to traffic load acting on the pavement and road class for a period of about 20 years. Given the practical aspects of road administration, pavement reconstruction is usually due only at the end of the life cycle, when the original materials are replaced by new materials and the layer strength is re-evaluated. Since the overall life cycle of the whole pavement is significantly longer than that of the surfacing, it is necessary to consider possibilities to extend the life cycle of the surfacing either through various technologies, i.e. reinforcement, overlays or recycling. Timing of execution of such action plays a paramount role, and it has impacts on future financial flows of road administrator as well as economic aspects of transportation for the whole society. This paper describes analytical calculations and experimental measurements of surfacing materials, as well as accelerated pavement testing process needed for ascertainment of operational performance of a pavement construction during its life cycle. Finally, a case study encompassing the whole method is presented.

Keywords: *Pavement management system, life cycle extension, pavement surfacing, accelerated pavement testing.*

1. Introduction

Life cycle of a pavement surfacing should be modelled in advance of a pavement construction and it should be a corner stone of a successful long term administration of given road section. Design and evaluation of pavement surfacing rehabilitation in the framework of the life cycle requires a combination of analytical and computational models, and experimental measurements on sections which are subject to traffic loading in real-life operation. In the analytical part, methods are proposed to calculate the design of the pavement construction, fatigue characteristics are defined as trend lines of asphalt material surfacing life-expectancy, computation models are defined for calculation of the life cycle and economic efficiency of all proposed variants. Experimental part consists of an experiment to determine the basic material and fatigue characteristics and deformation trend lines.

Life Cycle of surfacing materials in the pavement construction is defined through the analytical calculation method of pavement construction, where life expectancy is derived through the fatigue characteristics of materials used. However, the surfacing life cycle itself can be defined by other means than fatigue characteristics, for instance, permanent deformation expressed through pavement unevenness, foremost rutting (transverse unevenness).

Based on surfacing life cycle defined through the material fatigue and permanent deformation expressed by unevenness, it is possible to design rehabilitation variant - recycling or overlay at different times within the life cycle. These variants extend the original life cycle. In terms of efficiency, variants of the rehabilitation are evaluated by means of Cost Benefit Analysis (CBA) and mathematical optimisation model.

2. Experimental Pavement Model

Experimental pavement section was built on 1:1 scale, on which heavy truck axle acted as a simulated traffic load prescribed as equivalent single axle load, this is called accelerated pavement testing (APT). The general principle of APT testing is to apply artificially inducted load similar to real life traffic load in a compressed time period, thus providing an expedited means of evaluating factors associated with traffic-pavement interaction. APT is essentially a full-scale laboratory test during which loaded truck wheels are used to traffic sections of full-scale road pavement constructed using conventional techniques.

In order to define surfacing lifecycle in the pavement construction and the application of technological variants of rehabilitation, a standard pavement type usual for a primary road was designed. The pavement was designed according to standard methodology [1] for a minimum level of traffic load - $2x10^6$ design axles. The pavement design of built experimental pavement

* **Jan Mikolaj, Lubos Remek, Matus Kozel**
Faculty of Civil Engineering, University of Zilina, Slovakia
E-mail: jan.mikolaj@fstav.uniza.sk

section is shown in Fig. 1. Subgrade is simulated by a rubber layer on concrete with equivalent modulus of E_{def} 100 MPa. The complete APT tester is shown in Fig. 2. It is a Semi-mobile linear APT facility with axle load of 57.5 kN moving at 2.22 $m.s^{-1}$.

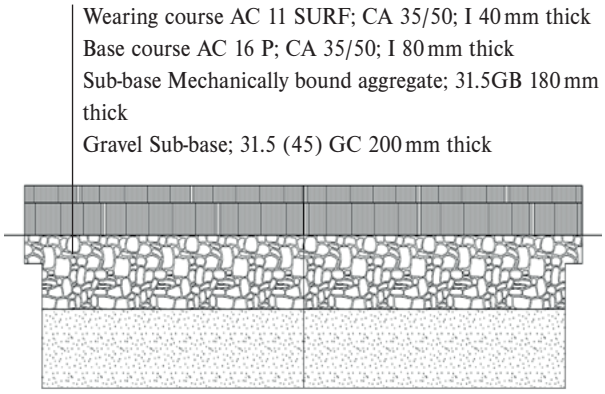

Fig. 1 Pavement Structure

Fig. 2 APT tester

Pavement structure layers are designed from generic materials defined in national standards. Table 1 contains material characteristics ascertained by the initial physical–measurement of surfacing materials. Two point bending test was used for this purpose. These values fall within the required interval for this particular type of pavement.

3. Asphalt Concrete Material Layer

3.1. Complex stiffness modulus

Measurement of complex stiffness modulus of a surfacing layer in the pavement structure was carried out according to national standard which is in compliance with European Union Standards [2]. Measurement of the complex stiffness modulus is performed with utilisation of short-term alternating harmonic load. It expresses the proportion of the maximum amplitudes of excitation tension and deformation induced by it and their phase shift. On the basis of measurements performed for different

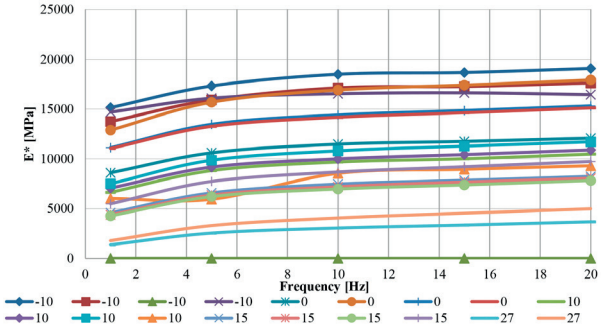

Fig. 3 E relation to frequency and temperature*

Material Characteristics of Pavement Layers — Table 1

Layer	Complex modulus	Strength	Poisson number	Layer Thickness
AC 11 SURF	10891 MPa	3.2 MPa	0.3	40 mm
AC 16 P	8317 MPa	2.4 MPa	0.33	80 mm
MBA, 31.5 GB	586 MPa	0.1 MPa	0.25	180 mm
Gravel Sub-base, 31.5	365 MPa	0.07 MPa	0.3	200 mm
Sub-grade	100 MPa	-	0.3	-

Complex modulus of AC11 measured at different frequencies — Table 2

Temperature °C	E* [MPa] Frequency Hz				
	1	5	10	15	20
-10	14532	16449	17390	17524	17715
0	10919	13261	14248	14664	15112
10	7060	9171	10002	10430	10891
15	4686	6721	7577	8026	8463
27	1581	2919	3556	3944	4334

temperature values ascertained are presented in Table 2 and Fig. 3.

3.2. Sub-base Layers

The measured values on sub-base layers are performed using an LDD and Clegg that, after conversion based on the equation (1) according to [3], were adjusted to CBR (California Bearing Ratio) values. The results are shown in chart in Fig. 4.

$$CBR_{STN721016} = 0.78 * CIV^{1.12} \quad (1)$$

Where:
CIV – Clegg impact value.

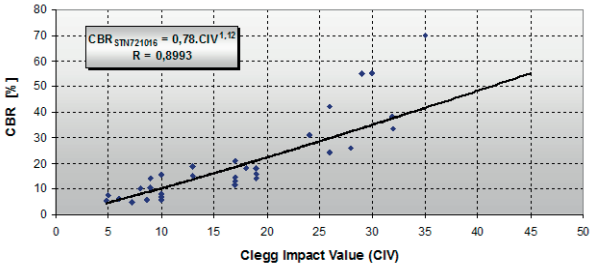

Fig. 4 Clegg and CBR Relationship

Subsequently, the CBR values were converted according to equation (2) [4] to (E_N) value with the use of following formula:

$$E_N = 17.6 * CBR^{0.64} \quad (2)$$

3.3. Fatigue Characteristics

Fatigue characteristics are used in the assessment of pavement resilience against repeated loading. Test temperature for the endurance test is 10 °C and the frequency of cyclic loading is 25 Hz. The test is carried out at a constant bend of the test sample during the test. Fatigue tests were carried out according to the European standard [5].

The results of research [6] carried out in the ambit of fatigue characteristics are presented in Fig. 5 and Table 3.

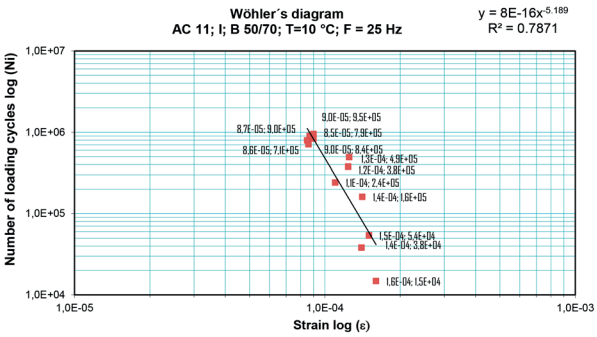

Fig. 5 Wohler diagram for AC 11 SURF

Values of fatigue parameters for mix AC 11 SURF — Table 3

Parameter	*a*	*1/b*	$\varepsilon_{,6}$ *10⁶*	r^2
Fatigue parameters	-15.0754	-0.1927	86.77	0.7871

4. Ascertainment of the Life Cycle

The life cycle of a surfacing layer can be defined through the means of bearing capacity evaluation on the basis of the stress and fatigue characteristics up until the point of a breakdown. In addition, however, the ACM (Asphalt Concrete Material) is subject to permanent deformation as a result of traffic loading, which may cause the loss of operational capability defined by the standard prior to its failure caused by fatigue. These deformations manifest as plastic deformations.

4.1. Bearing Capacity

Calculation of the life cycle is possible on the basis of the calculation method for the design of pavement structure [7 and 1]. This method imposes structural value for the surfacing layers which is expressed by comparing the calculated radial stress on the bottom of the considered layer with the strength in the same layer. That in view of the repeated loading is reduced by a fatigue factor S_N.

$$SV \geq \frac{\sigma_{ri}}{SN * R_i} \quad (3)$$

Where:
SV – structural value
σ_{ri} – radial stress,
R_i – strength,
SN – fatigue characteristic.

The calculated radial stress in the surfacing layer is calculated on the basis of the thickness of the layers, complex modulus and Poisson number by means of calculation in the layered elastic half space model [8]. Calculated stress (σ_{ri}) is based on the effects of repeated loading, which is expressed in terms of the design axle load with the axle weight of 10 tonnes (2P = 100 kN). Behaviour and properties of the materials used in the pavement construction pertain to certain climatic conditions, therefore under standard processes three different periods are considered during which the resiliency and elastic modulus change. In our case, the modelling of the pavement construction behaviour happens in constant conditions persisting in laboratory where the

experimental pavement section is built. These constitute medium conditions, i.e. constant temperature above + 10 °C.

Fatigue characteristic (S_N) is expressed via parameters (a) and (b) which represent the shape of the Wohler curve and the expected traffic load (N).

$$S_N = a - b * \log N_c \quad (4)$$

where:
a, b – fatigue characteristics.

On the basis of fatigue characteristic measurements (chapter 3.1) for AC 11 SURF mixture, the values of fatigue coefficients a, b are:

$$a = 1,\ b = 0.11 \quad (5)$$

The life cycle of ACM in the pavement construction can be expressed through the equation (1), on the basis of the stress calculation in pavement construction, strength and fatigue characteristics. The Structural Value must be less than 1, in order for the stress not to exceed the resiliency value. If it is exceeded, the surfacing layer is at the end of their useful life and collapses. The length of life cycle therefore defines stress in the surfacing layer and a decrease of strength depending on the traffic load expressed by the fatigue characteristics. For this reason, stress calculations were made for the pavement construction and its characteristics for the duration of the whole life cycle. In Table 4, stress values are listed in various stages of the life cycle depending on the number of loads and complex modules, whose values also decrease depending on the repeated loading.

The life-cycle itself, expressed by utilisation of Structural values in accordance with equation 1 is shown in Fig. 6. Calculations show that the life cycle of a surfacing in the testing pavement section is defined by 7.5 million of design axle passes. In this case, the annual traffic load will be max. 375 000 design axle loads, which, for given traffic intensity, equals to life expectancy of 20 years.

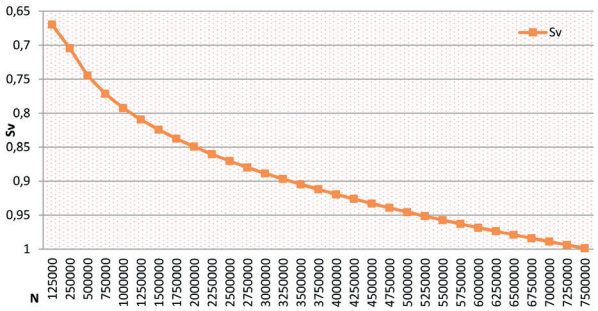

Fig. 6 Life cycle of surfacing in the pavement construction depending on the number of loading cycles

4.2. Permanent Deformation

Permanent deformations are induced by traffic loading and external environmental conditions such as temperature, humidity, radiation, etc. The material deteriorates to a point where it is no longer suitable from the viewpoint of operational characteristics, and thus ends its life cycle [9]. In contrast to fatigue and its relation to the residual life expectancy, which can be expressed by different coefficients [10], e.g. this can not be done for permanent deformation. It is foremost because of the fact that surfacing layer is, during deformation, neither in elastic nor in plastic state and the calculations are extremely sensitive to variety of conditions from the external environment. Therefore, experimental measurements are used to record pavement shape changes, and, by means of mathematical models environmental conditions are directly derived [11, 12 and 13]. In our research, deformation characteristics were obtained through measurements on the experimental pavement section after 50, 100 and 150 thousand loads. Deformations are shown in Fig. 7. Trend line of deformation in relation to load was derived and it is shown in Fig. 8.

Radial Stress and strength resiliency values in ACM layers based on Ni — Table 4

The number of Ni	0	1.5x10^6	3x10^6	4.5x10^6	6x10^6	**7.5x10^6**
AC 11 SURF E* (MPa)	10891	5998	5759	5620	5521	5445
AC 16 P E* (MPa)	8317	4580	4398	4291	4216	4158
Stress (MPa)	0.978132	0.634328	0.613133	0.600401	0.591348	0.584278
Strength (MPa)	2.4	0.769512	0.690040	0.643552	0.610568	0.584984

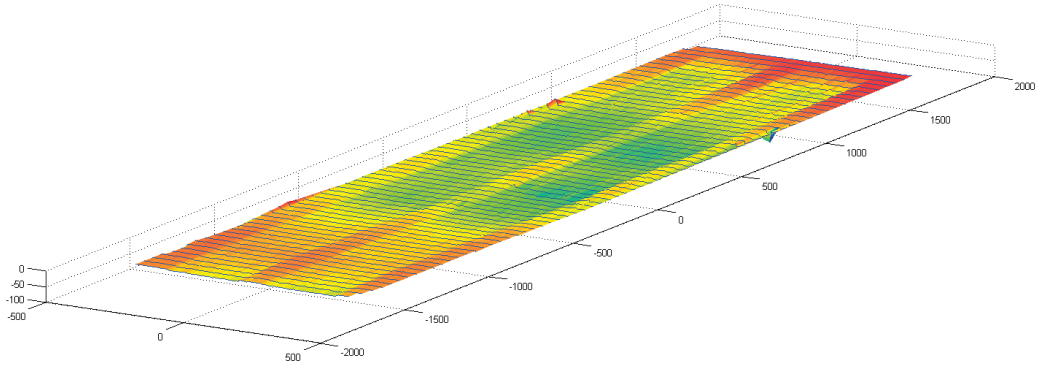

Fig. 7 Life cycle of surfacing in the pavement construction depending on the number of loading cycles - permanent deformations

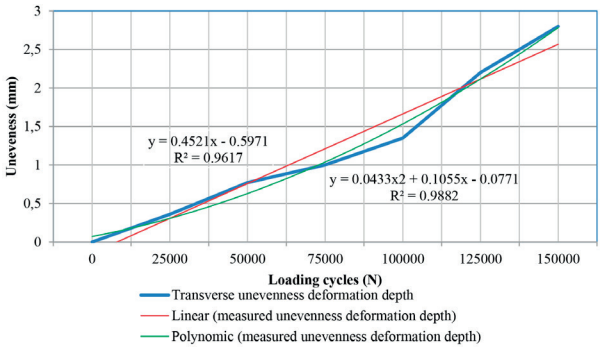

Fig. 8 Transverse Unevenness

5. Extension of the Life Cycle

The life cycle represents number of load repetitions acting on surfacing layer up to the state of a breakdown. For economic reasons, however, it may not be the cheapest or most efficient to wait until the very end of the surfacing life cycle, rehabilitation at earlier date may be more efficient. In our case, the rehabilitation of surfacing denotes improvements by means of overlay or mill & replace action, which restores the original properties of surfacing layer thus shifts the layer to the beginning of its life cycle [14]. This extends the life cycle of up to 20 years. In terms of analytical computational structural method, the rehabilitation manifests itself by increased complex modulus of surfacing layer and by adjusted thickness of the layer i. In Table 5, proposed rehabilitation is shown for three time periods of the life cycle

Stress Calculations Before and After Rehabilitation — Table 5

year	5	10	15	20	25	30	35	40
ACM layer thickness increase (mm)	36	52	62	71	-	-	-	-
AC 11-overlay E* (MPa)	10891	10891	10891	10891	5445	5445	5445	5445
AC 11 SURF E* (MPa)	5945	5682	5551	5445	5354	5304	5248	5205
AC 16 P E* (MPa)	4540	4339	4239	4158	4088	4051	4008	3975
Stress prior to rehabilitation (MPa)	0.751838	0.664456	0.620544	0.584984	0.48615	0.4465	0.42012	0.40146
Stress prior to rehabilitation (MPa)	0.508571	0.464004	0.429907	0.40146	0.477312	0.428528	0.404145	0.382118

– rehabilitation performed in year 5, 10, 15 and rehabilitation at the end of the initial life cycle in year 20. Thus there are four scenarios: Rehabilitation in 5th year, Rehabilitation in 10th year, Rehabilitation in 15th year and Rehabilitation in 20th year. The rehabilitation design constitutes various increase of surfacing thicknesses (without milling) in relation to current state of the surfacing material based on analytical calculation method [1]. The elastic modulus of surfacing layer is shown for each rehabilitation action year and the calculated stress before and after rehabilitation. Rehabilitation design in thickness increase (millimetres), rehabilitation year and extension of life expectancy are shown in Table 5. Graphically, individual variants of extended life in different years are shown in Fig. 9.

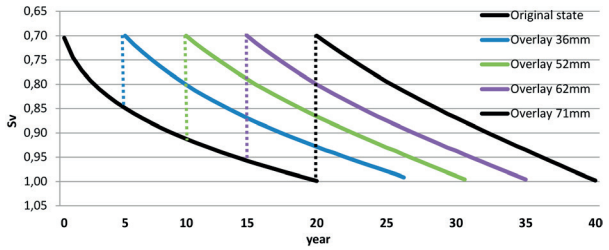

Fig. 9 Rehabilitation Design at Various Stages of the Life Cycle

6. Societal aspects and economic efficiency

The aim is to select rehabilitation variant and year which maximises economic efficiency, i.e. generates the most value for money. For calculation of economic efficiency, rehabilitation costs, increased maintenance costs and increased user costs have to be considered in case of postponed rehabilitation or for variant without any rehabilitation. Maintenance and user costs increase proportionally during the entire life cycle with operational capability of the pavement surface. The optimal time of rehabilitation can be calculated with the use of Cost Benefit Analysis in which the extension of the original life and related maintenance and user costs are taken into account. Optimisation is a mathematical relationship including all costs and surfacing layer operation.

The economic efficiency analysis is carried out with the use of Cost-Benefit Analysis (CBA). CBA evaluates positive impacts – benefits – related to improved operational parameters of the pavement in comparison to costs for applied rehabilitation actions. The Payback Period (PP), Internal Rate of Return (IRR) and Net Present Value (NPV) are economic indicators of CBA.

Calculation of economic efficiency for the experimental pavement section was performed on the basis of rehabilitation, maintenance and user costs for different variants according to Fig. 9. Quantification of road user costs was made for arterial road with usual traffic flow with yearly equivalent axle loads described in the previous chapters. The results are shown in Table 6. Rehabilitation costs are market averages, and user costs were quantified with the use of HDM-4 (Highway Development and Management Software) endorsed by the World Bank.

For quantification of user costs, vehicle fleet composed from personal car Skoda Octavia 1.6 TDI, light utility vehicle Fiat Ducato, medium truck Iveco Eurocargo, heavy truck Volovo FM9, articulated truck Volvo FH 12 + trailer Schwartzmuller and Bus Karosa C956. Their technical and economical parameters (unit

The results of the rehabilitation, maintenance and user costs — Table 6

Variant		Variant Scenario	Rehabilitation 5th year	Rehabilitation 10th year	Rehabilitation 15th year	Rehabilitation 20th year
Rehabilitation Action		-	Overlay 36 mm	Overlay 52 mm	Overlay 62 mm	Overlay 71 mm
Investment Cost		0 €	69 084 €	99 788 €	118 978 €	136 249 €
Maintenance Cost		846 938 €	858 066 €	941 350 €	1 162 456 €	1 581 330 €
Road Agency Cost		846 938 €	927 150 €	1 041 138 €	1 281 434 €	1 717 579 €
Road User Costs	Vehicle Operating Cost	8 316 431 €	9 995 382 €	11 689 165 €	13 594 956 €	16 045 362 €
	Travel Time Cost	822 241 €	973 891 €	1 125 826 €	1 290 801 €	1 569 194 €
	Total Road User Cost	9 138 673 €	10 969 273 €	12 814 991 €	14 885 757 €	17 614 555 €
Life Cycle Length		20	25	30	35	40
Optimisation index		0	475 857	461 871	461 920	483 303
CBA	NPV	-	20 333 €	26 739 €	14 527 €	1 438 €
	IRR	-	48.30%	155.10%	139.40%	99.50%
	PP	-	6	11	15	20

cost) were predefined in the HDM-4 calibration file for Slovak republic (unit cost were adjusted for year 2016). Vehicle travel speed was computed in the HDM-4 software, the road section was of average curvature (15 deg.km^{-1}) and level (2 m.km^{-1}). Speed limit was set to 90 km.h^{-1}. Vehicle operation costs and Travel time costs were subsequently calculate based on this imput. Accident cost were excluded from the computation since accident class of the road section wasn't influenced by the rehabilitation.

7. Conclusion

This paper describes topical issues of rehabilitation magnitude selection and timing of rehabilitation to ensure life cycle extension of pavement surfacing with consideration to economic efficiency of this process. The methods described in this article are based on analytical computation methods and actual measurements on experimental pavement section with the use of accelerated pavement testing. These methods are used to defined life cycle and ascertain how different rehabilitation technologies performed in different periods of the life cycle, this can be evaluated when modelling life cycle extension of the pavement surfacing. The aim of presented calculations and experiments is the search for optimal technology and time of rehabilitation, i.e., identification of methods to extend the life cycle for the lowest sum of economic costs. The calculations of surfacing life cycle and its extensions which are presented in this article are exemplificative, yet applicable in real life conditions. Values that are necessary to measure during pavement operation are derived from experimental pavement model. Economic calculations are made using common methods with the computation model of the World Bank.

Acknowledgement

The research is supported by the European Regional Development Fund and the Slovak state budget for the project "Research Centre of University of Zilina", ITMS 26220220183.

References

[1] GSCHWENDT, I.: *Pavement Structure Design. Technical Standards 3/2009.*Ministry of transport and telecommunication, Slovakia, p.52

[2] EUROPEAN COMMITTEE FOR STANDARDIZATION (CEN) EN 12697-26: Bituminous mixtures – Test method for hot mix asphalt – Part 26: Complex modulus, Brussels, Belgium 2003.

[3] ZGUTOVA, K.: *Non-destructive Determining CBR Values of Ground Structures of Engineering Constructions,* 14th Intern. Multidisciplinary Scientific GeoConference SGEM 2014.

[4] MINISTRY OF TRANSPORTAION OF CZECH REPUBLIC, Czech Pavement Design Manual, TP 170, VUT Brno, CVUT: Praha: SSZ: ODS, November 2004

[5] EUROPEAN COMMITTEE FOR STANDARDIZATION (CEN): EN 12697-24: Bituminous mixtures – Test method for hot mix asphalt – Part 24: Resistant to fatigue, Brussels 2003.

[6] SCHLOSSER, F., SRAMEKOVA, E., SRAMEK, J.: Rheology, Deformational Properties and Fatigue of the Asphalt Mixtures. *Advanced Materials Research*, vols. 875-877, 2014, ISSN 1662-8985 (web), ISSN 1022-6680 (print), pp. 578-583, 2014.

[7] CELKO, J., KOMACKA, J.: *Analysis of the Pavement Bearing Capacity on the Deflection Bowl Basis.* Fifth Intern. Conference on the Bearing Capacity of Roads and Airfields, Trondheim, vol. I, pp. 609-617, 1998.

[8] NOVOTNY, B., HANUSKA, A.: *The Theory of Multi Layered Half Space*, Veda : Bratislava, 1983.

[9] KATMAN, H., Y., et al: Evaluation of Permanent Deformation of Unmodified and Rubber-Reinforced SMA Asphalt Mixtures Using Dynamic Creep Test, *Materials Science and Engineering*, vol. 2015, Hindavi Publishing Corporation, ISSN 1687-8442 – online, ISSN 1687-8434- print, 2015.

[10] MINISTRY OF TRANSPORTAION OF CZECH REPUBLIC, Czech Pavement Design Manual, TP 170, VUT Brno, CVUT: Praha: SSZ: ODS, November 2004

[11] CELKO, J., DECKY, M., KOVAC, M.: An Analysis of Vehicle - Road Surface Interaction for Classification of IRI in Frame of Slovak PMS. *Maintenance and Reliability*. Polish Maintenance society, No. 1, 41, pp. 15-21, ISSN 1507-2711, 2009.

[12] CHYTCAKOVA, A.: *Evaluation Parameters of Operational Competence in the Pavement Management System*. PhD thesis, University of Zilina, November 2014.

[13] WORLD ROAD ASSOCIATION (PIARC): *Highway Performance Monitoring Systems.* Technical Committee 6 road management. ISBN 2-84060-052-8, p. 68, 1997.

[14] PENG, G., F., et al.: Mechanical Properties of Recycled Aggregate Concrete at Low and High Water/Binder Ratios, *Materials Science and Engineering*, vol. 2013, Hindavi Publishing Corporation, ISSN 1687-8442 - online, ISSN 1687-8434- print, 2013.

https://doi.org/10.26552/com.C.2016.4.90-98

Andrea Kocianova*

CAPACITY LIMITS OF BASIC TURBO-ROUNDABOUTS

Turbo-roundabouts with their specific design characteristics have become a suitable solution of a single-lane roundabouts capacity problem and a standard two-lane roundabouts safety problem. There is no doubt that turbo-roundabouts ensure a higher level of traffic safety in comparison to standard two-lane roundabouts due to a reduction of both conflict points and driving speed through the turbo-roundabouts. The question is if turbo-roundabouts can provide the same or a higher capacity than standard two-lane roundabouts. The answer, in the form of some important results of the basic turbo-roundabout total capacity at various traffic conditions and also in comparison with standard two-lane roundabouts, is presented in the paper. The capacity model is based on the gap-acceptance theory. Driver behaviour characteristics have been respected according to the Slovak technical guidelines. Redistribution of traffic flows into two lanes at entries and circulatory carriageway of roundabouts has been considered in the capacity calculations. An effective use of both lanes (left and right) has been assumed only at basic turbo-roundabout major entries. By contrast, low use of inner (left) lanes by drivers at entry and circulatory carriageway corresponding with real conditions in some countries has been assumed in the standard two-lane roundabout capacity calculations.

Keywords: *Traffic safety, capacity, two-lane roundabout, turbo-roundabout.*

1. Introduction

A turbo-roundabout is a relatively new type of roundabout. It was developed by the researcher Lambertus Fortuijn from the University of Delft in the Netherlands in 1996 as a solution of a capacity problem of single-lane roundabouts and a traffic safety problem of multi-lane roundabouts. Over the last ten years, turbo-roundabouts have been successfully implemented, apart from the Netherlands, in many European countries such as Germany, Slovenia, Belgium, the Czech Republic, Poland, Hungary and several others. Currently, over 400 turbo-roundabouts are built in Europe and this number continuously grows.

Foreign experience clearly confirms a higher traffic safety of turbo-roundabouts in comparison to multi-lane roundabouts, however, the question whether turbo-roundabouts can provide the same or higher capacity than multi-lane roundabouts is frequently discussed [1, 2 and 3]. In this article, a comparison of the total capacity of a basic turbo-roundabout and a standard two-lane roundabout (Fig. 1) at different traffic conditions is presented.

2. Main concept of turbo-roundabout

A turbo-roundabout is a specific type of multi-lane roundabout with a spiral arrangement of two or more circulating traffic lanes, where drivers are forced to follow a specific path according to their intended destination (Fig. 1, left) [3]. Traffic lanes in the entry, circulatory carriageway and exit zones are physically separated by specially shaped elements, which divert drivers to change traffic lanes in the roundabout [4]. Raised lane dividers are only interrupted at places of entry into the inner traffic lanes of circulatory carriageway.

The new circulating lane formed on the inner side of circulating carriageway of turbo-roundabouts (nested spiral lane) is designed opposite to the major entries (A and B in Fig. 1, left). Major entries are considered in dominant direction of the main traffic flow which is a criterion for selection of a suitable type of a turbo-roundabout (basic, egg, knee, spiral, rotor or star [5]).

The physical separation of traffic lanes and the specific geometry of turbo-roundabouts are the most important features affecting traffic safety and capacity differences in comparison to two-lane roundabouts.

3. Traffic safety improvements

In the simplest case, on a standard two-lane roundabout with two-lane entries and two-lane exits, there are 24 conflict points (Fig. 2, right). However, in reality, the traffic situation is much more complicated. Because there is no clearly specified legal framework for passing through the roundabout, drivers can enter the roundabout using any circulating lane, change lane at the

* **Andrea Kocianova**
Department of Highway Engineering, Faculty of Civil Engineering, University of Zilina, Slovakia
E-mail: andrea.kocianova@fstav.uniza.sk

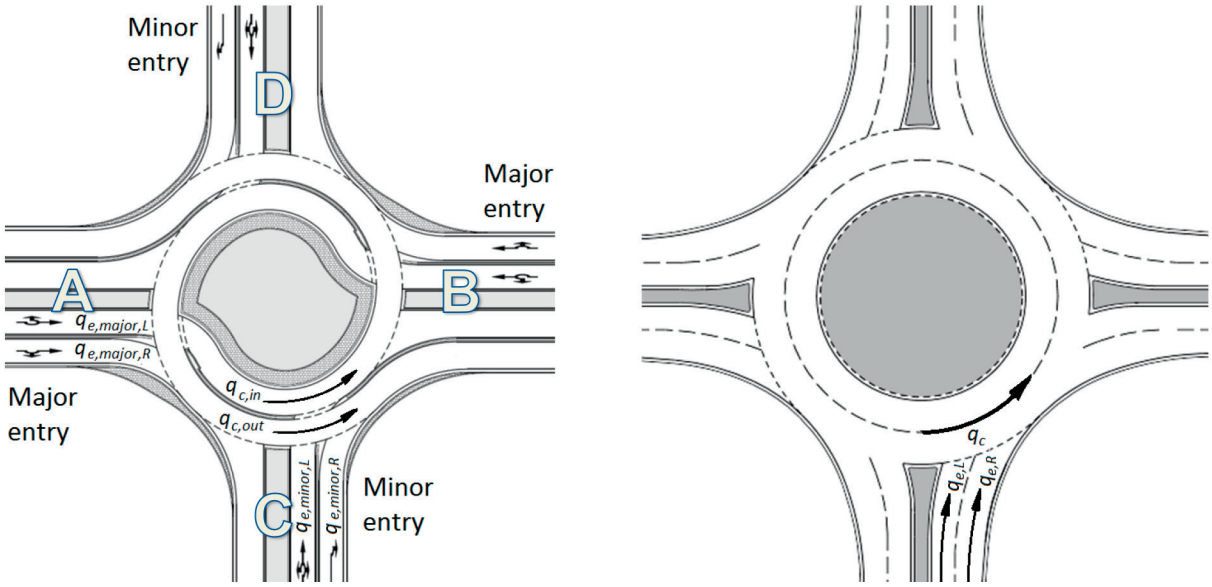

Fig. 1 Geometry of a basic turbo-roundabout (left) and a standard two-lane roundabout (right), Source: Author

circulatory carriageway and also they can leave the roundabout using any exit lane. This driver behaviour results in additional conflict points and weaving conflicts which, together with higher speeds, raise the risk of accidents. International experience has confirmed these functional problems. Accidents in the circulatory carriageway, although not usually serious, are frequent and often affect the normal traffic flow [2].

Traffic safety improvement of turbo-roundabouts in comparison with two-lane roundabouts is ensured thanks to the specific geometry (spiral alignment of circulating traffic lanes leading drivers to the correct exit) and the raised lane dividers. As a result, there are several advantages from the viewpoint of traffic safety: the reduction in conflict points from 24 to 14 (reduction of entry and exit conflict points including the elimination of very dangerous crossing conflict points at the exit from the inner circulating lane, see Fig. 2), the removal of weaving (lane changing) in the circulatory carriageway, the elimination of side-by-side accident risk and the reduction of driving speed through the roundabout. It ultimately means a global reduction of crash probabilities.

Several studies have shown that crash risk is reduced by 70% when the standard two-lane roundabout is converted into the turbo-roundabout [5]. Other study, based on the analysis of potential conflicts modelled in different layouts and traffic conditions, has shown that turbo-roundabouts provide about 40-50% reduction of total potential accidents and about 20-30% reduction of potential accidents with injuries in comparison with two-lane roundabouts [6]. Some studies even concluded that safety of turbo-roundabouts is comparable with the safety of single-lane roundabouts [5].

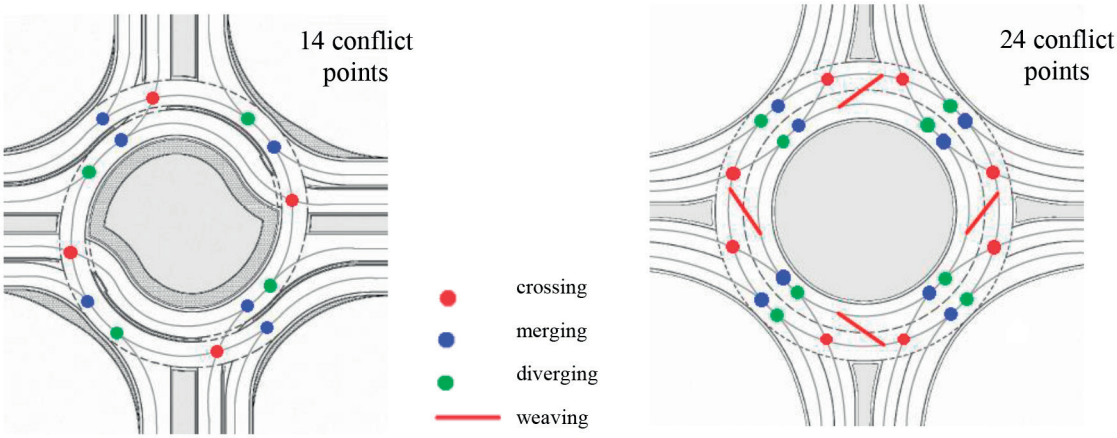

Fig. 2 Conflict points and weaving conflicts on standard two-lane roundabouts (right) and basic turbo-roundabouts (left), Source: author

In a study based on micro-simulation, it is shown that drivers using the outer circulating lane of turbo-roundabouts drive slower than on two-lane roundabouts. The reduction in the speed is from 48 km/h to 38 km/h [7]. One of the factors affecting the speed profile of drivers on turbo-roundabouts is the path curvature (system of inverse radii). The raised lane dividers play also an important role. They "force" drivers to use the predefined trajectory with smaller radii at lower speeds, thus contributing to the homogenous low-speed profiles [2]. On the contrary, drivers on two-lane roundabouts can ignore lane markings and pass the intersection on a shortened trajectory at high speed.

4. Capacity of turbo-roundabouts

Turbo-roundabouts have always larger capacity compared to single-lane roundabouts. The reason is turbo-roundabouts have usually two-lane entries, which directly continue into two-lane circulatory carriageway. When comparing capacity of turbo-roundabouts to standard two-lane roundabouts, it is necessary to take into account the geometry differences between the two kinds of roundabouts affecting the capacity performance at a variety of traffic conditions.

The main geometry differences between compared the basic turbo-roundabout and the standard two-lane roundabout with two lanes at all entries and exits (Fig. 1) are the following:

- A circulating traffic flow in front of the major entries (A and B) on the turbo-roundabout is concentrated in a single circulating lane, whereas on the two-lane roundabout, there are two circulating lanes available.
- While a through traffic flow can use only a left lane at the minor entries (C and D) on the turbo-roundabout, both left and right entry lanes on the two-lane roundabout are available.
- A right-turning traffic flow can use both left and right lanes at the minor entries (C and D) on the turbo-roundabout, whereas on the two-lane roundabout, only the right lane is used by the right-turning traffic.
- The change of lanes on the circulatory carriageway is not allowed (nor necessary) for drivers on the turbo-roundabout, whereas on the two-lane roundabout it is possible.

The above differences in geometry of roundabouts also affect the traffic redistribution at two-lane major and minor entries, and on two-lane circulatory carriageway. Because it has a significant influence on the entry capacity, it was further considered within the capacity calculations.

4.1 Capacity model

Capacity model used in this paper is based on the gap acceptance theory and capacity calculations are lane-based. Specifically, a formula proposed by Brilon [8] is used for capacity calculation of each entry lane to the basic turbo-roundabout and a formula proposed by Wu [9] is derived for capacity calculation of each entry lane to the standard two-lane roundabout.

The capacity model used for the basic turbo-roundabout is sensitive to the traffic flow allocation to both inner and outer lane on the two-lane circulatory carriageway. However, it does not take into account an influence of differences in critical headways and follow-up times which have a very low impact on the capacity compared with the traffic flow allocation in the circulating lanes [3].

Left-lane capacity at the minor entries (C and D in Fig. 1) considering the traffic flows in the inner circulating lane ($q_{c,in}$) and in the outer circulating lane ($q_{c,out}$) was calculated according to equation:

$$C_e = \frac{3600}{t_f} \cdot \left(1 - \frac{t_{\min} \cdot q_{c,out}}{3600}\right) \cdot \left(1 - \frac{t_{\min} \cdot q_{c,in}}{3600}\right) \cdot e^{-\frac{q_{c,out}+q_{c,in}}{3600}\left(t_c - \frac{t_f}{2} - t_{\min}\right)} \quad (5.1)$$

where:

C_e basic capacity of entry lane [pcu/h],
$q_{c,out}$ traffic flow on the outer circulating lane in front of entry [pcu/h],
$q_{c,in}$ traffic flow on the inner circulating lane in front of entry [pcu/h],
t_c critical gap [s],
t_f follow-up time [s],
t_{min} minimum gap between succeeding vehicles on the circulatory carriageway [s].

A considerable impact of the circulating traffic flow allocation in the inner and the outer circulating lanes on the entry lane capacity is shown in Fig. 3. The maximum capacity is achievable at equal distribution of the circulating traffic flow to circulating lanes (the curve 50/50 in Fig. 3) and the minimum capacity when the whole circulating traffic flow is in one circulating lane (the curve 100/0 in Fig. 3).

Right-lane and left-lane capacities at the major entries (A and B in Fig. 1), as well as the right-lane capacity at the minor entries (C and D in Fig. 1) were calculated considering the circulating traffic flow only in the outer lane ($q_{c,out}$) according to equation:

$$C_e = \frac{3600}{t_f} \cdot \left(1 - \frac{t_{\min} \cdot q_{c,out}}{3600}\right) \cdot e^{-\frac{q_{c,out}}{3600}\left(t_c - \frac{t_f}{2} - t_{\min}\right)} \quad (5.2)$$

Notations in Equation 5.2 have the same meaning as in Equation 5.1. Values of the gap acceptance parameters are taken from the Slovak technical guidelines [10]:

- left lane at minor entry: t_c = 3.9 s, t_f = 2.7 s, t_{min} = 2.1 s;
- right lane at minor and major entries: t_c = 4.0 s, t_f = 2.8 s, t_{min} = 2.1 s;
- left lane at major entry: t_c = 3.8 s, t_f = 2.7 s, t_{min} = 2.1 s;

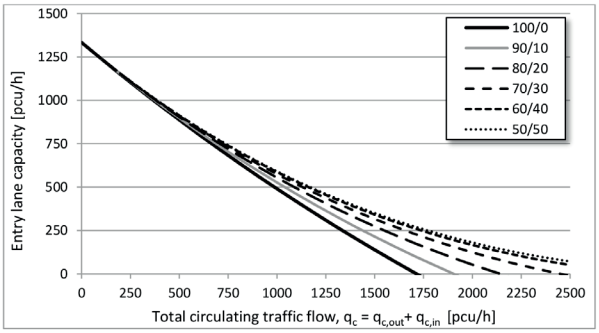

Fig. 3 Impact of the circulating traffic flow allocation on the entry lane capacity, Source: author

In the capacity model for the standard two-lane roundabout, only a total opposing circulating traffic flow in the two-lane circulatory carriageway (q_c) without a traffic flow allocation is considered. It is because drivers are not strictly keeping in one circulating lane as in turbo-roundabouts, but there is an option to switch lanes at any point. Capacity of each entry lane (left-lane and right-lane capacity) is calculated using the formula:

$$C_e = \frac{3600}{t_f} \cdot \left(1 - \frac{t_{\min} \cdot q_c}{3600}\right) \cdot e^{-\frac{q_c}{3600}\left(t_c - \frac{t_f}{2} - t_{\min}\right)} \qquad (5.3)$$

Where n_c is number of circulating lanes ($n_c = 2$) and other notations in Equation 5.3 have the same meaning as in Equation 5.1. Values of gap acceptance parameters are taken from the Slovak technical guidelines [11] and they are the same for left and right entry lanes: $t_c = 3.9$ s, $t_f = 2.7$ s, $t_{min} = 2.1$ s.

4.2 Entry traffic flows allocation procedure

Allocation of traffic flows to right and left lanes at major entries and minor entries of the **basic turbo-roundabout** is entirely different because of its specific geometry. As it has been written, while through traffic can use both left and right lanes at major entries, only a left lane at minor entries can be used (right minor entry lane is determined just for a right-turning traffic, see Fig. 1).

As a result, the allocation procedure at the major entries on basic turbo-roundabouts (A and B in Fig. 1) is based on the assumption that drivers going straight will choose the entry lane with the lowest degree of saturation and thus with the lowest waiting time (or queue). Therefore, the through traffic proportion using the right lane at major entries under assumption of equilibrium state at peak hours (lanes have equal levels of saturation) in the capacity model is given by formula:

$$p_{major} = \frac{C_{major,R} \cdot (q_1 + q_2) - C_{major,L} \cdot q_3}{q_2 \cdot (C_{major,L} + C_{major,R})}; \quad p_{major} \in \langle 0, 1 \rangle \qquad (5.4)$$

where q_1, q_2 and q_3 are left, through and right traffic flows respectively and $C_{major,R}$ and $C_{major,L}$ are right-lane and left-lane capacities at major entries calculated by the Equation 5.2. If $p_{major} \in (-\infty, 0) \Rightarrow p_{major} = 0$ or $p_{major} \in (1, \infty) \Rightarrow p_{major} = 1$.

Resulting traffic flows on right and left lanes at major entries ($q_{e,major,R}$ and $q_{e,major,L}$) are then given by the Equations (5.5) and (5.6):

$$q_{e,major,R} = p_{major} \cdot q_2 + q_3 \qquad (5.5)$$

$$q_{e,major,L} = q_1 + (1 - p_{major}) \cdot q_2 \qquad (5.6)$$

Because the right-turning traffic can use both left and right lanes at the minor entries on basic turbo-roundabouts (C and D in Fig. 1), its proportion using the right lane is given by formula:

$$p_{minor} = \frac{C_{minor,R} \cdot (q_1 + q_2 + q_3)}{q_2 \cdot (C_{minor,L} + C_{minor,R})}; \quad p_{minor} \in \langle 0, 1 \rangle \qquad (5.7)$$

where $C_{minor,R}$ is the right-lane capacity at minor entries calculated by the Equation 5.2 and $C_{major,L}$ is the left-lane capacity at minor entries calculated by the Equation 5.1.

If $p_{minor} \in (-\infty, 0) \Rightarrow p_{minor} = 0$ or $p_{minor} \in (1, \infty) \Rightarrow p_{minor} = 1$.

Resulting traffic flows on right and left lanes at minor entries ($q_{e,minor,R}$ and $q_{e,minor,L}$) are given by the Equations (5.8) and (5.9):

$$q_{e,minor,R} = p_{minor} \cdot q_3 \qquad (5.8)$$

$$q_{e,minor,L} = (q_1 + q_2) + (1 - p_{minor}) \cdot q_3 \qquad (5.9)$$

Allocation of traffic flows to right and left lanes at all entries of the **standard two-lane roundabout,** in comparison to the basic turbo-roundabout, is quite different because of free-flow conditions at two-lane entries, circulatory carriageway and exits. This allows drivers to use any entry lane and subsequently any circulating lane. However, the use of the inner circulating lane in reality is not too much attractive for drivers, since there is dangerous crossing conflict point at the exit from this lane or there is the need of weaving (see Fig. 2). As a result, drivers do not utilise the left lane at two-lane entries sufficiently and the traffic flows in both lanes at the entry are not equally distributed. It has been observed not only on two-lane entries at the German roundabouts [12], but at the standard two-lane roundabouts in the Czech Republic and Slovakia. As it follows from surveys, the right lane is used more frequently than the left lane, about 70% of the total entry traffic flow during peak hours, even if there is a long queue [13 and 14]. This has a significant impact on the two-lane entry capacity, which is not as high in reality as was assumed according to the original Wu capacity model.

Since the two-lane entry capacity at standard two-lane roundabouts is strongly dependent on the allocation of traffic flows to left and right entries (see Fig. 4), it was also taken into

account at the capacity calculations. Redistribution of traffic volumes to left and right entry lanes in the capacity model is assumed at a ratio of 30% : 70% (the curve 30/70 in Fig. 4). The entry capacity with such a flows allocation is by 29% lower than for equal allocation (the curve 50/50 in Fig. 4).

The capacity of two-lane entry shown in Fig. 4 is dependent on flow rate of each entry lane and on the degree of saturation of the critical lane, and it is computed in accordance with the model described in more details, for example, in [1, 15 and 16]

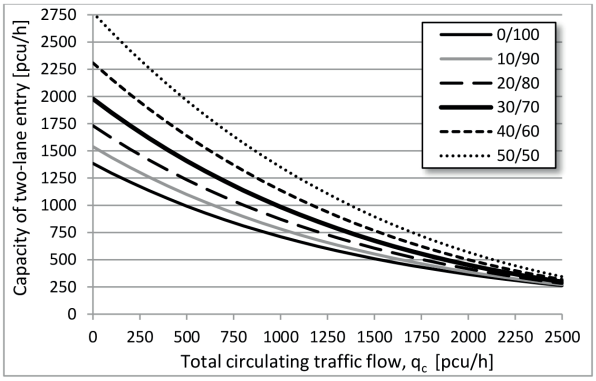

Fig. 4 Impact of the traffic flows allocation on the two-lane entry capacity; Source: Author

4.3 Traffic conditions

Since the proportion of traffic at major entries and proportion of left- and right-turning traffic have a significant influence on the intersection capacity, the following traffic conditions were modelled within capacity calculations:

- Various ratios of the total traffic load at major entries and minor entries: Major/Minor from 100/0 to 50/50 (Major/Minor = 90/10 means that the total traffic load at the major entries A+B is 90% and the total traffic load at the minor entries C+D is 10% of the total roundabout traffic load),
- Various left-turning traffic proportion of the total entry traffic load (%L): from 0% to 100%,
- Various right-turning traffic proportion of the total entry traffic load (%R): from 0% to 100%.

The variations were modelled under symmetric demand at major entries, symmetric demand at minor entries and equal traffic split at all entries.

4.4 Capacity performance of turbo-roundabouts

The total traffic volume, as the sum of traffic volumes at all entries to the roundabout, at specified traffic conditions has been progressively increased from zero in 10 pcu/h steps until the degree of saturation of any minor or major entry lane of the turbo-roundabout and the two-lane roundabout reached the value 1.0 (the capacity reserve is zero).

The total capacity has been calculated for every possible combination of traffic conditions in 2.5% steps. In this paper, only selected important results which show a clear impact of different pattern of traffic load on the total capacity of basic turbo-roundabouts are presented in Fig. 5. The total capacity of basic turbo-roundabouts in comparison with the total capacity of two-lane roundabouts and also differences between the total capacities in percentages are shown in Fig. 6 (green colour means a higher capacity and red colour means a lower capacity of turbo-roundabouts).

As it can be seen from the results, the influence of the right-turning proportion (%R) on the total capacity of turbo-roundabouts significantly depends on the demand flows at major and minor entries (Major/Minor) - see slope of the curves on the left graphs in Fig. 5. When having the substantial prevalence of the major traffic flow over the minor traffic flow (see the graph Major/Minor = 90/10) and the right-turning proportion is till 50%, the influence is negligible. The difference in the total capacity is only about 1-4%. However, at a higher proportion of right-turning traffic than 50%, the total capacity goes down sharply (for example at the left-turning traffic proportion L10%, the total capacity reduction is up to 60%). This is because only one lane (the right lane) at major entries for the right-turning traffic flow is determined and the lane becomes in terms of performance a critical lane.

The opposite situation occurs at a higher traffic load at minor entries, when increasing the right-turning traffic proportion up to 50%, the total capacity increases significantly. The increase may be at the ratio of Major/Minor = 70/30 approximately 15-50%, and at balanced demand flows at all entries even up to 70% depending on the left-turning traffic proportion. At a higher proportion of right-turning traffic than 50%, the total capacity is decreased, but not so sharply as at a high proportion of traffic load at major entries. For example, at balanced demand flows at all entries and at the left-turning traffic proportion L10%, the total capacity reduction is only 8%.

A significant influence of the low right-turning traffic proportion on the total capacity is also illustrated on the right graphs in Fig. 5. At minor entries of turbo-roundabouts, the low proportion of right-turning traffic results to insufficient use of right lanes (determined only for the right-turning traffic flow) and a higher saturation of left lanes at the same time. At a lower proportion of right-turning traffic than 40%, the total capacity of turbo-roundabouts thus can go down at increasing the minor traffic flow – see the breaking point in Fig. 5, right. The reason is the capacity failure of the left lane at minor entries.

The total capacity of turbo-roundabouts with increasing left-turning traffic proportion (%L) gets always decreased (it can be up to 70%) depending on demand flows at major and minor entries (Major/Minor) - see spacing of the curves in Fig. 5. When having

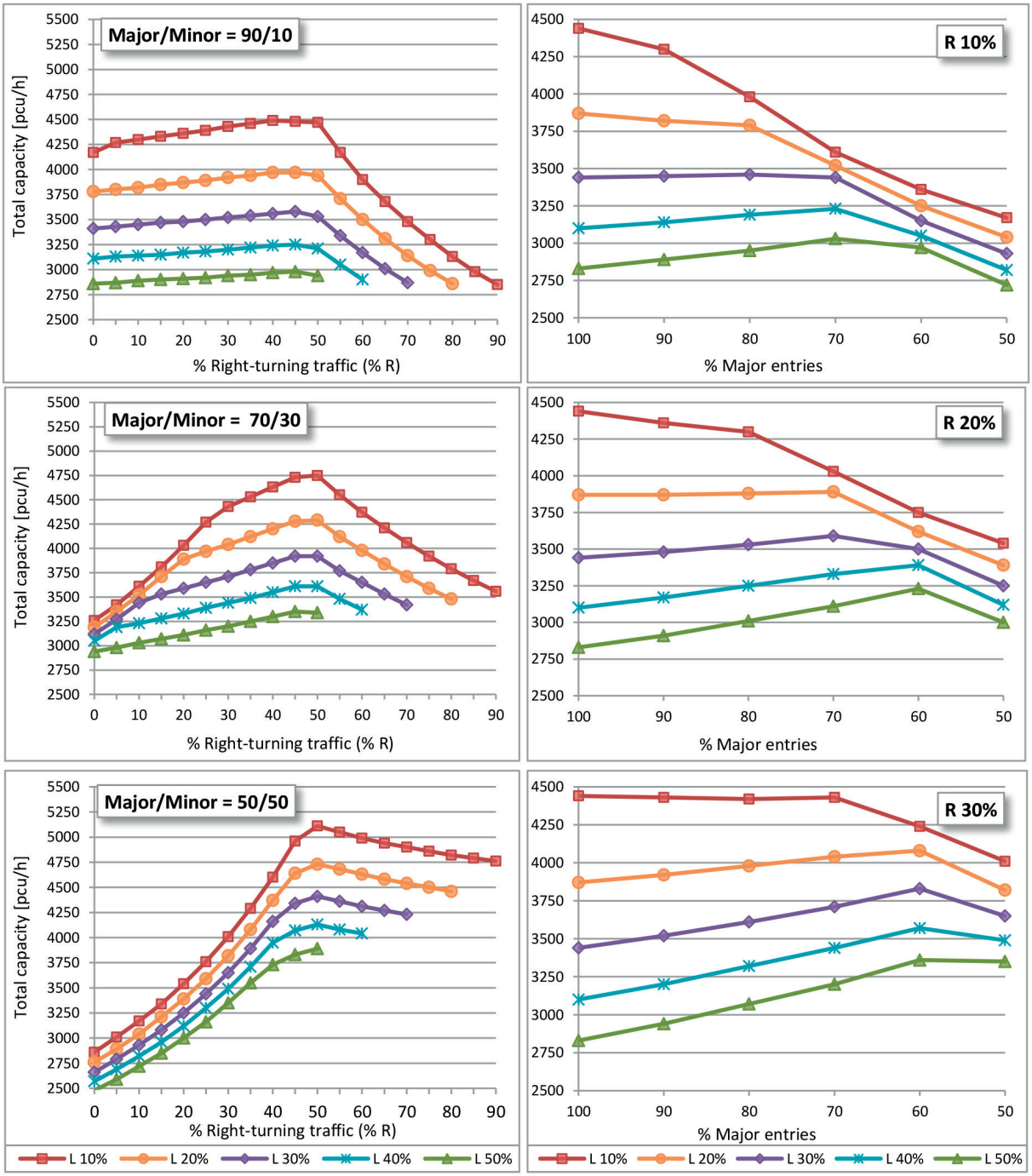

Fig. 5 Traffic condition influence on the total capacity of basic turbo-roundabouts; Source: Author

the substantial prevalence of the major traffic flow over the minor traffic flow (see the graph Major/Minor = 90/10), the influence of the left-turning traffic proportion at the right-turning traffic proportion up to 50% is significant and subsequently decreases. On the contrary, at balanced demand flows at all entries, the influence of the left-turning traffic proportion at the right-turning traffic proportion up to 50% is low and subsequently increases.

Differences in geometry and also in efficiency of the use of both right and left entry lanes on compared roundabouts result to different total capacities at various traffic conditions (Fig. 6). At a substantial prevalence of the major traffic flow over the minor

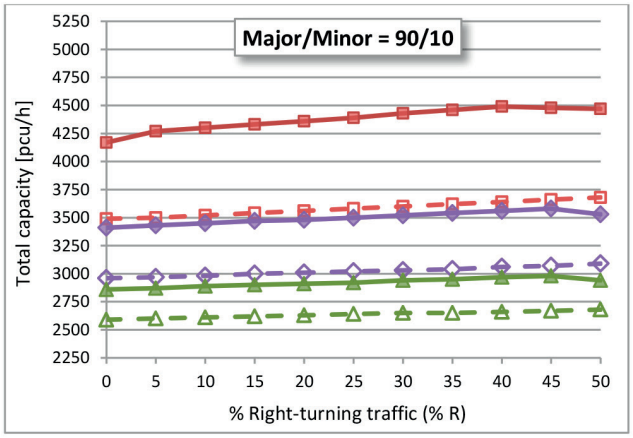

90/10		% L										
		0	5	10	15	20	25	30	35	40	45	50
% R	0	9	14	19	20	18	17	15	14	13	12	10
	5	14	20	22	20	18	17	15	14	13	12	10
	10	19	24	22	20	18	17	16	14	13	12	11
	15	24	24	22	20	19	17	16	14	13	12	11
	20	27	25	22	21	19	17	16	14	13	12	11
	25	27	25	23	21	19	18	16	15	13	12	11
	30	28	25	23	21	19	18	16	15	13	12	11
	35	28	26	23	21	19	18	16	15	13	13	11
	40	28	26	23	21	19	18	16	15	14	13	12
	45	29	26	22	21	19	18	17	15	14	13	12
	50	27	24	21	20	18	16	14	13	12	11	10

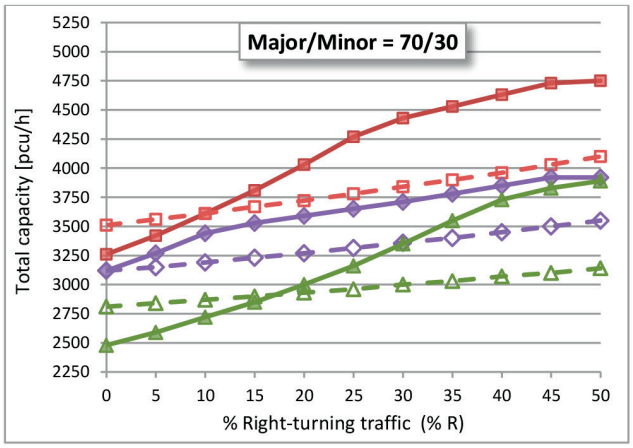

70/30		% L										
		0	5	10	15	20	25	30	35	40	45	50
% R	0	-11	-9	-7	-5	-3	-2	0	2	3	6	5
	5	-8	-6	-4	-2	0	2	4	6	7	6	5
	10	-6	-2	0	2	4	6	8	8	7	6	6
	15	-3	2	4	6	8	10	9	8	7	6	6
	20	1	5	8	11	12	11	10	9	8	7	6
	25	6	10	13	13	12	11	10	9	8	8	7
	30	10	15	15	14	13	12	10	10	9	8	7
	35	16	18	16	15	13	12	11	10	9	8	7
	40	20	18	17	15	14	13	12	10	10	9	7
	45	21	19	17	16	14	13	12	11	9	9	8
	50	19	17	16	14	13	11	10	10	8	7	6

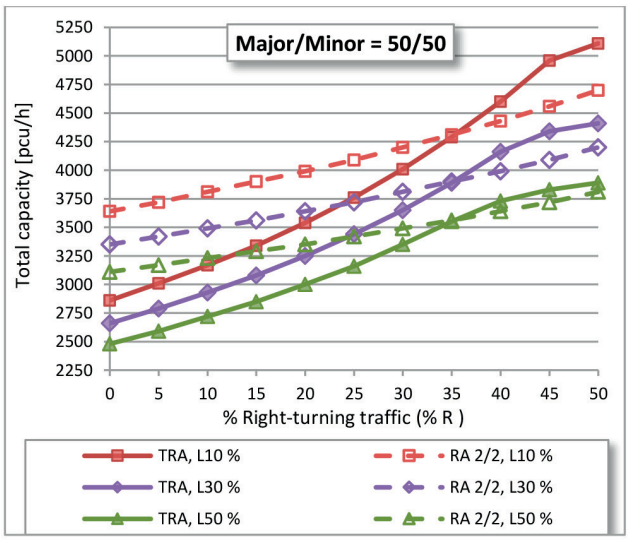

50/50		% L										
		0	5	10	15	20	25	30	35	40	45	50
% R	0	-22	-22	-21	-21	-21	-21	-21	-21	-20	-21	-20
	5	-20	-19	-19	-19	-19	-19	-18	-18	-18	-18	-18
	10	-17	-17	-17	-17	-17	-17	-16	-16	-16	-16	-16
	15	-14	-15	-14	-14	-14	-14	-13	-13	-13	-13	-13
	20	-12	-12	-11	-11	-11	-11	-11	-11	-11	-11	-10
	25	-9	-8	-8	-8	-8	-8	-8	-7	-8	-7	-8
	30	-5	-5	-5	-5	-5	-4	-4	-4	-4	-4	-4
	35	-1	-1	-1	-1	-1	-1	-1	-1	-1	-1	-1
	40	3	4	4	4	4	4	4	4	4	3	2
	45	8	8	9	8	7	7	6	5	4	4	3
	50	11	10	9	7	7	6	5	4	3	3	2

(+)	0 - 5 %	5 - 10 %	10 - 15 %	15 - 20 %	20 - 25 %	25 - 30 %
(-)	0 - 5 %	5 - 10 %	10 - 15 %	15 - 20 %	20 - 25 %	

Fig. 6 Total capacity comparison: basic turbo-roundabouts (TRA) versus standard two-lane roundabouts (RA 2/2), Source: author

traffic flow (Major/Minor = 90/10), turbo-roundabouts have a higher total capacity than two-lane roundabouts. The reason is in more efficient uses of both lanes at major entries on turbo-roundabouts. In contrast, a low efficient use of left-entry lanes on two-lane roundabouts leads to a faster overloading of critical right-entry lanes. Of course, in an increasing left-turning traffic

proportion over 70%, the possibility of using both lanes at entries on two-lane roundabouts for the left-turning traffic flow leads to a higher total capacity compared to basic turbo-roundabouts, where left-turning drivers are forced to use only one lane (the left lane) at major entries. This applies even at other demand flows at major and minor entries.

At increased proportion of the traffic flow at minor entries, the total capacity of roundabouts significantly depends on the right-turning traffic proportion. If the proportion is too low (%R = 10-20%), the total capacity of turbo-roundabouts can be less than the total capacity of two-lane roundabouts. Even, under balanced traffic load at all entries and at the right-turning traffic proportion less than 30%, the total capacity of turbo-roundabouts is always less than the total capacity of two-lane roundabouts. The reason is the right-entry lane at minor entries exclusively determined only for the right-turning traffic flow. At a low proportion of right-turning traffic, the entry lane is not used enough effectively and this leads to the capacity failure of the left entry lane, which has to ensure both through and left-turning movements.

5. Conclusions

The total capacity of turbo-roundabouts is, depending on traffic conditions, about 1.2 to 2.0 times higher than the capacity of single-lane roundabouts. Thanks to their specific geometry and ensuring the passage of vehicles through turbo-roundabouts with a significantly higher level of traffic safety, it can be achieved even from about 5% to 25% higher capacity in comparison to standard two-lane roundabouts. A higher performance of turbo-roundabouts can be achieved at a higher traffic load in dominant direction at major entries and lower traffic load at minor entries (more than about 70% proportion of the total traffic load at major entries). This is due to the more efficient use of both right and left lanes at major entries on turbo-roundabouts comparing to two-lane roundabouts, where only 30% proportion of the total entry traffic load on the left entry lane is expected. Furthermore, the total capacity of turbo-roundabouts is increased with an increasing proportion of right-turning traffic especially at minor entries (over 30% right-turning proportion).

On the other side, the total capacity of standard two-lane roundabouts can be about 5% to 20% higher in comparison to turbo-roundabouts. It is achievable at more balanced distribution of traffic loads on all roundabout entries and also at a higher proportion of left-turning traffic (more than 70%).

It can be concluded that the turbo-roundabouts provide a combination of high level of traffic safety with a relatively large capacity. Through their indisputable advantages following the successful foreign experience, their more extensive use in Slovakia is expected in a short time. Subsequently it will be possible to test the real capacities of turbo-roundabouts, choose the appropriate capacity model together with input parameters and also set microsimulations to real Slovak conditions.

Acknowledgement

This contribution/publication is the result of the project implementation:

Centre of excellence for systems and services of intelligent transport, ITMS 26220120028 supported by the Research & Development Operational Programme funded by the ERDF.

„Podporujeme výskumné aktivity na Slovensku/Projekt je spolufinancovaný zo zdrojov EÚ“

References

[1] MAURO, R., BRANCO, F.: Comparative Analysis of Compact Multilane Roundabouts and Turbo-Roundabouts. *J. of Transportation Engineering 136*, 316-322, 2010. ISSN 0733-947X.

[2] SILVA, A. B., SANTOS, S., GASPAR, M.: *Turbo-roundabout Use and Design.* CITTA 6th Annual Conference on Planning Research, Responsive transports for smart mobility, 2013.

[3] VASCONCELOS, A. L. P., SILVA, A. B., SECO, A. J. D. M.: *Capacity of Normal and Turbo-roundabouts: Comparative Analysis.* Proc. of the Institution of Civil Engineers (ICE), 11/2012.

[4] TOLLAZZI, T., TURNSEK, S., RENCELJ, M.: *Slovenian Experiences with Turbo-roundabouts.* Proc. of the 3rd Intern. Book on Roundabouts, TRB : USA, 2011.

[5] FORTUIJN, L. G. H.: Turbo Roundabouts: Design Principles and Safety Performance. *J. of the Transportation Research Board,* vol. 2096, pp. 16-24, 2009, ISBN 9780309126120.

[6] MAURO, R., CATTANI, M.: *Potential Accident Rate of Turbo-Roundabouts.* 4th Intern. Symposium on Highway Geometric Design, Valencia, 2010.

[7] FORTUIJN, L. G. H.: *Turbo-Kreisverkehre - Entwicklungen und Erfahrungen.* Seminar Aktuelle Theme der Strassenplanung. Bergisch Gladbach, 2007.
[8] BRILON, W., BONDZIO, L., WEISER, F.: *Experiences with Turbo-Roundabouts in Germany*. *5th Rural Roads Design Meeting,* Copenhagen. Available online at: http://nmfv.dk/wp-content/uploads/2014/04/Experiences-with-Turbo-Roundabouts-in-Germany-BrilonBondzio-Weiser.pdf, Accessed April 3-4, 2014.
[9] BRILON, S., WU, N., BONDZIO, L.: *Unsignalized Intersections in Germany - A State of the Art 1997*. Proc. of the Third International Symposium on Intersections without Traffic Signals, Portland: Oregon, 1997.
[10] TP 14/2015 Design of Turbo-roundabouts (in Slovak). *Technical regulations*. Ministry of Transport, Construction and Regional Development, Bratislava, 2015. Available online at: http://www.ssc.sk/files/documents/technicke-predpisy/tp2015/tp-14_2015.pdf.
[11] TP 16/2015 Roads Capacity Calculation (in Slovak). *Technical regulations*. Ministry of Transport, Construction and Regional Development, Bratislava, 2015. Available online at: http://www.ssc.sk/files/documents/technicke-predpisy/tp2015/tp-16_2015.pdf.
[12] BRILON, W.: Roundabouts: *A State of the Art in Germany.* National Roundabout Conference, Vail : Colorado, May 22-25, 2005.
[13] KOCIANOVA, A.: A New Approach to the Capacity Assessment of Two-Lane Entries on Roundabouts (in Slovak). *Silnicni obzor 76*, No. 7-8, 2015. ISSN 0322-7154.
[14] SMELY, M., RADIMSKY, M., APELTAUER, T.: Capacity of roundabouts with multi-lane entries (in Czech), *Dopravni inzenyrstvi*, 01/2011, ISSN 1801-8890.
[15] AKCELIK, R.: *Roundabout Model Calibration Issue and a Case Study*. TRB National roundabout conference: USA, 2005.
[16] GUERRIERI, M., CORRIERE, F., TICALI, D.: Turbo-Roundabouts: A Model to Evaluate Capacity, Delays, Queues and Level of Service. *European J. of Scientific Research,* vol. 92, No. 2, December, 2012, ISSN 1450-216X.

https://doi.org/10.26552/com.C.2016.4.99-102

Kamil Borko - Filip Pastorek - Stanislava Fintová - Branislav Hadzima*

CORROSION RESISTANCE OF HSLA STEEL AFTER VARIOUS SURFACE TREATMENTS IN CHLORIDE ENVIRONMENT

The effect of mechanical and chemical surface treatment of high-strength low alloy steel S355J2 on its electrochemical characteristics was investigated by voltamperic tests in corrosive environment of 0.1M NaCl solution simulating sea atmosphere. Mechanical surface treatment was done by grinding on 1200 grit paper and by sandblasting. Chemical surface treatment was performed by iron phosphating in aqueous solution of H_3PO_4 and $FeCl_3 6H_2O$. Thermodynamic and kinetic corrosion characteristics including corrosion potentials and corrosion current densities were measured and analysed by potentiodynamic polarisation curves and Tafel analyses respectively. The positive combination of these two techniques on corrosion properties of S355J2 steel surface was reported.

Keywords: *S355J steel, corrosion properties, iron phosphating, surface treatment.*

1. Introduction

There are two main grades of High Performance Steels (HPS), namely High Strength Low Alloyed (HSLA) and High Strength Steels (HSS). A major feature of these grades is low level of carbon and additions of micro alloying elements resulting in low value of Carbon Equivalent (CE) and improved weldability [1, 2, 3 and 4]. High strength low alloyed (HSLA) steels were primarily developed to replace low-carbon steels for the automotive industry in order to improve the strength-to-weight ratio and meet the need for higher-strength construction grade materials. HSLA steels demonstrate unique properties, such as high strength, excellent ductility, good weldability and also exhibit outstanding low temperature impact toughness superior to that of high yield strength (HY) steels. HSLA steels have much improved weldability compared to HY steels [4]. HSLA steels become an indispensable class for different applications like construction of large ships, oil and gas transmission lines, offshore oil drilling platforms, pressure vessels, building construction, bridges and storage tanks [5]. S355J2 steel is one of the most commonly used member of HSLA steel grade. However for many applications, proper surface pretreatment and painting has to be used to improve its surface quality.

Sandblasting, as a surface treatment method, is commonly used for surface modification [6], surface strengthening [7], surface clearing and rust removal [8]. Compared with shot peening, it has smaller abrasive particles and lower pressure of compressed air. Therefore, a smoother surface can be obtained by sandblasting in general. During the sandblasting process, the surface of specimens is blasted repeatedly by sand or other hard particles with high speed, which leads to the removal of oxide scale and generation of local plastic deformation in the surface layer. However, Wang et al. [9] observed decrease of corrosion resistance of steel after sandblasting, which limits the application possibilities of this technique [10 and 11].

Problems with lower corrosion resistance of sandblasted surface could be solved by application of chemical phosphating. Phosphate coatings are produced on ferrous and nonferrous metal surfaces and are composed of tiny crystals of iron, zinc, or manganese phosphates. These inorganic coatings produced on metal surfaces retard corrosion and promote better paint bonding. Iron phosphating is the workhorse of the general finishing industry because of the quality delivered with regards to the newer coatings, its ease of control, non-sludge characteristics, and economics [12].

For these reasons, the aim of this study is to compare these two techniques for surface treatment of steels applied individually and in mutual combination from the corrosion point of view.

* [1]Kamil Borko, [2]Filip Pastorek, [3]Stanislava Fintová, [1,2]Branislav Hadzima
[1]Department of Materials Engineering, Faculty of Mechanical Engineering, University of Zilina, Slovakia
[2]Research Centre, University of Zilina, Slovakia
[3]Institute of Physics of Materials, Academy of Sciences of the Czech Republic, Brno, Czech Republic
E-mail: filip.pastorek@rc.uniza.sk

2. Experimental material and methods

S355J2 steel was used as an experimental material. The chemical composition is listed in Table 1.

The samples for metallographic observation were prepared by conventional metallographic procedures. 3% Nital was used as an etchant for visualisation of the S355J2 steel microstructure (Fig. 1). The microstructure is created by ferrite-pearlite matrix with a low pearlite content (local pearlite occurrence) and with the grain size of about 10 microns. The microstructure was observed by the CARL ZEISS AXIO Imager.A1m (equipment financed by the project ITMS 26220220121) light metallographic microscope in the laboratories of Department of Materials Engineering, University of Zilina.

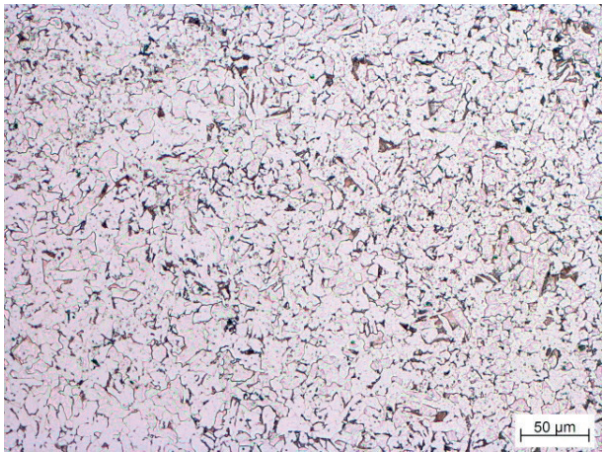

Fig. 1 Microstructure of S355J2 steel

S355J2 steel samples with surface area of 15 cm² were ground with 500 and 1200 grit SiC paper to ensure the same surface roughness, then rinsed with demineralised water and ethanol, and dried using a stream of hot air. The first pretreated samples were further sandblasted. Sandblasting was performed by sand particles on a mobile pressure sandblasting machine with a nozzle diameter 6 mm and pressure of 0.6 MPa. The second samples were treated chemically by iron phosphating. Composition of phosphating bath was 300 ml of demineralised water, 0.42 ml of H_3PO_4 and 0.999 g of $FeCl_3.6H_2O$. Phosphating process was performed for 5 minutes at the temperature of 90-95 °C. Third samples were treated by the combination of these techniques at defined parameters. Sandblasting was followed by iron phosphating in this case. All the samples were rinsed with demineralised water and ethanol, and dried using a stream of hot air after final surface treatment in order to remove chemical and mechanical residues.

The surface morphology of the treated samples was assessed by a stereomicroscope Nikon AZ100 (equipment financed by the project ITMS 26220220048) with a digital camera using NIS Elements software. The corrosion characteristics of S355J2 steel samples after various surface treatment were evaluated by potentiodynamic polarisation using a potentiostat/galvanostat/frequency response analyser VSP from BioLogic SAS France. All the corrosion experiments were performed in 0.1M NaCl at 22±1 °C. A saturated calomel electrode and a platinum electrode served as the reference and auxiliary electrodes, respectively. Treated S355J2 samples formed the working electrode in such a way that only 1 cm² area of the working electrode surface was exposed to the electrolyte solution in corrosion cell.

Potentiodynamic polarisation tests were carried out from -200 to + 300 mV vs SCE with respect to the OCP at a scan rate of 1 $mV.s^{-1}$. Measured potentiodynamic curves were analysed using Tafel fit by EC-Lab software (software financed by the project ITMS 26220220183). The potentiodynamic polarisation measurements were repeated at least three times, so that reproducibility of the test results was ensured [13].

3. Results and discussion

Surface 3D morphology of S355J2 steel after sandblasting is shown in Fig. 2. As can be seen, sandblasting caused mild surface deformation up to 10 microns of depth, which is appropriate in terms of surface roughness increase and surface oxide cleaning.

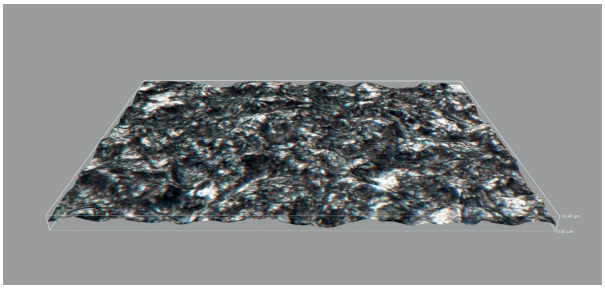

Fig. 2 Surface 3D surface morphology of S355J2 steel after sandblasting

When steel is exposed to the phosphating solution, iron dissolution is initiated at the micro-anodes present on the substrate due to the presence of free phosphoric acid in the bath and hydrogen evolution occurring at the microcathodic sites [14].

Chemical composition of S355J2 steel — Table 1

Component	C	Mn	P	S	Si	Cu	Fe
wt. %	0.200	1.600	0.025	0.025	0.550	0.550	balance

$$Fe + 2H_3PO_4 <=> Fe(H_2PO_4)_2 + H_2$$

The formation of soluble primary ferrous phosphate leads to a concurrent local depletion of free acid concentration in the solution resulting in a rise in pH at the metal/solution interface. Hence, a certain amount of free phosphoric acid must be present to repress the hydrolysis and to keep the bath stable for effective deposition of phosphate at the microcathodic sites [14 and 15]. The morphology of created iron phosphate is shown in Fig. 3 at maximal magnification of the used microscope. Iron phosphate forms a continuous layer homogeneously covering the entire surface of the base metal in such a way that no evidence of previous grinding process is noticeable on the surface although iron phosphate crystals are of very low size. However, the layer is significantly porous, which is a typical feature of chemically prepared phosphates. This porous character of the layer is beneficial for the further oil or paint preservation of the surface.

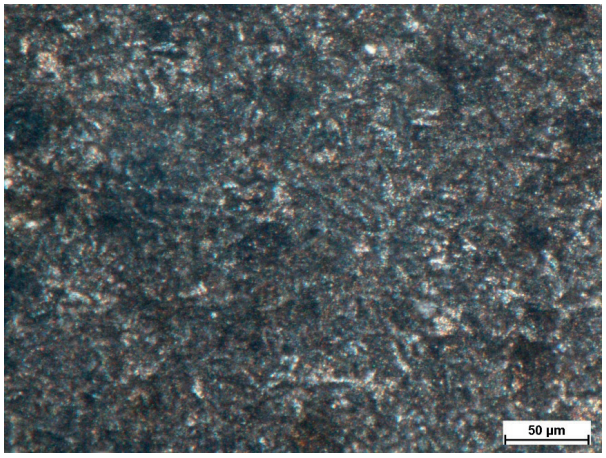

Fig. 3 Surface morphology of S355J2 steel after iron phosphating

Figure 4 shows the measured potentiodynamic curves of S355J2 steel samples after various surface treatments in 0.1M NaCl corrosive solution. The thermodynamic (corrosion potential) and kinetic (corrosion current density, corrosion rate) characteristics obtained from the measured curves are listed in Table 2.

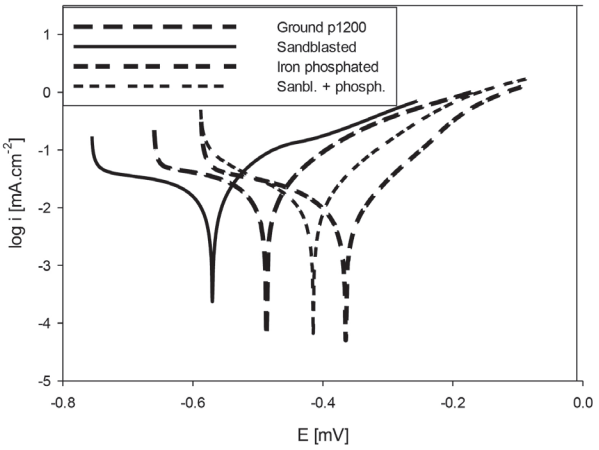

Fig. 4 Potentiodynamic curves of S355J2 steel after various surface treatments in 0.1M NaCl

Used mechanical and chemical surface treatment caused changes in both thermodynamic and kinetic characteristics of the base material. Thermodynamic stability of the surface is represented by the values of corrosion potentials E_{corr} in our case. More positive value of this electrochemical characteristic means that the surface is nobler and thermodynamically more stable. Sandblasting caused intensive destruction of the surface, which is an accompaniment to its cleaning process purpose. Destroyed surface with a higher concentration of structure defects and with larger area of an active surface resulted in lower electrochemical stability, which is reflected in 83 mV decrease of E_{corr} value in comparison with simply ground surface and sandblasted surface. A part of kinetic energy of sandblasting particles transformed into addition of internal energy of the base material, which caused its absolute value increase. As the result of higher surface activity, an increase of corrosion current density i_{corr} value and directly related value of corrosion rate rcorr is observed on sandblasted surface compared to the ground surface. However, this increase is not very significant and represents just 3.2 $\mu A.cm^{-2}$ and 0.07 $mm.y^{-1}$ respectively. It is a beneficial finding that corrosion resistance decrease caused by intensive sandblasting surface cleaning is acceptable.

Iron phosphating creates a stable layer of several microns that forms a mechanical barrier against corrosion process. The higher

Electrochemical characteristics of S355J2 steel after various surface treatments — Table 2

Surface treatment	E_{corr} $[mV_{SCE}]$	i_{corr} $[\mu A.cm^{-2}]$	r_{corr} $[mm.y^{-1}]$	β_a $[mV.dec^{-1}]$	β_c $[mV.dec^{-1}]$
Grinding (1200 grit paper)	-487	16.3	0.38	124	288
Sandblasting	-570	19.5	0.45	139	477
Iron phosphating	-365	7.7	0.18	108	213
Sandblasting + Iron phosph.	-415	10.4	0.24	102	177

stability of iron phosphate in 0.1M NaCl solution compared to the base metal resulted in more positive value of $E_{corr.}$ E_{corr} of iron phosphated surface is moved by 122 mV to nobler values. Thanks to mechanical barrier of iron phosphate the diffusion of oxygen to base metal active surface is more difficult and concentrated mainly to the more porous areas. This complication for kinetics of corrosion process results in decrease of i_{corr} and r_{corr} values too. Corrosion current density of the surface with iron phosphate represents just 47 % of base metal corrosion current density. These findings prove significant positive effect of iron phosphating on corrosion properties of S355J2 steel surface.

Very interesting combination of mechanical and chemical treatment of steel surface leading to preparation of pure and porous surface ideal for further preservation operations also brings positive effect on corrosion properties of S355J2 steel. In this case, positive effect of iron phosphating is more intensive than negative effect of sandblasting, which finally causes the improvement of both thermodynamic and kinetic electrochemical corrosion characteristics of double treated surface compared to simply ground surface with 1200 grit paper. Generally, two processes occur during iron phosphating in the first stage of this chemical treatment. The formation of iron phosphate on the one hand and the active dissolution of the base metal by phosphoric acid on the other hand. This active dissolution plays an important role in our case of sandblasted surface because at least a part of destroyed active surface layer can be removed in this way. However, the corrosion properties of this double treated surface are not of the same level as the corrosion properties of only iron phosphated surface.

4. Conclusions

On the basis of the measured data and analyses we concluded:

1. Sandblasting of S355J2 steel surface deteriorates corrosion properties of the surface by mild surface destruction.
2. Iron phosphating of S355J2 steel surface forms stable and effective porous barrier against corrosion process, which is proved by the best corrosion protection from tested surface treatment techniques.
3. Combination of surface treatment by sandblasting followed by iron phosphating improved corrosion protection of the base metal so it can be considered to be a suitable process for surface preparation prior to further preservation/painting.

Acknowledgements

The research is supported by Science Grant Agency of the Slovak Republic through project No. 1/0720/14. Authors are grateful for the support in experimental works to Slovak Research and Development Agency by the project No. APVV-14-0284 and No. APVV-15-0120.

References

[1] SLEZAK, T., SNIEZEK, L.: *Procedia Eng*., 114, 2015, 78-85.
[2] RAY, P. K., GANGULY, R. I., PANDA, A. K.: *Mat. Sci. Eng., A* 346, 2003, 122-131.
[3] SHOW, B. K., VEERABABU, R., BALAMURALIKRISHAN, R., MALAKONDAIAH, G.: *Mat. Sci. Eng., A* 527, 2010, 1595-1604.
[4] HIDETOSHI, F., LING, C., NOBUHIRO, T., MASAKATSU, M., KAZUHIRO, N., KIVOSHI, N.: *Mat. Sci. Eng*., A 429, 2006, 50-57.
[5] RAGU NATHAN, S., BALASUBRAMANIAN, V., MALARVIZHI, S., RAO, A. G.: *Def. Technol.,* 11, 2015, 308-317.
[6] CHINTAPALLI, R. K., MARRO, F. G., JIMENEZ-PIQUE, E., ANGLADA, M.: *Dent. Mater.,* 29, 2013, 566-572.
[7] CHINTAPALLI, R. K., MESTRA RODRIGUEZ, A., MARRO, F. G., ANGLADA, M.: *J. Mech. Behav. Biomed.,* 29, 2014, 126-137.
[8] RAYKOWSKI, A., HADER, M., MARAGNO, B., SPELT, J. K.: *Wear,* 249, 2001, 126-131.
[9] WANG, X. Y., LI, D. Y.: *Electrochem. Acta,* 47, 2002, 3939-3947.
[10] TRSKO, L., BOKUVKA, O., NOVY, F., GUAGLIANO, M.: *Mater. and Design,* 57, 2014, 103-113.
[11] GENG, S., SUN, J., GUO, L.: *Mater. and Design,* 88, 2015, 1-7.
[12] GRUSS, B.: Metal. Finish., 98, 2000, 54-56.
[13] PASTOREK, F., HADZIMA, B., DOLEZAL, P.: *Communications - Scientific Letters of the University of Zilina,* 14, 2012, 26-30.
[14] SANKARA NARAYANAN, T. S. N.: *Rev. Adv. Mater. Sci.,* 9, 2005, 130.
[15] KUMAR, A., BHOLA, S. K., MAJUMDAR, J. D.: *Surf. and Coat., Technol.,* 206, 2012, 3693-3699.

https://doi.org/10.26552/com.C.2016.4.103-111

Michal Petru – Jaroslav Mlynek – Tomas Martinec – Jozef Broncek*

MATHEMATICAL MODELLING OF FIBRE WINDING PROCESS FOR COMPOSITE FRAMES

This article describes the authors´ own mathematical modelling designed for the production process of a new type of low-weight composite frame. The used real technology is based on the winding of carbon or glass filament rovings around a polyurethane core which is a frame with a circular cross section (this type of composites is used, for example, to reinforce the doors and windows of airplanes). The core is attached to the end-effector of the robot (robot-end-effector) and successively passes through the fibre-processing head during the winding process. Quality production depends primarily on the correct winding of fibres around the polyurethane core. It is especially needed to ensure the correct angles of the fibre winding around the polyurethane core and the homogeneity of individual winding layers. The numerical model described in Euclidean space E3 of the manufacturing process is used when the fibre-processing frame is passing through the fibre-processing head. We use the described mathematical model and matrix calculus to enumerate the trajectory of the robot-end-effector to determine the desired passage of the core through the fibre-processing head. The calculated sequence of "tool-centre-point" values of the robot allows us to define the desired trajectory of the robot-end-effector and, thereby, the passage of the frame through the fibre-processing head. The calculation of the trajectory was programmed in the Delphi development environment. A practical example is analysed in the article.

Keywords: *Mathematical modelling, composite frame, winding fibre processing, robot technology.*

1. Introduction

This article describes the authors´ own mathematical modelling for the production process of a new type of low-weight composite frame. A new type of low-weight frame composite of high quality is used for example in the transport industry [1, 2 and 3]. Reasons for the use of composites not only in transport industry (car industry, aerospace industry, aeronautic industry, etc.) are derived from the current requirements for the low-weight parts. The construction of composite frames must be light because, for example, in car industry an optimal weight and power usage lead to emission reductions. But concurrently the construction of design parts must be sufficiently solid and rigid. We will describe technology of carbon or glass filament rovings wound around the polyurethane core which is a frame shape in 3D with a varying shape and size of cross-section of the frame. In the following part of the article we will consider only a circular cross-section. If the frame cross-section is not circular, we consider an imaginary cylindrical "envelope" (with minimum possible radius) stretched on the frame surface. Traditional procedures of composite manufacturing are labour-intensive and time-consuming. Moreover, the traditional techniques do not ensure accurate fibre winding around the core. The use of industrial robots in composite production greatly reduces production costs, production time and minimises scrap rate. Other problems of industrial robot trajectory are also solved in publications, e.g. [4 - 7]. Composites offer an attractive material properties-to-production cost ratio. One of the possible methods for producing composites is to stretch the fabric from the fibres on a core with an arbitrary geometry. However, if the core of the composite is a 3D frame or a frame with a very complicated 3D shape or several layers of the fibre strands are wound simultaneously around the core, then this method is not suitable. In such cases, the method of dry winding of endless fibre strands around a core geometry using a rotary fibre-processing head is often used for the composite production. This method provides full control over the placement, laying direction, and the amount of fibres on the core as well as the homogeneity of the structure. The final composite is obtained after dry winding of the required layers of strands around the core by injection of the resin to the mould using heat and pressure. Now, we are describing the process of producing composites with a polyurethane core of

* [1]Michal Petru, [2]Jaroslav Mlynek, [1]Tomas Martinec, [3]Jozef Broncek
[1]The Institute for Nanomaterials, Advanced Technologies and Innovation, Technical University of Liberec, Czech Republic
[2]Department of Mathematics and Didactics of Mathematics, Faculty of Science, Humanities and Education, Technical University of Liberec, Czech Republic
[4]Department of Design and Mechanical Elements, Faculty of Mechanical Engineering, University of Zilina, Slovakia
E-mail: michal.petru@tul.cz

a frame shape by the method of dry winding around the core. We tested this manufacturing process in our experimental laboratory (Fig. 1). The key equipment in our experimental laboratory is an industry robot KR 16-2 and fibre-processing head as shown in Fig. 2.

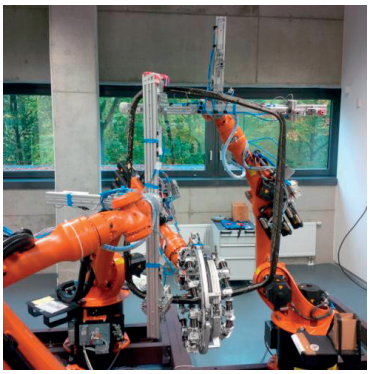

Fig.1 Experimental laboratory for manufacturing process of winding fibres around the frame

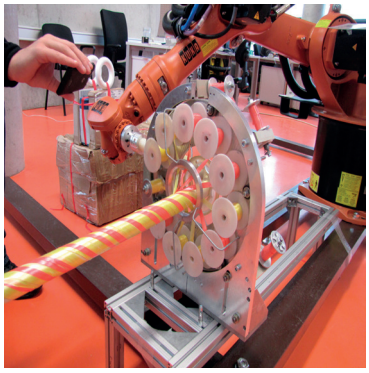

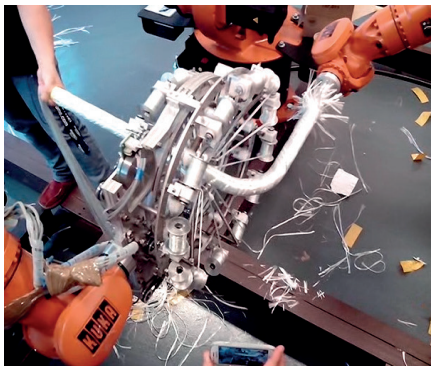

Fig.2 Fibre-processing head with one guide line (up) and with three guide lines on the frame (down).

The fibre-processing head is fixedly placed in the workspace of the robot and coordinates of its parts are specified in the basic coordinate system of the robot. The used fibre-processing head contains three guide lines (Fig. 2). Each guide line contains twelve fixed fibre coils along its periphery. The outer guidelines rotate around a common axis and the intermediate guideline is static. The polyurethane core of a frame shape is attached to the robot-end-effector. The passage of the core through the fibre-processing head is controlled by the movement of the robot-end-effector. When polyurethane core passes through fibre-processing head the strands are successively wound on the surface of the core at a targeted angle. First, the outer rotating guide line ensures winding strands under the angle 45° (relative to the axis of the head and the moving direction of the core). Subsequently, the middle static guide winds the second layer of strand under the angle 0° and the second outer rotation winds the final layer of strands -45°. Our goal is for the core to pass through the fibre-processing head orthogonal to the guide lines of the head as far as possible. The principle of the winding solution is shown in Fig. 2 (fibre processing head contains only one rotation line in this figure). To optimise the manufacturing process we made a numerical model for calculating the robot-end-effector trajectory to achieve an optimal directional orientation of the fibre placement in the manufacture of the composite frame profile. The mathematical calculation of trajectory was programmed in the Delphi development environment. This article describes a numerical model for quality of the manufacturing process technology of a shaped composite in 3D space. As already mentioned, providing the correct angles for winding of strands around the core is mainly conditioned by the determination of the appropriate trajectory of the robot-end-effector. Orthogonal direction of passage of the core (of a closed frame shape) to the guide line in the place of its own winding of fibres around the core surface ensures the correct angle and uniformity of winding. The quality of fibre winding also depends on the material properties of polyurethane core and fibres (especially on adhesion of the fibre to the core).

2. Numerical model describing the fibre winding process for a composite frame

This chapter briefly describes the numerical model of the optimal process of winding strands around a 3D polyurethane core with a circular cross-section. The core shape is a frame and the radius of the circular cross section of the frame may be generally different for individual parts of a frame. The actual process of strand winding is carried out using a fibre-processing head and an industrial robot. The polyurethane core is attached to the robot-end-effector and the winding head is fixed in the workspace of the robot. Within the described numerical model (Fig. 3), we will consider the right-handed Euclidean coordinate system E_3 of the robot (*BCS*). We will describe the positions of the individual parts of an experimental workplace of winding strands to frame using this coordinate system. Subsequently, we will consider the local right-handed Euclidean coordinate system of the robot-end-effector (*LCS*). To avoid any misunderstanding, we will label the points and vectors with coordinates in *BCS* with the subscript *BCS* and points and vectors with coordinates in

LCS with the subscript *LCS*. Activities of the industrial robot are controlled using a robot control unit (in our case unit KR C4) and the library of instructions. For our purposes it is crucial to set the desired position of the robot-end-effector using the library of instructions. The position and orientation of the robot-end-effector is defined by using the *LCS*. The origin of the *LCS* is positioned in the robot-end-effector while at the same time the robot-end-effector is oriented in the direction of the positive part of the *z*-axis in the *LCS* with regard to the *BCS*. The actual position of the *LCS* with regard to the *BCS* is determined by the values listed in the "tool-centre-point" (*TCP*). The tool centre point contains six values *TCP* = (*x, y, z, a, b, c*). The first three parameters specify the coordinates of the origin of the *LCS* with regard to the *BCS*. The values *a*, *b* and *c* indicate the angle of the rotation of the *LCS* around the axes *z*, *y* and *x* with regard to the *BCS*. The non-bearing polyurethane frame can be described by the central axis *o* (see Fig. 4) and radius r_{TUBE} of the cross-section of the frame. The central axis of the frame *o* is entered in the *LCS* of the robot-end-effector using a discrete set of *N* points stored in the array *B*:*array*[1..*N*,1..3] where *B*[*i*,1] indicates the *x*, *B*[*i*,2] indicates the *y* and *B*[*i*,3] indicates the *z* coordinate of the *i*-th point $B[i]_{LCS}$ lying on the axis *o* (see Fig. 4). At the same time, the array *vector*1*B*:*array*[1..*N*,1..3] is entered where *vector*1*B*:*array*[*i*,1], *vector*1*B*:*array*[*i*,2] and *vector*1*B*:*array*[*i*,3] indicate the coordinates of the unit vector $vector1B{:}array[i]_{LCS}$ tangent to the axis *o* at point $B[i]_{LCS}$. In addition, the array *vector*2*B*[*i*, 1] is defined where , *vector*2*B*[*i*, 2] and *vector*2*B*[*i*, 3] indicate the coordinates of the unit vector $vector2B[i]_{LCS}$ which, when passing the point $B[i]_{LCS}$ through the fibre-processing, characterises the necessary rotation of the frame about an axis head. All the time $vector1B{:}array[i]_{LCS} \perp vector2B{:}array[i]_{LCS}$ holds. We assume that the discrete set of points $B[i]_{LCS}$ lying on the axis *o* is specified sufficiently densely and defines with a sufficient accuracy the shape of the frame. We suppose the distance of two consecutive points $B[i]_{LCS}$ and $B[i+1]_{LCS}$ has a constant distance *h*. If the polyurethane frame is closed, then the first entered point on the axis *o* is identical to the last entered point ($B[i]_{LCS} \equiv B[N]_{LCS}$, $vector1B[i]_{LCS} \equiv vector1B[N]_{LCS}$ and $vector2B[i]_{LCS} \equiv vector2B[N]_{LCS}$). The coordinates of the individual components of the fibre-processing head are entered in the *BCS* coordinate system. The first outer rotating guide line is presented by the circle *k*1 with the centre $S1_{BCS}=[x_{S1}, y_{S1}, z_{S1}]_{BCS}$, the second outer rotating guide line is presented by the circle *k*2 with the centre $S2_{BCS}=[x_{S2}, y_{S2}, z_{S2}]_{BCS}$, both circles *k*1 and *k*2 have the same radius r_{CIRCLE}(we assume $r_{CIRCLE} > r_{TUBE}$). Points *S*1 and *S*2 lie on the axis *s* of the fibre-processing head (see Fig. 5). The middle guide line, which enables the placement of the fibres in the longitudinal direction, is static and so it is not necessary to consider this guide line in the model in the subsequent calculations. Point H_{BCS} is entered, this point lies in the middle of the abscissa $S1_{BCS}S2_{BCS}$. Subsequently, the unit vectors $vector1H_{BCS}$ (this vector indicates the direction of passage frame through the fibre-winding head) and vector $vector2H_{BCS}$ are entered, while the relation $vector1H_{BCS} \perp vector2H_{BCS}$ is valid. In our test examples we selected $vector1H_{BCS}=(S1_{BCS} - S2_{BCS})/\|S1_{BCS} - S2_{BCS}\|$, where $\|S1_{BCS} - S2_{BCS}\|$ is the length of the abscissa $S1_{BCS} - S2_{BCS}$. The point H_{BCS} together with $vector1H_{BCS}$ and $vector2H_{BCS}$ allow us to calculate the passage of polyurethane frame through the fibre-processing head while the frame possibly rotates around the tangent of its axis *o* in point $B[i]_{BCS}$. In the following chapter we will describe the use of the mathematical model to calculate the trajectory of the robot-end-effector.

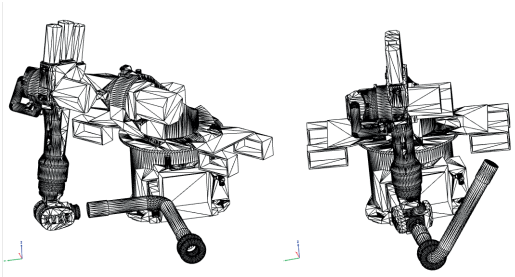

Fig.3 Numerical model describing of fibres winding process for a new composite frame

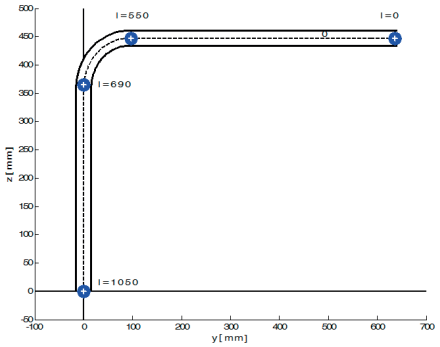

Fig. 4 Geometry of a polyurethane frame

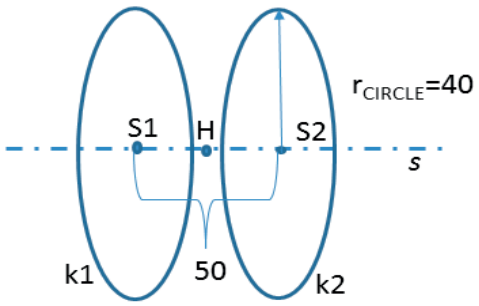

Fig. 5 Points S1 and S2 lie on the axis s of the fibre-processing head

2.1 Mathematical model for calculating the trajectory of the robot-end-effector

In the derivation procedure of trajectory calculation, we used results listed in [1 and 7]. Note that the Denavit-Hartenberg method is often used to determine the trajectory of robot (e.g. see [8]). In this chapter we will calculate such a trajectory of the robot-end-effector when the polyurethane frame attached to the robot-end-effector passes gradually through the fibre-processing head. Recall that the fibre-processing head and its parts are fixedly positioned in the *BCS* and a position of the polyurethane frame is defined in the *LCS* of the robot-end-effector. Determination of the trajectory is made on the basis of calculating the sequence of N of the TCP_i values, where $1 \le i \le N$. Then the robot-end-effector changes its position in relation to changes in parameters based on their linear interpolation (or the use of cubic splines) during the transition from the current TCP_{i-1} to the subsequent TCP_i. Consequently, the frame passes through the fibre-processing head. The calculated parameters of the current TCP_i ensure that point $B[i]_{BCS}$ of the axis o of the frame will be the same as point H_{BCS} (the middle of the fibre-processing head) in the i-th step of the polyurethane frame passing through the fibre-processing head. At the same time the vector $vector1B[i]_{BCS}$ of the tangent of the axis o of the frame at the point $B[i]_{BCS}$ identifies with the vector $vector1H_{BCS}$ (this vector indicates the direction of passage frame through fibre-winding head) and the vector $vector2B[i]_{BCS}$ identifies with the vector $vector2H_{BCS}$ (identification of this pair of vectors allows the polyurethane frame to turn around the tangent of the axis of the frame o in the point $B[i]_{BCS}$). When the described identifications are complete (i.e. the two orthogonal vectors and their common starting point entered in the *LCS* are in the same position in *BCS* as the two orthogonal vectors and their common starting point in the *BCS*) the parameters of the corresponding TCP_i are unambiguously determined and, therefore, the position and orientation of the robot-end-effector relative to the *BCS* in the i-th step of passing the frame through the fibre-processing are also unambiguously determined. When calculating the sequence of the TCP_i values ($1 \le i \le N$) of the robot-end-effector, we use a matrix calculus to perform a transformation of the *LCS* of the robot-end-effector relative to the *BCS*. We will write points, vectors and matrices in a homogeneous form (i.e. point $V = [x_v, y_v, z_v, 1]^T$ vector $u = (x_u, y_u, z_u, 1)^T$) in the following text. We also use the Euclidean norm $\|u\|$ of vector u, where $\| u \| = \sqrt{x_u^2 + y_u^2 + z_u^2}$.

I. Calculation of the Passage of Frame Thorough the Fibre-processing Head

We calculate for $i = 1,...N$ the TCP_i of the robot-end-effector so that at the same time $B[i]_{BCS} \equiv H_{BCS}$, $vector1B[i]_{BCS} \equiv vector1H_{BCS}$, $vector2B[i]_{BCS} \equiv vector2H_{BCS}$. After determining TCP_i all of the TCP_{i-1} parameters are continuously changed to the parameters of to the TCP_i. By this procedure we determine partial passage of the frame through the fibre-processing head. The initial *TCP* indicates the position and orientation of the robot-end-effector before the start of the passage of the frame through fibre-processing head. In the following section of this chapter we will focus on the procedure for determining TCP_i.

II. Determining the Transformation Matrix

We assume that $TCP_{i-1} = (x_{i-1}, y_{i-1}, z_{i-1}, a_{i-1}, b_{i-1}, c_{i-1})$ is entered. With the aim of determining the transformation matrix $\mathbf{T}_i$ (which we will apply to *LCS*) in the form Eq. (1) we perform the following steps.

$$\mathbf{T}_i = \mathbf{L}_i \cdot \mathbf{Q}_i. \tag{1}$$

i. We determine the coordinates of the vector $vector1B[i]_{LCS}$ in the coordinate system *BCS* (under the assumption that the coordinate systems *BCS* and *LCS* have the same origin, this assumption is used when finding the required rotation matrix). The matrix Q_{i-1} of the rotation *LCS* towards *BCS* is in the form of Eq. (2).

$$Q_{i-1} = Rot(z,a_{i-1})\, Rot(y,b_{i-1})\, Rot(x,c_{i-1}), \tag{2}$$

where $Rot(z,a_{i-1})$ is the orthogonal matrix of rotation of *LCS* around axis z at angle a_{i-1}, $Rot(y,b_{i-1})$ orthogonal matrix of rotation of *LCS* around axis y at angle b_{i-1} and $Rot(x,c_{i-1})$ orthogonal matrix of rotation of *LCS* around axis x at angle c_{i-1} (3).

$$\left.\begin{aligned} Rot(z,a_{i-1}) &= \begin{pmatrix} \cos a_{i-1} & -\sin a_{i-1} & 0 & 0 \\ \sin a_{i-1} & \cos a_{i-1} & 0 & 0 \\ 0 & 0 & 1 & 0 \\ 0 & 0 & 0 & 1 \end{pmatrix} \\ Rot(y,b_{i-1}) &= \begin{pmatrix} \cos b_{i-1} & 0 & \sin b_{i-1} & 0 \\ 0 & 1 & 0 & 0 \\ -\sin b_{i-1} & 0 & \cos b_{i-1} & 0 \\ 0 & 0 & 0 & 1 \end{pmatrix} \\ Rot(x,c_{i-1}) &= \begin{pmatrix} 1 & 0 & 0 & 0 \\ 0 & \cos c_{i-1} & -\sin c_{i-1} & 0 \\ 0 & \sin c_{i-1} & \cos c_{i-1} & 0 \\ 0 & 0 & 0 & 1 \end{pmatrix} \end{aligned}\right\} \tag{3}$$

Subsequently, we can express the coordinates of the vector $vector1B[i]_{LCS}$ in the *BCS* system in the form $vector1B[i]_{BCS} = Q_{i-1} vector1B[i]_{LCS}$.

ii. By using the scalar product of vectors $vector1H_{BCS}$ and $vector1B[i]_{BCS}$ we determine their deviation α.

iii. We determine the cross product $p_{BCS} = vector1H_{BCS} \times vector1B[i]_{BCS}$.

iv. Vector p_{BCS} is orthogonal to vectors $vector1H_{BCS}$ and $vector1B[i]_{BCS}$.

We normalise vector p_{BCS}, i.e., we ensure its unit length $p_{BCS} = p_{BCS} / \|p_{BCS}\|$. We perform the rotation of vector $vector1B[i]_{BCS}$ by angle α around vector p_{BCS} (we consider the correct

$$Rot(p_{BCS},\alpha)=\begin{bmatrix} c+n_1^2(1-c) & n_1n_2(1-c)+n_3s & n_1n_3(1-c)-n_2s & 0\\ n_1n_2(1-c)+n_3s & c+n_2^2(1-c) & n_2n_3(1-c)-n_1s & 0\\ n_1n_3(1-c)-n_2s & n_2n_3(1-c)-n_1s & c+n_3^2(1-c) & 0\\ 0 & 0 & 0 & 1 \end{bmatrix}, \quad (4)$$

orientation of angle $vector1B[i]_{BCS}$, i.e. rotate vector $vector1B[i]_{BCS}$ to vector $vector1H_{BCS}$). Then $vector1H_{BCS}=Rot(p_{BCS},\alpha)\,vector1B[i]_{BCS}$. If we denote $p_{BCS}=(n_1, n_2, n_3,0)^T$, then the matrix $Rot(p_{BCS},\alpha)$ will have the form (4), you can see in [1].

Where s and c indicate $s=\sin\alpha$, $c=\cos\alpha$. At the same time we determine the vector l_{BCS} (5).

$$l_{BCS}=Rot(p_{BCS},\alpha)\cdot Q_{i-1}vector2B[i]_{LCS}. \quad (5)$$

The cases where $\alpha=0$ or $\alpha=\pi$ need to be solved separately.

v. By using the scalar product of the vectors, we determine the deviation β of vectors $vector2H_{BCS}$ and l_{BCS}.

vi. The resulting matrix of rotation Q_i has the form of Eq. (6).

$$Q_i=Rot(vector1H_{BCS},\beta)\cdot Rot(p_{BCS},\alpha)\cdot Rot(z,a_{i-1})\cdot \cdot Rot(y,b_{i-1})\cdot Rot(x,c_{i-1}) \quad (6)$$

where the elements of the matrix $Rot(vector1H_{BCS},\beta)$ are analogously defined as elements of the matrix $Rot(p_{BCS},\alpha)$ in relation (4). In relation (6) we use the correctly determined angle orientation of angle β, i.e. we rotate the vector l_{BCS} (5) around the vector $vector1H_{BCS}$ to the vector $vector2H_{BCS}$.

vii. The translation vector is defined (7) as

$$u(i)_{BCS}=H_{BCS}-Q_iB[i]_{LCS}-(x_{i-1},y_{i-1},z_{i-1},0)^T, \quad (7)$$

where matrix Q_i is determined by the relation (6). We remember that x_{i-1}, y_{i-1}, z_{i-1} are the first three parameters of TCP_{i-1}. The resulting transformation matrix T_i in the i-th step of the passing of the frame through the fibre-processing head is in the form (8).

$$T_i=Trans(x_{u(i)},y_{u(i)},z_{u(i)})\cdot Q_i, \quad (8)$$

where translation matrix

$$Trans(x_{u(i)},y_{u(i)},z_{u(i)})=\begin{pmatrix} 1&0&0&x_{u(i)}\\ 0&1&0&y_{u(i)}\\ 0&0&1&z_{u(i)}\\ 0&0&0&1 \end{pmatrix}$$

and $x_{u(i)}$, $y_{u(i)}$, $z_{u(i)}$ are components of vector $u(i)_{BCS}$ in Equation (7).

After performing the *LCS* of the robot-end-effector the corresponding transformation matrix T_i determined by relation (8) will be valid $H_{BCS}\equiv B[i]_{BCS}=T_i\cdot B[i]_{LCS}$ and $vector1B[i]_{BCS}\equiv vector1H_{BCS}$, $vector2B[i]_{BCS}\equiv vector2H_{BCS}$.

III. Calculation of the Euler Angles

We will calculate the Euler angles. Any right-handed rotation in Euclidean space E_3 around the given unit vector p by angle φ is determined by the orthogonal matrix $\mathbf{Q}=\mathbf{Rot}(\mathbf{p},\varphi)$, its elements are in the form (3) and $\det\mathbf{Q}=1$. Each rotation matrix can be written as a product of the matrices of rotation around the coordinate axes z, y and x, i.e. $Q=Rot(z,a)\cdot Rot(y,b)\cdot Rot(x,c)$, where the matrices $Rot(z,a)$, $Rot(y,b)$ and $Rot(x,c)$ are in the form (3); a, b and c are the corresponding Euler angles. We note that the determination of Euler angles a, b and c is not unique (see [7]). The matrix of rotation Q_i defined by the relation (9) can be decomposed into the product of the orthogonal matrices.

$$Q_i=Rot(z,a_i)\cdot Rot(y,b_i)\cdot Rot(x,c_i) \quad (9)$$

By multiplying the left and right sides from the left of the matrix $Rot(z,a_i)^{-1}$ because the matrix $Rot(z,a_i)$ is orthogonal $Rot(z,a_i)^{-1}=Rot(z,a_i)^T$) and comparing suitably selected corresponding elements from the resulting matrix on the left and right sides of equation (8) modified in this way, we can determine the rotation angles a_i, b_i and c_i (see [4], pp. 32). When calculating the angles of rotations, we use the *ATAN*2 function (part of the library of most programming languages), which calculates from the two input parameters arg_1 and arg_2 the value of the function arctangent for argument arg_1/arg_2. Moreover, the signs of both input parameters are used to determine the quadrant in which the resulting value function is located (it is valid that $-\pi<ATAN2(arg_1,arg_2)\le\pi$ part). We write the matrix of rotation Q_i in the form by (10).

$$Q_i=\begin{pmatrix} q_{11}(i)&q_{12}(i)&q_{13}(i)&0\\ q_{21}(i)&q_{22}(i)&q_{23}(i)&0\\ q_{31}(i)&q_{32}(i)&q_{33}(i)&0\\ 0&0&0&1 \end{pmatrix}. \quad (10)$$

Using the procedure described above for comparing the corresponding elements of the matrices in the modified equation (9) it is possible to obtain (11).

$$\left.\begin{aligned} a_i&=ATAN2(q_{21}(i),q_{11}(i)),\\ b_i&=ATAN2\begin{pmatrix}-q_{31}(i),q_{11}(i)\cos a_1+q_{21}\\ (i)\sin a_1\end{pmatrix},\\ c_i&=ATAN2\begin{pmatrix}q_{13}(i)\sin a_i-q_{23}(i)\cos a_i,\\ q_{22}(i)\cos a_1-q_{12}\sin a_i\end{pmatrix}\end{aligned}\right\} \quad (11)$$

Thus, we determined rotation angles a_i, b_i, c_i in the equation (9) and the corresponding TCP_i defining the position and orientation of the *LCS* of the robot-end-effector in relation to the *BCS* of the robot. The TCP_i can be expressed in the form (12).

$$TCP_i = (x_{u(i)}, y_{u(i)}, z_{u(i)}, a_i, b_i, b_i) \quad (12)$$

where the elements of the vector $u(i)_{BCS}$ are given by the relation (7).

3. Results and discussion

We focus on the practical problem of the passage of the non-bearing polyurethane frame with a circular cross-section through the fibre-processing head. The central 2D axis o of the frame is composed of two interconnected perpendicular arms (see Fig. 4). The axis o is entered into the *LCS* of the robot-end-effector using a discrete set of points $B[i]_{LCS}$, $1 \le i \le N = 105$. The total length d of the axis o from the starting point $B[1]_{LCS}$ to the end point $B[N]_{LCS}$ of the axis is $d = 1050$. The continuous distance of the points $B[i]_{LCS}$ on the axis o from the starting point is denoted by the variable l. The distance between two consecutive points $B[i]_{LCS}$ and $B[i+1]_{LCS}$ is $h = 10$ mm. Vectors $vector1B[i]_{LCS}$ and $vector2B[i]_{LCS}$ are specified, radius of the frame is $r_{TUBE} = 20$ mm. The fibre-processing head is represented by the circles $k1$ and $k2$ with the centres $S1_{BCS}$ = [-1000,1105,990] and $S2_{BCS}$ = [-1000,1035,990] having the same radius $r_{CIRCLE} = 40$ MM. The length of abscissa $S1_{BCS}$ $S2_{BCS}$= *70 mm*. It is valid $H_{BCS} = (S1_{BCS} + S2_{BCS})/2$, $vector1H_{BCS} = (S1_{BCS} - S2_{BCS})/\|S1_{BCS} - S2_{BCS}\|$, $vector2H_{BCS}$=(0,0,1). The frame needs to be rotated at a distance of 550 mm from the beginning of the axis o to the distance of 690 mm around a tangent to the frame of axis o during the passing of point $B[i]_{BCS}$ (for $56 \le i \le 69$) by point $H_{BCS}$when placing the longitudinal fibres relative to the axis o of the frame. This is a uniform right-handed rotary motion with an overall rotation angle $\omega = \pi$. The rotation is performed during the passage of the bent portion of the frame through the fibre-processing head. The calculation of the trajectory of the robot-end-effector from numerical model referred to in the previous chapter was applied to the described problem. Fig. 6 shows the position of the robot-end-effector when passing the polyurethane frame through winding head. Part a) shows the position of the robot-end-effector (first three parameters of *TCP*) and part b) the orientation of the robot-end-effector (last three parameters of *TCP*). Figures 7 and 8 compare the numerical model and the real experiment and illustrate the individually calculated values of *TCP* during the passing of the frame through the fibre-processing head. The comparison of an ideal sample and real sample from winding processing is seen in Fig. 9. Our article solves problem in which a composite frame with a circular cross-section is attached to

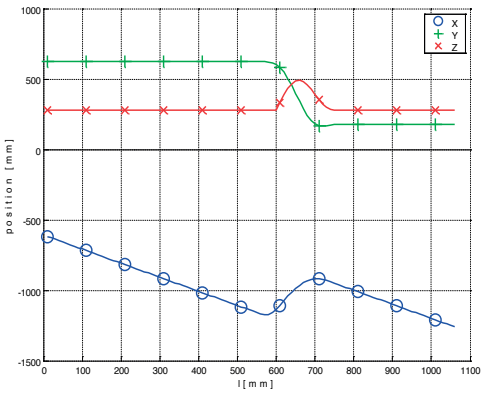

a)

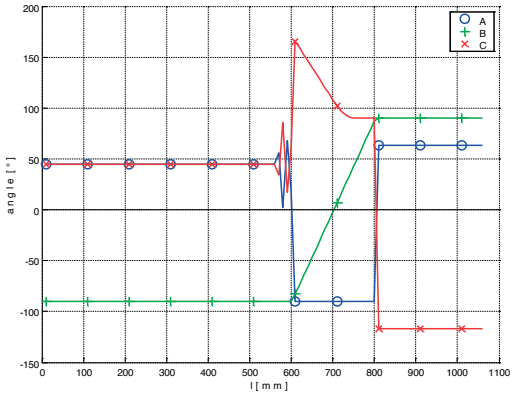

b)

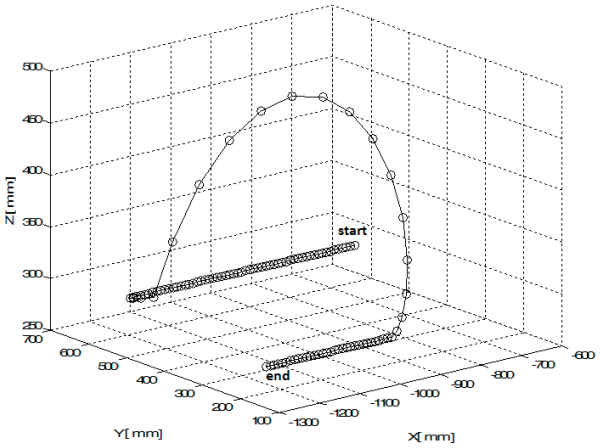

c)

Fig. 6 Diagram showing numerical simulation of the course of the TCP during the passing of the frame through the fibre-processing head, a) parameter values of the first three parameters of TCP, b) parameter values of the last three parameters of TCP, c) trajectory of the robot-end-effector: start and end

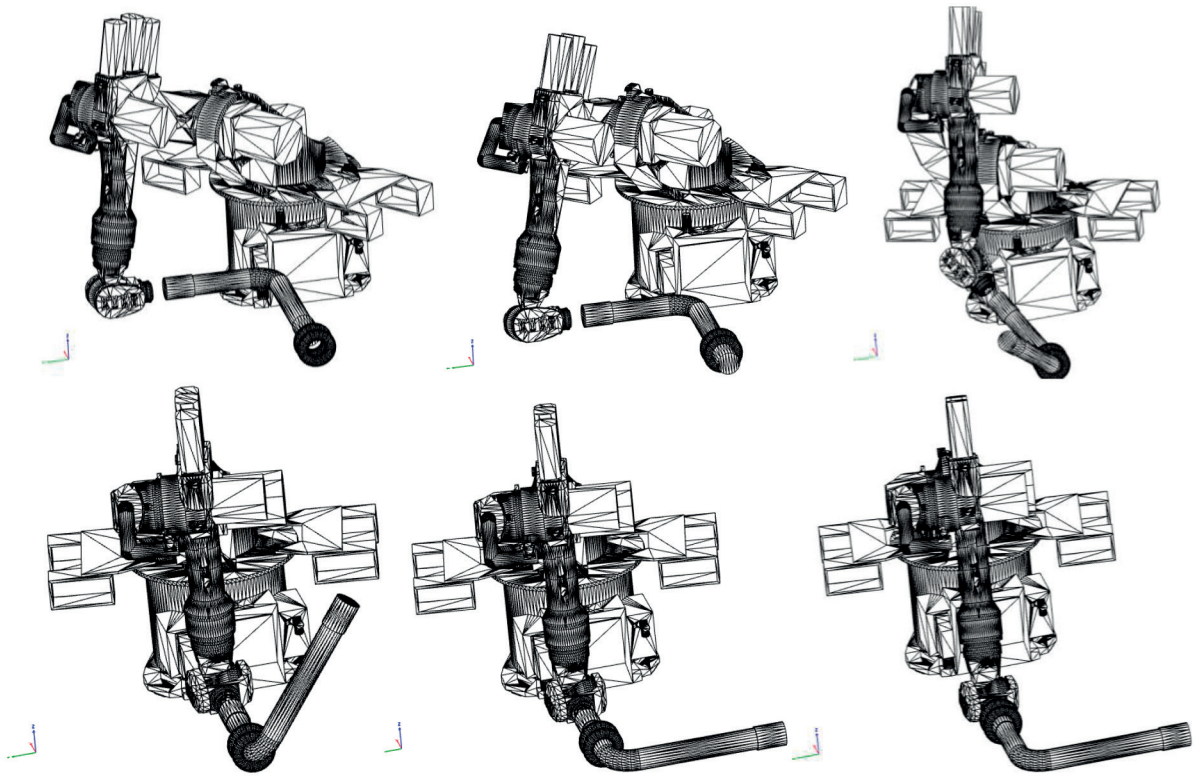

Fig. 7 Time response of a numerical model for optimal trajectory of fibre winding process

the end-effector of the industrial robot and successively passes through the fibre-processing head during the winding process. It is a similar problem as in [1 and 7]. We don't know any other robotic workplace where similar technical problem production of composite with frame shape (the frame could be closed) is solved. This is the main problem to compare effectiveness of approach

Fig. 8 Time response of real fibre winding process with data from a numerical model

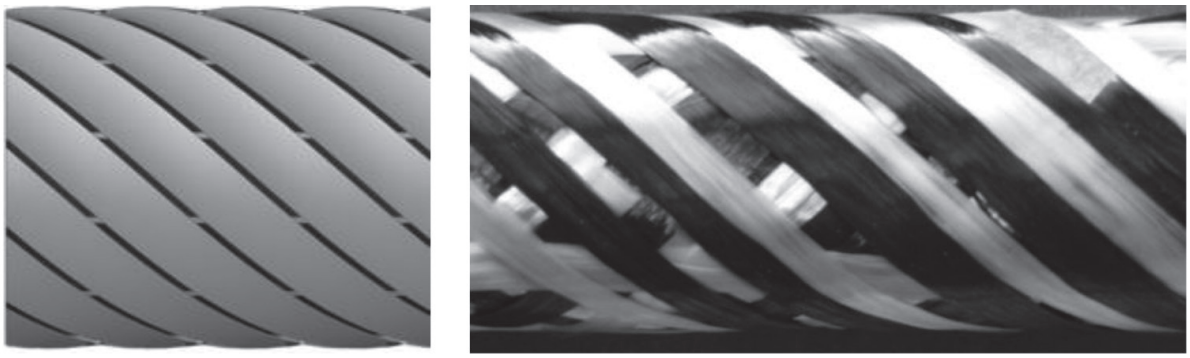

Fig. 9 Comparison an ideal sample and real sample from winding processing with data from a numerical model

of our production procedure with the other one. We solved determining of the robot-end-effector trajectory by our procedure in several practical examples and we have obtained good results. Of course in the world you can find a number of professional teams that are trying to find an optimal algorithm for computing the trajectory toward solving a particular problem. All these methods are, but intended for surface coating technology fibres. Therefore not directly comparable with the method presented in this article (which is designed for winding fibres). Their basic aim is that the product (its surface) is placed firmly in the space robot and carries a tool for applying fibres. They are known methods such as point *Tag generation for flat open surfaces* [9], where it is the automatic generation of points based on a CAD product model and tools. *Fibre steering* is method for determining the trajectory of the robot, the robot gives fibres along a circular path on a flat or complex surface (helix) [9]. *Surface-curve algorithm for RFP (SCAR)*, where is the basic principle of this method is defining an initial curve for laying fibres to form [10]. *Roller path planning method* is the method similar to method RFP (SCAR), but examines not only the position of the fibre to be laid, but also the availability of trajectory from a pressure roller [11].

4. Conclusion

The described mathematical or numerical model with algorithm allows the accurate calculation and determination of the 3D trajectory of the robot-end-effector of the industry robot during the production of composite profile using the dry fibre winding technology on a open and closed non-bearing frame. This provides a significant advantage over users of the extended teach-in principle. The determination of the trajectory of the robot-end-effector using the given method can be used for optimising the trajectory of the robot-end-effector, too. Evolutionary optimising algorithms, in particular genetic algorithms or differential algorithms are often used in solving technical problems (see e.g. [6 - 8]). The described algorithm trajectory calculation can be applied to any manufacturing process where it is necessary to determine the 3D trajectory of a robot-end-effector. Suppliers of industrial robots currently offer specific software tools facilitating control of the robot-end-effector when programming specific tasks (e.g. welding, pressing, laser cutting, grinding). However, none of them are suitable to solve a technical problem of composite production and other general tasks related to the use of industrial robots. The use of the described algorithm is completely independent on the type of industrial robot and software tools. The procedure for determining the trajectory of the robot-end-effector induces virtually no additional costs to the manufacturer and can significantly speed up the determination of the desired trajectory of the robot-end-effector.

Acknowledgements

The results of this project No. LO1201 were obtained through the financial support of the Ministry of Education, Youth and Sports, Czech Republic in the framework of the targeted support of the "National Programme for Sustainability I".

References

[1] PETRU, M., MARTINEC, T., MLYNEK, J.: Numerical Model Description of Fibres Winding Process for new Technology of Winding Fibres on the Frames, *Manufacturing Technology*, vol.16, No. 4, pp. 778-785, 2016.

[2] NOVAKOVA-MARCINCINOVA, L., NOVAK-MARCINCIN, J.: Production of ABS-aramid Composite Material by Fused Deposition Modeling Rapid Prototyping System. *Manufacturing Technology*, vol. 14, No. 1, pp. 85-91, 2014.

[3] PETRU, M., BRONCEK, J., LEPSIK, P., NOVAK, O.: Experimental and Numerical Analysis of Crack Propagation on Light Composite Materials under Dynamic Fracturing, *Communications - Scientific Letters of the University of Zilina*, vol. 16, No. 3A, pp. 82-89, 2014.

[4] SCIAVICCO, L., SICILIANO, B.: *Modelling and Control of Robot Manipulators,* p. 378, 2004, Springer : London.

[5] JAZAR R., N.: *Theory and Applied Robotics,* p. 883, 2004, Springer : New York.

[6] SCIAVICCO, L., SICILIANO, B.: *Modelling and Control of Robot Manipulators,* p. 378, 2004, Springer : London.

[7] MARTINEC, T., MLYNEK, J., PETRU, M.: Calculation of the Robot Trajectory for the Optimum Directional Orientation of Fibre Placement in the Manufacture of Composite Profile Frames, *Robotics and Computer-Integrated Manufacturing,* vol. 35, pp. 42-54, 2015.

[8] BALOCKOVA, L.: The Method for Solving Kinematics of an Industrial Robot, *Applied Mechanics and Materials*, vol. 283, pp. 279-281, 2013.

[9] SHIRINZADECH, B., ALICI, G., FOONG, C. W., CASSIDY, G.: Fabrication Process of Open Surfaces by Robotic Fibre Placement. *Robotics and Computer-Integrated Manufacturing*, vol. 20, pp. 17-28, 2004.

[10] SHIRINZADECH, B., CASSIDY, G., OETOMO, D., ALICI, G., ANG, M. H.: Trajectory Generation for Open-Contoured Structures, Robotic Fibre Placement. *Robotics and Computer-Integrated Manufacturing* , vol. 23, pp. 276-286, 2007.

[11] LONG, Y., ZEZHONG, CH. CH., YAOYAO, S., RONG, M.: An Accurate Approach to Roller Path Generation for Robotic Fibre Placement of Free-Form Surface Composites. *Robotics and Computer-Integrated Manufacturing*, vol. 30, No. 3, pp. 277-286, 2014.

https://doi.org/10.26552/com.C.2016.4.112-116

Ladislav Janosik - Ivana Janosikova - Pavel Polednak*

ASSESSMENT OF ECONOMIC LIFE OF FIREFIGHTING AND RESCUE APPLIANCES BASED ON CHASSIS RENAULT MIDLUM IN THE ZLIN REGION

This paper is focused on the evaluation of economic data obtained from operational records of fire-fighting equipment with a focus on Firefighting and Rescue Appliance type of vehicles, especially on exit vehicles based on the chassis Renault Midlum, during the period 2006 - 2013. These vehicles were operated by professional units of the Fire and Rescue Service of the Zlin Region. The paper's aim is to specify the optimum lifetime of the fire-fighting vehicles by the marginal analysis of fire-fighting vehicles' economical operation. Theoretic calculations of the optimum lifetime have been processed with implementing both the method of exponential trends, and Brown method. The residual value of vehicles has been calculated both according to the current Czech tax law, and to the Expert Standard Valuation of motor vehicles in force in the Czech Republic.

Keywords: *Acquisition value; costs; amortization; residual value; economic life.*

1. Introduction

This paper follows on previous publications of the author focused on the functional reliability assessment of Firefighting and Rescue Appliances based on the chassis Renault Midlum [1, 2 and 3]. These vehicles were deployed at professional units of the Fire and Rescue Service of the Zlin Region during the reporting period. Results of alternative calculations of theoretical economic lifetime are presented in this paper.

2. Characteristics of observed Firefighting and Rescue Appliances

Key operational and economic characteristics of the monitored equipment for the period 2005-2013 are given in Table 1. Basic tactical and technical characteristics of vehicles type Renault Midlum 270.14 P 4x4, for example, can be traced in the literature [3 and 4].

Basic characteristics of referred vehicles during years 2005-2013 Table 1

Vehicle dislocation	Registration mark	Date of commissioning	Purchase price [CZK]	Mileage [km]	Machine work at the site [hour]	Amount of fuel [litr]	Repair costs [CZK]
Zlin	2Z7 8478	20/09/2006	5 805 200	31 278	328	7 264	304 644
Zlin	3Z3 4693	17/12/2007	5 000 000	23 490	112	4 561	201 366
Slavicin	3Z5 7550	16/12/2008	5 000 000	9 993	223	3 868	97 669
Otrokovice	2Z7 8479	20/09/2006	5 805 200	22 860	407	6 632	331 197
Valasske Mezirici	2Z6 2647	20/02/2006	5 805 200	39 260	670	8 141	369 931
Valasske Mezirici	3Z5 7540	17/12/2008	5 000 000	10 241	97	3 721	99 661
Valasske Mezirici	3Z3 4692	14/12/2007	5 000 000	14 618	96	2 856	209 404
Uhersky Brod	3Z2 3957	30/12/2007	5 307 400	28 908	479	9 314	211 802
Uherske Hradiste	3Z6 6297	05/01/2009	5 307 400	15 584	415	6 780	213 246

* [1]Ladislav Janosik, [2]Ivana Janosikova, [1]Pavel Polednak
[1]Faculty of Safety Engineering, VSB - Technical University of Ostrava, Czech Republic
[2]Faculty of Economics, VSB - Technical University of Ostrava, Czech Republic
Email: ladislav.janosik@vsb.cz

3. Methods

Primary operating data [5] for the years 2010-2013 received from the information system IKIS II, were exported to Excel file format and used for failure rate of monitored vehicles evaluating. Data for the years 2005 to 2009 were investigated by the author personally from machinery service records at individual Regional Departments of the Zlin region.

Service life is the ability of the technical system to perform desired functions in order to achieve the ultimate state [6]. *Economic life* of the vehicle can be generally characterized as reaching the limit state when further operation is economically unsustainable [7].

The *economic efficiency of the investment* is calculated to assess the economic life of the technical system in the business environment. This procedure would be relatively difficult to apply for the evaluation of firefighting appliances. The methodology of these calculations is based on the input data extremely difficult to define in the sphere of public service [8 and 9]. Expected annual returns and/or annual operating costs in dealing with accidental incidents are representatives of these data. Revenues are primarily represented by preserved properties during the liquidation of accidents. Property owners and insurance companies usually have different views on the amount of damages. Forensic expert opinion and/or the court proceedings decide in these disputes thereafter. The total amount of investment, bank loans, the tax rate for the calculation of investment income taxes and annual depreciation might be examples of detectable data. Further reason for the impossibility of using this calculation method is the requirement of the initial setting of the technical system's lifetime. The approximate lifetime can be only theoretically assumed from the Machinery Service Order [10].

Therefore, the calculation of the monitored vehicles' economic life was performed by use of two simple and generally known methods, both *exponential trends method*, and the *Brown method* [11 and 12]. Calculations according to both methods were performed for 5-year operation time period. The *residual value* of appliances, which is one of data used for calculations, was variously calculated according to the Act No. 586/1992 Coll. on Income Taxes [13], and according to the Expert Standard No. I/2005 - Valuation of motor vehicles [14].

3.1. Exponential trend method

The exponential trends method is based on the theoretical assumption that the value of firefighting appliances in time $N_p(t)$ has the shape of downward sloping exponential curve [11]. The curve is defined by the equation:

$$N_p(t) = C \cdot e^{-\alpha \cdot t} \tag{1}$$

Similarly, we can define by using an upward sloping exponential curve the trend of costs for maintenance and repairs $N_u(t)$ according to the equation:

$$N_u(t) = A \cdot e^{\beta \cdot t} \tag{2}$$

The total value of firefighting appliances $N_c(t)$ is a sum of equations (1) a (2):

$$N_c(t) = C \cdot e^{-\alpha \cdot t} + A \cdot e^{\beta \cdot t} \tag{3}$$

Further, we can count the local extreme of the function (3) by derivation. The local extreme ($N_c(t)$ minimum in this case) represents the optimal time T_{opt} for replacing the appliance:

$$T_{opt} = \frac{1}{\alpha + \beta} \cdot \ln\left(\frac{\alpha \cdot C}{\beta \cdot A}\right) \tag{4}$$

After reaching the minimum point the function $N_c(t)$ rises, due to declining price of the firefighting vehicle $N_c(t)$ and increasing maintenance and repair costs $N_u(t)$. The constants A, C and exponent coefficients α, β are obtained after processing the input of economic data, building charts and drawing or exponential curve of these charts by using appropriate software, e.g. MS Excel.

3.2. Brown method

This method was first published over 55 years ago in the journal Railway Age, in Brown's paper "What's the Life of a Diesel?" Theoretical foundations were then summarized and published in 1963 [15]. The method was used for the preliminary determination lifetime of rail vehicles [11]. The optimum lifetime T_{opt} is given by:

$$T_{opt} = \sqrt{\frac{2 \cdot H_0}{B}} \tag{5}$$

Here, H_0 is the vehicles' acquisition value given as a percentage = 100 % and B is the linear incremental trend coefficient of the maintenance and repair costs. This coefficient is obtained likewise from the charts using linear regression of data. Application of this method is connected with some weaknesses, as discussed below in the results.

3.3. Vehicle's residual value calculations

Calculations of the vehicle's residual value according to the Act on Income Tax [13] consider the depreciation period of 5 years in Article 30 within motor vehicles for special purposes, according to the classification in Appendix No. 1 of the Act. Depreciation percentages are fixed for the first year at the level

of 11 % and for the next four years they are changed to 22.25 %. Calculating the relative technical value of the vehicle *PTHS* in any year of operation is carried out in a percentage of the purchase price, in accordance with the Expert Standard [14], by the equation:

$$PTHS = \frac{THSN \cdot (100 - ZA) \cdot (100 \pm TS) \cdot PDS}{10^6} \quad (6)$$

Initial technical value of the group *THSN* = 100 %, technical condition changes *TS* = 0.0 % and the relative group proportion value *PDS* = 100 % were applied in the equation, in the case of maintained and operational firefighting appliances. Basic amortization *ZA* [%] which is calculated as the arithmetic average of the following equation was the only variable in the equation (6):

$$ZA = \frac{ZAD + ZAP}{2} \quad (7)$$

ZAD parameter is the basic percent reduction during the operation defined in Annex No. 1.4 of the Expert standard [14] and ranges from 20 % in the first year of operation to 90 % in the tenth and following year of operation. *ZAP* parameter [%] determines the percentage of the basic reduction for the mileage (see ibid.).

4. Results

Overall results of calculations are stated in the following tables and graph exemplifications of which are evident constants and coefficients exponents values used for the calculations in equations (4) and (5).

The difference of calculated results of the vehicle's residual value was set in Figs. 1 and 2, as demonstrated on the case of the vehicle registration number 3Z2 6957, deployed at the fire station Uhersky Brod. It is evident that the Expert Standard is more suitable for both longer amortization time, and mileage consideration. These factors can significantly affect the vehicle wearing. Expert Standard gives even higher residual value of the particular vehicle in the final outcome.

The difference in resulting functions of repair costs (for the same vehicle) obtained by the method of exponential trends and Brown's method can be seen in Figs. 3 and 4. The vehicle registration number 3Z2 3957 of the station Uhersky Brod was chosen as an example because due to the highest calculated value of economic life, which is closest to the expected present reality. The appliance was included into exit vehicles on December 31, 2007. Unfortunately, even in these calculations is reflected the fact that operation records were not conducted complexly before 2010 [1 and 2]. Thus, it was found that the vehicle mileage had reached 13,600 km in years 2008 and 2009 but recorded repair costs had been zero in the same period.

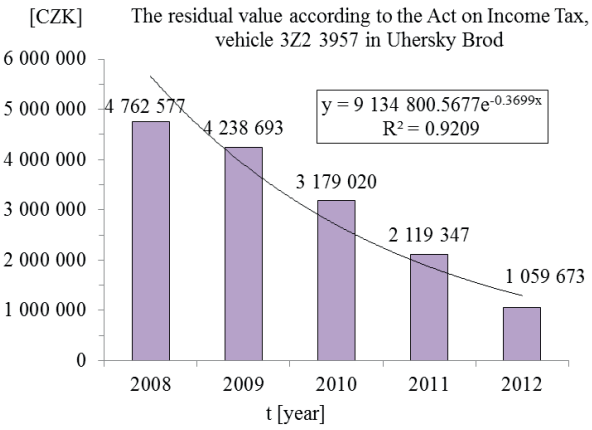

Fig. 1 The residual value according to the Act on Income Tax

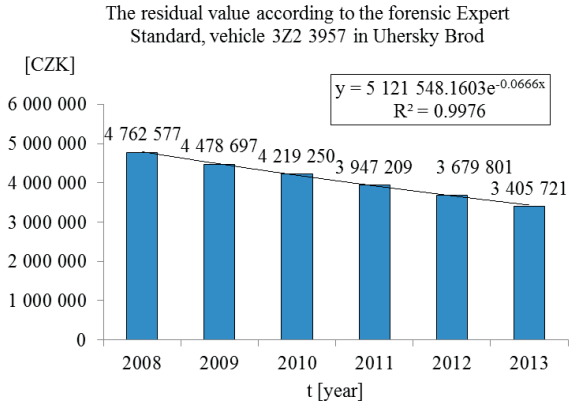

Fig. 2 The residual value according to the forensic Expert Standard

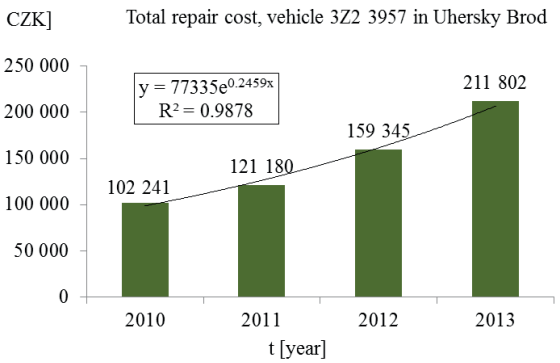

Fig. 3 Total repair costs according to the exponential trends method

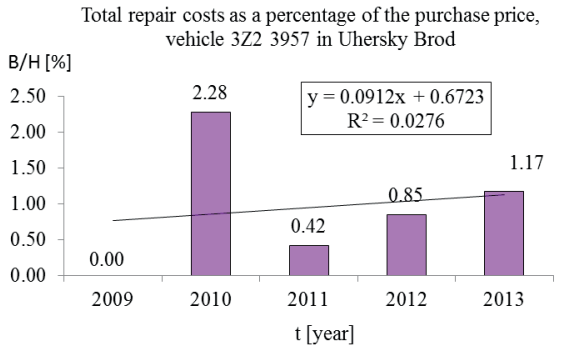

Fig. 4 Repair costs according to the Brown method

Results of the recovery time when depreciating according to the Act on Income Tax are shown in Table 2 [13]. Table 3 presents alternative results of calculations while using the depreciation according to the Expert Standard [14]. Both results are counted when applying the method of exponential trends. As written above next to Figs. 1 and 2, the influence of valuation methods is reflected in the final size of the recovery time.

Results acquired by the Brown method with using linear trends are shown in Table 4. Calculations show that the Brown method application is inappropriate for fire equipment. Calculation results are completely out of reality. Correlation coefficients of each regression curve are very low. The optimal economic life calculations by the equation (5) for negative values of constant B cannot be accomplished thereafter.

Recovery time in accordance with the Brown method Table 4

Vehicle dislocation	Registration mark	B [-]	Correlation coefficient R	T_{opt} [year]
Zlin	2Z7 8478	0.2871	0.4303	26
Zlin	3Z3 4693	-0.0119	0.0608	
Slavicin	3Z5 7550	0.042	0.1682	69
Otrokovice	2Z7 8479	0.1074	0.1327	43
Valasske Mezirici	2Z6 2647	-0.1507	0.1503	
Valasske Mezirici	3Z5 7540	0.0787	0.3746	50
Valasske Mezirici	3Z3 4692	0.4995	0.7030	20
Uhersky Brod	3Z2 3957	0.0769	0.1661	51
Uherske Hradiste	3Z6 6297	0.3754	0.9027	23

Using this method has its disadvantages. The method was formulated for rail vehicles, which have high initial costs, and the expected optimum life is considerably longer than 10 years. For

Recovery time in accordance with the Act on Income Tax Table 2

		Maintenance and repairs cost ratio $N_u(t)$			Residual value of firefighting appliances in time $N_p(t)$ coefficients			T_{opt} [year]
Vehicle dislocation	Registration mark	A [CZK]	β [-]	Correlation coefficient R	C [CZK]	α [-]	Correlation coefficient R	
Zlin	2Z7 8478	36 512	0.5899	0.907	8 444 634	0.3699	0.960	5.2
Zlin	3Z3 4693	37 561	0.3529	0.961	7 660 778	0.3699	0.960	7.4
Slavicin	3Z5 7550	27 164	0.3397	0.909	8 605 720	0.3699	0.960	8.2
Otrokovice	2Z7 8479	64 958	0.4619	0.890	8 453 027	0.3699	0.960	5.6
Valasske Mezirici	2Z6 2647	32 249	0.5644	0.832	7 926 425	0.3699	0.960	5.4
Valasske Mezirici	3Z5 7540	4 763	0.6637	0.952	8 605 720	0.3699	0.960	6.7
Valasske Mezirici	3Z3 4692	3 447	0.7005	0.966	7 715 162	0.3699	0.960	6.6
Uhersky Brod	3Z2 3957	77 335	0.2459	0.994	9 134 800	0.3699	0.960	8.4
Uherske Hradiste	3Z6 6297	23 196	0.5493	0.999	9 134 800	0.3699	0.960	6.1

Recovery time in accordance with the Expert Standard Table 3

		Maintenance and repairs cost ratio $N_u(t)$			Residual value of firefighting appliances in time $N_p(t)$ coefficients			T_{opt} [year]
Vehicle dislocation	Registration mark	A [CZK]	β [-]	Correlation coefficient R	C [CZK]	α [-]	Correlation coefficient R	
Zlin	2Z7 8478	36 512	0.5899	0.907	5 553 636	0.0638	0.9982	4.3
Zlin	3Z3 4693	37 561	0.3529	0.961	4 779 616	0.0631	0.9987	7.5
Slavicin	3Z5 7550	27 164	0.3397	0.909	4 822 246	0.0652	0.9989	8.7
Otrokovice	2Z7 8479	64 958	0.4619	0.890	5 565 664	0.0637	0.9980	4.7
Valasske Mezirici	2Z6 2647	32 249	0.5644	0.832	5 655 152	0.0704	0.9894	4.9
Valasske Mezirici	3Z5 7540	4 763	0.6637	0.952	4 795 414	0.063	0.9993	6.3
Valasske Mezirici	3Z3 4692	3 447	0.7005	0.966	4 779 616	0.0631	0.9987	6.3
Uhersky Brod	3Z2 3957	77 335	0.2459	0.994	5 121 548	0.0666	0.9988	9.2
Uherske Hradiste	3Z6 6297	23 196	0.5493	0.999	5 095 852	0.0641	0.9996	5.3

example, rail kit CityElefant type 471/071/971 costs CZK 217 million within the lifetime of 30 years or rail kit RegioSprinter BR 654 costs CZK 47 million within the lifetime of 25 years. Application of this method assumes steady and in time rising repair costs. To evaluate the lifetime of less costly firefighting equipment, then the results are not those we expected.

5. Conclusion

Calculations results show that we can theoretically expect the optimum lifetime close to 9 years operation of firefighting vehicles based on the chassis Renault Midlum. This theoretical aim was achieved without major problems in six of the nine observed trucks. This lifetime depends on the current operational load. The firefighting vehicle lifetime can be prolonged by relocating trucks from the group of emergency vehicles to reserves that are in lower service load. Using the Expert Standard for more accurate and more realistic residual vehicle value determination than using the Act on Income Tax is the next recommendation. Confirmation of the Brown method unsuitability for these calculations is the last major finding.

Acknowledgements

This paper was supported by an internal grant of specific research *"SP2014/44 - Determining aspects of operational and functional reliability of firefighting equipment."*

References

[1] JANOSIK, L.: *Evaluation of Fire Appliances on Renault Midlum chassis with Brigades of Fire and Rescue Service of the Zlin region.* Fire Protection 2014, Ostrava : Association of Fire and Safety Engineering, 2014, ISBN 978-80-7385-148-4, 108-111.

[2] MONOSI, M., JANOSIK, L.: *An Essay of Firefighting Vehicles' Reliability.* Production Management and Engineering Sciences: Proc. of the Intern. Conference on Engineering Science and Production Management, London : CRC Press, 2016, ISBN: 978-1-138-02856-2, 201-206.

[3] JANOSIK, L.: *Functional Reliability of Operation of Selected Firefighting Vehicles* (in Czech), PhD. thesis, Ostrava : VSB-Technical university of Ostrava, 2015, 142 p.

[4] MONOSI, M., SLOBODA, A., PALUCH, B., HAJDUOVA, Z.: *Fire Equipment* (in Slovak), EDIS : University of Zilina, 2013, ISBN 978-80-554-0705-0, 402 p.

[5] BALCAREK, V.: *Personal Consultation and Operational Data Export from IKIS II* (in Czech). Fire Rescue Service of Zlin Region : Regional Directorate Zlin, Prirucka 213, December 2013.

[6] CSN IEC 50(191) - *International Electrotechnical Vocabulary. Chapter 191: Dependability and Quality of Service* (in Czech), Praha : Czech office for Standards, Metrology and Testing, 1993, 166 p.

[7] STODOLA, J.: *Operational Reliability and Diagnostics (in Slovak),* Brno : University of Defence, 2002, 88 p.

[8] SPACILOVA, L., JANOSIKOVA, I., HON, M.: *Microeconomics B. Workbook,* 1st ed. (in Czech). Ostrava : Faculty of Economics : VSB-Technical University, 2014 vol. 19, ISBN 978-80-248-3608-9, 121 p.

[9] JURECKA, V., JANOSIKOVA, I. *Microeconomics. Textbook for Bachelor Studies,* 1st ed. (in Czech). Ostrava : Faculty of Economics : VSB-Technical University, 2005, ISBN 978-80-248-0910-6, 315 p.

[10] *Instructed the Director General of the Fire and Rescue Service and the Deputy Minister of Interior of 13. 3. 2006 issued Order Machinery Fire Rescue Services of the Czech Republic* (in Czech). Praha : The collection of internal management Director General of Fire Rescue Service of the Czech Republic and the Deputy Minister of the Interior, 2006, No. 9, 28 p.

[11] DANEK, A., SIROKY, J.: *Theory of Replacement of Conveying Vehicles* (in Czech), Ostrava : VSB-Technical University, 1999, ISBN 80-7078-568-3, 156 p.

[12] HOLUB, R., VINTR, Z.: *Fundamentals of Reliability* (in Czech). Brno : University of Defence, 2002, 174 p.

[13] Czech National Council Act No. 586/1992 Coll., On income taxes, as amended (in Czech). Collection of Acts, 1992, part 117, 48 p.

[14] KREJCIR, P., BRADAC, A.: *Expert standard No. I / 2005 - Valuation of Motor Vehicles* (in Czech). Brno : Academic publishing CERM Ltd., 2005, 103 p.

[15] BROWN, R. G.: *Smoothing Forecasting and Prediction of Discrete Time Series*. Englewood Cliffs : NJ : Prentice-Hall Inc., 1963, 464 p.

https://doi.org/10.26552/com.C.2016.4.117-122

Silvie Benesova - Isabela Bradacova - Thomas Jager*

EVACUATION OF PERSONS FROM SELECTED DEPARTMENTS IN HIGH-RISE BUILDINGS OF HEALTHCARE FACILITIES

The article deals with the evacuation of persons from hospital bed wards in high-rise buildings of medical facilities. It presents a proposal for a systems approach and provides a subsequent supportive methodology and tools for planning and implementation of the evacuation of persons with disabilities, which is based on data collection and analysis.

Keywords: *Evacuation, evacuation plan, bed wards, patient classification, systematic methodology for evacuation.*

1. Introduction

The issue of evacuation of persons with disabilities from selected hospital wards presents a multifunctional problem which is significantly extensive and complex. There are actually two groups of patients: walking patients and patients confined to bed who are often in poor physical condition and have psychological problems, which in the event of an emergency evacuation situation requires increased coordination and a higher number of the staff involved. The evacuation itself, and in this respect also the safety of people from the point of time available for their evacuation in general, is still the subject of research [1].

So far no complete methodology, which would serve the medical facilities to develop their evacuation plans for high-rise buildings, has been created in the Czech Republic.

It is necessary to mention that medical facilities due to their typical character of operation create specific positive and negative factors, which have impact on the evacuation of persons [2].

Positive factors are, for example:

- Sufficient space to enable a possible evacuation of persons;
- Constant on-site presence of staff members in facilities enabling to detect danger;
- Constant on-site presence of staff members to be able to carry out the evacuation of persons;
- Possible assistance of staff members from other departments which are not endangered;
- Preparation and training of staff members to be able to handle emergency situations;
- Demanding requirements for construction and operation of medical facilities from the point of view of fire safety and protection of population (legal and technical standards);
- Systematic attention of supervising authorities focused on providing high level safety (e.g. the authority responsible for state fire inspection).

Factors considered as negative are, for example:

- A relatively high concentration of people (especially in multi storey buildings);
- Persons with limited mobility or immobile patients;
- Patients permanently attached to medical devices safeguarding their life functions (e. g. department of anaesthesiology and intensive care (DAIC), intensive care unit (ICU), division of neonatology);
- The necessity to complete some surgical interventions in specialist departments under any situation (e. g. operating rooms);
- Psychological instability of patients having health problems being exposed to sudden unexpected threat [2].

On December 31 2013, there were 188 hospitals with a capacity of 56 807 beds (including 47 033 acute care beds, 7 652 beds in after care and 2 122 new-born beds) registered in the Czech Republic [3] - Fig. 1.

* [1]Silvie Benesova, [1]Isabela Bradacova, [2]Thomas Jager
[1]Department of Fire Protection, Faculty of Security Engineering, VSB-Technical University, Czech Republic
[2]Munchen, Psytech GmbH, Germany
E-mail: Benesova.Silvie@fnbrno.cz

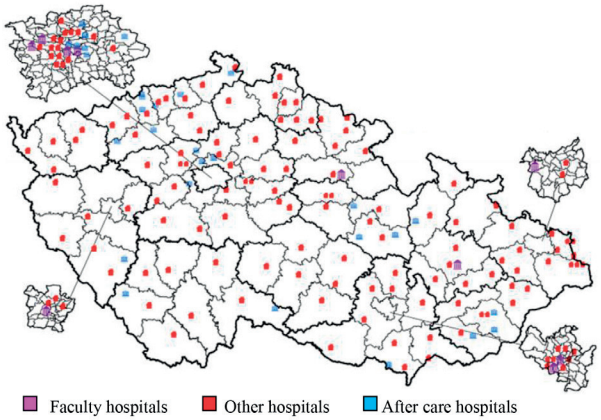

Fig. 1 Hospitals in the Czech Republic (Dec. 31 2013)

2. Analysis of risks and factors affecting the evacuation of patients from a healthcare facility

An analysis of risks which might in any way adversely affect either the operation of the healthcare facility or the evacuation process should be done before every planning of evacuation training as well as before creating partial evacuation plans. Regulation of risks is one of the fundamental building blocks of modern management [4].

In our opinion the combination of SWOT analysis and the checklist method is the most suitable to be used in medicine. The reason is that both these methods are relatively simple and easily accessible to the management of a healthcare facility [5].

To evaluate the extent (degree) of risks in the Faculty Hospital Brno (FH Brno), the point semi-quantitative method of risk acceptance was applied, using the formula:

$$R = P \times Z \text{ [4]}$$

where

R - resultant extent of the risk (the degree of risk acceptance),

P - probability of the risk occurrence,

Z - severity of the possible risk consequences.

The results of the dot product of individual risks were processed using a matrix and are shown in the table which served for the evaluation of individual risk acceptances (see Table 1).

Dot product – the acceptance of individual risk types Table 1

R / Risk degree	Risk acceptability
1 - 2	Minimal risk
3 - 5	Low risk
6 - 8	Medium risk
9 - 14	High risk
15 - 25	Very high risk

On January 1 2016, the Catalogue of risks of the FH Brno contained 155 risks; the catalogue is constantly updated and extended once in a period of 2 years.

3. Selected risks associated with the evacuation of persons

For research purposes the analysis of extent of risks selected from the Catalogue of risks of the FH Brno was conducted. The selected risks might affect the evacuation of persons from the healthcare facility (see Table 2).

A summary of achieved levels of risks associated with the evacuation Table 2

Risk type	R / Risk degree
Gas explosion	2.95
Lack of evacuating staff	2.28
Risks associated with the operation of technological systems	0.42
Fire outbreak	4.19
Toxic chemicals formed by burning	0.90
Disruption of organisational operation - energy, water, gas supply breakdowns	2.30
Disruption of organisational operation - air-conditioning problems	1.36
Disruption of organisational operation - disruption of medical gas supplies	1.04
Limited functionality of alternative sources of electric energy	1.18
Malfunction or breakdown of lifts	1.25
Flooding	1.73
Local damage to buildings	1.31
Disruption of the building statics	0.61
Contamination of people and material	0.55
Impassable access paths	1.03
Suspicious objects (e.g. explosive)	1.98
Failure of safety systems	0.82
Explosion – a terrorist attack, collision	0.86
Panics initiated and spread	2.13
Helicopter/airplane crashes	0.50
Impassable escape routes	1,71
Late announcement of an emergency situation	1.96

4. SWOT analysis of patient evacuation in the FH Brno

Our work experience and risk analyses created in the years 2012 and 2014 enabled us to create the SWOT analysis for patient evacuation in the Faculty Hospital in Brno - Fig. 2.

SWOT analysis is an efficient and simple tool for evaluating the real situation, possible risks, necessary changes and inevitable steps to be taken to transform weak points into strong points and eliminate risks. Simultaneously, it is a tool for long-term planning due to the fact that it comprehensively evaluates the operation of an organisation and helps to detect problems and new growth challenges. It is the method which enables to determine the strong and weak points, opportunities and threats of the organisation [5].

The strengths of the FH Brno are, for example, prior experience of the staff with evacuations, permanent presence of the Emergency dispatching (EMOFF), cooperation with other hospitals in the city of Brno and anti-fire security of the building. Some examples of weaknesses include: the presence of people with impaired mobility, placement of these patients on upper floors, constant high number of people in the building (outpatients, visitors) as well as human factors, such as panic.

Examples of opportunities for the FH Brno are: constant modernisation of the current departments, frequent trainings of evacuation scenarios as well as the preparedness of the medical staff to deal with an emergency situation.

Threats, which the FH Brno is facing, represent possible health and property losses, a high number of visitors in medical facilities, possibility of hidden fire spread, as well as possibility of fire initiation (intentional ignition in the hospital area).

Individual points were evaluated according to the knowledge and information about evacuation plans of the FH Brno. After both the internal and external parts were added together, the sum of 1.5 was obtained, which means that the result achieved using SWOT analysis is highly favourable for the FH Brno.

		Positive			Negative	
INTERNAL	**STRENGTHS**	*Importance*	*Rating*	**WEAKNESSES**	*Importance*	*Rating*
	1 Staff experience with evacuation	0.3	4	1 Presence of people with limited mobility (immob	0.5	4
	2 Sufficient staffing	0.1	4	2 People with limited mobility are placed upstairs	0.2	2
	3 Cooperation with other hospitals	0.1	4	3 Slower evacuation	0.1	1
	4 Emergency dispatching	0.3	5	4 Large number of people inside the buildings	0.1	3
	5 Building fire protection	0.2	4	5 Panic caused by some patients	0.1	2
	Total	4.3			3	
EXTERNAL	**OPPORTUNITIES**	*Importance*	*Rating*	**THREATS**	*Importance*	*Rating*
	1 Hospital modernisation	0.2	3	1 Number of other people in the hospital area	0.3	3
	2 Evacuation training	0.3	4	2 Insufficient staffing at night	0.1	3
	3 Preparedness of medical staff	0.3	3	3 Hidden spread of fire	0.2	3
	4 Building an outside staircase	0.1	1	4 Possibility of setting objects on fire deliberately	0.3	3
	5 Grant	0.1	2	5 Possible health and property damages	0.1	1
	Total	3			2.8	

SWOT - rating		**TOTAL**	**1.5**
Strengths	4.3		
Weaknesses	3		
Total (internal)	**1.3**		
Opportunities	3		
Threats	2.8		
Total (external)	**0.2**		

Fig. 2 SWOT analysis of patient evacuation in FH Brno

5. The evacuation of patients in the event of fire

In the event of an emergency or catastrophe there may be situations when the evacuation plans need to be activated. If a hospital ward is endangered by fire the situation gets very serious, since the transportation of patients can result in the worsening of their medical conditions or it can even cause their death.

The statistical survey obtained from the software programme ISV 5.0 ("Statistical monitoring of situations") of the General Directorate of Fire Rescue Service of the Czech Republic reports that the major causes fire initiation are:

- Fire,
- Fire manipulation,
- Discarded cigarette butts,
- Disregard of safety regulations,
- Leak of a harmful substance,
- Bomb threats or suspicious objects,
- Dysfunctional infrastructure (power outage, water, gas disruption),
- Technical defects in wiring, machines and equipment,
- Disruption of a building statics,
- Natural disasters.

Fires in buildings of medical facilities are special because of the presence of patients who are unable to move independently, whose mobility is reduced or who are connected to life supporting equipment (electricity, oxygen). Some patients cannot be moved with their beds, their medical conditions can possibly be worsened, others have the lower ability to react and lower self-control which can lead to their panic reactions.

6. Analysis of preparedness of the faculty hospitals in the Czech Republic for emergency evacuations

The evacuation of persons from the premises of medical facilities represents a serious problem in the event of emergency. The character of this issue is complicated also due to variability of types of people present in the hospitals at the time of evacuation. These can be outpatients, hospitalised patients or random visitors. The core of the problem is the fact that any manipulation or transport of immobile patients can lead to the worsening of their health conditions or even to their death.

In order to avoid negative effects of emergency evacuations of patients in hospitals or at least to eliminate their adverse consequences, all the hospitals should have the scheme **containing following points:**

- Pre-planned emergency evacuation scheme;
- Unambiguous marking of escape routes in the buildings (regular inspections);
- Establishment of a crisis committee or centre;
- Introduction of registration and classification (sorting) of patients;
- Ways of safeguarding medical records;
- Assigning of persons responsible for activation of evacuation plans in the departments;
- Evacuation workflow for an intensive care unit (ICU) and department of anaesthesiology and intensive care (DAIC) - (order of patient and equipment evacuation);
- Consultation of the prepared plan with the fire brigade (responsibility, coordination);
- Means of transport and technical provision (face masks, special mattresses, evacuation mats, etc.).

To monitor and analyse the state of preparedness of the Czech hospitals for emergency evacuations, we developed Checklists which were sent to 14 biggest hospitals (mostly faculty hospitals) in the Czech Republic. From the 14 addressed hospitals only one hospital rejected to participate and so the return of checklists represented 92.85 %.

In the first phase we wanted to know to which category (in compliance with the Fire Safety of Building Regulations in the Czech Republic) the addressed hospitals belong. We further wanted to know which parts their high-rise buildings consist of (outpatient departments, hospital wards and bed complements), how often they train evacuation scenarios and how long the evacuation of the ward block with the highest number of immobile patients would last (see Fig. 3).

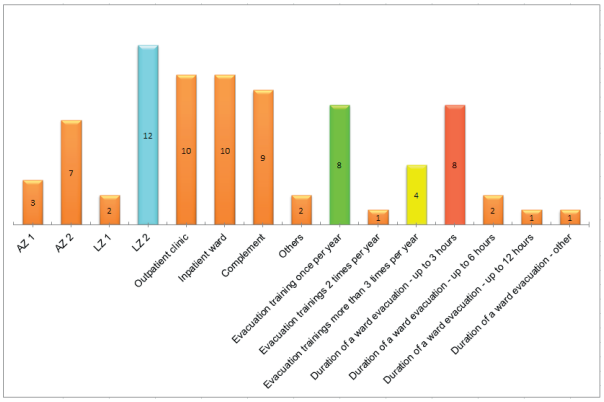

AZ 1- outpatient clinic – maximally 3 offices, AZ 2 – outpatient clinic - more than 3 offices, LZ 1 - small hospital without bed wards, LZ 2 - hospital with 1 or more bed wards

Fig. 3 The 1st- graphical illustration of the number of hospitals included in the given category of questions

The graph shows that from the total number of 13 hospitals participating in the survey:

- 12 hospitals belong to the LZ 2 group (hospitals with 1 or more bed wards),

- 8 hospitals undergo evacuation drills at least once per year,
- 4 hospitals undergo evacuation drills at least 3 times per year,
- 8 hospitals would evacuate the wards with a maximum number of immobile patients within 3 hours.

In the second phase, the questions related to the creation of evacuation plans, existence of the map of risks, the mapping of staffing and number immobile patients on the wards and number of devices to assist for transportation of immobile patients, were processed. Answers are shown in the graph (see Fig. 4).

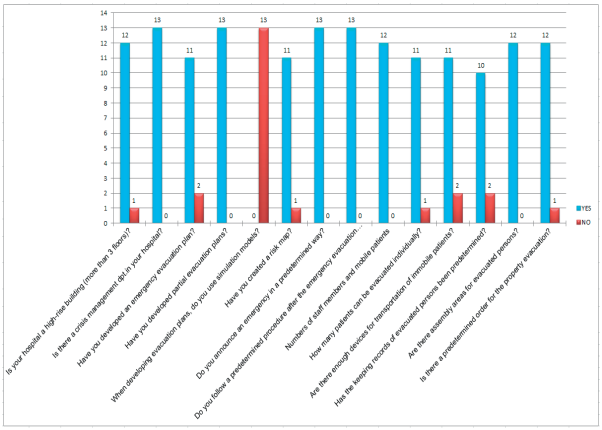

Fig. 4 The 2nd phase - graphical illustration of the number of hospitals included in the given category of questions

The graph shows that from the total number of 13 hospitals participating in the surveys:

- 12 hospitals have a high-rise building with more than 3 floors,
- 13 hospitals have developed partial evacuation plans,
- 11 hospitals have elaborated the risks (the methods for risk evaluation differ),
- 13 hospitals did not use software simulation models when designing their evacuation plans,
- 10 hospitals have a predetermined way of labelling and registration of evacuated people,
- 2 hospitals have not sufficient devices to assist for transportation of immobile patients and have no predetermined way of their labelling and registration.

We can see that none of the 13 surveyed hospitals used software simulation models for development of their emergency evacuation plans. Instead, they use software AutoCad (software for 2D and 3D design and construction of the Co. Autodesk) within pasportisation of hospitals.

From the analysis of answers related to problems occurring during emergency evacuation training we can see that **the hospital faced following problems during evacuation drills:**

- Inaccessibility of the evacuation means of transport;
- Passing on information to fire and rescue service members;
- Decreased audibility when telephoning during the evacuation broadcast;
- Lack of evacuation lifts (old-fashioned hospital building);
- Impassability of the access roads to buildings, late activation of fire safety devices;
- Responsibility for children patients (up to 19 years) – permanent supervision

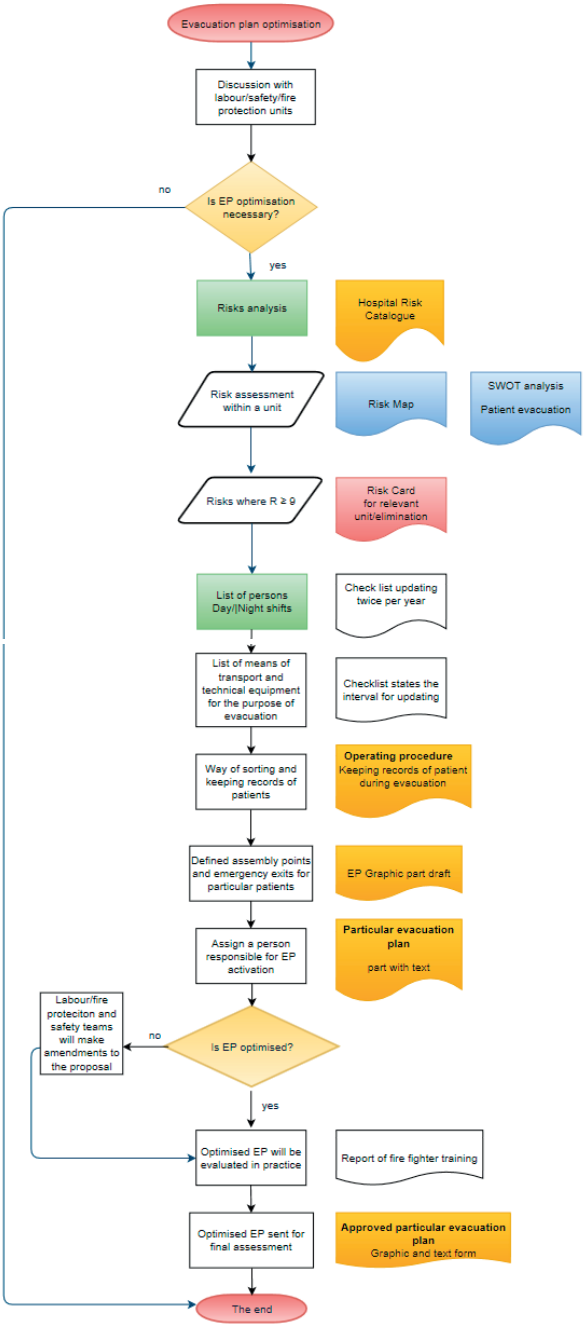

Fig. 5 Flow diagram of the evacuation plan optimisation

- Difficult evacuation of children – incubators in the neonatal units;
- Unwillingness of the staff to participate in the evacuation drills ("Why?")
- The clinic management role versus staff members during the initial phase of an emergency evacuation;
- Technical character (bed widths, lifts, etc.).

7. Flow diagram of the methodological progress for the evacuation plan optimisation

Before anyone begins either to develop an emergency evacuation plan or to optimise the existing one, the first step to do should be **to make an analysis and control of risks and their evaluation.** The objective of this article was to contribute to the issue of evacuation of persons from selected departments located in high-rise buildings in health care facilities and **to design a model (of a flow diagram) and consequent methodology (principles) for creation of partial evacuation plans** or for optimisation of existing evacuation plans.

The acquired data enabled us to formulate the steps which should precede the development of partial plans or their optimisation.

Figure 5 illustrates the flow diagram of the whole methodological process designed for those involved in development of evacuation plans.

8. Conclusion

With the help of the abovementioned methods and analyses we obtained data and results which confirmed the introductory hypothesis saying that in order to avoid negative impacts on patients evacuated from hospitals or at least eliminate the effects of emergency evacuation, **the hospitals should complete the following steps:**

1. To create a catalogue of risks (focus on the risks which could cause or influence the evacuation);
2. To carry out a survey of the departments with a higher probability of risks which might result in emergency evacuation initiation;
3. To make lists of people (patients and staff members) present on average in day and night shifts;
4. To decide on how to register and sort the patients;
5. To assign people responsible for the evacuation plan activation in departments;
6. To determine assembly locations and deviation tracks for specific categories of patients;
7. Workflows for activation of "partial" evacuation plans of a particular clinic;
8. Workflows for evacuation of UIC/DAIC (the order of patient transportation);
9. To decide on how to secure the medical documentation.
10. To make a list of means of transport and technical equipment for emergency evacuation;
11. To make regular inspections of exit routes labelling;
12. To organise fire fighting training courses (functional verification of optimised evacuation plans);
13. To provide the training of staff members on the evacuation course.

The methodology proposed in this article is based on a thorough theoretical background, but it also enables to perform more sophisticated preparation in a simpler way and to execute a demanding evacuation in a complicated environment of medical facilities.

References

[1] MOZER, V., POKORNY, J., KUCERA, P., VRABLOVA, L., WILKINSON, P.: Utility of Computer Modelling in Determination of Safe Available Evacuation Time. *Communications - Scientific Letters of the University of Zilina,* vol. 17, No. 1, 2015, pp. 67-72, ISSN 1335-4205.

[2] FOLWARCZNY, L., POKORNY, J.: *Evacuation of Persons in Health Care Facilities,* 1st ed. (in Czech), [online], p. 13, [cit. 2015-04-17], Ostrava : The Association for Fire and Safety Engineering, 2006. ISBN 80-86634-92-2. Available from: http://www.unbr. cz/Data/files/Konf%20MeKa07/III3_folwarczny.pdf

[3] TYPLTOVA, J.: *Hospitals in the Czech Republic in the Year 2013,* Ustav zdravotnickych informaci a statistiky CR, [online], 2014 [cit. 2016-03-17]. Available from: http://www. uzis.cz/rychle-informace/nemocnice-ceske-republice-roce-2013#_ftn4.

[4] SKRLA, P., SKRLOVA, M.: *Regulation of Risks in Healthcare Facilities,* 1st ed., Prague : Grada Publishing, 2008, ISBN 978-80-247-2616-81.

[5] SMEJKAL, V., RAIS, K.: *Regulation of Risks in Companies and other Organisations,* 4th updated and extended edition, Prague : Grada, 2013, Expert, ISBN 978-80-247-4644-9.

https://doi.org/10.26552/com.C.2016.4.123-128

Cyril Diatka - Jan Ligus*

THINKING ABOUT CERTAINTY AND TOLERANCE WITH MICHEL EYQUEM DE MONTAIGNE

Michel Montaigne's thinking, though primarily relevant to and based upon his own historical context, exhibits unique traits and provides inspiration to current socio-political, ethical, and philosophical discourse. This study deals with Montaigne's peculiar epistemological skepticism, arguing that, if adequately understood, it may prove an important factor in human striving for tolerance. With his emphasis on the emancipation (and separation) of politics from religion and positing the will of an individual human person as the determining factor in the development of human societies, Montaigne brings a significant contribution.

Keywords: *Michel Montaigne, skepticism, tolerance, epistemology, certainty.*

1. Introduction

The legacy of Michel de Montaigne (1533-1592), an important French intellectual from the 16th century, should be considered in the historical context of his life and, even more importantly, within the wider historical framework of late-medieval Europe. [1, 2 and 3] As a continent as well as a civilization, Europe was undergoing significant political, economic, military, as well as cultural changes in the 16th century. Montaigne dies exactly 100 years after the discovery of the "New World". European nations such as England, Portugal, Spain (etc.) are stretching their muscles while expanding the horizons of their influence. Murderous raids of the Spanish conquistadors are contrasted by pious heroism of great religious figures like St. Ignatius of Loyola, St. Francis Xavier, Theresa of Avila, St. John of the Cross (among others). Nicolaus Copernicus publishes his groundbreaking work *De revolutionibus orbium coelestium* in 1543 and the German reformers manage to bring the mightiest ruler in Europe to sign the Peace Treaty of Augsburg in 1555, though only after ruthless religious fighting and mutual persecution among Protestants and Catholics throughout Charles V. German speaking domain and beyond [4, p. 213-215]. The Catholic reform is successfully launched at the Council of Trent in 1545 (the concluding session in 1563), marking the beginning of the Catholic counter-reformation movement that would claim many lives and result in the greatest war that Europe was to experience up until then (the 30-Year War, 1618-1648). The Battle of Lepant (1571) stopped the seemingly unstoppable Turkish invasion into the Mediterranean, while the Sultan Suleiman II launched his mighty campaign against the Southern and Eastern provinces of Hungary and the Balkan countries.

Events like these bring Europe to a new epoch. Old securities are waning and new ones, though tantalizing, are unproved and uncertain. The situation, on the one hand, calls for a simple order, a clear system that would order the lives of individuals and societies and rid it of excessive privileges, while at the same time promoting individual freedom and responsibility; on the other hand, a robust continental struggle is picking up its pace in which individual countries and principalities are drawn into an unavoidable confrontation of the existing hierarchical system with the emerging world of individualism and rationalism [5, p. 197], culminating in the subsequent rise of science, industry and trade. Modern age, though not yet fully born, knocks at the gates of the passing age, promoting the ideology of rejecting the things of the old world. Moral relativism creeps in, expressing itself in the rising reception of epicureism and stoicism, which only further helps emphasizing the individual disposition of a human person to freely make decisions regarding the matters of one's life [6]. In France, the policy of the state is to centralize power in order to face the alliance of its Spanish rival with the Papal State in Italy. The internal social and political changes result in the devastating civil war of 1562-1598 [7]. Michel de Montaigne lives in these volatile times. With his emphasis on the emancipation (and separation) of politics from religion and positing the will

* [1]Cyril Diatka, [2]Jan Ligus
[1]University of Constantine the Philosopher, Faculty of Arts, Nitra, Slovakia
[2]Hussite Theological Faculty, Charles University in Prague, Czech Republic
E-mail: cdiatka@ukf.sk

of an individual human person as the determining factor in the development of human societies [8, p. 137-138], Montaigne brings a significant contribution [9].

2. Historical Self-awareness as Condition for Free Action

Michel de Montaigne shares the criticism of the old order and the energy to think for himself with other important figures of his century (such as Martin Luther) but he turns out to be an intellectual of his own (new) sort. One of his main principles is his conviction that understanding one's own life (as historically situated) is a necessary precondition for free decision-making and action.

Suffice it to say, in the limited space of this current study, Michel de Montaigne was well aware of the role that his own upbringing came to play on his values and character formation. He came from an aristocratic family where his father, Pierre Eyquem de Montaigne, was a provincial judge (in Bordeaux) and his mother, Antoinette de Luppes, a member of a wealthy, Jewish Portugal family. His own parents, thus, embodied not only a rich diversity of family origins and outlooks on life but also a live example of tolerance and mutual understanding. In addition to this, Michel's father was a hardworking, well-read, and innerly disciplined man with a profound effect on his son. His inclination to the values of moral pathos of the Renaissance Stoicism, promoted by the efforts of humanist intellectuals of the time, had its roots in the Platonic body-soul dualism. Pierre de Montaigne thus came to the conclusion that human being is a self-aware, personal being with a clear inner drive for self-realization. As such, human being is responsible to God (understood in a more or less deistic sense). Michel de Montaigne's father was, therefore, convinced that his son must be thoroughly educated from his early childhood, including the study of music, arts and literature, and, above all, proper philosophy, exercised not only intellectually but also existentially in the sense of making concrete decisions and taking responsibility for them.

Michel de Montaigne's study of classical ancient philosophy started early on and continued throughout his life. By placing emphasis on his own, subjective deliberation, however, Montaigne invented a new "rhetorical system" for re-structuring and re-interpreting numerous classic philosophical ideas in a modern fashion: "If being a philosopher means being insensitive to human frailties and to the evils or to the pleasures which befall us, then Montaigne is not a philosopher. If it means using a "jargon", and being able to enter the world of scholars, then Montaigne is not one either. Yet, if being a philosopher is being able to judge properly in any circumstances of life, then the Essays are the exemplary testimony of an author who wanted to be a philosopher for good. Montaigne is putting his judgment to trial on whatever subject, in order not only to get to know its value, but also to form and strengthen it." [10, http://plato.stanford.edu/entries/montaigne/#Con].

"Get to know yourself" [11, p. 153] and "get to know the world" [11, p. 218] - these continued to be the leading mottos of Michel's education at home and beyond. Already at the age of 13, young Montaigne begins to contemplate the intricacy of relationships between humans and nature and the ambiguity of dimensions of life and death. His contemplative, thoughtful nature comes into conflict with his strict upbringing at this juncture. Instead of disciplined memorization, Montaigne came to promote independent reflection and creative thinking [12]. The power of "nature" (e.g., natural curiosity), according to Montaigne, should be allowed to play its part, unhampered by human devices (this approach might place Montaigne in the position of a forerunner to J.J. Rousseau and a precursor to L.N. Tolstoj, in a certain sense). He shocks his contemporaries with statements like: "I have, as I have said elsewhere, quite simply and crudely adopted for my own use the ancient rule that we cannot go wrong in following nature, and that the sovereign precept is to conform to her. I have not, like Socrates, corrected my natural disposition by force of reason, nor used any art to interfere with my native inclinations;" [11, p. 338] and then he adds: "May I say this in passing, that I find we attach more value than it deserves to a certain idea of scholarly integrity, almost the only one in vogue amongst us, which makes learning a slave to precept and fetters it with hope and fear? I would have it not formed, but perfected and justified, by laws and religions, conscious of being able to sustain itself without help, springing up within us with its own roots from a seed of universal reason, which is implanted in every man who is not corrupt by nature." [11, p. 339] Instead of pedantic memorization, thus, learners should be encouraged to, so to speak, create their own being/personhood face to face to the fullness of the world [13]. Such creative freedom enables one to form their own attitudes, inner dispositions, and value judgements about the outer reality as well as one's own relationship to the outer world. Montaigne embodies this ideal in his own creative approach. In his magnum opus work – *Essays* – "Montaigne shows himself to be programmatically unphilosophical. He sets out to write not impersonally but personally, not comprehensively but partially and inconsistently, not supra-temporally but consciously immersed in the passage of time; he relies on an unsystematic mixture of anecdote, quotation, and moral reflection, into which in the course of the last twelve years of his life he interpolated intermittently yet more thoughts and quotations; his text rarely takes on the character of a sustained argument that is explicit about its own forms of validation" [14, p. 143-144].

Young Montaigne was not excited about most of the contents of his study at Colege de Gyuenne, preferring rather the study of Roman classics, especially Ovidius and, later on, the philosophical school of Skepticism. In his adult life, Montaigne got his share of administrative (as counselor in Bordeaux Parliament) and political duties (as the mayor of Bordeaux and royal counselor). His political career, however, did not bring much satisfaction

to thoughtful and contemplative Montaigne. Thus, having the means to lead a comfortable life at his mansion in Montaigne (about 45 km east of Bordeaux), he decided to step down from his political and administrative duties and live a relatively secluded life, being fully devoted to philosophy and writing. He collected his ideas into his famous *Essays* – "Essais de Messier de Michel Seigneur de Montaigne. Livre et premier et de second" (Bordeaux 1580) [15]. However, at the height of civil war, Montaigne decided to try to mediate between the fighting camps of Protestant Huguenots and the Catholic League. He traveled personally to Paris in 1588 but his efforts only led to his imprisonment in the hated Bastille prison. However, with the rise of Henry IV. as king of France in 1589, Montaigne was not only vindicated but offered a high position at the royal court. Due to his deteriorating health, Montaigne politely rejected the offer and spent the rest of his days in his mansion, where he died on September 13, 1592.

3. Hopeful Skepticism as a Way to Epistemological Sobriety

Montaigne is intellectually provoked by a peculiar type of ignorance on the side of humans regarding life and its meaning. His way of dealing with this situation is to free human innermost beliefs and convictions from the authorities of this world (especially those of the church). He then attempts to lead the human subject to a conjunction of a transformed faith – i.e. faith ridden of institutional ideologies and morphed into an intense, personal experience – and of free, emancipated, though necessarily incomplete knowledge. This subjective experience of faith in the sense of emancipated self-knowledge may serve as a certain satisfaction vis-à-vis one's realization of one's own contingency and limitedness. Everything in nature, all living things, are bound to die. The ensuing sense of meaninglessness and/or nihilism can be countered by one's self-knowledge and self-realization. To know oneself is thus an ever emerging and growing theme in Michele de Montaigne's intellectual reflection, placing him among thinkers such as Heraclitus, Socrates, Chrisyppos, Epictetus, Abelard, Dante, Petrarca, Erasmus of Rotterdam, etc.

Montaigne recognized human natural need for knowledge, the source of which were primarily reason and experience. He did not connect these directly with faith and religious sensitivity, for the spheres of religion and knowledge must be, according to Montaigne, strictly separated [11, p. 309, 314, etc.]. For, as Montaigne exclaims, using Livy's words: "Nothing has a more deceptive face than a corrupt religion, in which the divine will acts as a screen for crimes"; [11, p. 319] and a few pages later he states: "It is a doctrine ruinous to every society, and far more harmful than clever or subtle, which persuades people that religious belief alone, without morality, is sufficient to satisfy divine justice. Practice shows us an enormous difference between piety and conscience" [11, p. 339].

is human frailty and finitude. Our senses are not fully reliable and do not convey the certainty one wishes for. Thus Montaigne soberly realizes that "As for the natural faculties within me, of which my writing is the proof, I feel them bending under the burden. My ideas and my judgement merely grope their way forward, faltering, tripping, and stumbling; and when I have advanced as far as I can, I am still not at all satisfied. I can see more country ahead, but with so disturbed and clouded a vision that I can distinguish nothing" [11, p. 50]. Our attempts to prove their validity by our reason only lead us from one argument to another in an infinite progression of proofs – which, ultimately, leads nowhere.

The ensuing epistemological humility is explicated by Montaigne in one of his longest essays titled "Apology of Raymund de Sabonde" (originally intended as a separate work). In it he offers a sharp criticism of human cognitive abilities. When we focus on our knowledge of nature, for example, we are confronted with a labyrinth of conflicting ideas and experiences. Thus, neither in natural philosophy, nor in the intimate knowledge of one's soul is there a fully true knowledge. The world is full of blabber of various untruths, philosophical absurdities, and sophistry. The human subject is entangled in human traditions and bound by his blind faith in authorities (such as Aristotle, or the authority of ecclesiastical offices). His true essence and capacities remain hidden. Neither can we find certainty in moral laws, since that which is valid and binding in one country may not be valid in another. That, which is lifted up as ideal in one historical and geographic context, may be considered a vice in another. Humans are not able to understand with certainty the general laws of the world (including moral conduct). One may say, in a sense that the world is a heap of disordered realities, full of confusion and paradoxes.

The sobering recognition of this fact may lead us to a humbler approach to learning about and interacting with other people and the world. This epistemological uncertainty may open us up to a more diverse approach, to a willingness to look at things from different angles. This is why Montaigne "distrusts universal statements, and seems enamored of the exception, of the particular case... We move from a general rule to an exception, then to an exception to the exception, until we seem to be left hanging. The impression of open-endedness that many chapters of the *Essays* convey is linked to the author's willingness to indulge any sort of particular case" [16, p. 1]. The goal of Montaigne's skepticism "is not to ruin arguments by opposing them, as it is the case in the Pyrrhonian 'antilogy', but rather to counterbalance a single opinion by taking into account other opinions" [10, http://plato.stanford.edu/entries/montaigne/#MonSce] Only when humans grasp the fact that they are finite and fallible, that their ability to know is limited at best and prejudiced at worst, can they alter their behavioral patterns in relation to other (i.e. different) people.

Truly inspiring are Montaigne's views on the position of morality in the social dimension. Having lived through times of

abrupt changes and horrifying cruelties in 16th century France, he comes to the conclusion that social life with its rules and customs, needs and interests, cannot be the true, genuine foundation of virtues. The wellbeing of French society (which, in itself, is difficult to define), understood as the ultimate goal of social interactions, is often being pursued by illegitimate, or inadequate means, including treachery, torture, and murder. From this follows, according to Montaigne, that "social usefulness" must be clearly distinguished from "virtue". Virtue and social usefulness (a form of utilitarianism) part ways at the moment when necessary acts mutate into recklessly ambitious plans. Though Montaigne is no idealist, he does maintain that, under certain conditions, one must always act in accordance with virtue, even if it meant sacrificing one's wellbeing (or social wellbeing) in the anticipation that God's gracious providence will not refuse to support the just and pure action of humans. Since humans are not almighty, they must often hand over the navigation of their "ship" to God, seeing in Him the anchor of safety. In a similar fashion to that of Kant, though not discursively but rather intuitively, Montaigne moves in solving this issue to a position of expectation, to anticipating God's gracious, providential care. Among other things, this also implies that any reward of virtuous actions should not be expected in this historical reality but that one should rather rely on God's providence as it plays out in a future state of things.

We might, in a way, sense an anticipation of the stance that we later see in Blaise Pascal and, centuries later, in Soren Kierkegaard [17]. In contrast to that, we see a dramatically different approach in Rene Descartes who defines morality as the freedom of will to do that which human reason presents to us as our comprehension of the truth and the good. The capacity of our reason to determine/discern that which is true and good then implies that genuine understanding is identical with virtue. Montaigne, in fact, made it a point of his philosophic endeavor to show that such identification is not only intellectually illegitimate but also socially dangerous. "Not only does Montaigne criticize philosophers for their inattentiveness to their own humanity, but he intentionally fashions his own writings to be unlike philosophy" [16, p. 1].

4. Towards a New Foundation for Tolerance

Montaigne concludes his contemplation of virtue with the following points that carry promising potential for establishing a new foundation for tolerance in society [18]. One should respect one's historical context. Humans should abide by the given order, instituted in a particular country (where these humans are historically situated) – so there is room for civic obedience – but the society must not interfere in personal opinions of individuals – which is a clear reference to the freedom of conscience [19]. Montaigne promotes the principle of cultivating benevolence to others with different opinions. This we can achieve by an intentional effort on our part to understand the position of the "other", trying to view the disputed matter from his point of view (through his eyes). We should not succumb to the temptation of comparing others with us, employing our standards of measurement, but we ought instead to consider them in their own context, how they measure up to their own standards of conduct. Montaigne articulates his conviction in this respect on several places of his *Essays* with vigor and resolve: "Everyone thinks himself the master pattern of human nature; and by this, as on a touchstone, he tests all others. Behavior that does not square with his is false and artificial. What brutish stupidity! For my part, I consider some men, particularly among the ancients, greatly superior to me; and though I clearly recognize my inability to follow in their footsteps, still I follow them with my eyes, and observe the force that lifts them so high" [11, p. 232]. Even if we do not adopt the customs and expressions of other cultures, we can still be free to see positive aspects in them and to show our respect (3). It is not enough if we flee from other people; we must flee from the attributes of the crowd which sends its roots deep into our inner selves. One must part with oneself, only in order to find oneself again. We should not cling to our accrued status or wealth. Instead, we should vigorously practice self-control, [20] which happens to be the most important thing in the world.

Montaigne is offering his society a bold new outlook on the goals and meaning of life. The aim of human life should be subordinated to the human individual, not some external values that are anchored in transcendence. Each human life has its own rich resources and is thus, in a sense, self-consistent and self-sufficient. Human individual is sovereign to himself, though each individual bears the image of the whole human plight. From this follows that each person should love all people, trust only a few, and harm no one.

5. Conclusion

Montaigne understood skepticism as an ethics of judgement rather than as vicious tool to defeat enemies or a self-negating tool that leads to oblivion. The path to a mature, personal judgement leads through a thoughtful, intentional absorption and mental processing of personal experience, wider historical circumstances, and (yes, this too!) doctrines and dogmas. "[T] he development of character integrity must remember the organic nature of moral experience" [21, p. 107] Montaigne's hopeful skepticism demolishes absolute certainty only to reinstitute what we might label "viable probability" – that what seems (often intuitively) right and true to us. This, however, is nothing like modern individualism, or absolute subjectivism. We are dealing here with an informed judgement of a qualified subjectivism, i.e. subjectivism shaped by one's intentional struggle to understand oneself as a product of as well as a critic of one's circumstances. Human thought is and should always be perceived as dialogic in

nature. Instead of arriving at absolute truth and then defending and promoting it, often at the expense of those disagreeing with us, we should keep the dialogue going because none of us can claim an absolute perspective [22]. This stimulates a new disposition of the human heart, a new outlook of tolerance. It also helps us preserve a genuine freedom: if we don't have to find and defend absolute truth, we are free to disagree; we are free to fail to comprehend completely; we are free to accept the fact that someone might know more and we might learn from them. As Stefan Zweig said: "Montaigne helps us answer this one question: 'How to stay free? How to preserve our inborn clear-mindedness in front of all the threats and dangers of fanaticism, how to preserve the humanity of our hearts among the upsurge of bestiality?'" [10, http://plato.stanford.edu/entries/montaigne/#Con].

Lest this line of reasoning lead us to hopeless relativism, on the other hand, Montaigne emphasizes personal responsibility of every human individual to make mature judgements in order to arrive at the most convincing conclusion that is possible. One should do it by examining and weighing the strengths and weakness of all conceivable positions, patiently listening to arguments of others, even being willing to place oneself in other's "shoes" in attempt to see the world through their eyes. Personal experience of a lifetime is at our disposal and our task is to actively process it. What awaits us at the end is a "joyful wisdom" – the fruit of our humility, openness, perseverance, and ever-present doubt. The loss of epistemic certainty may ultimately yield true wisdom of life. In this sense, Montaigne brought philosophy to its original starting point – to the sense of awe that keeps a philosopher curious and humble at the same time. Thus we may agree that "[t]he path to an authentic subjectivity seems to lead inevitably through the complicated and sometimes painful struggles of life. One should not expect to make sense of his own life without an arduous struggle to interpret one's existence in relation to self, the world, and to God" [21, p. 106].

References

[1] HEN, J.: *I, Michel de Montaigne* (in Czech), Praha : Odeon, 1990.

[2] MARCI, L.: *Autonomy of Personality and the Problem of Power in the Views of N. Macchiavelli and Michel de Montaigne* (in Slovak), Nitra : Univerzita Konstantina Filozofa, 1999.

[3] SVITAK, I.: *Montaigne*, Praha : Orbis, 1966.

[4] VALCO, M.: *Setting the Stage for a Meaningful Engagement: The Need for a Competent Public Theology in the Post-Communist Context of Slovakia.* In: M. Valco & D. Slivka (eds.), Christian churches in post-communist Slovakia: current challenges and opportunities, Salem, Virginia, Center for religion and society, Roanoke college, 2012, 185-256. "Confiscated church buildings and schools, forced labor in mines, torture, extortion, discrimination in the religious, political, social, as well as academic sense - all these belonged to the harsh reality of those times" (p. 213).

[5] We need to pay more attention to "how the ideas and methods of the Enlightenment" (p. 197) influenced the religious, social, and political thinking of not only Montaigne's era but how they continue to influence our own paradigms. See: VALCO, M.: *Alternative viewpoint: Edwards and the world religions.* McDermott, G. (ed.). Understanding Jonathan Edwards: An introduction to America´s theologian. Oxford : Oxford University Press, 2009, pp. 195-200.

[6] TRETERA, I.: *Historical Outline of European Thinking* (in Czech), Praha : Litomysl : Paseka, 1999.

[7] MAUROIS, A.: *History of France* (in Czech), Praha : NLN, 1994.

[8] With regard to this topic, one might consider Montaigne a precursor to certain elements in the existential thinking of S. Kierkegaard. A mature, self-aware, responsible individual is by both considered as the foundational building block of a healthy society. See: VALCO, M.: Rethinking the role of Kierkegaard´s authentic individual in liberal capitalist democracies today. *European J. of Science and Theology*, vol. 11, No. 5 (2015), 129-139. ISSN 1841-0464. "Kierkegaard's calling the human self to what we may call a 'relational authenticity' may constitute the much needed inception (or inculcation) that will then grow to fuller complexity and beauty of transformed individuals and societies." (Ibid., p. 137); VALCOVA, K., PAVLIKOVA, M., ROUBALOVA, M.: Religious Existentialism as a Countermeasure to Moralistic Therapeutic Deism, *Communications – Scientific Letters of the University of Zilina*, vol. 18, No. 3, 2016, 98-104.

[9] Gregory, M. E. conducted an incisive study on the nature and capacity of the human will according to Michel de Montaigne (as compared with other selected thinkers), placing him in the "soft determinism" camp along with David Hume, Baruch Spinoza, Thomas Hobbes, John Locke, Jean-Jacques Rousseau, François-Marie Arouet de Voltaire, G.E. Moore, A.J. Ayer and Harry G., Frankfurt. See: GREGORY, M. E.: *Free will in Montaigne, Pascal, Diderot, Rousseau, Voltaire and Sartre*, New York : Peter Lang, 2012, 9.

[10] FOGLIA, M.: *Michel de Montaigne*, in *The Stanford Encyclopedia of Philosophy* (Spring 2014 Edition), Edward N. Zalta (ed.), URL = <http://plato.stanford.edu/archives/ spr2014/entries/montaigne/>. [cit. Feb 05, 2016]

[11] DE MONTAIGNE, M.: *Essays,* J. M. Cohen (transl. and ed.), London : Penguin, 1993.

[12] DE MONTAIGNE, M.: *Principles of Upbringing* (in Czech)*,* Valaske Mezirici : Fr. Vanek, 1886.

[13] For a recent inspiring study on how to holistically integrate creative freedom and intrapersonal responsibility in current educational contexts, see: CABANOVA, V.: Social Attitudes and Values of Young People in the Context of Multicultural Education. *Communications - Scientific Letters of the University of Zilina,* vol. 16, No. 3, 2014, 4-8. ISSN 1335-4205.

[14] MACLEAN, I.: *Montaigne and the Truth of the Schools*, in U. Langer (ed.), The Cambridge Companion to Montaigne : Cambridge : Cambridge University Press, 2005, 142-162.

[15] Here it is worth mentioning that Montaigne's *Essays* were placed on the Index of prohibited books (*Index Librorum Prohibitorum*) by the Papal Office in Vatican in 1676.

[16] LANGER, U.: *Introduction*, in U. Langer (ed.), The Cambridge Companion to Montaigne : Cambridge : Cambridge University Press, 2005, 1-8.

[17] "For Kierkegaard, truth is more than a noetic, objective category, accessible to intellectual inquiry by a thinking subject. There must be a deeper, existential basis, related to the deepest aspirations and, yes, fears and doubts of the individual - a desire permeated by passion. The truth cannot be meaningful and relevant without this ‚subjective desire,' whose doubt is the beginning of the highest form of existence", (p. 27), VALCO, M. & VALCOVA, K.: The epistemological challenge of Kierkegaard's truth is subjectivity principle, *Communications - Scientific Letters of the University of Zilina*, vol. 16, No. 3, 2014, 25-28. ISSN 1335-4205. For recent studies on Kierkegaard's thought in our geographic provenience, see also: VALCO, M.: Kierkegaard's 'Sickness unto death' as a resource in our search for personal authenticity, *European J. of Science and Theology*, vol. 12, No. 1, 2016, 97-105. ISSN 1841-0464; KRALIK, R.: Kierkegaard and his influence on Tillich's philosophy of religion, *European J. of Science and Theology*, vol. 11, No. 3, 2015, 183-189. ISSN 1841-0464; KONDRLA, P. & KRALIK, R.: The Specifics of Mission of the Thessalonian Brothers and the Potential for their Actualization (in Slovak), *Konstantinove listy*, vol. 9. No. 2, 2016, 90-98, ISSN 1337-8740; KONDRLA, P. & PAVLIKOVA, M.: From formal ethics to existential ethics, *European J. of Science and Theology*, vol. 12, No. 3, 2016, 101-111. ISSN 1841-0464; KONDRLA, P. & KRALIK, R.: Authentic being and moral conscience, *European J. of Science and Theology*, vol. 12, No. 4, 2016, 155-164. ISSN 1841-0464; KRALIK, R. & TOROK, L.: The "Moment" Kierkegaard's attack upon christendom, *European J. of Science and Theology*, vol. 12, No. 3, 2016, 45-53. ISSN 1841-0464; PAVLIKOVA, M.: The concept of anxiety and its reflection in Auden's work „the age of anxiety", *European J. of Science and Theology*, vol. 12, No. 4, 2016, 111-119. ISSN 1841-0464; REPAR, P.: The Existential Dialectics of Decision and the Scandalon (in Slovak), *Filozofia*, vol. 67, No. 8, 2012, 689-704. ISSN 0046-385X, (etc.).

[18] Theological philosophy is also dealing with the relationship between human freedom and conscience and both concepts are also linked with responsibility. The theological ethics of Dietrich Bonhoeffer deals with the same issue in the first half of the 20th century, as it is explicitly shown in doctoral thesis of N. Bravena: "The two concepts: freedom and conscience are inextricably linked with responsibility", especially in certain human actions. It also means that "responsibility, which would force to act against human own conscience would condemn itself". See: BRAVENA, N.: *Jesus Christ, a brother and a neighbor act in my place. Vicariousness in the theology of Dietrich Bonhoeffer (in Czech),* Edice Pontes : Pragensis, vol. 56, Brno : L. Marek, 2010, p. 166. The relationship of conscience, freedom and responsibility closer illuminates Montaign's philosophy of life (for more details, see: CETL, J., HORAK, P. et al.: *History of European Thought* (in Czech), Praha : Panorama, 1984, p. 258-260.

[19] In his *Essays*, Montaigne is also interested in the importance of education for human life and society. His pedagogical principles correspond with his philosophy of life according to which "education does not only lead man to book learning and verbal knowledge, but understanding the nature of things that could humanly organize his life." CETL, J., HORAK, P. et al.: *History of European Thought* (in Czech), Praha : Panorama, 1984, p. 260. For proper education, therefore, it is very important recognize the "impact of teacher's personality on the development of natural talents and endowments and action of real-life people and books." (Ibid., p. 260). This was often forgotten and overlooked in education. Montaigne's emphasis on personal influence and example in education leads to appreciation of each individual person. Its intentional cultivation is highlighted by "the transcendent dimension of pedagogy" which emphasizes "the uniqueness of human You (Thou), its capabilities and ...it offers help for any individual neglect in upbringing." BRAVENA, N.: *Do not be Preoccupied with Merely yourself ... Overlap and its Significance for the Socialization and Formation of a Child as Personality* (in Czech), Praha : UK PedF, 2016, p. 159.

[20] "Montaigne's watchword, like Goethe's, is *Restraint (Je m'abstiens),* which he took from the Greek sceptics, and inscribed, in Greek, on the reverse side of his famous medal." COHEN, J. M.: *Introduction, in Michel de Montaigne*, *Essays,* J. M. Cohen (transl. and ed.), London : Penguin, 1993, 12.

[21] VALCO, M., KRALIK, R., BARRETT, L.: Moral Implications of Augustine's Philosophical and Spiritual Journey in his Confessions. *Communications - Scientific Letters of the University of Zilina*, vol. 17, No. 2, 2015, 103-108. ISSN 1335-4205.

[22] PETRO, M.: *Human Being as a Person - Hope for Europe* (in Slovak), P. Dancak (ed.), *The Sapiential Character of John Paul II's Anthropology in the Context of the European Integration*, Presov : University of Presov, 2006, 96-111. In his study, Petro argues that Europe's future depends on the consistent cultivation of a free dialogue of values, the starting point of which is the notion of intrinsic dignity of all humans.

Translated by Michal Valco.

https://doi.org/10.26552/com.C.2016.4.129-133

Milan Kubina - Gabriel Koman*

BIG DATA TECHNOLOGY AND ITS IMPORTANCE FOR DECISION-MAKING IN ENTERPRISES

Rapid development in the field of information-communication technologies, which has been recorded in recent years, caused the increase from 40 to 50% in the volume of data in companies last year. At present enterprises are able to use only a quarter of the data available. It is expected that by 2020, the volume of data will have reached 35 zettabytes [1]. By analyzing large amounts of data, it is possible to get the information important for an enterprise which will facilitate decision-making process of managers. Technology for large volume data called Big Data is nowadays largely employed for effective use of data.

Keywords: *Big Data, Technology, Management, Decision-making.*

1. Introduction

The occurrence of large amounts of data was recorded in the 1970s, when researchers from Berkeley identified that there should be more than 1.5 trillion bits of information generated by 1999. Subsequently, in 2003, the repetitive study showed that the amount of information would be doubled within three years. Thus it was established that the amount of data continues to grow. The basis for the definition of large data (Big) in 2001 was formulated by **an** analyst Doug Laney, who described the ever-increasing amount of data, i.e. diversity, volume and speed. The problem of large amounts of data was firstly introduced in 1997, when NASA scientists identified the problem with the graphics as data visualization, this amounted to such a size that the data files could not be placed in computer's memory or on the hard drive of the computer [2] and [3].

2. Big Data

In terms of information-communication technologies Big Data (BD) represents rapidly changing and expanding field. Big data is associated primarily with modern, trendy technologies that generate a wealth of data, where appropriate, the amount of data used, as for example, semantic technology, sound processing and voice, whether or not the internet of things. For this reason, it is very difficult to clearly define the concept of Big Data. Other reasons are also temporal changes in the meaning of rapid technological development, i.e. data, which represented large data-intensive processing in the 1990s, can be handled by common computers or mobile devices just because of the influence of developed technology [4].

As it is not clearly defined there is a number of definitions of data, from which it is possible to mention the following:

Big data represents a loosely defined term that describes a large amount of complex data sets, and, at the same time, it describes advanced technology for the collection and storage of the data [5].

Big Data is currently a modern way of working with information, the importance of which depends on the number of enterprises. The very concept of Big Data can be misleading, as shows the survey conducted by IBM, in which 18% of Directors see Big Data just as a larger amount of data, and 8% as a new term, or a term to describe the amount of data [6].

In general, it is possible to talk about big data in three basic senses. These data consist of three different types – data too bulky to be processed in a reasonably short period of time with the appropriate performance (e.g. information about the gravitational potential of each star located in two galaxies, which are currently subjected to collision), flat data (e.g. searching for information within text, video or audio files), and real time data of the process, (such as traffic information from thousands of cameras and satellites) [7].

Big Data constitutes data of very large size, typically up to such an extent that their handling and management brings significant logistical challenges [7].

* **Milan Kubina, Gabriel Koman**
Department of Management Theories, Faculty of Management Science and Informatics, University of Zilina, Slovakia
E-mail: Milan.Kubina@fri.uniza.sk

Big Data shall relate to data files whose size is within the current database systems and it captures storage and processes capabilities over their analysis [8].

Large data relate to large amounts of data collected over time and are difficult to analyze and handle using ordinary tools to manage a single database. Analyzed data include the data in the field of marketing trends, as well as in the field of production, medicine and science. Types of input data are, e.g., commercial transactions, e-mail messages, photos, camera records, logs of activities, unstructured text, for instance from blogging and social media, as well as a large amount of data, which are generated by a variety of sensors [9].

Big Data is a term describing exponential growth and availability of structured as well as unstructured data. Big Data can have the same meaning for business and society as the Internet at present, but these data may lead to more accurate analyses [10].

The term Big Data refers to a large amount of information coming from a variety of sources, such as transaction records, boot files, social media, sensors, third parties, Web applications, etc. Big Data, however, is not only a large amount of data, but also extremely varied type of data, distributed at different speeds and frequencies [11].

Big Data is generated everywhere around us at all times. It is created by each digital process and the exchange of information through social media. It also generates different systems, sensors and mobile devices. Big Data comes from multiple sources at very great speed, in large volume and wide diversity. In order to obtain meaningful values from the major data, it is essential to feature optimum computing power, analytical abilities and skills [12].

Big Data can be defined in situations where sets of data are so great that traditional technology, technique and tools for their extraction are no longer usable within a reasonable time frame, and they are also ineffective due to the cost [13].

Big Data represents an ocean of information, in which we swim every single day. These are the extensive data from our computers, mobile devices and zettabytes machine sensors. The right solution will allow organizations to delve into all of the data and to gain valuable insights, which were previously unthinkable [14].

The concept of big data generates data that are too big, too demanding or too quick for processing of existing instruments. Too big means that enterprises must constantly deal with the petabytes data, which come from reports, transaction systems, sensors, etc.. Too quick data for processing of existing systems designate detection of frauds at the point of sale or detection of ads which should be provided to users on a website. Too demanding data means that processing of data by using existing tools for particular analyses is complicated and difficult and it cannot be provided [15].

The term Big Data defines large volumes of data, which are so complex that traditional data processing systems have problems to work with. Three main problems in large data include a number of data collections, speed at which it is necessary to analyze the data, and a variety of collected data formats [16].

Big Data is a collection of large amounts of disparate information, usable for an understanding of the environment, medicine and the human experience [17].

The concept of Big Data currently defines the broad use of data obtained through digital technology and analog sources. Big data is used for better understanding of business environment and markets, leading to better understanding of customers and at the same time increasing the performance of organizations [17].

Big Data constitutes data files whose size exceeds the possibilities of most current hardware and software technologies, so they can be paired and processed within a reasonable time. In addition, these data have a different texture, are heterogeneous, or they may be completely unstructured (such as multimedia or text documents) [18].

Big Data is a term used to describe the storage and analysis of large and complex data sets, by using a variety of technologies (MapReduce, NoSQL, etc.) [19].

With the advent of new technological options, such as social sites, mobile devices, cameras, and a variety of interfaces with sensors to data networks, many companies and institutions have become capable of generating huge volumes of data that potentially contain interesting information, but they are not directly evaluated by man or by the usual calculation means, only to a limited extent. These kinds of data are referred to as big data [20].

Big Data designates such amounts of data that are difficult to handle by using traditional, commonly available means or financially demanding [21].

Big Data represents the next generation of data warehousing and business analyses. The concept is designed to provide maximum support for the needs of the investigation costs and increasing the efficiency of businesses [22].

Big Data is data that require an inordinate amount of time/space for storage, transmission, processing, and use of available resources [23].

Based on the similarities of the aforementioned definitions, it is possible to establish Big Data as large amounts of data that are constantly generated from a variety of sources (social networks, sensors, Internet, text files, etc.), and whose processing by traditional technologies is financially and temporally unfeasible for enterprises. There are also new technologies focused on the collection, storage and analysis of data through a variety of advanced analytical tools. This work with the data (diverse data that is structured, flat and semi-structured) in the context of Big Data technology is characterized by high speed. The ability to process large amounts of disparate data has a major impact on the acquisition of relevant information, the detection of business opportunities and streamline activities in the framework of all the processes in the enterprise.

3. Characteristic of Big Data technology

Big Data is a new generation of technologies and structures for processing of large amounts of disparate data. This technology allows rapid collection, sorting, analyzing and extracting valuable data from large volumes of data.

According to IBM, Big Data brings platform with options how to handle large amounts of data in relation to business opportunities of an enterprise. Big Data platform includes technologies for processing of structured and unstructured data with traditional links to new technologies focused on speed, flexibility, and task force exploring, discovering, analyzing the data. According to IBM Big Data is defined by the following features [24] - Fig. 1:

- ***volume*** represents a very large number of collected data for analytical processing (e.g. Airbus aircraft generates up to 40 TB of data every half an hour, Twitter generates 12 TB of data a day, Facebook 25 TB, etc.) [25 and 26], which presents an opportunity for businesses to process voluminous data in a single database summary structure.
- ***diversity*** means that data are well structured in a structured form, i.e. the data entered into the form of messages, images, and other types of data generated by the GPS signals via the Internet and telecommunications equipment.
- ***speed*** indicates that data must be gathered and processed very quickly, i.e. in real or near real time, which enables businesses to respond flexibly to changes in the market, or gain a competitive advantage.
- ***truthfulness*** represents the possibility of obtaining distorted output as processing a large number of diverse data is accompanied by certain amount of data that contain noise or distortion (e.g. data from social networks).

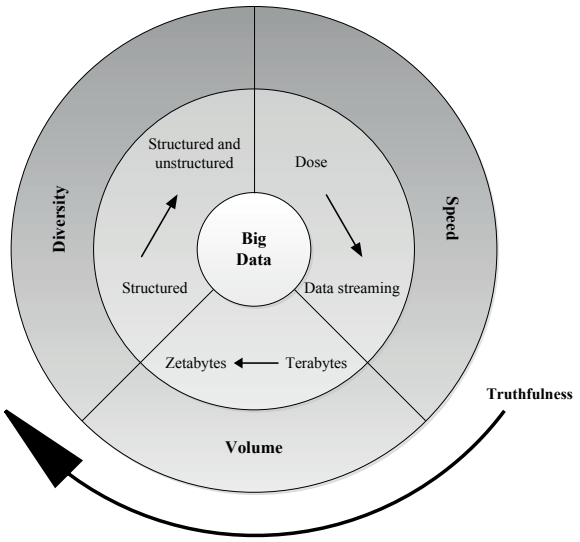

Fig. 1 Characteristics of Big Data, according to the IBM
Source: Edited according to ZIKOPOULOS, 2011, p. 5

The original characteristic of Big Data technology is defined by the three above-mentioned factors: volume, speed of data processing and diversity. The fourth factor, truthfulness, represents the extension of the three preceding characteristics of Big Data, as defined by IBM [26].

4. Benefits of Big Data technology

Big Data solutions are able to analyze almost all data sources that contain structured or unstructured data. Precisely for this reason, it is very rewarding, especially for large technologies and medium-sized enterprises that generate bulks of disparate data. The technology of Big Data can be utilized by small businesses to create positive influence on decision making and processes in enterprises, to ensure increase in sales and market growth. An example of this may be small businesses that operate call centers. Big Data platform is convenient exactly for this kind of enterprises as it generates a number of unstructured data. Assuming that a company knew how to analyze the quality of large volumes of unstructured data, in particular, it would receive more detailed information on the basis of which would be possible for example [6]:

- ***Streamlining marketing enterprise***, for example, in the context of the call centers which carry out Direct Marketing. Success rate in mass marketing in this case is currently between 0.2% and 3.1% [3], which is inefficient from a marketing perspective. By analysis of unstructured data, using Big Data technology in the form of e.g. Event Driven Marketing, it is possible to increase the rate to a range from 18% to 34% [6], which represents a significant difference compared to the present.
- ***Reducing the risk of loss***, by analyzing the behavior of clients using the Big Data technology. Analysis of the characteristics of the management of individual clients, the system can warn you about potentially risky procedures and thus, ultimately, to save money and time to prepare corrective measures against possible threats.
- ***Adjust bids according to the needs of customers***, using information obtained in the analysis of unstructured data. On the basis of this information it is possible to predict purchase behavior of consumers and subsequently adapt the products according to their needs, requirements and expectations or situations. The information provided can be used not only by Internet sales and marketing campaigns, but also in the marketing of a brick and mortar store.
- ***Streamlining work of the call center***, based on the processing of recorded interviews. Information that can be obtained from this data, they can improve the work of the operators, who then can offer the customer service that you need, or to solve his problem in a short time.

- ***Streamlining maintenance processes***, for example, in the industrial sphere, where businesses use numerous sensors that generate large volumes of data. By analyzing these data, it is possible to prevent accidents, or more accurately plan their service and maintenance, allowing the company to reduce costs and downtime caused by malfunctioning equipment.
- ***Understanding the spoken word***, in connection with the recognition of the voice, its analysis and sorting. This will allow businesses to save time and increase efficiency.
- ***Improving the quality of provided service***, for example, in healthcare, where doctors decide on the treatment of their patients based on their experience. However, in the future the analysis of large scale of patients´ data might enable doctors to make decisions on the basis of information and knowledge from a range of other doctors. Even in the field of business management, managers make decisions in various situations, not only on the basis of the information and outputs of the system, but also on the basis of their expertise.

Big Data technology can be applied in almost all areas of business where it is necessary to carry out decisions on the basis of readily available and relevant information obtained by analyzing large volumes of data.

5. Conclusion

The main problem in management and decision-making of enterprises is constantly growing amount of data generated within undertaking and its surroundings. These data reach the volumes and structures, which is not possible to manage through current management information systems due to time and cost.

The fastest increasing volumes of data are unstructured data, which may contain data with significant information value, for the purposes of decision-making in enterprises. Following the principle of processing data in the existing MIS, i.e. processing of structured data, companies do not have efficient tools to capture, analyze and transform the data.

Big Data brings solution to the problem of processing and integrating data of different types. This technology allows handling different kinds of data, from a variety of data sources, in a very short amount of time (in milliseconds).

Big Data technology provides business managers with the opportunity to carry out decision-making process on the basis of a larger quantity of available information. In general, the more information the better decision may be taken. Based on the above facts, it is thus possible to answer the question: *how much data do we need to achieve the best decision*? The answer to this question is: *it is never enough.*

References

[1] *What we Need Big Data* (in Slovak) [on-line] [cit. 2016-02-25]. Available at: https://www.datalan.sk/tmp/asset_cache/link/0000014602/DATALAN%20NEWS-01-2014_web.pdf

[2] BEZWEEK, S., EGBU, C.: *Impact of Information Technology in Facilitating Communication and Collaboration in Libyan Public Sector Organisations,* [on-line], [cit. 2016-02-02], available at: http://usir.salford.ac.uk/12835/1/530.pdf, 2010.

[3] *What Is ´Big Data,´ Anyway?,* [on-line], [cit. 2016-02-12], available at: http://www.strategy-business.com/blog/What-Is-Big-Data-Anyway?gko=28596

[4] CERNY, M.: *Eight Technology Trends that Transform Libraries in the Information Society* (in Czech), [on-line] [cit. 2016-02-12]. Available at: http://itlib.cvtisr.sk/buxus/docs/30_ osm%20technol%20trendu.pdf, 2013.

[5] KIM, J.: *Big Data Sharing Among Academics.* In: HU, W., KAABOUCH, N. 2014. Big Data Management, Technologies, and Applications. USA: Information Science Reference, 2014, pp. 177-194, ISBN 9781466647008.

[6] *Reasons Why Big Data Easier Life for Companies* (in Slovak), [on-line], [cit. 2016-02-22], available at: http://www.zive.sk/clanok/66175/7-dovodov-preco-big-data-ulahcia-firmam-zivot

[7] *Oxford English Dictionary - Big Data,* [on-line], [cit. 2015-03-01], available at: http://www.oed.com/view/Entry/18833?redirectedFrom=Big+Data#eid301162177.

[8] *Big Data: The next Frontier for Innovation, Competition, and Productivity,* [on-line], [cit. 2016-02-15], available at: http://www.mckinsey.com/business-functions/business-technology/our-insig hts/big-data-the-next-frontier-for-innovation.

[9] *Definiton of: Big Data,* [on-line], [cit. 2016-02-20], available at: http://www.pcmag.com/encyclopedia/term/62849/big-data.

[10] *Big Data. What is it & why it matters,* [on-line], [cit. 2016-02-10], available at: http://www.sas.com/en_us/insights/big-data/what-is-big-data.html.

[11] STANIMIROVIC, Z., MISKOVIC, S.: *Efficient Metaheuristic Approaches for Exploration of Online Social Networks.* In: HU, W., KAABOUCH, N.: *Big Data Management, Technologies, and Applications.* USA: Information Science Reference, 2014, pp. 222-269, ISBN 9781466647008.

[12] *What is Big Data,* [on-line], [cit. 2016-02-25], available at: http://www.ibm.com/big-data/us/en/.

[13] BAKSHI, K.: *Technologies for Big Data*, In: HU, W., KAABOUCH, N. 2014. *Big Data Management, Technologies, and Applications.* USA : Information Science Reference, 2014, pp. 1-22, ISBN 9781466647008.

[14] *Explore the World of Big Data,* [on-line], [cit. 2016-02-01], available at: *http://go.sap.com/solution/big-data.html.*

[15] MADDEN, S.: *From Databases to Big Data,* [on-line], [cit. 2016-02-22], available at: https://www.computer.org/csdl/mags/ic/2012/03/mic2012030004.pdf, 2012.

[16] MATTMANN, CH. A. et al.: *Scalable Data Mining, Archiving, and Big Data Management for the Next Generation Astronomical Telescopes.* In: HU, W., KAABOUCH, N.: Big Data Management, Technologies, and Applications, Information Science Reference, 2014, pp. 196-221, ISBN 9781466647008.

[17] *Best Practice Guideline: Big Data,* [on-line], [cit. 2016-02-05], available at: http://www.adma.com.au/assets/Uploads/Downloads/Big-Data-Best-Practice-Guidelines2.pdf.

[18] SEVVAS, K. I, et al.: *Applying the K-Means Algorithm in Big Raw Data Sets with Hadoop and MapReduce Data.* In: HU, W., KAABOUCH, N.: Big Data Management, Technologies, and Applications. Information Science Reference, pp. 23-46, 2014, ISBN 9781466647008.

[19] *The Big Data Conundrum: How to Define It?* [on-line], [cit. 2016-02-05], available at: http://www.technologyreview.com/view/519851/the-big-data-conundrum-how-to-define-it/.

[20] STRASIK, S.: FlexPod Select Hardware Platform for Hadoop (in Slovak), *INFOWARE X*., vol, 1-2, 2014, pp. 20-21.

[21] SYNEK, T.: How to Save IT Costs with Big Data Technology (in Slovak), *INFOWARE X.,* vol. 1-2, 2014, pp. 23-24.

[22] MINELLI, M., CHAMBERS, M., DHIRAJ, A.: *Big Data, Big Analytics. Emerging Business Intelligence and Analytic Trends for Today´s Businesses.* John Wiley & Sons, 2013, 187 p., ISBN 9781118147603.

[23] YILDIRIM, A., A. et al.: *Parallel Data Reduction Techniques for Big Datasets.* In: HU, W., KAABOUCH, N.: Big Data Management, Technologies, and Applications, Information Science Reference, 2014, pp. 72-93, ISBN 9781466647008.

[24] *Big Data for Beginners and Advanced* (in Czech), [on-line], [cit. 2016-02-10], available at: http://data.computerworld.cz/file/BigData/BigData-2012-web.pdf.

[25] *How Can we Use Big Data* (in Slovak), [on-line], [cit. 2016-02-01], available at: http://www.itnews.sk/2012-05-02/c148464-ako-mozno-vyuzit-big-data.

[26] *Data and Big Data - Prepare to Handle the New Paradigm?* (in Slovak), [online], [cit. 2016-02-20], available at: http://issuu.com/jozefsupsak/docs/zbornik_marec2013_final/3?e=2664486/ 8836631.

COMMUNICATIONS – Scientific Letters of the University of Zilina
Writer's Guidelines

1. Submitted papers must be unpublished and must not be currently under review for any other publication.
2. Submitted manuscripts should not exceed 8 pages including figures and graphs (in Microsoft WORD – format A4, Times Roman size 12, page margins 2.5 cm).
3. Manuscripts written in good English must include abstract and keywords also written in English. The abstract should not exceed 10 lines.
4. Submission should be sent by e-mail – as an attachment – to one of the following addresses: komunikacie@uniza.sk or holesa@uniza.sk (or on CD to the following address: Zilinska univerzita, OVaV – Komunikacie, Univerzitna 1, SK – 010 26 Zilina, Slovakia).
5. Uncommon abbreviations must be defined the first time they are used in the text.
6. Figures, graphs and diagrams, if not processed in Microsoft WORD, must be sent in electronic form (as JPG, GIF, TIF, TTF or BMP files) or drawn in high contrast on white paper. Photographs for publication must be either contrastive or on a slide.
7. The numbered reference citation within text should be enclosed in square brackets - in numerical order. The reference list should appear at the end of the article (in compliance with ISO 690).
8. The numbered figures and tables must be also included in text.
9. The author's exact mailing address, full names, E-mail address, telephone or fax number, the name and address of the organization and workplace (also written in English) must be enclosed.
10. The editorial board will assess the submitted paper in its following session. If the manuscript is accepted for publication, it will be sent to peer review and language correction. After reviewing and incorporating the editor's comments, the final draft (before printing) will be sent to authors for final review and minor adjustments
11. Submission deadlines are: September 30, December 31, March 31 and June 30.

COMMUNICATIONS

SCIENTIFIC LETTERS OF THE UNIVERSITY OF ZILINA
VOLUME 18

Editor-in-chief:
Prof. Ing. Otakar Bokuvka, PhD.

Editorial board:
Prof. Ing. Jan Bujnak, CSc. – SK
Prof. Ing. Otakar Bokuvka, PhD. – SK
Prof. RNDr. Peter Bury, CSc. – SK
Prof. RNDr. Jan Cerny, DrSc. – CZ
Prof. Eduard I. Danilenko, DrSc. – UA
Prof. Ing. Branislav Dobrucky, PhD. – SK
Prof. Ing. Pavol Durica, CSc. – SK
Prof. Dr.hab Inž. Stefania Grzeszczyk – PL
Prof. Ing. Mário Guagliano – IT
Prof. Ing. Vladimír Hlavna, PhD. – SK
Prof. RNDr. Jaroslav Janacek, PhD. – SK
Prof. Ing. Hermann Knoflacher – AT
Prof. Ing. Tomas Lovecek, PhD. – SK
Doc. RNDr. Mariana Marcokova, CSc. – SK
Prof. Ing. Gianni Nicoletto – IT
Prof. Ing. Ludovít Parilak, CSc. – SK
Prof. Ing. Pavel Polednak, PhD. – CZ
Prof. Bruno Salgues – FR
Prof. Dr. Miroslaw Skibniewski, PhD. – US
Prof. Andreas Steimel – DE
Prof. Ing. Marian Sulgan, PhD. – SK
Prof. Dr. Ing. Miroslav Svitek – CZ
Prof. Josu Takala – FI
Doc. Ing. Martin Vaculik, PhD. – SK
Doc. PhDr. Michal Valco, PhD. - SK

Address of the editorial office:
Zilinská univerzita
Office for Science and Research
(OVaV)
Univerzitna 1
SK 010 26 Zilina
Slovakia

E-mail: komunikacie@uniza.sk

Each paper was reviewed by two reviewers.

Journal is excerpted in **COMPENDEX** and **SCOPUS**.

It is published by the University of Zilina in
EDIS – Publishing Institution of Zilina University
Registered No: EV 3672/09
ISSN 1335-4205

Published quarterly

Single issues of the journal can be found on:
http://www.uniza.sk/komunikacie

ICO 00397 563
November 2016